The University of Adelaide
Australia

A PMAC Motor Drive with a Minimum Number of Sensors

Li Ying

Submitted to the Faculty of Engineering, Computer and Mathematical Sciences for the degree of Doctor of Philosophy

School of Electrical and Electronic engineering

The University of Adelaide

October 2002

Abstract

Permanent magnet AC motors have a wide range of applications mainly because of their high efficiency and high power density. To implement a self-synchronous control system, the conventional PMAC motor drives require some form of mechanical position sensors, usually attached directly to the motor shaft. However, mechanical sensors have a number of drawbacks in practical applications, such as increased number of wires and their sensitivity to the environmental factors. Therefore, elimination of the mechanical position sensor is desirable.

A number of position detection techniques have already been reported in the literature for PMAC motor drives, which may be named as indirect position sensing techniques. However, they have a number of limitations, such as math intensive calculations, limited operating speeds, sensitivity to the measurement noise and motor parameter variations, which all reduce the accuracy of the position data and the operating speed range of the motor drive.

In this thesis, a robust indirect position sensing technique is proposed and implemented in real time using a DSP based motor controller. The technique is based on a rotor position estimation using the measured phase voltages and currents of the motor. In this study, however, an incremental algorithm is used to estimate the flux linkage increments, which effectively eliminates the integration involved in the flux linkage estimation. Thus, the integration that exists in the outer loop is moved to the position calculation section forming an internal closed-loop. With the help of a phase-locked loop (PLL) algorithm, the internal closed-loop can significantly reduce the drift in the position estimation, which may be due to the parameter deviations or measurement inaccuracies. It was demonstrated that this feature provides a wider operating speed range and robustness. Theory analysis and real time implementation of the proposed indirect position detection technique are detailed in the thesis. In addition, a number of real-time tests are performed using a PMAC motor drive to demonstrate the accuracy and the robustness of the technique.

A PMAC motor drive always requires signals of phase currents and voltages to achieve the closed-loop current control or rotor position estimation. The phase voltages and currents are measurable quantities, but they can also be reconstructed from DC link measurements of the inverter for some low cost applications. This thesis also proposes and develops a novel three-phase currents reconstruction technique that is based on an adaptive current observer. The observer uses the mathematical model of a PMAC motor drive to estimate the three-phase currents, and then reconstructs the DC link current based on the relationship with switching states as its output. The correction section of the observer is the comparison between the measured and the estimated DC link currents and the result is used to compensate the DC link voltage to correct any deviations, assuming that three phases of the motor are symmetrical. A number of experimental results are provided in this thesis to demonstrate the accuracy of the current reconstruction for both sinusoidal and rectangular current excitations. A set of real-time experimental results also show that the reconstructed currents can replace phase current measurements as feedback signals to implement current closed loop control with single current sensor only.

In the final section of the thesis, two methods, the position estimation and the current reconstruction, are combined together to achieve a PMAC motor drive utilising a minimum number of sensors in the motor drive. The real time experimental results provided in this section illustrate that a good steady-state and dynamic performance can be achieved using the methods proposed, which effectively reduces the number of sensors in the motor drive to two, one voltage and one current sensors on the DC link. The number can further be reduced to one if the DC link voltage is assumed constant during the operation of the motor drive.

Declaration

This work contains no material which has been accepted for the award of any other degree or diploma in any university or other tertiary institution and, to the best of my knowledge and belief, contains no material previously published or written by another person, except where due reference has been made in the text.

I give consent to this copy of my thesis, when deposited in the University Library, being available for photocopying and loan.

Signed: **Date:** 05/11/02

Acknowledgements

I wish to express sincere gratitude to my supervisor Dr. Nesimi Ertugrul for his guidance, inspiration, support, and knowledge during my research. He has made this project both challenging and enjoyable. Above all he has shown great warmth and friendship, and for that I am very grateful.

I would like to thank all the technical staff for their help and assistance during my research in the power projects laboratory.

I would also like to acknowledge Dr. Soong Wen L. for his suggestions and encouragements during my research.

The University of Adelaide provided me with a scholarship during my studies, for which I am grateful.

I am grateful to every member of the Department who has helped me during my stay here.

This thesis would not have been possible without the love and support of my wife. I deeply love and appreciate my wife's encouragement and understanding during my long hour working.

Li Ying

October 2002, Adelaide.

Abbreviations

List of variables used throughout this thesis

Abbr.	Variable Name	Unit
$i_{a,\,b,\,c}$	Three-phase currents	A
$\Delta i_{a,\,b,\,c}$	Three-phase current increments	A
$i_{d,\,q}$	D- and Q-axis currents	A
I_{dc}	DC link current	A
I_m	Amplitude of phase current	A
$\vec{i}_s$	Current phasor	A
$v_{a,\,b,\,c}$	Three-phase voltages	V
$v_{d,\,q}$	D- and Q-axis voltages	V
V_{dc}	DC link voltage	V
$\vec{v}_s$	Voltage phasor	V
$v_{A,\,B,\,C}$	Terminal voltages	V
v_N	Floating neutral voltage	V
$e_{a,\,b,\,c}$	Three-phase back-EMF voltages	V
$e_{1,\,2,\,3}(\theta_e)$	Three-phase back-EMF functions	-
E_m	Amplitude of back-EMF	V
$\vec{E}$	Back-EMF phasor	V
$\psi_{a,\,b,\,c}$	Three-phase total flux linkages	Wb
$\Delta\psi_{a,\,b,\,c}$	Three-phase flux linkage increments	Wb
$\psi_{pma,\,pmb,\,pmc}$	Three-phase flux linkages of permanent magnet	Wb
ψ_m	Amplitude of flux linkage	Wb
$\vec{\psi}$	Flux linkage phasor	Wb
$R_{a,\,b,\,c}$	Three-phase winding resistances	Ω
R	Winding resistance	Ω
$L_{a,\,b,\,c}$	Three-phase self-inductances	H
$L_{d,\,q}$	D- and Q-axis inductances	H
$M_{ab,\,bc,\,ca}$	Three-phase mutual inductances	H
L_{sl}	Leakage inductance	H
L_{s0}	Inductance of fundamental air-gap flux linkage	H
L_{s2}	Inductance of rotor position dependent flux linkage	H
L_s	Self-inductance	H

M_s	Mutual inductance	H
L	Equivalent inductance	H
k_e	Back-EMF constant	V/rad/s
θ_e	Electrical rotor position	rad
θ_r	Mechanical rotor position	rad
$\Delta\theta_{ae,\ be,\ ce}$	Three-phase electrical rotor position increments	rad
$\Delta\theta_e$	Electrical rotor position increment	rad
$\delta\theta_e$	Position increment error	rad
φ	Angle of power factor	rad
ω_r	Angular speed	rad/s
ω_e	Angular speed in electrical	rad/s
$\mu_{a,\ b,\ c}$	Measurement noise of the three phases	V
Δt	Sampling interval	s
N_p	Number of pole pairs	-
p_e	Input instantaneous power	W
p_{mech}	Mechanical power	W
$p_{e\phi}$	Phase instantaneous power in electrical	W
$p_{m\phi}$	Phase instantaneous power in mechanical	W
T_e	Electromagnetic torque	Nm
T_l	Load torque	Nm
$T_{e\phi}$	Phase electromagnetic torque	Nm
J	Inertia	$Kg.m^2$
$f_{d,\ q}$	Torque map functions	-
$S_{a,\ b,\ c}$	Three-phase switch states	-
K	Constant used in phase voltage reconstruction	-
K_p	Constant in PI a regulator	-
K_i	Constant in PI a regulator	-
ε_{dc}	DC link current error	A
p	Subscript denoting three phases	-
(k)	Subscript denoting order number in real time	-
*	Superscript denoting reference values	-
^	Superscript denoting predicted values	-

Table of Contents

Chapter 1
Introduction

1.1 Overview and Background

Electrical motor drives are widely used in industrialised nations. For example, 95% of all prime movers in industry are electric motors. In the last century, most of the motor drives in industrial systems, commercial equipments, and domestic appliances were designed to operate essentially at constant speed, mainly because of the absence of the efficient variable speed drives. With the advancement in power electronics and developments of industrial automation within the last 20 years, many mechanical loads, such as elevators, paper and steel mill drives, machine tools, and robots, were accommodated adjustable speed motor drives, which significantly improved the performance, productivity, and energy efficiency [1].

Among the motor types, due to their simple construction, induction motors have been the most popular type, which are also inherently reliable and require minimum maintenance. Although such motors are widely used in constant speed applications, after the development of vector control methods in the early 1970's, their speed control performance became very close to the performance of the conventional brush DC motor (with commutators). Moreover, the rapid advancements in power electronics and microprocessor technologies made the induction motor drives very competitive in terms of real-time performance and overall system efficiency. As a result of these developments, the applications of adjustable speed AC motor drives have increased tremendously with the improvement of the performance and the reduction of the cost [2].

Permanent magnets (PMs) have been used in electrical machines as replacements for the electromagnetic excitation systems almost from the beginning of the development of such machines. However, the low energy densities of the earlier magnetic materials limited their use to small or brush DC machines. After the introduction of advanced permanent magnet (PM) materials, however, such as rare earth PMs, the use of PM motors has become more attractive than the vector controlled induction motor drives in the recent years [3].

The PMs in motors produce the air gap magnetic field, which eliminate the use of excitation or field windings as in the conventional brush DC motor. The PMs not only can improve the motor's performance, but also make it possible to design a motor with much higher efficiency characteristics. The higher efficiency is mainly due to the absence of the field windings and associated copper losses. In addition, higher magnetic flux density in the air gap can be achieved by using high performance PM materials. This higher magnetic flux density made it possible to design the motor with impressively high values of power density and torque-to-inertia ratios. The superior characteristics of PMs make them very attractive candidate in numerous applications including actuators and servo motor applications that demand the fastest possible dynamic response. Furthermore, the absence of the field windings simplifies the construction and maintenance of the PM motors while increasing the flexibility of their usage in special applications. In general, compare to their counterparts, modern PM motors are competitive both in performance and cost, which also improves continuously with the significant drop in their cost.

A brushless permanent magnet AC (PMAC) motor has magnets mounted on the rotor and three-phase armature windings mounted on the stator, which are usually connected star configuration. The armature currents of the motor flow through the stator windings, and due to the absence of the rotor windings this arrangement allows excellent heat dissipation in the motor.

However, the brushless configuration means an electronic switching converter has to be accommodated to perform the similar function of the mechanical commutators/brushes that exist in the conventional brush DC motor. The principal function of the electronic switching converter is to produce excitation current for each phase, which must be synchronised with the back-EMF voltage of that phase. Since the back-EMF voltage is related to the magnet positions in the rotor, the rotor position of the PMAC motor has to be known for correct current commutation. With the development of power electronics, microprocessor and motor control technology, nowadays, PMAC motor control is becoming much easier and inexpensive opening a wide range of applications where such motor drives are utilized.

1.2 Objectives and Contributions

Effectively, PMAC motors are synchronous motors and in the absence of auxiliary rotor windings, power electronics devices must be used to synchronise the AC exciting currents with the instantaneous rotor position accurately. This is a requirement to obtain smooth

electromagnetic torque from the motor drive. As stated earlier, generally, a three-phase inverter is used to power the PMAC motor. The conventional method of ensuring synchronism is achieved by switching the power devices of the inverter directly from a shaft-mounted rotor position sensor. This action is commonly known as self-synchronisation, which effectively keeps the torque angle of the synchronous PMAC motor constant at zero degrees. This function is analogous to the role of the mechanical commutators and brushes where the current commutation is achieved mechanically. Therefore, the PMAC motors with trapezoidal back-EMF voltages are also known as brushless PMDC motors [4].

However, mechanical shaft-mounted position sensors, such as resolvers, absolute position encoders and Hall-Effect sensors, have many drawbacks and their applications are restricted. Firstly, a special mechanical arrangement is needed to mount the position sensor on the motor shaft, and the mounting accuracy directly affects the accuracy of the position detection. Secondly, a number of signal wires are needed between the motor and the controller. Such wires increase the cost and decrease the reliability of the motor drive system. Thirdly, these sensors, particularly Hall-Effect sensors, are sensitive to the environmental factors, such as temperature, humidity and vibration, so that their applications are limited in many applications. Moreover, using a shaft-mounted position sensor increases the moment of inertia and motor size. In addition, using a position sensor increases the system cost significantly, which should consider the sensor itself and associated electronic circuit [5].

One of the most active research areas of PMAC motor controls during recent years has been the rapid development of new techniques for eliminating the rotor position sensors. It can be concluded that the position sensors are the most expensive and fragile components in the entire motor drive. Therefore, elimination of the shaft-mounted position sensor is a very desirable objective in many applications. Although the elimination of the direct sensor does not eliminate the requirement for the position information, there are a number of benefits of this, such as the elimination of electrical connections to the sensor and associated environmental factors, and reduction in overall size. Of course, the absence of the direct sensor should not limit the operation of the motor drive at zero, low and higher speeds.

A number of position sensor elimination, or indirect position detection, techniques have been proposed for the PMAC motor drives. These techniques can broadly be classified in three groups.

In the first group, the position sensing is based on the back-EMF sensing. However, since the back-EMF voltages are too low to be sensed at low speed range, this technique is not suitable at start and at low-speed operation, which may be critical in certain applications. In the second group, the position information is obtained by measuring and processing the phase voltages and the currents of the PMAC motor. However, in this group, computationally intensive real-time algorithms are needed. The methods are also very sensitive to the motor parameter variations and measurement inaccuracies. In addition, these techniques may also suffer at low speed operation that may be due to integration drift in the algorithms. The third group of indirect position techniques is based on the detection of the rotor saliency due to structure or magnetic saturation in certain PMAC motors. Therefore, these techniques are not suitable for surface permanent magnet (SPM) motor, which has no rotor saliency.

In order to estimate continuous rotor position information, most of the proposed position estimation algorithms require the measurements of three-phase currents and voltages of the motor. In addition, the three-phase currents are also used in the drive to implement the closed-loop current control. The most effective method is to measure all five quantities directly.

In practice, Hall-Effect sensors for current measurements and isolation amplifiers for voltage measurements are utilized, which also provide electrical isolation between high-voltage inverter and low-voltage control circuit. Additional hardware, such as A/D converters, is still needed to implement digital control. However, using current sensors and associated conditioning circuits may result in increased complexity, cost, space and a reduction of system reliability. Therefore, employing a minimum number of sensors, which also increase the reliability of the system and reducing cost, are desirable in many applications. This is the primary aim of this project.

In this research, a robust position sensorless technique, which is suitable for both sinusoidal and trapezoidal PMAC motors without rotor saliency, is proposed and implemented in real time with a DSP controller. The method proposed here is based on the estimation of rotor position using phase voltages and line currents. In this study an incremental algorithm is utilised to transfer the integration from flux linkage calculations to the position calculation, which forms an internal closed loop. With the help of a phase-locked loop (PLL) algorithm, the internal closed loop corrects any position drift caused by the motor parameter deviations or measurement inaccuracies. Therefore, the position sensorless technique can operate in a wider speed range, and has robustness with respect to motor

parameter variations and the measurement errors. In comparison with other position estimation methods, moreover, the algorithm has less mathematical computations, which makes the real-time implementation of the method easier. A wide range of experimental results is provided in the thesis to demonstrate the high accuracy of the position estimation. Moreover, parameter variations and measurement inaccuracies are also investigated thoroughly. It was shown that the estimated rotor position can replace the measured position signals to implement a closed-loop position sensorless control. Furthermore, real time experiments demonstrated that the position sensorless drive system has good static and dynamic performances, and achieve high robustness and reliability that are required in any practical applications.

The second major contribution of this thesis is the proposition and implementation of a novel three-phase current reconstruction technique. The technique is based on an adaptive current observer, which estimate the three-phase currents according to the mathematical model of a PMAC motor drive. Based on the relationship among the switching states, a DC link current is reconstructed from the estimated three-phase currents and used as an output of the adaptive current observer. The output is then compared with the actual measured DC link current and the result is used to correct the estimated current from the observer. Under the assumption of the symmetry of the three phases of a PMAC motor, the correction factor is utilised to compensate the DC link voltage, so that all of the three-phase estimated currents can be corrected at all time. With the adaptive current observer, therefore, the three-phase current can be reconstructed from DC link measurements and switching signals of the inverter. The phase currents reconstruction technique is suitable for both trapezoidal and sinusoidal PMAC motor drives with rectangular or sinusoidal current excitation. The experimental results demonstrate that the reconstructed three-phase currents can follow the actual winding currents accurately and have good dynamic performances. This makes it possible to replace the phase current measurements with a single current sensor on the DC link. Real time steady state and dynamic results were obtained under a single current sensor operation of the PMAC motor

The key contribution of this thesis is to combine the novel position sensorless and current reconstruction techniques to demonstrate a practical PMAC motor drive with a minimum number of sensors. In the final method developed, the three-phase voltages and currents required by the position estimation are reconstructed using the DC link current measurements and switching signals of the inverter, and then the rotor position is estimated using these

reconstructed phase voltages and reconstructed phase currents. Effectively, this final implementation requires only two sensors: DC link current and DC link voltage sensors. It is worth noting here that if dc link voltage remains constant, only one measurement, DC link current, is sufficient. Real time experimental results are also given under steady state and dynamic operating conditions using a single sensor in the DC link.

1.3 Outline of Thesis

The contents of this thesis are organised as seven chapters.

The objective of Chapter 2 is to introduce the operation principle and control methods of two major classes of PMAC motors (trapezoidal and sinusoidal) in order to provide a theoretical basis for the research work presented in the thesis. As it is shown, due to the differences in their configurations, these two types of motors PMAC motors have some notable difference in their performances and their controls. Therefore, a major portion of this chapter is devoted to a comprehensive discussion on commonalities, differences and controls of these two classes of PMAC motors. The particular requirements of the PMAC motors for the synchronization of the phase currents with the rotor position are also addressed.

Chapter 3 provides a review of previous position sensorless and phase current reconstruction techniques. The advantages and disadvantages of each method are discussed with reference to their application targeting a practical PMAC motor drive. The position sensorless methods can be broadly divided into three groups, based on back EMF sensing, based on an estimation method using the measured three-phase currents and voltages, and based on the inductance variations that has to be identified indirectly. In this chapter, it is summarised that previous position sensorless methods have limitations, mainly based on the accuracy of position data and limited operation under low and high speeds. In addition, it is explained in this chapter that three-phase voltages and currents of a PMAC motor powered from an inverter can be directly measured or reconstructed from DC link measurements in order to reduce the cost. The chapter also reviews the previous current reconstruction techniques and highlight their limitations in term of accuracy and operation in a closed-loop real time system.

Chapter 4 develops a mathematical model suitable for the application of digital control techniques for both trapezoidal and sinusoidal PMAC motor drives. The derivation of the model is briefly reviewed to show the theoretical control principles of PMAC motor drives.

Based on the mathematical model, a general dynamic simulation Virtual Instrument (VI) for a PMAC motor drive is established using a graphical programming language, LabVIEW. In this study, the developed simulation tool is used to predict the static as well as the dynamic performances of the motor drive, and the results are verified by the experimental data. Of course, the main purpose of the development of the simulation tool is to provide an evaluation platform to simulate the rotor position estimation and phase current reconstruction algorithms before they are actually been implemented in the practical real time motor drive.

Chapters 5, 6 and 7 compose the core of this thesis, which cover the major contributions of this research.

Chapter 5 concentrates on the development of the robust position sensorless technique for a wide range of PMAC motor types. Based on the discussion of all possible approaches to derive rotor position information from ideal mathematical model and measurable quantities of a PMAC motor drive, the derivation of the novel incremental position estimation algorithm is detailed at the beginning of the chapter. The characteristics of this algorithm are also covered in the chapter. To demonstrate the validity and reliability of the new position sensorless technique, the Chapter provides some computer simulations and examines the robustness of the method with respect to the motor parameter variations and the measurement errors. In addition, the real data obtained from the actual motor drive are used to estimate the rotor position, and the results are compared with the actual rotor position signals to demonstrate the validity and the robustness of the position estimation algorithm. Finally, the position sensorless technique is implemented in real time using a DSP based motor controller. The hardware and software details are provided, and a wide range of experimental results is given to demonstrate the ability of the position sensorless PMAC motor drive.

Chapter 6 primarily focuses on the three-phase current reconstruction from DC link measurements of an inverter. In a three-phase inverter, DC link current fully depends on the switching states of the inverter and the three-phase currents. Based on the discussions of all possible operating modes of a three-phase inverter, this Chapter first presents a novel approach to analyse the switching states, and then establishes a background discussion to reconstruct the DC link current using the estimated three-phase currents. Assuming a three-phase symmetry in the PMAC motor, a novel approach of three-phase current reconstruction using the DC link measurements is proposed, which is based on an adaptive state observer. Similar to the previous chapter, the phase current reconstruction technique is also validated using the computer simulation developed. Following this section, the real data obtained from

the DC link current and the switching signals measurement are used to reconstruct the three-phase currents. The experimental verifications demonstrated that the accuracy of the reconstruction is good to be used as a current feedback signals. Finally, the phase current reconstruction technique is implemented in real-time in a closed-loop current control system, and experimental results are given at the end of the chapter.

In chapter 7, two of the novel techniques, the position estimation and the phase current reconstruction, are combined to achieve a PMAC motor drive with a minimum number of sensors. First, the chapter reviews the reconstruction techniques of phase voltages and currents and discuss the possible approach to estimate the rotor position using the reconstructed phase voltages and currents. Then, a real PMAC motor drive with a minimum number of sensors is implemented. Hardware and software details of the combined system are given. Finally, a wide range of experimental results is given to demonstrate the performance of the motor drive. In this section a discussion is provided to highlight the implementation of the method in sinusoidal and trapezoidal PMAC motor drives.

The appendices are used to supplement the work found in the chapters. Appendix A details the hardware of the actual motor drive. The major features of IRMDAC3 3-Phase 460VAC 3HP Motor Drive Board and ADMC 300 DSP-based Motor Controller as well as the processor board of the controller are given. Appendix B describes the hardware and software of the data acquisition system, which includes two analogue boards of PCI-6110E boards and one high-speed digital board of PCI-6534. The principal features of these boards are given, and the software diagrams with LabVIEW are also provided here to show the implementation of the synchronization technique of the data acquisition. Appendix C details the derivation of the different position estimation errors, which are used to discuss the robustness of the position estimation algorithm.

Chapter 2

Permanent Magnet AC Motors and Control

2.1 Introduction

Permanent magnet (PM) motors fall into a generalized classification known as double-excited motors, which have two sources of excitation: usually known as the armature and the field excitation. In conventional synchronous and brush DC motors, both of these excitation sources are electrical windings connected to an external source of electrical energy. In PM motors, however, the field excitation windings are replaced by PMs and, of course, no external source of electrical energy is required. The use of permanent magnets to replace the field excitation windings in a motor brings several benefits. First, no electrical energy is absorbed by the field excitation system, and thus there is no excitation loss that means substantial increase in the efficiency. Second, higher magnetic flux density in the air gap can be achieved by using high performance PM materials. This make it possible to design a PM motor with higher torque or output power per volume and better dynamic performance compared with motors with electromagnetic excitation. In addition, the absence of electromagnetic excitation can simplify construction and maintenance of the PM motors and also increase flexibility of size and shape for special application [3].

When the PMs are mounted on the stator of a motor, the motor falls into a PMDC commutator motor since a special commutator must used to connect the armature rotor with an external electrical power supply. Because of the action of the commutator, of course, the control of a PM brush DC motor is comparatively simple and so, it is still widely used in many applications. However, the commutator of the motor and its brushes also cause several construction and maintenance problems, so that brushless or replacement of the mechanical commutator with an electronic switching converter is required in some applications, which is named as brushless PM motor [4].

A brushless PM motor has PMs located on the rotor and a polyphase, usually three-phase, stator similar to conventional synchronous or induction motor. The most obvious advantage of the brushless configuration is the removal of the brushes, which are subject to wear and

require maintenance. Another advantage of the brushless configuration, in which the rotor is always inside the stator, is that more cross sectional area is available for the power armature winding that make the condition of heat through the frame improved. Consequently the power per volume and the efficiency of a brushless PM motor is likely to be higher than that of a PM brush DC motor. In addition, the absence of commutator and brushes reduces the motor length and rotor inertia and eliminate brush fiction and speed dependent current limitations. Thus, considerable improvements in dynamics can be achieved specifically for servo-type applications.

However, the brushless configuration does not come without some disadvantages. When rotor with PMs rotating, the back EMF voltages induced in the stator windings are AC. Thus, the excitation currents fed to stator armature should also be AC in order to produce constant torque. This means that the brushless PM motor actually is an AC motor. Consequently, one of the main disadvantages compared with the PM brush DC motors is that PMAC motors require more complicated electronic controller to provide AC excitation currents. In addition, the excitation currents should be synchronous with the back EMF voltages, that is, the rotor position. Therefore, a position sensor should be mounted on the shaft of the PMAC motor to achieve a correct current commutation, that is, a self-synchronous control. However, these disadvantages have been surmountable with the development of power electronics and motor control technology [2].

The objective of this chapter is to examine the principal control techniques of PMAC motor drives in order to provide basic concepts for the research work presented in this thesis. Two major classes of PMAC motors, trapezoidal and sinusoidal, will be introduced that have some notable difference in their respective control requirement and performance characteristics. A major portion of this chapter will be devoted to a discussion of the commonalities and differences associated with their controls. The particular requirements of PMAC motors for the synchronization of excitation currents with the rotor position will also be addressed.

2.2 Configuration of PMAC Motor

As stated above, the stator of a PMAC motor is essentially identical to that of a synchronous or induction motor, which is usually formed from punched soft magnet steel laminations. On inner surface of the stator lamination, there are several slots, which are used to hold the armature windings, which are usually connected to a three-phase source as star or

delta form. Since the distinguishing feature of PMAC motors is the present of a set of PMs in the rotor, a great variety of PMAC motor configurations do exist, and much of this variety is due to the location of the PMs within the rotor structure. Thus, PMAC motors may be classified according to their rotor configurations [2].

One of the simplest rotor configurations is shown in cross section in figure 2.1(a). The rotor has an iron core that may be solid iron or made of punched laminations. Thin PMs are mounted on the surface of this core using adhesives. Alternating magnets of opposite magnetization direction produce radially directed flux density across the air gap. This flux density then interacts with currents in the armature windings to produce torque. The surface PM motors usually have equal inductances in direct-axis and quadrature-axis. Because of their high efficiency, such PM motors have the potential to replace the induction motors in a number of industrial, commercial, and domestic variable speed drives. However, constant power operations of these motors are very limited. This is due to the fact that a large demagnetising component of stator current is required to produce a significant reduction in magnet flux.

If some of the properties of a reluctance motor are incorporated into the PMAC motor, effective flux reduction can be achieved. A simple example is an inset PM motor, in which the PMs are inset into the rotor core as shown in figure 2.1(b). Due to the near unity relative permeability of the PM material, the direct-axis inductance of the inset PM motor is smaller than the quadrature-axis inductance, which is due to the small iron-to-iron gap throughout the quadrature sector. Because of the presence of a reluctance torque, in these types of motor flux reduction can be effectively achieved by advancing the stator current phase angle from a maximum torque. Therefore, they are suitable for constant power speed range applications.

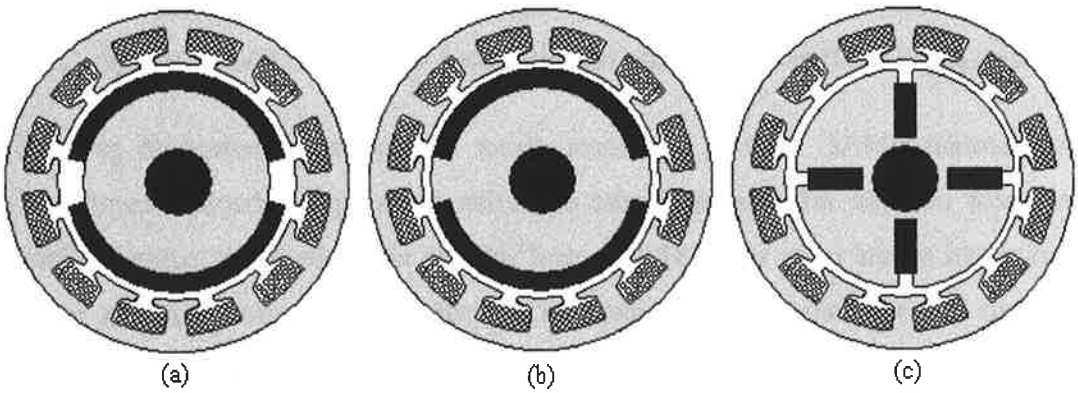

Figure 2.1 Cross section of PMAC motors: (a) Surface magnets, (b) Inset magnets, (c) Interior magnets

Another rotor configuration for a PMAC motor is shown in figure 2.1(c). In this interior PMAC motor, the magnets are directed circumferentially to supply flux to the iron poles, which then produce radially directed air gap flux. To increase air gap flux, the shaft should be nonmagnetic. This type of structure can achieve a high air gap flux density. The direct axis inductance of this motor is low because its flux path is largely through low permeability magnets, while the quadrature-axis inductance is high since its flux can circulate in and out of each pole face. Many structural variants of interior PM motor have been proposed. Since the magnets are very well protected against centrifugal forces, some of them are well suitable for high frequency and high-speed applications.

Apart from the rotor configurations given in figure 2.1, many other rotor geometries have been proposed for PMAC motors. Most of the research and advance developments in PMAC motors today is focus on the optimum rotor structure, which may be based on weight minimization or cost minimization or both. However, in terms of motor parameters, an optimum rotor should maximize the air gap flux density and minimize the leakage flux between magnets that does not contribute to energy conversion process. Structure integrity and ease of assembly are also concerns in the optimisation process.

Although there are a number of the PMAC motor configurations, from the control point of view, they can be broadly classified into two principal classes: sinusoidal current excited and rectangular current excited motors. Due to the sinusoidal back-EMF waveforms, a sinusoidal current excited motor should be powered by three-phase sinusoidal currents to produce constant torque, so that it is usually called sinusoidal PMAC motor. Also, since it operates on the principle of a rotating magnetic field as other synchronous motors, it is simply called PM synchronous motor. Rectangular current excited motors are also fed with three-phase currents shifted by 120^0 one from another, but due to the trapezoidal back-EMF waveforms, the current waveforms should be rectangular and precisely synchronized with the rotor instantaneous position. These motors are usually called trapezoidal PMAC motors [2].

In trapezoidal PMAC motors, the most direct and popular method of providing the required rotor position information to the controller is using an absolute angular position sensor mounted on the rotor shaft. This control scheme is an electronic commutation that is analogous to the mechanical commutation in a brush PMDC motor. For this reason, the rectangularly excited motors are also known as brushless PMDC motors, or simply brushless DC motors.

In practice, only surface magnet rotor configurations are used with both trapezoidal and sinusoidal PMAC motors, while inset and interior magnet rotor configurations are used only with sinusoidal PMAC motors [3].

2.3 PMAC Motor Control Characteristics

2.3.1 Trapezoidal PMAC Motor

As stated above, trapezoidal PMAC motors are usually of surface magnet rotor configuration. The magnets mounted on the surface of the rotor core are usually designed as wide magnet pole arcs, such as 180^0. In ideal case, therefore, a rectangular distribution of magnet flux can be achieved in the air gap, as shown in Figure 2.2(a). In practice, however, fringing causes the corners to be somewhat rounded.

In addition, the stator windings of a trapezoidal PMAC motor are always concentrated in a few slots, as an example of 12 slots for three-phase winding (that is two slots per pole per phase). If the two adjacent full-pitch coils are connected in series as one phase winding, the back-EMF induced in the winding will ideally produce a stepped shape, as shown in Figure 2.2(b), when rotor of the motor rotates. In practice, fringing will cause corners in the back-EMF waveform to be round. As a result, a roughly trapezoidal back-EMF voltage will be produced in each stator phase winding during rotation, as shown by the dotted lines in Figure 2.2(b). Thus, the back EMF waveform has the trapezoidal shape that is characteristics of trapezoidal PMAC motors [4].

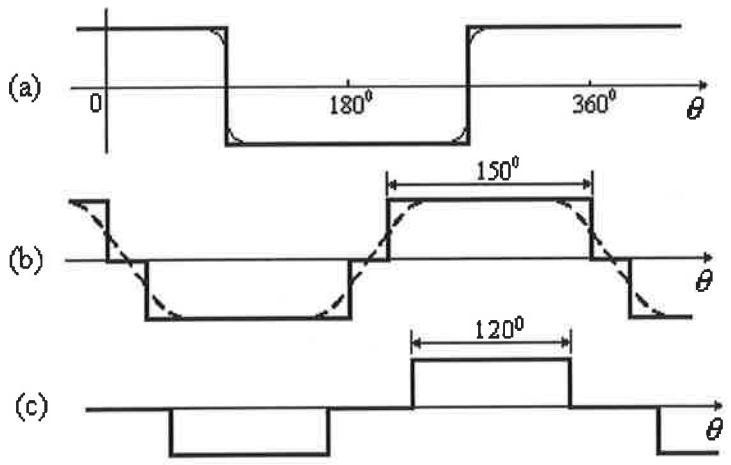

Figure 2.2 Trapezoidal PMAC motor with ideal waveforms of flux density, back EMF, and current: (a) Magnet flux density around the air gap. (b) Back EMF waveform, (c) Ideal phase current waveform.

With 180^0 magnet arcs and two slots per phase, the crest of the back EMF waveform is ideally 150^0 wide, but in practice the fringing field reduces this to a somewhat smaller value, possible as little as 120^0, which is required to maximise the smoothness of the resulting output torque. The back-EMF amplitude E_m is proportional to rotational angular frequency ω_r, as follow,

$$E_m = k_e \cdot \omega_r \tag{2.1}$$

where K_e is back-EMF constant.

If a current with fixed amplitude I_m is flowing into the motor phase during the time interval when the back-EMF is cresting as indicated in Figure 2.2(c), the instantaneous power converted by this phase from electrical form ($P_{e\phi}$) into mechanical form ($P_{m\phi}$) will be,

$$P_{e\phi} = E_m I_m = P_{m\phi} = \omega_r T_{e\phi} \tag{2.2}$$

where ($T_{e\phi}$) is instantaneous electromagnetic torque developed by the excited phase. Using the equation (2.1), the torque is given by,

$$T_{e\phi} = k_e I_m \tag{2.3}$$

These dual direct proportionalities of back-EMF to speed and torque to current expressed in equations (2.1) and (2.3) are identical in form to expressions characterising a conventional brush DC motor with constant field excitation. Some of the control techniques for brush DC motor can be used in trapezoidal PMAC motor drive. This is also the reason of naming trapezoidal PMAC motor as brushless DC motor. Despite the popularity of this name, however, it should be noted that the trapezoidal PMAC motor is fundamentally a synchronous AC motor, and not a DC motor as the name implies.

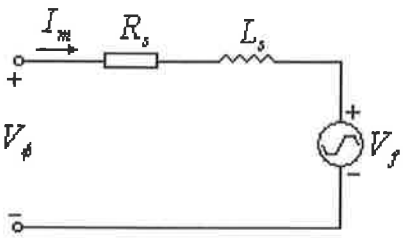

Figure 2.3 Basic per phase equivalent circuit of a trapezoidal PMAC motor.

The standard per phase equivalent circuit model, as shown in Figure 2.3, can be used to analyse a three-phase trapezoidal PMAC motor [1]. The equivalent phase inductance in this model is constant since the rotor of a surface magnet motor presents virtually no net magnetic saliency, which would result in inductance variations at the motor stator terminals. The back-EMF voltage source included in this model delivers the signature trapezoidal voltage waveform shown by the dotted lines in Figure 2.2(b), corresponding to the open circuit back-EMF waveform measured across each of the phase terminals.

2.3.2 Sinusoidal PMAC Motor

Unlike the trapezoidal PMAC motor with concentrated stator windings, the windings of a sinusoidal PMAC motor are typically distributed over multiple slots on the inner surface of the stator in order to approximate a sinusoidal distribution. The resulting back-EMF waveforms generated by sinusoidal PMAC motors have sinusoidal shape. In addition, the air gap flux density distribution of a sinusoidal PMAC motor is also modulated to reduce the harmonics of the back-EMF waveforms.

Trapezoidal PMAC motors strongly favour surface magnet designs, so that the phase inductances remain constant as the rotor rotates. In contrast, besides the basic surface magnet design, sinusoidal PMAC motors can provide flexibility for adopting a variety of rotor configurations including inset or interior magnets. Hence, sinusoidal PMAC motors can offer various performance characteristics for a wide range of applications.

Similar to the induction motors, the most convenient analysis method for the sinusoidal PMAC motors is to use instantaneous current, voltage, and flux linkage phasors in a synchronously rotating reference frame locked to the rotor [1]. In the analysis, three-phase sinusoidal currents, voltages and flux linkages can be integrated as synchronously rotating phasors. When a synchronously rotating reference frame is set up and d-axis is aligned with the PM flux linkage $\vec{\psi}$, the phasors of current, voltage and flux linkage can be given as in Figure 2.4. The three-phase back-EMFs obtained from the flux linkages can also be integrated as a phasor $\vec{E}$, which will be aligned with the quadrature or q-axis. The amplitude of the back-EMF phasor is proportional to rotational angular frequency ω_r and can be expressed as:

$$E_m = N_p \cdot \omega_r \cdot \psi_m \tag{2.4}$$

where N_p is the number of pole pairs and ψ_m is the amplitude of the magnet flux linkage.

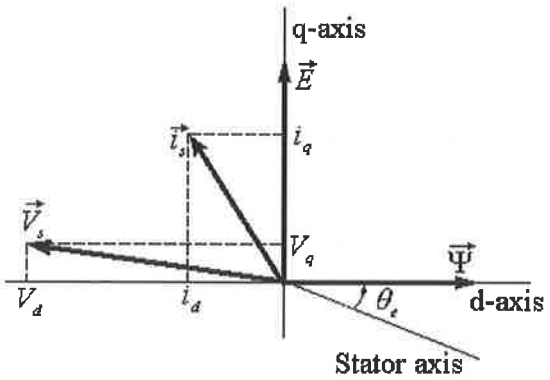

Figure 2.4 Basic phasor relationships for the sinusoidal PMAC motors

As shown in Figure 2.4, the current phasor $\vec{i}_s$ can be divided into d- and q-axis scalar components i_d and i_q in the synchronously rotating reference frame. Similarly, the applied stator voltage phasor $\vec{V}$ can also be divided into two scalar components v_d and v_q. The components of the d-q frame and the abc three-phase reference frame are interrelated by the Park transformation, which can be written for currents as follows:

$$\begin{bmatrix} i_a \\ i_b \\ i_c \end{bmatrix} = \sqrt{\frac{2}{3}} \begin{bmatrix} \cos(\theta) & \sin(\theta) \\ \cos(\theta - \frac{2\pi}{3}) & \sin(\theta - \frac{2\pi}{3}) \\ \cos(\theta + \frac{2\pi}{3}) & \sin(\theta + \frac{2\pi}{3}) \end{bmatrix} \cdot \begin{bmatrix} i_d \\ i_q \end{bmatrix} \tag{2.5}$$

The basic voltage equation describing the sinusoidal PMAC motor in the synchronously rotating reference frame is given by:

$$\begin{aligned} v_d &= R \cdot i_d + L_d \cdot \frac{di_d}{dt} - \omega_e \cdot L_q \cdot i_q \\ v_q &= R \cdot i_q + L_q \cdot \frac{di_q}{dt} + \omega_e \cdot L_d \cdot i_d + \omega_e \cdot \psi_m \end{aligned} \tag{2.6}$$

where R is the winding resistance, L_d and L_q are the d- and q-axis stator phase inductances respectively, and ω_e is the angular electrical speed.

The values of the stator phase inductances L_d and L_q are equal in a non-salient PMAC motor with surface magnet rotor. However, L_d will be small than L_q in salient-pole PMAC motor using inset or interior magnets.

This $d-q$ phasor representation given in figure 2.4 leads to the following general expression for the instantaneous electromagnetic torque developed in a sinusoidal PMAC motor,

$$T_e = 1.5N_p \cdot \left[\psi_m \cdot i_q + i_d \cdot i_q \cdot (L_d - L_q)\right] \tag{2.7}$$

The torque equation consists of two terms and each of them has a useful physical interpretation. The first magnet torque term is independent of i_d but is directly proportional to stator current component i_q, which is in phase with the back-EMF. In contrast, the second reluctance torque in equation (2.7) is proportional to the current component product $(i_d i_q)$ and to the difference in the inductance values along the two axes ($L_d - L_q$). For a non-salient surface magnet PMAC motor, the reluctance term naturally disappears since L_d equals L_q. However, since L_q is typically larger than L_d in a salient pole PMAC motor, it is worth noting that i_d and i_q must have opposite polarities for the reluctance torque to contribute a positive torque component and therefore the total torque is no longer linearly proportional to the stator current amplitude as in trapezoidal PMAC motor [1].

2.4 Current Control of PMAC Motor

2.4.1 Control Requirements

As discussed above, sinusoidal and trapezoidal PMAC motors have different control characteristics. These differences will be reflected in their respective current control requirements, which are naturally derived from their fundamentally different excitation current waveforms.

In order to produce a smooth torque in a PMAC motor with trapezoidal back-EMF, an ideal rectangular waveform of phase current should be provided to the phase windings. The current pulses should be 120^0 electrical wide and of magnitude I_m, and the positive direction of the current must be against the back EMF. The conduction periods of the three phases are

symmetrically phased so as to produce a three-phase set of balanced 120^0 square waveforms, as shown in Figure 2.5(a).

In contrast, a PMAC motor with sinusoidal back-EMF should be fed by the sinusoidal current in order to produce a constant electromagnetic torque. The excitation waveforms for sinusoidal PMAC motors are shown in Figure 2.5(b).

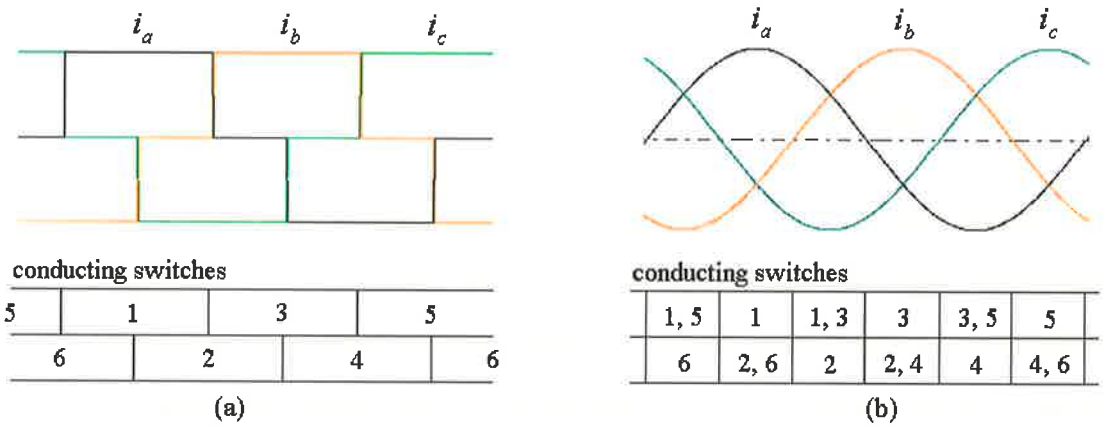

Figure 2.5 Excitation current waveforms and conducting switches in a three-phase inverter: (a) Trapezoidal PMAC motor, (b) Sinusoidal PMAC motor

There are some different control techniques to achieve the current requirements of sinusoidal and trapezoidal PMAC motors. For high performance current controller, however, the differences between them are only in the method used to generate the reference current waveforms. A sinusoidal PMAC motor need a sinusoidal reference current generator, while a trapezoidal PMAC motor need a rectangular reference current generator, but similar current control techniques can be applied to both motors.

2.4.2 Power Converter

For PMAC motor drives supplied from utility power lines, some form of power electronic converter is required to transform the fixed frequency, fixed amplitude input power into the variable frequency, variable amplitude power needed to excite the PMAC motors. The most popular approach is to use a converter with an intermediate DC link between the input rectifier and output inverter. There are two types of intermediate DC link. One uses an inductance in the DC link as a current source, so the inverter is called current source inverter. The second type accommodates a large capacitor in the DC link as a voltage source, so the inverter is called voltage source inverter [1].

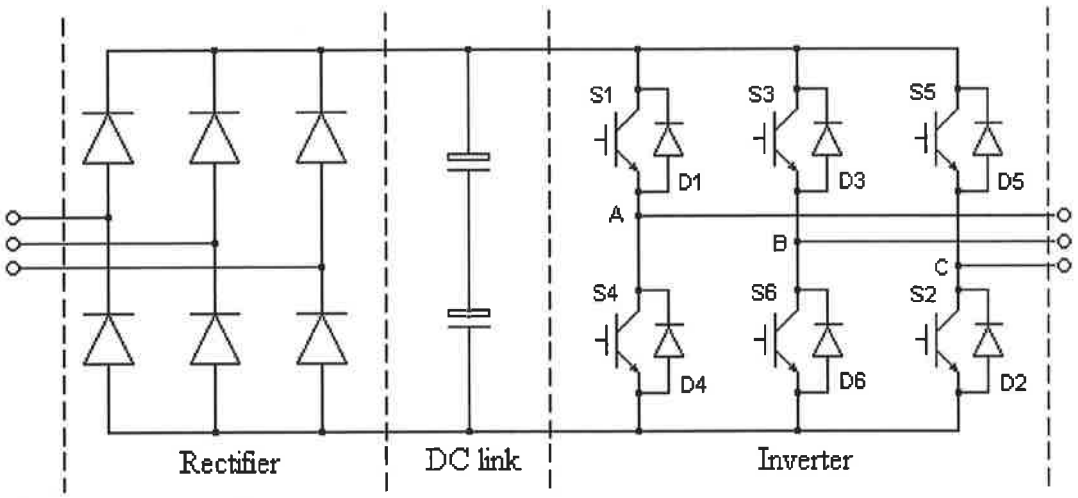

Figure 2.6 Three-phase AC-to-AC converter with voltage source DC link

To produce the required three-phase symmetrical sinusoidal or rectangular excitation currents, the most typical structure for a PMAC motor is a three-phase AC-to-AC converter with voltage source DC link, which consist of a three-phase (or a single-phase) diode bridge rectifier, voltage source DC link and a three-phase power switch inverter as shown in Figure 2.6. The rectifier with diodes is uncontrollable, so the DC link voltage only depends on the input voltage. The power switches in the inverter are the key elements of the converter, which achieve the regulation of the phase currents in the motor drive.

The inverter has two primary functions for the PMAC motor control. The first function is position synchronization that requires the inverter to direct excitation to the proper phases at each time instant to maintain synchronisation and to maximise the torque output. The second function is the current regulation, taking the advantage of the direct proportionality between the current amplitude and the output torque.

2.4.3 Position Synchronization

Since the PMAC motors discussed here are also from the synchronous motors family, a constant torque can be produced only when the excitation currents are precisely synchronized with the instantaneous rotor position. The most direct and powerful method of ensuring this requirement is to continuously measure the rotor position and switch the excitation to make sure the PMAC motor phases are in exact synchronism with the rotor's motion. This method, commonly known as self-synchronization showing in Figure 2.7, uses direct feedback of the rotor position to ensure that the PMAC motor never experiences loss of synchronization [1].

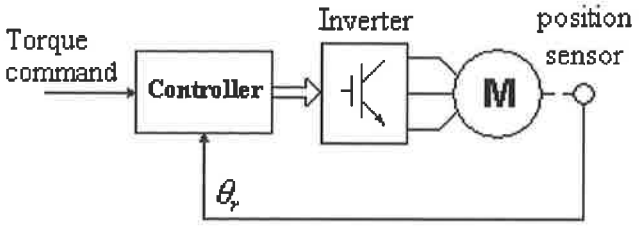

Figure 2.7 Block diagram of a self-synchronising PMAC motor controller.

For the trapezoidal PMAC motors, the concept of self-synchronization is always known as electronic commutation since this action is functionally equivalent to the mechanical commutator's role in a DC motor. The electronic commutation function can be easily accomplished by opening and closing the power switches in the inverter according to the rotor position of the PMAC motor. The most direct means is to detect the rotor poles with six position sensors, such as Hall-Effect sensors, which are shifted from each other by 60^0 (electrical), and hence to obtain six discrete switching points per electrical cycle. Each of the position sensors is used to trigger on one power switch in the inverter during 120^0 electrical per cycle. However, it can demonstrated that only three Hall-Effect sensors are sufficient to generate six discrete switching points per electrical cycle by using a logic circuit. In the trapezoidal PMAC motors, the power switches conduct in a six-step sequence, and only two power switches (one in the upper DC rail and one in the lower DC link) conduct at any instant, as shown in Figure 2.5(a).

For the sinusoidal PMAC motors, however, the self-synchronization requires continuous rotor position information to produce the sinusoidal excitation. Moreover, the self-synchronization should be implemented together with the current regulated. This means that six power switches of the inverter have the added responsibility of sinusoidally shaping the applied excitation waveform in addition to adjusting their amplitudes and frequency. A PWM switch control algorithm is typically used to eliminate all major low-order harmonics of the desired fundamental frequency excitation waveforms.

Various PWM algorithms can be used to obtain the sinusoidal current excitation. If a voltage source inverter is used, a typical approach is to use a closed-loop current control to achieve high-performance motion control in the sinusoidal PMAC motor drive. In this case, a rotor position sensor is required to feedback continuous position information to generate

required sinusoidal reference current, and the actual phase currents track the reference currents in the current controlled inverter, as will be described in the next subsection.

Although there are different current control techniques that can be used in trapezoidal PMAC motor drives, such as using a single current sensor in DC link [6], the similar PWM algorithms for current control can also be used for high-performance trapezoidal PMAC motor drives. The only difference is the three-phase reference currents generated from rotor position, which are rectangular waveforms.

2.4.4 Current Regulation

The purpose of current regulation in PMAC motor drives is to force the actual phase currents to track the reference currents. The closed-loop current regulation conventionally requires at least two current sensors to directly measure two-phase currents (assuming that the motor is star connected). Although several different schemes have been proposed to implement such current regulation, only two basic schemes, hysteresis and PWM current control, will be discussed below.

a) Hysteresis Current Control

Figure 2.8(a) shows the block diagram of one phase of the hysteresis current controller [5]. Three of these controllers are required for a three-phase motor drive, one for each phase. In this diagram, a current sensor is used to feedback the actual instantaneous phase current signal to the controller. The measured signal is compared with the current reference signal, which is ideal rectangular or sinusoidal waveform produced using the current command and the rotor position signal. Then the current error signal is used to generate switching signals for the power switches of the inverter, so that the current error can be minimized.

Figure 2.8(b) illustrates the typical waveform produced by a simple hysteresis current controller for a sinusoidal reference current. As shown in the figure, if the actual current is more positive than the reference current value, the upper power switch is turned off and the lower power switch is turn on causing the actual motor current to decrease by applying a negative voltage to the related phase. Conversely, when the actual current is more negative than the reference current value, the upper power switch is turned on and the lower power switch is turned off causing the motor current to increase by applying a positive voltage. The hysteresis comparator has a bandwidth that determines the permitted deviation of the actual phase current from the reference value before a switching is initiated. Thus, the actual current

can track the reference value without significant amplitude error or phase delay. Although setting a small hysteresis bandwidth, a nearly sinusoidal or rectangular phase current with small current ripple can be obtained, this results very high switching frequency in the inverter causing high switching losses.

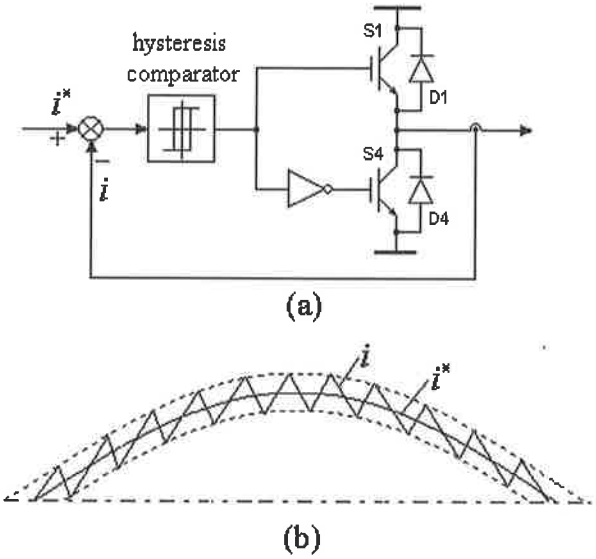

Figure 2.8 Hysteresis current control: (a) block diagram; (b) basic current waveform, *i* is the actual current and *i is the reference current.**

This control scheme is simple to implement and has high dynamic performance. However, there are some inherent drawbacks [7]. One of the drawbacks is that the switching frequency is not constant. This is because the switching frequency not only depend on the hysteresis bandwidth but also the back-EMF and inductance of the motor at a given speed and position respectively. For a given supply voltage, when the back-EMF of the motor is low, the switching frequency may rise excessively.

b) PWM Current Control

Figure 2.9(a) shows the block diagram of one phase of a PWM current controller. Similar to the hysteresis current control, a current sensor is required to feedback the actual instantaneous phase current signal, but the error between the reference current and actual current is regulated by a proportional integral (PI) controller to derive the reference signals u^* for the pulse width modulator (PWM). The output of PWM is used to drive the inverter power switches, so that the actual current is forced to track the reference current.

The switching procedure for a PWM current controller is illustrated in Figure 2.9(b). If the reference current is more positive than actual current, the PWM reference signal u^* derived from PI controller may be positive. The reference signal is compared with triangular carrier signal u_{cr} from the carrier generator. If the reference signal u^* is more positive than the carrier signal u_{cr}, the upper power switch is turned on and the lower power switch is turned off, so that positive voltage is applied to the related phase. While, if the reference signal u^* is more negative than the carrier signal u_{cr}, the upper power switch is turned off and the lower power switch is turned on causing negative voltage power applied to the related phase. Since the reference is positive, the interval of applying positive voltage will be longer than that of applying negative voltage within one PWM cycle. This will reduce the current error and force the actual current to track the reference current. Conversely, if the reference current is more negative than actual current, the PWM reference signal u^* may be negative, so that the interval of applying negative voltage will be longer than that of applying positive voltage within a PWM cycle. This also forces to reduce the current error and make the actual current to track the reference current closely.

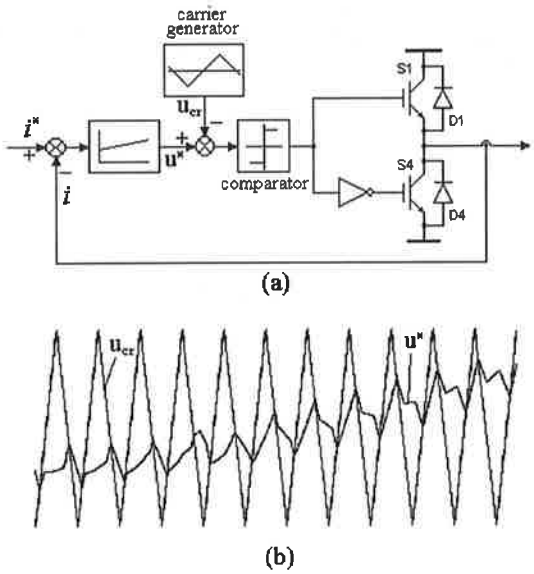

Figure 2.9 PWM current control: (a) block diagram; (b) Carrier signal (u_{cr}) and reference current (u^*).

The switching frequency in the PWM controller is defined by the triangular carrier signal. It is preset and therefore will ensure the inverter switching capability not exceeded. The tracking error can be kept low by choosing a high gain of the PI controller. The gain is limited, on the other hand, as it also amplifies the harmonic currents. In order not to impair

the proper operation of the pulse width modulator, the slop of the current error signal must be always less than the slop of the triangular carrier signal.

2.5 PMAC Motor Drive

2.5.1 Control Structure

Regardless of whether the PMAC motor is sinusoidal or trapezoidal, the control structure of a PMAC motor drive shares important common characteristics. Figure 2.10 shows how control loops can be cascaded using classic techniques to achieve, successively, torque, speed, and position control in a PMAC motor motion control system [1].

a) Torque Control

Torque control is the most basic control function for a motion control system. Due to the close relationship between current and torque produced in any PMAC motors, as described in

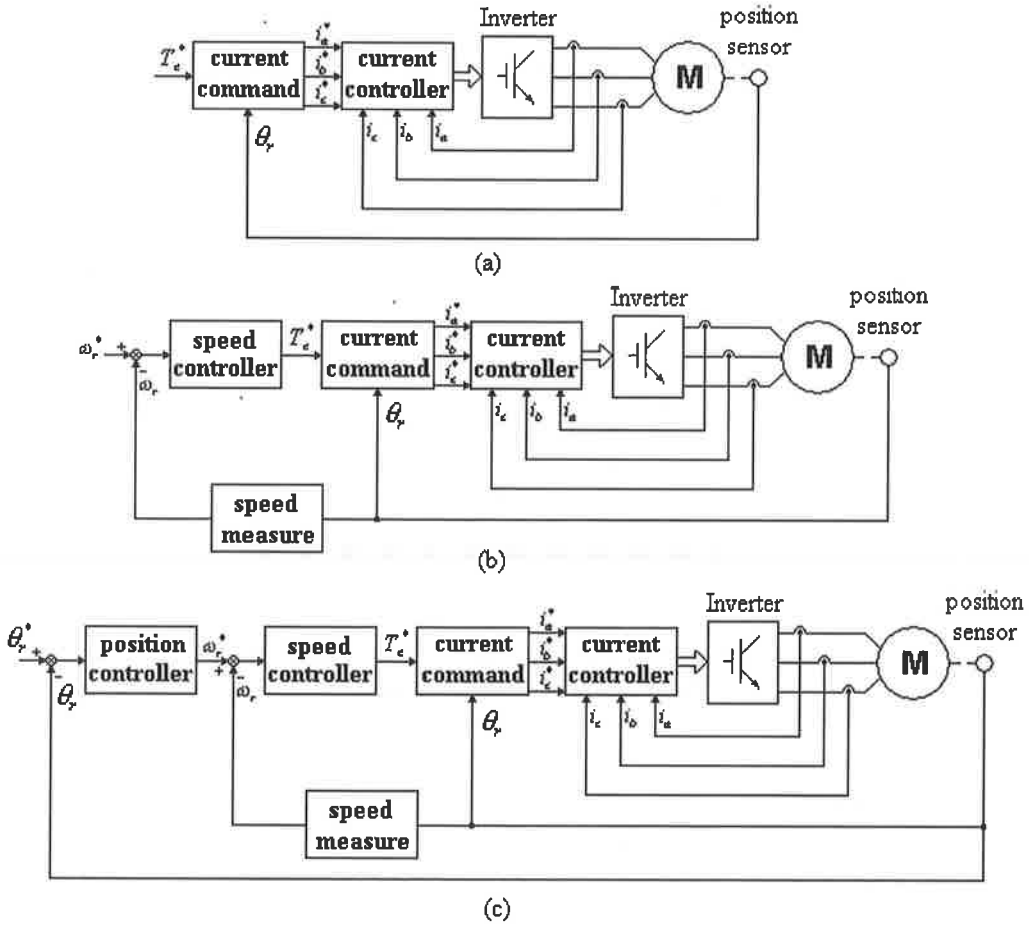

Figure 2.10 Typical cascaded control structures for high performance PMAC motor drives: (a) current-regulated torque control; (b) closed-loop speed control with inner current loop; (c) closed-loop position control with inner speed and current loops.

more detail in Section 2.3, torque control of a PMAC motor drive can directly map into current control. In order to achieve high-performance motion control, the majority of PMAC motor drive applications incorporate closed loop regulation of the phase current as shown in Figure 2.10(a). Note that this basic torque control configuration also incorporates the self-synchronization concept using rotor position feedback discussed previously in Section 2.4.3.

For trapezoidal PMAC motors, if the rectangular excitation currents are exactly in phase with the trapezoidal back-EMF, the relationship between electromagnetic torque and current amplitude is almost perfectly linear, so that the torque command can map directly into the current command with only a simple proportionality constant.

In contrast, sinusoidal PMAC motors usually require a non-linear mapping between torque and current command. One basic approach to implement this non-linear mapping for high-performance torque control of sinusoidal PMAC motor drives is shown in Figure 2.11. According to this approach, the incoming torque command T_e^* is mapped into commands for *d-q* axis current components i_d^* and i_q^* using functions f_d and f_q respectively, which are extracted from torque equation (2.7). These current commands in the rotor *d-q* reference frame (DC quantities for a constant torque command) are then transformed into the instantaneous sinusoidal current commands for the individual stator phase currents (i_a^*, i_b^*, and i_c^*) by using the Park transformation in Equation (2.5). The most common means of defining functions f_d and f_q to map the torque command T_e^* into the d-q current component commands i_d^* and i_q^* is to set a constraint of maximum torque-per-amp operation, which is nearly equivalent to maximizing operation efficiency [8].

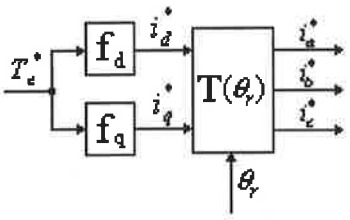

Figure 2.11 Current command for high performance sinusoidal PMAC motor drive

Since d- and q-axis stator phase inductances, L_d and L_q are equal, the torque-per-amp in the non salient sinusoidal PMAC motor can be maximized by simply setting i_d to zero for all values of the torque, that is, f_d is equal to zero and f_q is a proportional constant. In this case,

the torque is proportional to the amplitude of the excitation currents and the sinusoidal currents are always exactly in phase with the back-EMFs of the motor. This control scheme is similar to that of the non-salient trapezoidal PMAC motor as described above.

In contrast, the maximum torque-per amp for a salient PMAC motor can be developed by advancing the phase angle of the stator phase currents, so that they lead their respective back-EMF waveforms by angles between zero and 45^0 electrical. This means that two non-linear functions f_d and f_q, which define the maximum torque-per-amp trajectory for the salient PMAC motor, should be used to produce the commands of $d-q$ axis current components i_d^* and i_q^* for the control of the stator current [9].

b) Speed Control

Speed control can be conveniently achieved in PMAC motor drives by closing a speed feedback loop around the inner torque/current loop as illustrated in Figure 2-10(b). Usually, this speed feedback signal can be derived from the same shaft- mounted sensor used to detect the rotor position, eliminating the need for an additional sensor. In many cases, a simple proportional integral (PI) controller is sufficient to achieve the desired dynamic performance requirements. The output of the speed controller will be the torque command for the torque control.

c) Position Control

A position control loop may be needed for position control applications. Using a similar loop cascading procedure, position control can be accomplished by closing an outer position loop around the nested current and speed loops as shown in Figure 2.10(c). If a gearbox or some other power transmission device couples the motor to a load, it is often necessary to introduce a second position sensor attached to the movable output load. This direct measurement of the load position will make it possible to compensate any non-linear effects in the mechanical drive train and free the controls from the problems associated with tracking the absolute position of the load over multiple turns of the motor shaft. On other hand, cost pressures or other considerations may make it necessary to sacrifice some of the position accuracy in order to eliminate the extra sensor.

As in the case of speed control, a basic PI controller may be sufficient in many position applications. Using classic servo control techniques, the dynamic characteristics of the nested

loops are typically designed, so that the innermost current loop has the fastest dynamic response, while the outermost position loop is the slowest. However, a wide variety of alternate controller configurations are also possible to achieve desired performance for PMAC motor position applications.

2.5.2 Torque Ripple

Due to the magnet flux density distribution and the exciting current of a practical PMAC motor drive cannot be as perfect as described in Section 2.3, the drive always has some periodic torque ripple components that may pose problems in some applications. There are two major sources contributing to the torque ripple, one principally motor related while the other predominantly inverter related. The motor related source causes the back-EMF waveform distorted, such as the round back-EMF top (not flat) of a trapezoidal PMAC motor or the harmonic components in the back-EMF of a sinusoidal PMAC motor. Various PMAC motor design improvements have been suggested to minimize this torque ripple [10].

The inverter related source is that no ideal sinusoidal or rectangular excitation current may be supplied by a practical inverter. For trapezoidal PMAC motors, the most trouble torque ripple components are caused by the phase current commutation. When current is transferred from an off-going inverter phase to the next on-coming active phase at the end of each 60^0 electrical interval, the commutation between the two phases will take some time, which depends on the phase inductance and the available voltage. During this time, the sum of the currents in the off-going and on-coming motor phase is never constant. This causes the commutation torque ripple, which occurs every 60 electrical degrees, giving rise to a torque ripple component with a fundamental frequency of six times electrical excitation frequency. In order to reduce the amplitude of the commutation torque ripple, several techniques have been proposed for modifying the current PWM regulation scheme [11].

In addition to the commutation torque ripple, there is an inverter related torque ripple component, which is directly proportional to the high-frequency PWM ripple in the motor phase currents. This torque ripple component is generally not significant because the mechanical load inertia is typical large enough to filter out its effect on the speed of the motor.

The inverter related torque ripple component is only produced by the high-frequency PWM ripple in the motor phase currents, so that the torque ripple associated with sinusoidal

PMAC motors is generally less than that developed in trapezoidal motors. This is due to the fact of sinusoidal PMAC motors do not experience the abrupt phase-to phase current commutations as that of trapezoidal PMAC motors. Therefore, sinusoidal PMAC motors are preferred in high-performance motion control applications, such as servo systems.

2.5.3 High-Speed Operation

As discussed earlier in Section 2.3, the amplitude of the back-EMF of a PMAC motor increases linearly with the rotor speed. When the speed increases to a value where the amplitude of the peak line-to-line back-EMF approaches the DC link source voltage, the current controller of the PMAC motor drive will gradually degrade in quality. Eventually the current regulators saturate, losing their ability to force the actual currents to track the command currents, so that the inverter naturally reverts to its basic voltage source operation.

For a trapezoidal PMAC motor, when rotor speed is relatively low, the current controller can force the actual currents to track the reference current and a good quasi-rectangular current waveform, as shown in Figure 2.12(a), can be produced in each phase of the trapezoidal PMAC motor. This is called low speed operation with current control model. However, when the sum of the back-EMF voltages of the two conducting motor phases approaches the DC link source voltage with the rotor speed increase, the actual phase current amplitudes and the motor torque will both fall off quite abruptly. Since the phase currents in this case depend only on the phase voltage and the back-EMF, the actual current waveforms are not quasi-rectangular. This is because the back-EMF of the off-going phase during commutation is in such a direction as to drive the current down and assist commutation. In addition, the back-EMF in the on-coming phase is of equal value and in a direction as to oppose the current build-up, so that the phase current waveform as shown in Figure 2.12(b) will be produced. For this reason, this is called high-speed operation without current control model. The non-rectangular current waveforms also will cause more commutation torque ripple components. Under such conditions, however, the effect of these torque disturbance on motor speed tend to be less troublesome due to the effective low-pass filtering action of the rotor inertia at high-speed range.

As mentioned before, when the speed increases above the threshold value, the torque drops quite heavily for the trapezoidal PMAC motor. In order to expand the speed range, a technique of advancing the phase angle of the excitation transition points relative to the back-EMF may be used to restore some degree of torque production at the high-speed operation.

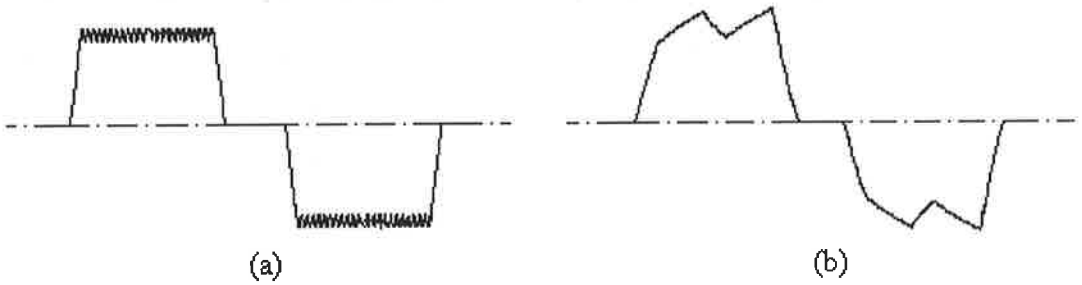

Figure 2.12 Typical phase current waveform of a trapezoidal PMAC motor. (a) Low speed with current control. (b) High speed without current control.

As the phase angle is advanced, the current in the on-coming phase is given a controlled time interval to build up before the back-EMF increases and limits further current increase. Unfortunately, the available range expansion with this approach is relatively modest and comes at a price of increased peak phase current amplitude and significant increases in the torque ripple [12].

High-speed operation of sinusoidal PMAC motors has similar constraint from back-EMF increase with the rotor speed. However, the current regulators for sinusoidal PMAC motors will naturally saturate to six-step voltage excitation with 180^0 switch conduction intervals (that is three inverter switches on at all times) then the peak line-to-line back-EMF approaches the DC link source voltage. This makes it easier to achieve extended high-speed operation in sinusoidal PMAC motor drives.

Similar to the conventional DC and induction motor drives, high-speed constant power operation can be achieved in the sinusoidal PMAC motor drives by flux weakening. For simplicity, a non-salient sinusoidal PMAC motor is used as an example to introduce this concept here. As mentioned in Section 2.5.1(a), to maintain maximum torque-per-amp operation at low-speeds is to hold d-axis current component i_d at zero. As the speed is increased toward the threshold value, a d-axis current component i_d can be added to produce a negative d-axis stator flux ($L_d\, i_d$), which counteracts the positive d-axis magnet flux ψ_m, so that a limited amount of flux weakening can be achieved. This demagnetising current component can be implemented by advancing the phasor angle of the stator phase currents. The flux weakening can develop greater torque for a sinusoidal PMAC motor drive in high-speed regime, but it is no longer in maximum torque-per-amp operation. Although this concept is introduced by using a no salient PMAC motor, flux weakening for high-speed

operation can be used more effectively in a salient PMAC motor by advancing the current phasor angle from the maximum torque-per-amp trajectory [13].

Chapter 3

Survey of Sensorless Techniques in PMAC Motor Drives

3.1 Introduction

A PMAC motor with a squirrel cage winding on the rotor can produce asynchronous torque, hence can be started and operated from an inverter without any rotor position data. In such motor, a simple constant volt-hertz (V/Hz) control algorithm can be used to achieve open-loop speed control in applications such as pumps and fans that do not require fast dynamic response. However, rotor position information is always required in any other type of PMAC motors, which effectively synchronize the phase excitation currents to the back EMF waveforms.

As described in the previous chapter, a trapezoidal PMAC motor with an electronic switching converter is basically equivalent to a brush DC motor with the mechanical commutators. The principal function of the electronic switching converter is to switch the DC source according to the rotor position information. Therefore, the motor can produce constant electromagnetic torque and never lose synchronism. Because of the high cost of the power switches, the number of the phases is kept much smaller than the equivalent number of the commutator segments on the brush DC motor's rotor. For a three-phase winding motor, six power switches (equivalent to six commutator segments) should be used to switch the DC source and to generate three-phase symmetrical excitation currents. This means that the rotor position information must be obtained at a 60^0 interval to ensure that two of the power switches in the inverter are on for the correct current excitation and for the synchronisation. However, because of the small phase numbers, the electronic commutation of the trapezoidal PMAC motor is quite coarse compared to the mechanical commutator.

In contrast, since the back-EMF waveforms of a sinusoidal PMAC motor rotate continuously at a constant speed with the rotor rotation, continuous rotor position information must be obtained to generate the required sinusoidal excitation currents and maintain the phase currents at a fixed angle. If a similar analogy is applied to the sinusoidal PMAC motor,

the continuous rotor position information makes such motor drives similar to a brush DC motor having an infinite number of commutator segments. Consequently, in such motor drives, a very low level of high-frequency torque ripples are produced because of the limited resolution of the practical rotor position sensors resulting a high-frequency harmonics in the excitation currents.

In addition to the position synchronization, it should be noted here that the rotor position information may also be used to derive the rotor speed for closed-loop speed control of the PMAC motors.

In order to obtain the rotor position information, the simplest method is using some form of rotor position sensor on the motor's shaft. Such a sensor measures the mechanical position of the rotor based on either optical or electromagnetic principle. For trapezoidal PMAC motor, for example, Hall-Effect position sensors may be preferred to detect the rotor position. Normally, a group of three Hall-Effect sensors are mounted on the stator positioned by 120^0 electrical. When the shaft rotates, such sensors are triggered either by the rotor magnets or by a separate magnets ring, so that the rotor position information can be obtained at a 60^0 electrical resolution.

To obtain more accurate digital position information, optical encoders are used, which consist of a coded disc mounted on the shaft of the motor, a light emitting diode (LED) acting as a light source, and a phototransistor to detect light. The coded disc can either block or pass the emitted light to the phototransistor at different position, so that the on-off states of the phototransistor can be transferred to rotor position information as the motor is running. There are two main classes of optical encoders, incremental and absolute encoders. Incremental encoders usually use a coded disc with certain number of equally spaced slots. In these sensors, the position information is obtained by counting the slots as the shaft rotates. However, such encoders require a reference position to determine the absolute position reference to this reference, and their operation is strictly limited in the case of a power supply failure. An incremental encoder can also be made using electromagnetic position sensor. In such sensor, the coded disc is replaced with a metal-toothed wheel and the light emitter is replaced with a form of electromagnetic sensor that can detect the change of the electromagnetic permeability as the metal wheel rotates.

Absolute encoders provide a series of uniquely coded positions, such as eight different slot patterns with eight detectors arranged concentrically for an eight-bit encoder. These encoders

can output digital signals that can directly be interfaced to a computer controller. Unlike the incremental encoders, absolute encoders cannot lose the absolute rotor position in the case of a power supply failure, but they are more expensive specifically if a higher resolution sensor is needed.

Resolvers are also a type of rotor position sensors attached directly to the shaft of the motor. Their operation is based on inductive coupling between its stator and rotor windings of a special rotating electrical machine. Normally, the rotor winding of a resolver is excited by a reference voltage at 50 Hz or 400 Hz, so that the induced voltages in the stator windings can be processed to output sine and cosine signals. Then the output signals are processed and converted to highly precise absolute digital position information using a Resolver to Digital converter. However, resolvers together with the associated electronic circuits are expensive for many applications of PMAC motor drives.

Although direct position sensing is readily available and widely used in industrial applications, their usage has a number of disadvantages in practical PMAC motor drives. Some of these disadvantages may be summarized as below [5]:

a) A special mechanical arrangement is needed to mount the position sensor on motor shaft since the accuracy of the mechanical mounting directly affects the accuracy of detection. In addition, direct sensors always require maintenance.

b) A number of connection wires are required for the shaft sensors, between the motor and the controller, which have to be shielded against EMI. This increases the overall cost and reduces the reliability of the motor drive.

c) The direct position sensors are sensitive to environmental factors, such as dust, temperature, humidity and vibration. This tends to reduce the reliability of the motor drives and limits their application areas.

d) The shaft mounted position sensors increase the inertia of the motor system, and the size and cost of the system.

Because of the above listed disadvantages, direct rotor position sensor elimination techniques for PMAC motor control received a wide range attention within the last decade. The position sensor elimination techniques are also known as position sensorless operation. However, the term of position sensorless doesnÆt means that the drive operates without rotor

position data, but it means that the position data is obtained indirectly using different sensors that already exists, easy to connect and reliable.

Recently, a number of position sensorless control scheme for PMAC motors have been developed. In the following sections of this chapter, a comprehensive review of the operation of these previously proposed position estimation methods will be given, and the advantages and disadvantages of each method will be discussed with reference to the implementation in practical PMAC motor drives. Section 3.2 provides the survey of the indirect rotor position determining techniques particular for trapezoidal PMAC motors. While, Section 3.3 gives the summaries of rotor position estimation techniques developed for sinusoidal PMAC motors, although some of them may also be used for trapezoidal PMAC motors. Most of the position sensorless, or indirect position sensing methods are not self-starting techniques. Therefore a special starting strategy is needed for start up the motor drive. Several starting strategies are described in Section 3.4.

In order to estimate the rotor position, most of the proposed position sensorless techniques require a number of voltage and current measurements. Unfortunately, the sensors used to measure such quantities are expensive due to the need of isolation. Therefore, a reduction of the number of the sensors, and as a result the cost of the drive, is desired in many PMAC motor drive applications. Several current reconstruction techniques to reduce the number of the sensors will be reviewed in Section 3.5.

3.2 Position Sensorless Techniques for Trapezoidal PMAC Motors

As discussed previously, a trapezoidal PMAC motor has trapezoidal back-EMF waveforms with 120^{o} flat top. In order to produce maximum torque, phase currents of the motor should be 120^{0} rectangular waveforms and in phase with the corresponding back-EMF waveforms. The excitation currents are delivered to the motor phases via a three-phase inverter that commutates the currents at every 60^{0} electrical. This means that the rotor position information must be known at the same interval to generate the correct switching sequence to maintain the synchronisation of the excitation currents. Several methods have been reported in literatures to indirectly determine the rotor position in trapezoidal PMAC motor drives.

3.2.1 Using Back-EMF

Since the back-EMF of a PMAC motor is a function of the rotor position, the most common approach to estimate rotor position is to extract the rotor position information from its back-EMF waveform. As stated previously, in a trapezoidal PMAC motor, each phase conducts 120^0, which means that only two of three phases are excited at any instant of time, and ideally there is no current on the third phase. Therefore, no current instant of a phase can be used to observe the back-EMF voltage of that phase, which ideally contains the zero crossing levels of the back-EMF voltage. Therefore, using the terminal voltages of the motor and switching sequence of the inverter, the back-EMF in an unexcited phase can be easily detected [14].

Several specific algorithms have been developed that use the back-EMF waveform measurement of the unexcited phase to determine the electronic commutation instants for trapezoidal PMAC motors. One of these algorithms is based on detecting the instant when the back-EMF voltage in the unexcited phase crosses zero [15,16]. In this algorithm, three terminal voltages V_a, V_b, V_c, and the neutral voltage V_n of the motor with respect to the negative DC link voltage are measured. At the instants of the zero crossing of the back-EMF waveform, the terminal voltage is equal to the neutral voltage. For example, when the back-EMF of phase A crosses zero, then $V_a = V_n = V_{dc}/2$. In order to use this zero crossing point to derive the switching sequence, the phase of this point has to be shifted by 30^0. The simplest method to implement the phase shift can be achieved by using the zero crossing signal to trigger a timer, which may be as simple as an R-C time constant, so that the next sequential inverter commutation occurs at the end of this timing interval.

The price for this simplicity tends to be vulnerable to noise in detecting the zero crossing and also shows a degraded performance over wide speed ranges due to the phase shifting variations with different speeds. An alternative approach for phase shift is to use phase-locked loop (PLL) techniques to lock the back-EMF waveform of the unexcited phase during each 60^0 interval, so that the proper instant for next inverter commutation can be derived from the phase-locked loop circuit [17]. The phase-locked loop system can be simple but sensitive to switching noise at the output of the inverter and may also not operate over a wide speed range.

A significant improvement of this method, comparing with the basic zero-crossing algorithm introduced above, has been proposed in reference [18]. Instead of using the zero

crossing point of the back-EMF waveform to trigger a phase shifter directly, this method uses a back-EMF integration approach in virtue of less switching noise sensitivity and automatic adjustment of the inverter switching instants with the variation of the rotor speed. In this method, a signal selector circuit selects the phase-to-neutral motor voltage of the unexcited phase, which is equal to the desired back-EMF for position sensing. The absolute value of the selected back-EMF is integrated starting from the zero crossing point. The output of the integrator will be proportional to the amplitude of the back-EMF because the instantaneous back-EMF voltage is varying approximately linearly with time in the vicinity of the zero crossing point. When the output value reaches a pre-set threshold value, the next commutation device of the inverter can be initiated. Since the amplitude of the back-EMF is proportional to the rotor speed, the conduction intervals automatically scale inversely with the speed with a fixed threshold value. The choice of the threshold value and the integrator constant for a given motor determine the specific alignment of the excitation phase current waveform with the back-EMF voltage.

However, one of the special control issues for any such scheme, which uses back-EMF sensing, is starting from standstill at which point the back-EMF voltage is zero. A typical approach for handling this condition is to initially override the position signal by sequentially stepping the commutation at a fixed rate in the desired direction of the rotation. This open loop excitation sequence provides initial acceleration to the rotor and generates a back-EMF signal with sufficient amplitude for the back-EMF sensing scheme to smoothly take over control of the interval switch commutation sequencing.

3.2.2 Using Stator Third Harmonic Voltages

A trapezoidal PMAC motor also has approximately trapezoidal stator voltage waveforms, which include significant third harmonic voltage components that can be used for position sensing [19,20]. It is well know that, the third harmonic components of a symmetrical three-phase star connected motor can be extracted from the stator phase voltages while the fundamental as well as other polyphase components are eliminated via a simple summation of the three phase voltages. In the method proposed in [19], the third harmonic voltage is directly measured between the actual neutral point and an artificial neutral point created by three high value external resistors, which are connected to the motor terminals. The measured third harmonic signal keeps a constant phase relationship with the back-EMF waveforms for any motor speed and load condition. If the third harmonic signal is integrated, the zero

crossing point of the integrator output will be exactly at every desired current commutation instant, so that the zero crossing signal can be used to determine the switching sequence of the inverter.

In contrast with the back-EMF sensing scheme, the key advantages of this technique are simplicity of the implementation and low susceptibility to the switching noise. The high frequency zero sequence components including the result of the summation of the three-phase voltages can be easily eliminated by a low pass filter. This filtering action will not introduce a significant phase delay in the third harmonic signal, so that this method can achieve a better performance for a wide speed range. In addition, since the third harmonic signal has a frequency three times higher than the fundamental back-EMF, the signal detection at low speeds is possible. This allows the method to operate in a wider speed range than the techniques based on the direct back-EMF sensing. However, because of the relatively low value of the third harmonic voltage at low speed, the major disadvantage of the method is the difficulty in detecting the correct relative phase relationship between the third harmonic signal and the corresponding phase at low speed. If the sequence is lost, the system has to be restarted.

3.2.3 Using Conducting States of Freewheeling Diodes

A special method to obtain the switching sequence has been presented in reference [21]. This method is based on the conducting states of freewheeling diodes in an inverter bridge. For a trapezoidal PMAC motor fed from a three-phase voltage source inverter, only two of three phases should be excited at any instant of time, and the excitation current flows through two legs of the inverter. During this conduction period, two of the power switches on the third leg of the inverter are in off state. However, the freewheeling diodes connected across these Power switches may conduct current resulting from the back-EMF produced in the motor winding of this phase. In the proposed method, a special alternative chopping control approach is used to make sure that only one of the two power switches in the on state of the two conducting phase legs is turned on and off at a chopper frequency. When the chopped power switch is turned off, the excitation current will circulate within the inverter bridge, not flowing via the DC link voltage source. In this case, one of the freewheeling diodes on the unexcited phase leg may conduct a current if the direction of the back-EMF of this phase is the same as the diode. Therefore, the zero crossing point of the back-EMF voltages can be detected by checking whether the corresponding freewheeling diode is conducting or not. In

this sensing method, similar to the back-EMF sensing method, the detected signal leads the next commutation by 30^0. Therefore, a phase shifter must be used to shift the signal to initiate the next commutation of the inverter.

This method is considered to be an indirect detection of the back-EMF voltage through the freewheeling diodes, and makes it possible to detect the rotor position over a wider speed range compared with the conventional method of direct back-EMF voltage sensing. However, the inverter needs to be operated in a special alternative chopping control approach in order for the algorithm to work properly. Moreover, the starting problem also exists in this method.

3.3 Position Sensorless Techniques for Sinusoidal PMAC Motors

Due to the sinusoidal back-EMF waveforms, a sinusoidal PMAC motor requires sinusoidal excited currents to produce a constant torque. In order to synchronize the sinusoidal excitation currents with the rotor position, a continuous rotor position feedback signal (compared with the rotor position information for every 60^0 in trapezoidal PMAC motors) is required to control the inverter. Due to the sinusoidal excitation currents, all three-phases of the sinusoidal PMAC motor conduct currents at any instant of time, and therefore no unexcited phase winding exists. This makes it impossible to measure the back-EMF voltage directly using the terminal voltages. As a result, estimation and observer techniques used in such motors are more complex, which usually requires multiple phase voltage and current measurements. A number of algorithms have been proposed for the rotor position estimation in sinusoidal PMAC motors, and several of these can be extended to trapezoidal PMAC motor drives. These techniques will be discussed below.

3.3.1 Position Information Based on the Flux Linkage Calculation

Several sensorless position detection methods have been developed, which measure the phase currents and voltages and estimate the flux linkages of the PMAC motor. The basic principle of these methods is based on the field orientation in the stationary reference frame. As mentioned in Section 2.3.2, three-phase sinusoidal currents, voltages and flux linkages of a sinusoidal PMAC motor can form three rotating phasors. These phasors rotate synchronously in a stationary reference frame and therefore the phase of the stator flux linkage phasor reflects the rotor position information of the motor. Fortunately, the stator flux

linkages can easily be calculated by an integrator using the measured stator voltages and currents.

When the stator flux linkage phasor has been determined, the instantaneous phase angle of the rotating phasor can be directly derived by an arc tangent function. If the stator power factor has to be unity, the phase angle can be used as the rotor position information to produce required excitation current command signals [22]. The motor drive system controlled by this position information can achieve near unity power factor over a wide range of torque and speed. However, unity power factor is not always required by most applications of sinusoidal PMAC motor drives. In addition, the integration drift in the calculation of stator flux linkages significantly changes the accuracy of the position calculation even though an offset compensation is applied. To eliminate this, an improved method has been proposed in reference [23]. The proposed method uses the voltages and currents to directly calculate the phase angle of the stator flux linkage instead of conventional flux linkage calculation based on an integration method. Moreover, a load angle, which is estimated based on the steady-state relationship between the torque and the flux linkage, is introduced to compensate the difference between the rotor position and the stator flux linkage angle. However, two major problems still exist in this approach. One is that it is very sensitive to the noise from the measured voltages and currents, which are directly used to calculate the phase of the stator flux linkage. The voltages and currents may include high frequency harmonic components due to the PWM control, and the use of a low pass filter will cause phase delay. Another is the difficulty of the trigonometric function calculation for the phase of the stator flux linkage using two flux linkage components, which are sinusoidal functions.

An extension to the above mentioned technique has been given in references [24,25]. The new algorithm still uses measured stator voltages and currents to calculate the flux linkages of the PMAC motor, but it has two current-loop structures. At each time step, the previously estimated flux linkages and a prediction of rotor position are used to generate an estimate of stator currents in two stages. These estimated values are compared with the measured stator currents and form the two current-loop structures to correct the predicted rotor position and the estimated flux linkage respectively. In this way, an accurate rotor position can be estimated over a wide speed range, even at very low speed. Since the calculations are based on the ABC reference frame model of the PMAC motor, another advantage of this algorithm is that it can be applied to both trapezoidal and sinusoidal PMAC motors [26]. However, the performance of the algorithms depends on the quality and accuracy of the estimated flux

linkages and measured values of voltage and current. Parameter variations due to temperature and saturation also affect the accuracy of the estimated rotor position.

3.3.2 Position Information Based on a Hypothetical Rotor Position

Another rotor position estimation technique is based on the vector control principle of AC motors in the synchronously rotating reference frame [27-30]. In this estimate strategy, the difference between the detected actual variables and the estimated state variables is used to determine the rotor position information. Firstly, a hypothetical synchronous rotating reference frame is set up, which doesnÆ necessarily coincide with the actual rotor po sition. Then, the detected three-phase voltages and currents are transformed to this hypothetical coordinate system. Under the ideal condition, in which the hypothetical rotor position is equal to the actual position, the ideal applied voltage can be calculated by using the instantaneous voltage equation of the motor and the measured current. The error between the actual and the ideal voltages is approximately proportional to the angular difference between the hypothetical and the actual rotor positions. Therefore, self-synchronisation is possible by reducing the angular difference to zero, by changing the speed of the motor, and the hypothetical rotor position will be an estimation of the actual rotor position.

There are two approaches in this method. First approach is based on the voltage model of the PMAC motor, as mentioned above, and the second method is based on the current model. The strategies used in the current model are similar to those of the voltage model; the estimation of the rotor position is performed by using a current error (instead of voltage error) that is the error between the actual current and the calculated current using the motor model. A comparative study of the two self-synchronization approaches is presented in [29], and some of the important implementation problems are described in [30]. Since the accuracy of the detected voltages and currents and the steadiness of the motor parameters are vital to this algorithm, it has the same drawbacks as the method based on calculating the flux linkages. In addition, this algorithm cannot operate normally at very low speed.

3.3.3 Sensorless Operation Based on a Kalman Filter

Kalman filter is an optimum state estimator, which provides an optimum estimation from noisy sensed signals and processes that are disturbed by some random noise. This assumes that measurement noise and disturbance noise is uncorrelated. Kalman filter is a viable and

efficient approach for on-line estimation of the speed and the rotor position of the PMAC motor. This is because the mathematical model describing dynamic performance of the PMAC motor is sufficiently well known. If measured three-phase voltages and the currents are transformed to a stationary frame, the voltage equations in this stationary frame, as well as the motion equation of the PMAC motor can consist of the state equations in this approach. When some state variables of the state equation (stator voltages and currents) are detected from the motor drive, the missing state variables (rotor position and velocity) can be estimated using a Kalman filter [31-33].

The Kalman filter consists of a two-step process, prediction and filtering. The prediction part of the algorithm calculates the next estimation values for the variables and the state covariance matrix before the new measurement is made. In doing so, the predictor uses the state variable equations, state transition matrix, disturbance covariance and measurement covariance matrixes. The function of the filter is to correct the estimation process in a recursive manner. The filter constantly works on the output and corrects its quality in a recursive manner based on the measured values. Based on the deviation from the estimated value, the filter provides an optimum output value at the next output instant.

However, the critical step in the Kalman filter design is to select the coefficient values to yield the best position estimation performance. Moreover, the Kalman filter approach is computationally intensive, all of the step involved require a vector or a matrix operation, and depends on the accuracy of the parameter of the model and the motor.

3.3.4 Sensorless Operation Based on State Observers

Numerous research papers have been published, which estimate the rotor position of the sinusoidal PMAC motor using state observers. These techniques are based on the space control theory. The mathematical model of the PMAC motor is used as a state space model, or state estimator, which has the same input signals as the actual motor. The outputs of the actual motor and the estimator are compared and the error is fed back to the estimator, so that the behaviour of the estimator can be corrected. The internal state, such as rotor position, of the estimator can be monitored directly, so that it can be used to estimate the actual rotor position.

One of these methods constructed a state observer based on the motor model, including electrical and mechanical equations, in the synchronous rotating coordinate [34]. In this

observer, the output is defined as a combination of the state variables, and this output is compared with the equivalent measured output of the actual motor. Any error between the two output values is used to correct the state trajectory of the observer. The stability of this observer is an important consideration in providing accurate estimation of the rotor position information for the motor drive system. Loss of observer stability would result in erratic and possible destructive motor operation. In order to stabilise the system, the gain of the observer has to be optimised. However, because of non-linearity of its electrical equation, it is difficult to determine the optimum gains of the observer under different operation conditions.

To improve this issue, a reduced order state observer has been proposed in [35]. In this reduced order state observer, the non-linear terms are eliminated by introduction of a group of control inputs, so that a linear control strategy can be used to estimate state variables of the observer. The use of reduced order observer also simplifies the system and reduces the computational burden in implementation.

Instead of a direct estimation of the rotor position, another reduced order observer has been used to estimate the back-EMF voltages of the motor in the references [36,37]. Since the mechanical time constant is usually much larger than the electrical time constant of the motor, this method is the reduced order observer by assuming the motor speed approximately constant during a short time interval in the calculation of the electrical state variables. According to the relationship between the rotor position and the back-EMF voltages, the rotor position can be easily derived using the estimated back-EMF voltages.

Another indirect approach to estimate the rotor position, which is based on disturbance observer, is proposed in [38]. The non-linear term in the voltage equation of a PMAC motor is the back-EMF voltage, which includes information of the rotor position. This non-linear term is considered as a disturbance and can be estimated using a disturbance observer. A common conclusion from these reviews is that, whatever type of state observer is used, the key problem remains same, how to obtain the initial information of the state, which is required for proper convergence of the observer.

3.3.5 Position Information Based on Inductance Variations

As mentioned in Section 2.2, sinusoidal PMAC motors have various geometrical designs. Interior permanent magnet (IPM) motors and surface permanent magnet (SPM) motors are the two main kinds of sinusoidal PMAC motors. The inductance in the direct and quadrature

axis of an SPM motor is approximately equal and constant, while an IPM motor has different inductances in both axis due to the saliency. In most designs, the motor inductance along the q-axis is greater than the inductance along the d-axis because of the low permeability of the magnet material. The different inductance between the d-axis and q-axis means that the variation of the inductance is a function of the rotor position.

Based on the inductance variation with the rotor position, two approaches of rotor position estimation have been proposed, which are based on detecting the variation of the inductance with position. One method is the direct use of the fundamental voltage and current signals under conventional PWM modulation to calculate the motor inductances, which include rotor position information [39-43]. An IPM motor fed by a voltage-source pulse width modulation (PWM) inverter will generate current ripples. The measurements of the amplitude and the rise time of the current, as well as the causing voltage vector can be used to determine the inductances within each cycle of the PWM, and then the rotor position information can be derived from the inductances using their relationship with the rotor position. This approach can also be used in the SPM motor without rotor saliency as proposed in [44]. In this reference, the measurements of the current ripple are not used to calculate the inductances but the back-EMF voltages. Then, the rotor position information is derived from the estimated back-EMF voltages. Since this algorithm does not use integration operation, it works well at very low speeds. However, the implementation of this approach based on current ripple measurements is quite difficult in practice. This is because the time intervals of the current ripples sometimes are very short, so that it is very hard to measure the current ripples accurately, and the measurement noise will significantly influence the accuracy of the rotor position estimation.

Another method based on detecting the variation of the inductance of the IPM motor is to inject a high frequency sinusoidal signal into the stator windings of the motor. The rotor position information in this method is extracted from the responses of the high frequency excitation [45-50]. Usually, the high frequency signals can be used to modify the PWM modulation and can be injected into the motor under normal excitation together via the inverter. The corresponding responses, which contain frequency components depends on the rotor position, can be extracted from the current measurements using a high pass filter. In this method, the rotor position estimator based on a phase-locked loop technique contains the saliency models and the model of the mechanical subsystem.

A key advantage of the methods based on the inductance variation is that the estimation accuracy does not rely on the rotor speed, specifically at zero speed operation. Moreover, the methods are less sensitive or completely insensitive to the parameter variations of the motor. However, since the method requires prior calculation of the inductance, the rotor position information depends on the accuracy of the calculation, and the inductance calculation may lead to the position errors due to sub transient effect [49].

3.4 Starting Strategies

Unlike the position sensorless induction motor drives, the starting procedure of position sensorless PMAC motor drives is more difficult. Since the rotor has a PM and due to the absence of the rotor position at start, the application of the magnet field at an arbitrary position may be accompanied with a temporary reverse rotation or may lead to a starting failure. Most of the position sensorless techniques proposed for PMAC motor drives are not self-starting techniques. In order to detect the back-EMF voltage or to calculate the position from the measurements of the stator currents and the voltages, the motor must be first started and brought up to a certain speed where the terminal quantities are detectable.

Most of the starting strategies presented for trapezoidal PMAC motor drives are based on open-loop control or arbitrarily exciting the two or three stator windings and expecting the rotor to align to a certain definite position. In [16], the motor phases are excited by specific currents at an increasing frequency in an open loop mode. Then, when the back-EMF voltage of the motor is sufficiently high to allow the determination of the rotor position using the terminal voltages, the motor drive is switched to the self-synchronous mode. Another arbitrary starting procedure is described in [21]. In this strategy, two arbitrary phases of the motor are excited with limited current for a preset interval. This causes the rotor of the motor to rotate in the direction corresponding to the excited phases. When the rotor aligns to a certain position due to this excitation, the next commutation signal that advances the switching pattern by 120^0 is generated and the motor drive switches immediately from open loop commutation to self-commutation.

The similar starting strategies can also be used in the sensorless sinusoidal PMAC motor drives. In [22], an open loop control approach is used to accelerate the motor from standstill to the speed at which the flux linkage angle can reliably be determined. In [28], the motor is started by applying a specific PWM pattern (say device T1, T2, and T6 are turn on and off) to

the inverter for about 200 μs. This pattern is repeated several times to align the rotor in the direction of the A-phase winding, and then the specific sensorless control strategy is applied.

The above starting strategies have poor dynamic response and the rotor can be in the hunting mode due to the absence of position information at standstill and arbitrary increase speed. In addition, the switch from starting stage to normal position sensorless operation may not be smooth, which is required in some applications.

Due to the saturation effect of the core in the magnetic circuit, the phase inductances vary slightly with the rotor position in a PMAC motor. This principle is indirectly used to start a trapezoidal PMAC motor [51]. Instead of measuring the inductance, the sign and the amplitude of the current waveform is determined when two phases are excited. After a given time T, the current is reversed, and the sign and the amplitude are determined again. If the current difference sign is positive, the PM flux has the same sign as the flux created by the positive current. If the current difference sign is negative, the PM flux has the same sign as the flux created by the negative current. The process is repeated for other phases, and the information obtained is used to determine the rotor position. This algorithm is used repeatedly until sufficient back-EMF is developed to use it for obtaining the correct switching patterns. Similar method is also used to start the sinusoidal PMAC motors as described in [26, 52]. However, this method is difficult to estimate the rotor position accurately due to the problem in detecting the current amplitude accurately. In addition, the exciting current pulses may generate rotating torque, which may change the initial rotor position.

For the salient PMAC motors, the saliency of the rotor can be used to determine the rotor position at standstill. Several different uses of the saliency have been proposed. One of the methods proposed in [53] is based on the current locus. Due to the rotor saliency, an IPM motor has different d-axis and q-axis inductances. The difference of the inductances makes the locus of the stator current vector as an oval when the stator voltage is balanced with the three-phase sinusoidal waveforms. The major diameter direction of the current vector ellipse gives the information of the rotor position. In [54], a second method utilizing the rotor saliency is proposed. In this method, when the IPM motor is excited by a current controller, the phase difference between the magnetizing current and the voltage reference makes it possible to estimate the rotor position without using the motor parameters, which uses the ratio of the d-axis and q-axis inductances only.

In the starting, the methods based on the injection of high frequency test signals proposed in [45-50] claim to offer accurate rotor position information even at standstill, which can also be used to derive the initial rotor position and requires no additional starting strategy. Although these methods can achieve high dynamic performance in closed loop position control, no practical test results have been reported to verify this claim.

3.5 Current Reconstruction Techniques

In many servo applications, the PMAC motor drive often needs to operate together with a fast acting closed-loop current controller, which requires the knowledge of the three-phase winding currents of the motor. In addition, the current measurements are always required in most of the position sensorless techniques to estimate the rotor position information in PMAC motor drives.

As indicated in the previous chapters, the most effective method to measure the winding currents is to use low value resistors or Hall-Effect current sensors in series with the windings. The later is usually preferred since they provide electrical isolation at relatively high frequency bandwidth. However, a three-phase motor drive requires three Hall-Effect current sensors that are expensive specifically at high frequency switching applications. Although the number of current sensors in the star-connected three-phase motor drives can be reduced from three to two, this method may introduce errors in the calculation of the third phase current because of the discrepancies in the gain constants and the DC offsets of the two current sensors. As can be predicted, using less number of sensors, such as a single sensor on DC link, can reduce the error introduced by the gain constant of a sensor.

A number of studies were reported in the literatures, which reconstructs the phase currents of an AC motor using the DC link current measurement. As reported in [55-58], the reconstruction of phase currents of the trapezoidal PMAC motor with rectangular current excitation is relatively easy, since only two of the three phase windings conduct currents at a given time. In such motor drives, since two-phase windings conduct currents at a given time, the values of the two-phase currents exactly equal to the DC link current. However, the direction of the currents may be the same or reverse, depending upon the switching states of the inverter. With the help of switching states of the inverter, the three-phase currents can be reconstructed from the DC link current measurement as described in [55]. However, during the current commutation period (the current transfer period from one phase to the other),

current flows in all three phases of the motor, hence three-phase currents cannot be reconstructed. In [56], a simple single current sensor technique for the trapezoidal PMAC motor is proposed. The major feature of this method is that the switching information of the inverter is not needed in the current sampling processing.

An estimation method of three-phase currents using the DC link current measurement is proposed in [57] and [58] for the trapezoidal PMAC motors. This method involves the application of a state observer, which uses the error between the actual and estimated DC link current of the drive and updates its phase current estimates. The major advantage of this method is that the measurements are made equally on all three phases of the motor, so that the effects of sensor imbalance are eliminated. However, when all three-phase windings conduct currents during the current commutation period, the phase current estimation is not possible since the state observer is observable if the current flows only through two-phase windings.

In the PMAC motors with sinusoidal current excitation, however, all three-phase windings carry currents at any instant. Although the current reconstruction is still possible in these motor drives [59-65], it is not as easy as in the trapezoidal PMAC motors with the rectangular current excitation.

A three-phase inverter consists of six switches and their associated freewheeling diodes. If all of the three phases conduct current simultaneously, the inverter only has eight possible switching states, which can be represented with two zero-states and six active-states. During the six active states, one of the phase currents flows through the DC link. At two zero-states, however, the phase currents circulate inside the inverter bridge, not passing through the DC link. Under the normal PWM modulation mode, there are two possible active-states in each PWM cycle. Thus, the two-phase currents can be derived from the DC link current at the two consecutive points. If the PWM frequency is high enough, the phase currents vary slightly over one PWM cycle. Hence, the derived two-phase currents can represent current values of the two phases within this PWM cycle, and the third phase current can easily be calculated using the two derived currents if the motor is star connected [59]. However, under certain operating conditions of the PWM control, either two active-states of the inverter may last very short period of time. As a result, due to the finite switching time of the power devices, the dead bands, and the delays in the electronic circuits, actual phase current may not be visible on the DC link measurement.

Different approaches have been proposed to solve this problem. In [60], a sample-and hold technique is used to sample a phase current through DC link current in the period of the phase current passing through the DC link and hold the value until the same active-state take place again. The second phase current can be sampled using the similar method, and the third phase current can be calculated from these two currents. This method is used in a simple control scheme for an induction motor in [61]. Although the test results in [61] are satisfactory, the problems related to the very low modulation index and the delay of current sampling are not discussed in this reference. When the period of the active-state is too short, a solution by replacing all active-states less than 30 μs with a zero-state has been proposed in [62] and [63], in which the missing time is added to the next PWM cycle. This makes the DC link current composed of wider pulses, and therefore it is more suitable for phase current reconstruction. However, this approach delays the current feedback signals and makes the current control more difficult, specifically at low speed operation.

In [64], it is proposed to sample the DC link current in the center of each active state that gives a better current sampling. Under the narrow-pulse conditions, this paper proposes two adjustment schemes for the duty-cycles in a single-ended modulation strategy. One of the adjustment schemes is based on reducing the zero-state time if one of the active states is too short. The second method uses no zero-states when the active states are too short but uses two complementary voltage vectors closest to those already used. This approach introduces more switchings but information about all three-phase currents exists in one PWM cycle. Two other methods are also proposed in [65-67] that can work in the whole operation area of the inverter. When duty-cycles of two phases are almost equal, one method is to adjust the duty-cycle within one PWM cycle by shifting the switching signals one forward and one backward. Thus, clear and visible two active states can be obtained, but the average voltages applied to the two phases remain same during this PWM cycle. The second method is to adjust the duty-cycle in two PWM cycles by adding the duty-cycle of one phase in first PWM cycle and reducing it in the next, which ensures the average voltage applied to the phase remaining same. Both of the methods are capable to operate at low speed and can easily be implemented in practice using a computer-based controller. In [68] and [69], the problem of all possible fault protections based on one DC link current sensor is also discussed. A comparative study of the different approaches to reconstruct the three-phase currents is presented in [70].

An alternative approach to reconstruct the three-phase currents from DC link measurement is proposed in [71, 72] for the PM synchronous motors. This approach is based on a state observer. The method proposed in these references can provide reliable phase current feedback to the controller under all operation conditions of the motor drive. However, the impacts of the parameter variations of the motor are not discussed in these papers.

The above proposed methods of three-phase current reconstruction from DC link current measurement have been used in low-cost AC motor drives and demonstrated good experimental results. However, in general, there still are some limitations in these methods. For example, since the DC link current waveforms are narrow pulses, it is not very easy to sample the current values accurately at determined point. The measurement noise always influences the reconstructed currents. In addition, these methods can only obtain the average values of the phase currents within one or several PWM cycles. Therefore, the current variation within a PWM cycle cannot be obtained, which is required in the fast acting closed loop current controllers.

3.6 Conclusion

It can be seen from above discussion that the research of position sensorless techniques is one of the most active and widespread area of the control of the PMAC motor drives in the recent years. A comprehensive review of the existing position sensorless techniques are discussed in the chapter. Since only two of the three stator windings are excited at any instant of time and since the voltage induced in the unexcited winding can be used to determine the rotor position, the position sensorless strategy is much simpler to implement in the trapezoidal PMAC motors. In the sinusoidal PMAC motors, however, the position detection is more complex, mainly due to current conduction in all three windings of the motor.

The most commonly used position detection scheme for the trapezoidal PMAC motors is based on the back-EMF sensing. In this scheme, since there is no sufficient back-EMF signal at low speeds, it is not suitable at low-speed operation. In addition, this method requires a special strategy to start the motor from standstill.

The position detection schemes used in the sinusoidal PMAC motors are mainly based on the position estimations utilizing the phase voltages and the currents of the motor. By using these quantities, the rotor position can be determined by a state observer, Kalman filtering technique, or by direct calculations. However since these techniques are computationally

intensive, significant rotor position detection error occurs mainly resulting from quantisation, truncation errors, and measurement inaccuracies. The variation of the motor parameters due to the temperature and the saturation also affects the accuracy of the position estimation in these methods. Moreover, these techniques may also suffer from low speed operation, mainly due to the integration drift in the algorithms.

For the PMAC motors with rotor saliency, the position information can be extracted from the variation of the inductances. The most popular method is to inject a high frequency test signal and extract the rotor position by analysing its response. Since the high frequency injection exists independent from the motor speed, these techniques can operate at low speed including at standstill. However, they are not suitable for the surface permanent magnet (SPM) motors that have no rotor saliency.

Finally, the elimination or the minimization of the discrete current sensors in the PMAC motor drives is also addressed in the chapter. As discussed, the researches in the area indicate that the three-phase currents of the PMAC motor can be reconstructed from the DC link current measurement using a single current sensor. However, the key issue of further research is how to minimize the degradation of the current regulator performance that appears in the form of increased waveform distortion, even though the system's dynamic response is still very fast.

The review results summarized in this chapter demonstrate that there is a need to improve sensorless technique, which can accommodate a minimum number of sensors. This will be discussed in detail in the successive chapter.

Chapter 4

Mathematical Model and Simulation of PMAC Motor Drives

4.1 Introduction

As mentioned in Chapter 2, under the ideal conditions, it is possible to predict the steady-state performances of a PMAC motor under various operating modes using analytical methods. However, when the motor is fed from a power electronic converter, which naturally generates some non-ideal waveforms, the analysis of dynamic behavior of the motor using analytical methods is impossible. Therefore, computer simulation provides a very useful medium to analyze the behavior of the motor drive under steady state as well as dynamic conditions without the implementation of hardware. If the simulation model of the drive is done accurately, it is possible to predict the performances of the motor drive under practical operating conditions, including start up, and step load changes. In addition to this, once the accurate simulation model of the drive is achieved, the simulations can easily be forced to operate under an extreme operating condition without the fear of damaging the motor drive. Although a number of modeling and simulation approaches have been developed previously [73-78], they all have varying degrees of complexity and accuracy.

The main objective of this chapter is to develop a general simulation algorithm for both trapezoidal and sinusoidal PMAC motor drives, which include the components of PMAC motor, inverter and the controller. The primary aim of the simulation algorithm is to simulate the components of the drive during transient conditions for all modes of motor operation, and predict the dynamic as well as the steady-state performances of the motor drive. Moreover, it is aimed to calculate the currents and voltages of the motor accurately to utilize them in the novel rotor position estimation and phase current reconstruction schemes of the PMAC motor drive, which will be described in the consecutive chapters. Therefore, the performances of the rotor position estimation and the phase current reconstruction algorithms under various operating conditions can be analyzed and tested, and possible problems can be identified and corrected before they are actually used in a practical real time motor drive system.

All the simulation studies in this thesis are done using LabVIEW. LabVIEW (Laboratory Virtual Instrument Engineering Workbench) is a graphical programming language, which is widely used for data acquisition and analysis as a computer based instrument. In comparison with the other software tools, simulation with LabVIEW provides easy debugging features and a user-friendly environment [79]. In addition, the simulation results can be easily compared with the real data acquired from the test motor drive implemented.

Since the validity of the simulation results mainly depends on the accuracy of the simulation model, establishment of an accurate motor drive model is the key step to consider. Section 4.2 gives the detailed descriptions of the mathematical models used in both trapezoidal and sinusoidal PMAC motor drives. The actual implementation method of the simulation with LabVIEW is detailed in Section 4.3. In Section 4.4, various simulation results are presented, which are then compared with the measured waveforms obtained from the practical motor drive system.

4.2 Mathematical Model of PMAC Motor Drives

A three-phase PMAC motor has symmetrical three-phase stator windings almost identical to the windings of a three-phase induction motor, while its rotor has magnets mounted on the surface of or buried inside the rotor. As indicated in [80], a three-phase star-connected PMAC motor can be modelled by a star-connected three-phase lumped parameter network consisting of a winding resistance, an equivalent winding inductance, and a back-EMF source per phase, all connected in series. The following assumptions are made in the derivation of the motor model:

a) Because of the high electrical resistivity of the magnets and the stainless steel retaining sleeves, the induced eddy currents are neglected, and hysteresis losses are ignored.

b) Since no significant demagnetisation is experienced under normal operation conditions, the stator current effects on the magnet flux distributions are ignored.

c) Because of the large low-permeability air-gap between stator and rotor, the saturation may be neglected, although it can be taken into account by parameter changes.

d) There are no cage windings on the rotor, so self-starting is not possible.

4.2.1 Voltage Equations

Under the above assumptions, the voltage equation of a sinusoidal PMAC motor may be given in various reference frames and in different forms (synchronous rotation reference frame, two-axis stationary reference frame and three-phase stationary reference frame). However, a trapezoidal PMAC motor has non-linear flux distributions and back-EMF waveforms. Therefore, the space-vector transformation theory is not suitable for analysis of trapezoidal PMAC motors. In order to establish general mathematic expressions valid for both trapezoidal and sinusoidal PMAC motors, the three-phase stationary abc reference frame is used in this thesis. Therefore, the voltage equations of a three-phase PMAC motor can be expressed in the matrix form as:

$$\begin{bmatrix} v_a \\ v_b \\ v_c \end{bmatrix} = \begin{bmatrix} R_a & 0 & 0 \\ 0 & R_b & 0 \\ 0 & 0 & R_c \end{bmatrix} \begin{bmatrix} i_a \\ i_b \\ i_c \end{bmatrix} + \frac{d}{dt} \begin{bmatrix} \psi_a \\ \psi_b \\ \psi_c \end{bmatrix} \tag{4.1}$$

where v_a, v_b, and v_c are the phase voltages; i_a, i_b, and i_c are the phase currents; ψ_a, ψ_b, and ψ_c are the total flux linkages; and R_a, R_b, and R_c are the winding resistances of the phases a, b, and c respectively. If the three-phase windings are symmetric, it may be assumed that the three-phase winding resistances are equal, that is, $R_a = R_b = R_c = R$.

The total flux linkages given above include the flux linkages established by PM and the stator currents, and can be expressed in matrix form as follow:

$$\begin{bmatrix} \psi_a \\ \psi_b \\ \psi_c \end{bmatrix} = \begin{bmatrix} L_a & M_{ab} & M_{ac} \\ M_{ba} & L_b & M_{bc} \\ M_{ca} & M_{cb} & L_c \end{bmatrix} \begin{bmatrix} i_a \\ i_b \\ i_c \end{bmatrix} + \begin{bmatrix} \psi_{pma} \\ \psi_{pmb} \\ \psi_{pmc} \end{bmatrix} \tag{4.2}$$

where L_a , L_b and L_c are the self-inductances of the phases a, b, and c respectively; and M_{ab}, M_{ac}, M_{ba}, M_{bc}, M_{ca}, and M_{cb} are the mutual inductances between the two phase windings. When the three-phase windings are symmetrical, the mutual inductances are also symmetric, that is, $M_{ab}=M_{ba}$, $M_{bc}=M_{cb}$, and $M_{ca}=M_{ac}$.

ψ_{pma} , ψ_{pmb} , and ψ_{pmc} are the flux linkages established by permanent magnet as viewed from the stator windings and they are functions of the rotor position. When the rotor

rotates, the derivatives of the flux linkages with respect to time are the back-EMF voltages induced in the phase windings that are due to the permanent magnets on the rotor.

For a PMAC motor with surface mounted PMs, it can be assumed that the self-inductances and the mutual inductances are constant and independent of the rotor position, while the self-inductances and the mutual inductances of an interior PM motor are functions of the rotor position due to the saliency. In general, the self-inductances of each phase can be expressed as [81]:

$$\begin{aligned} L_a &= L_{sl} + L_{s0} + L_{s2}\cos(2\theta_e) \\ L_b &= L_{sl} + L_{s0} + L_{s2}\cos(2\theta_e + 2\pi/3) \\ L_c &= L_{sl} + L_{s0} + L_{s2}\cos(2\theta_e - 2\pi/3) \end{aligned} \tag{4.3}$$

And the mutual inductances between two phases can be given by:

$$\begin{aligned} M_{ab} &= M_{ba} = -\frac{1}{2}L_{s0} + L_{s2}\cos(2\theta_e - 2\pi/3) \\ M_{bc} &= M_{cb} = -\frac{1}{2}L_{s0} + L_{s2}\cos(2\theta_e) \\ M_{ca} &= M_{ac} = -\frac{1}{2}L_{s0} + L_{s2}\cos(2\theta_e + 2\pi/3) \end{aligned} \tag{4.4}$$

where L_{sl} represents the leakage inductance of a phase; L_{s0} is the component of the self-inductance due to the fundamental air-gap flux linkage; L_{s2} is the component of the self-inductance due to the rotor position dependent flux; and θ_e is the electrical rotor position angle.

Substituting Equation (4.2)-(4.4) into (4.1), a common voltage equation can be obtained, which is suitable for all types of PMAC motors. However, this thesis only focuses on the sensorless techniques of surface PM motors, which includes sinusoidal and trapezoidal PMAC motors. Therefore, non-salience has been considered, that is, $L_{s2} = 0$. Therefore, the self-inductances and the mutual inductances are assumed constant and independent of the rotor position. Hence, the self-inductances can be given by:

$$L_a = L_b = L_c = L_{sl} + L_{s0} = L_s \tag{4.5}$$

and the mutual inductances are written as:

$$M_{ab} = M_{ba} = M_{bc} = M_{cb} = M_{ac} = M_{ca} = -\frac{1}{2}L_{s0} = M_s \tag{4.6}$$

Therefore, based on these assumptions, the above given voltage equation can be simplified for the surface permanent magnet motors as:

$$\begin{bmatrix} v_a \\ v_b \\ v_c \end{bmatrix} = \begin{bmatrix} R_a & 0 & 0 \\ 0 & R_b & 0 \\ 0 & 0 & R_c \end{bmatrix} \begin{bmatrix} i_a \\ i_b \\ i_c \end{bmatrix} + \begin{bmatrix} L_s & M_s & M_s \\ M_s & L_s & M_s \\ M_s & M_s & L_s \end{bmatrix} \frac{d}{dt} \begin{bmatrix} i_a \\ i_b \\ i_c \end{bmatrix} + \begin{bmatrix} e_a \\ e_b \\ e_c \end{bmatrix} \tag{4.7}$$

where e_a, e_b, and e_c are the back-EMF voltages induced in each phase winding due to the magnet flux linkage.

As discussed in Chapter 2, the differences between the sinusoidal and the trapezoidal PMAC motors mainly depend on the shape of their back-EMF waveforms. If the stator windings are symmetrically displaced, the ideal back-EMF waveforms for a sinusoidal PMAC motor can be given as:

$$\begin{aligned} e_a &= E_m \sin(\theta_e) \\ e_b &= E_m \sin(\theta_e + 2\pi/3) \\ e_c &= E_m \sin(\theta_e - 2\pi/3) \end{aligned} \tag{4.8}$$

For a trapezoidal PMAC motor, the ideal back-EMF waveform of phase A can be given in piecewise linear form as:

$$e_a = \begin{cases} \dfrac{E_m}{\pi/6}\theta_e & 0 < \theta_e \le \dfrac{\pi}{6} \\ E_m & \dfrac{\pi}{6} < \theta_e \le \dfrac{5\pi}{6} \\ -\dfrac{E_m}{\pi/6}(\theta_e - \pi) & \dfrac{5\pi}{6} < \theta_e \le \dfrac{7\pi}{6} \\ -E_m & \dfrac{7\pi}{6} < \theta_e \le \dfrac{11\pi}{6} \\ \dfrac{E_m}{\pi/6}(\theta_e - 2\pi) & \dfrac{11\pi}{6} < \theta_e \le 2\pi \end{cases} \tag{4.9}$$

Note that Equation (4.9) only gives the back-EMF voltage of phase A. Therefore the definition can be repeated for the remaining two phases simply by introducing 120° electrical

phase difference between the phases. In addition, the practical back-EMF waveforms always deviate from these ideal assumptions mainly due to the fringing field and manufacturing inaccuracies. If more accurate model of the practical motor is desired, the back-EMF waveforms can be modelled by using a look-up table or multiple harmonic components of the real waveform [5].

In Equations (4.8) and (4.9), E_m is the amplitude of the back-EMF that is proportional to the angular speed ω_r of the motor and can be given by:

$$E_m = k_e \omega_r \tag{4.10}$$

where K_e is the back-EMF constant; and the electrical rotor position angle θ_e is given by:

$$\theta_e = N_p \theta_r = N_p \int \omega_r dt \tag{4.11}$$

where θ_r is the mechanical rotor position angle and N_p is the number of pole pairs of the motor.

Also, since the sum of the three-phase currents is equal to zero ($i_a + i_b + i_c = 0$) in the star connected motor with isolated floating neutral; the following equation can be given:

$$M_s i_a + M_s i_b = -M_s i_c \tag{4.12}$$

Substituting Equation (4.12) into (4,7), the voltage equation of the surface permanent magnet motor can be simplified as:

$$\begin{bmatrix} v_a \\ v_b \\ v_c \end{bmatrix} = \begin{bmatrix} R_a & 0 & 0 \\ 0 & R_b & 0 \\ 0 & 0 & R_c \end{bmatrix} \begin{bmatrix} i_a \\ i_b \\ i_c \end{bmatrix} + \begin{bmatrix} L & 0 & 0 \\ 0 & L & 0 \\ 0 & 0 & L \end{bmatrix} \frac{d}{dt} \begin{bmatrix} i_a \\ i_b \\ i_c \end{bmatrix} + \begin{bmatrix} e_a \\ e_b \\ e_c \end{bmatrix} \tag{4.13}$$

where $L = L_s - M_s = L_{sl} + \frac{3}{2} L_{s0}$ and is called as the equivalent winding inductance, which is equal to the direct and the quadrature inductances of the surface permanent magnet motor.

As seen from Equation (4.13), the voltage equation has been decoupled by simply introducing the equivalent inductance term (L), which is equal to half of the open-circuit line-to-line inductance and it is easy to calculate or measure. This makes it easy to simulate the transient behaviour of the surface PM motor using a computer. The accuracy of the proposed

model predicting instantaneous voltage and current waveforms during various operation conditions has been demonstrated in the previous study in [5]. The predicted waveforms are also verified in this thesis using the measured waveforms in the practical PMAC motor drive.

4.2.2 Electromagnetic Torque Equations

An electrical machine is an energy conversion device, which can convert the energy from electrical to mechanical or vice versa. The electromagnetic torque of a motor can be directly derived from the relationship with its mechanical output power. In a symmetrical three-phase motor, the total input instantaneous power, p_e, is equal to the sum of the instantaneous powers produced by each of the three phases, that is,

$$p_e = v_a \cdot i_a + v_b \cdot i_b + v_c \cdot i_c \tag{4.14}$$

For simplicity, only the voltage equation of the surface PM motor is given here. Substituting Equation (4.13) into (4.14), the instantaneous power p_e of the surface PM motor can be expressed as:

$$p_e = R(i_a^2 + i_b^2 + i_c^2) + \frac{1}{2}\left(\frac{di_a^2}{dt} + \frac{di_b^2}{dt} + \frac{di_c^2}{dt}\right) + (e_a i_a + e_b i_b + e_c i_c) \tag{4.15}$$

As seen from the equation above, the input instantaneous power consists of three parts. The first term on the right hand side of the equation represents the power losses in the stator winding resistances. The second term is the change rate of the energy stored in the magnetic field. According to the energy conservation principle, the third term will be the power converted into mechanical power and is called mechanical output power.

From the viewpoint of a rotating mechanical system, the mechanical power is also equal to the product of the electromagnetic torque T_e and angular rotor speed ω_r, that is,

$$p_{mech} = e_a i_a + e_b i_b + e_c i_c = T_e \cdot \omega_r \tag{4.16}$$

Thus, the electromagnetic torque in the surface PM motor can be expressed as:

$$T_e = \frac{1}{\omega_r}(e_a i_a + e_b i_b + e_c i_c) \tag{4.17}$$

As seen in Equation (4.17), the electromagnetic torque is inversely proportional with the rotor angular speed and directly proportional with the sum of the products of the phase current and back-EMF voltage. This torque equation is not suitable to calculate electromagnetic torque for zero speed operation. Since the back-EMF voltages are also proportional with the rotor angular speed as described in (4.8) and (4.9), the electromagnetic torque may be conveniently expressed as:

$$T_e = k_e[e_1(\theta_e)\cdot i_a + e_2(\theta_e)\cdot i_b + e_3(\theta_e)\cdot i_c] \tag{4.18}$$

where $e_1(\theta_e)$, $e_2(\theta_e)$, and $e(\theta_e)$ are the unit back-EMF functions of the rotor position, and their relationships with the back-EMF voltages are given as,

$$\begin{aligned} e_a &= k_e\,\omega_r\,e_1(\theta_e) \\ e_b &= k_e\,\omega_r\,e_2(\theta_e) \\ e_c &= k_e\,\omega_r\,e_3(\theta_e) \end{aligned} \tag{4.19}$$

For a sinusoidal PMAC motor, the unit back-EMF functions are the sinusoidal function of the rotor position, while the unit back-EMF functions of a trapezoidal PMAC motor are the trapezoidal function of the rotor position.

Similar to the other drive systems, the mechanical equation of the PMAC motor drive system can be given as:

$$T_e - T_l = J\frac{d\omega_r}{dt} \tag{4.20}$$

where T_l is the load torque; J is the inertia of the motor and connected load. In this equation, the damping coefficient B, is assumed zero.

This relationship is often called the motion equation of a motor and is used to describe the dynamic behaviour of the drive system.

4.2.3 Inverter and Phase Voltages

Generally, a three-phase PMAC motor is fed from a three-phase voltage source inverter as described in Chapter 2. Due to the switched step voltages, the currents and voltages generated by such inverter often are non-sinusoidal waveforms. Therefore, in order to produce an

accurate transient simulation result, the inverter should be modeled together with the PMAC motor.

The equivalent circuit of a common three-phase inverter with a motor load given in Figure 4.1 is used in the computer simulation study in this research. The derivation of the circuit will be discussed in detail later in Chapter 6. As shown in the figure, the inverter consists of six power switches, which are controlled to generate the desired AC voltages or currents for the motor load. i_a, i_b and i_c are the instantaneous three-phase currents of the motor and their directions are indicated with the arrow signs. The DC link voltage V_{dc} is assumed constant, and the mid-point of the DC link voltage is defined as the reference point for the voltages. Therefore, the voltages of the positive and the negative supply rails are $+V_{dc}/2$ and $-V_{dc}/2$ respectively.

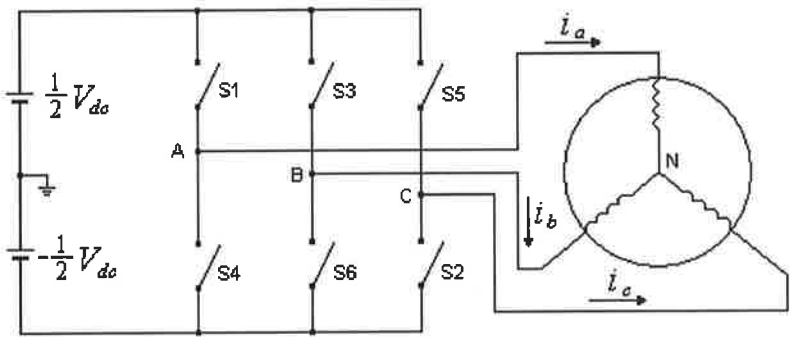

Figure 4.1 Equivalent circuit of a three-phase inverter with motor load

In this inverter configuration, when one of the switches in one phase is turned on, the terminal voltage of this phase will be either $+V_{dc}/2$ or $-V_{dc}/2$. For example, if switch S_1 is on, terminal point A will be connected to the positive supply rail, so the terminal voltage of the phase A is equal to $+V_{dc}/2$. Inversely, if switch S_4 is on, terminal voltage of the phase A is equal to $-V_{dc}/2$. When the two switches in one phase are all turned off, the terminal voltage of the phase A is independent of the DC link. Since the two switching on at the same time will causes short circuit in the inverter, this state is not permitted in a practical system. Therefore, two switches in one phase can compose three possible switch states, which can be expressed by a state variable S_p (p = a, b, c) having three different states. For example, when the upper leg switch of phase p is on, S_p=1, when the lower leg switch of phase p is on, S_p=-1, and when the two switches on the same leg are off, S_p=0.

In the practical simulation model, the values of the switch state variable S_p are determined by both the switching signals of power switches and direction of the winding current of the

motor. More detail explanations will be provided later in this thesis, in Section 6.2.2 and in Table 6.3.

With the help of the switch state variables, the terminal voltages of each phase can be easily expressed as:

$$\begin{aligned} v_A &= \frac{V_{dc}}{2} S_a \\ v_B &= \frac{V_{dc}}{2} S_b \\ v_C &= \frac{V_{dc}}{2} S_c \end{aligned} \tag{4.21}$$

where v_A , v_B, and v_C are the terminal voltages of the point A, B, and C with respect to the mid-point of the DC supply voltage.

However, the voltages required in the voltage equation are the phase voltages that are the voltages between the terminals and the floating neutral point of the star connected motor. Then, the relationships between the terminal voltages and the phase voltages can be given as:

$$\begin{aligned} v_A &= v_a + v_N \\ v_B &= v_b + v_N \\ v_C &= v_c + v_N \end{aligned} \tag{4.22}$$

where v_N is the voltage of the floating neutral with respect to the mid-point of the DC supply voltage. However, due to the inverter switching the floating neutral voltage is not constant.

To derive the floating neutral voltage, Equation 4.22 can be substituted into the voltage equations in (4.13),

$$\begin{aligned} v_A &= R\, i_a + L\frac{di_a}{dt} + e_a + v_N \\ v_B &= R\, i_b + L\frac{di_b}{dt} + e_b + v_N \\ v_C &= R\, i_c + L\frac{di_c}{dt} + e_c + v_N \end{aligned} \tag{4.23}$$

In a star-connected PMAC motor, it is always true to say that the sum of the three phase currents is equal to zero. Therefore, when all three phases conduct current, the floating neutral voltage of the motor can easily be derived by summing the above equations:

$$v_N = \left(\frac{v_A + v_B + v_C}{3}\right) - \left(\frac{e_a + e_b + e_c}{3}\right) = \frac{1}{3}\left[(S_a + S_b + S_c)\frac{V_{dc}}{2} - (e_a + e_b + e_c)\right] \tag{4.24}$$

Hence, substituting Equation (4.24) into Equation (4.22), the phase voltages of the inverter driven PMAC motor can be obtained. If the back EMF of the motor is sinusoidal, the sum of three back EMF voltages is equal to zero. Therefore, the three-phase voltages of a sinusoidal PMAC motor can be simply given by:

$$\begin{aligned} v_a &= \frac{V_{dc}}{2}\left[S_a - \frac{1}{3}(S_a + S_b + S_c)\right] = \frac{V_{dc}}{6}(2S_a - S_b - S_c) \\ v_b &= \frac{V_{dc}}{2}\left[S_b - \frac{1}{3}(S_a + S_b + S_c)\right] = \frac{V_{dc}}{6}(2S_b - S_a - S_c) \\ v_c &= \frac{V_{dc}}{2}\left[S_c - \frac{1}{3}(S_a + S_b + S_c)\right] = \frac{V_{dc}}{6}(2S_c - S_a - S_c) \end{aligned} \tag{4.25}$$

As can be seen in Equation (4.25), the phase voltages of the sinusoidal PMAC motor only depend on the switching states and the DC link voltage of the inverter. This means that the phase voltages do not have to be measured directly, but can be reconstructed from the switching signals and the DC link voltage. This is very important in the PMAC motor control if the use of a minimum number of sensors is aimed, which will be discussed in Chapter 7.

Similarly, if only two of the three phases (say Phase A and B) are conducting currents, the floating neutral voltage of the motor can be derived as:

$$v_N = \left(\frac{v_A + v_B}{2}\right) - \left(\frac{e_a + e_b}{2}\right) = \frac{1}{2}\left[(S_a + S_b + S_c)\frac{V_{dc}}{2} - (|S_a|e_a + |S_b|e_b + |S_c|e_c)\right] \tag{4.26}$$

Substituting Equation (4.26) into Equation (4.22), the phase voltages of the current conducting phases can be obtained when only two phases of the motor conducting current. Combining these two cases together, a unified expression of the voltage of phase p (p = a, b, c) for the PMAC motor can be given as follow:

$$v_p = \frac{1}{K}\left[(K \cdot S_p - S_a - S_b - S_c)\cdot\frac{V_{dc}}{2} + (|S_a| \cdot e_a + |S_b| \cdot e_b + |S_c| \cdot e_c)\right] \tag{4.27}$$

where K is a constant, and K = 3 when all three phases conduct current, and K = 2 when only two of the three phases conduct current.

When only two of the three phases conduct current, the phase voltage of the remaining phase is equal to the back-EMF voltage, that is,

$$If \quad S_p = 0, \quad v_p = e_p \tag{4.28}$$

4.3 Virtual Instrument of the PMAC Motor Drive

In this study, LabVIEW is used as a powerful computer simulation tool to study the PMAC motor drive. LabVIEW is a graphical programming language that uses icons instead of lines of texts to create applications. In contrast to text-based programming languages, where instructions determine program execution, LabVIEW uses dataflow programming, where the flow of data determines execution.

LabVIEW programs are called virtual instruments, or simply VIs, because their appearance and operation imitate physical instruments, such as an oscilloscope and a multimeter. Every VI uses functions that manipulate input from the user interface or other sources, and display that information or move it to other files or other computers. A VI contains the following three components [79]:

- **Front panel** -- Serves as the user interface.
- **Block diagram** -- Contains the graphical source code that defines the functionality of the VI. In some ways, the block diagram resembles a flowchart.
- **Icon and connector pane** -- Identifies the VI so that it can be used in another VI. A VI within another VI is called a subVI, which corresponds to a subroutine in text-based programming languages.

With LabVIEW, a user interface may be built by using controls and indicators, which are the interactive input and output terminals of the VI, respectively. Controls are knobs, push buttons, dials, and other input devices. Indicators are graphs, LEDs, and other displays. Controls simulate instrument input devices and supply data to the block diagram of the VI. Indicators simulate instrument output devices and display data that the block diagram acquires or generates. After the front panel is built, these front panel objects appear as terminals on the block diagram. By adding some codes, which use graphical representations of functions, the front panel objects can be controlled.

Therefore, the computer simulation of the motor drive was implemented in LabVIEW by providing all the motor and drive parameters from the front panel and by displaying the estimated values on the front panel, which is similar to the oscilloscope measurements. In order to build a general simulation tool for the PMAC motor, a number of VIs were constructed, which each consists of several functional subVIs, and each implements one component of the practical motor drive system.

4.3.1 Virtual Instrument of the PMAC Motor

In this section, the VI that simulates the three-phase PMAC motor is given. This VI implements the mathematical models of the motor that was described earlier in Section 4.2. As can be seen in Equation (4.13), the voltage equations are non-linear differential equation because the back-EMF voltages are the functions of the rotor position.

It can be said that if the time step in the simulation is small enough, the back-EMF variations within one calculation interval may be neglected. Under this assumption, the complete simulation VI can be divided into four functional sub-components.

In the first component, the unit back-EMF functions are implemented (as in Equation (4.8) and Equation (4.9)). The block diagram of the back-EMF function sub-VI is shown in Figure 4.2. The sub-component has two input terminals: Mode and Position. The "Mode" is used to select either trapezoidal or sinusoidal back-EMF functions. Note that this figure shows the state of the trapezoidal back-EMF selection and one of the discrete intervals describing the back-EMF function. The "Position" is the input terminal for the rotor position signal. The three output terminals are the three-phase unit back-EMF functions of the simulated motor.

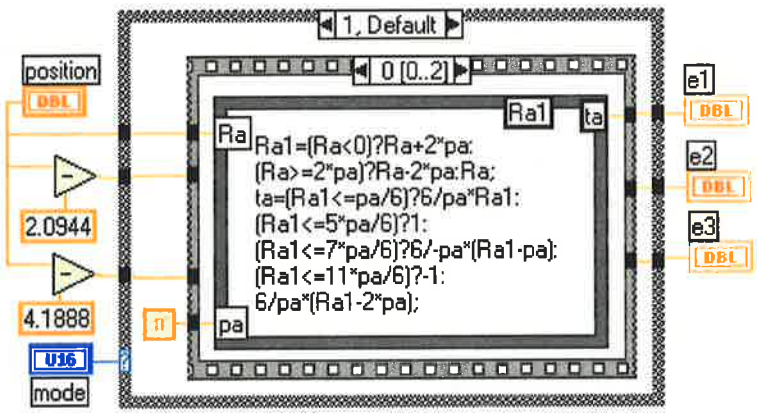

Figure 4.2 Block diagram of the three-phase back-EMF function sub-VI.

The second sub-component is used to simulate the inverter and to produce the state variables of the inverter as described in Section 4.2.3. Figure 4.3 shows the block diagram of this sub-component. The input terminals in the sub-component are the switching signals and the three-phase currents. The phase current inputs are used to identify the direction and the zero state of the motor currents. Similar to the practical inverter, where the switching signals are used to drive the six power switches, the six switching signals in this sub-component are used to generate (together with the phase currents) the values of the state variables for each phase, which determine the instantaneous output voltages of the inverter.

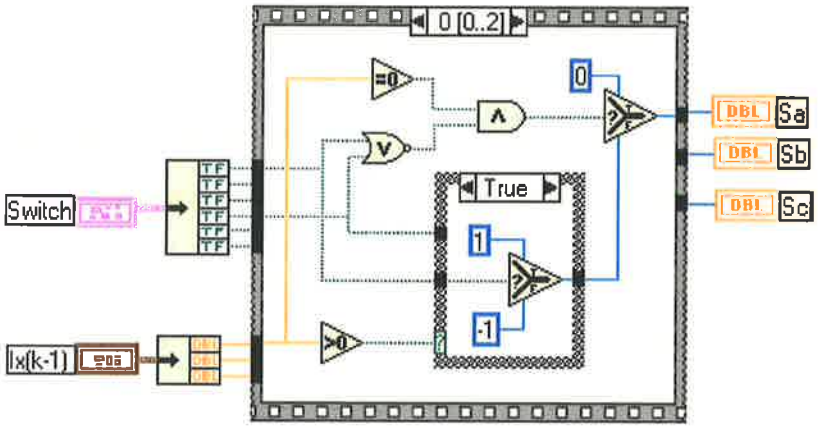

Figure 4.3 Block diagram of the three-phase inverter sub-VI

The two sub-components described above are also integrated as a sub-VI and used in the simulation VI of the PMAC motor as icons. The block diagram of the PMAC motor VI is given in Figure 4.4. The remaining two sub-components of the motor VI are directly programmed in this block diagram. One of the blocks calculates the electrical rotor position from the angular speed that is based on Equation (4.11). Although more complex discrete integration methods can be used for a better accuracy, a simple Eular integration method is utilized here, which is found to be sufficient. The second block, an Equation Node, in the figure performs the calculations of the phase voltages, the currents, and the electromagnetic torque of the motor. In this block, the back-EMF voltages are calculated using Equation (4.19), and the three-phase voltages are calculated using Equation (4.27) and (4.28). Therefore, the voltage equation can be solved using the solution of the differential equation that produces the phase current value for the consecutive time step. Eular integration method is also used here for simplicity. Finally, the electromagnetic torque of the motor is calculated using Equation (4.18).

It should be noted here that the value of zero current in the trapezoidal PMAC motor drive simulation has to be identified. This is also implemented in this block diagram. Under the normal double pole modulation (two of the power switches on the conducting current legs are turned on or off together, that is different from the single pole modulation used in the position sensorless technique based on the conducting states of the free-wheeling diodes as mentioned in Section 3.2.3), the two power switches on the phase have to be turned off together. So the current in this phase decays to zero through one of the freewheeling diodes. Then, no current flows in this phase until one of the power switches turns on again in the next cycle. Therefore, the zero current in the simulation can be identified by checking the direction of the current. This is done by observing the direction of the calculated current within the free current decay interval, where the current is equal to zero as shown in the block diagram.

As a unique feature of LabVIEW programming, the PMAC motor VI can also be integrated as a sub-VI and used in the overall drive system as an icon, which is identified by a name of "*motor*". The "*motor*" VI has six inputs and four outputs terminals. One of the inputs is the array of the switching signals, which are generated by the current controller of the motor drive and used to control the power switches in the inverter. The parameters of the

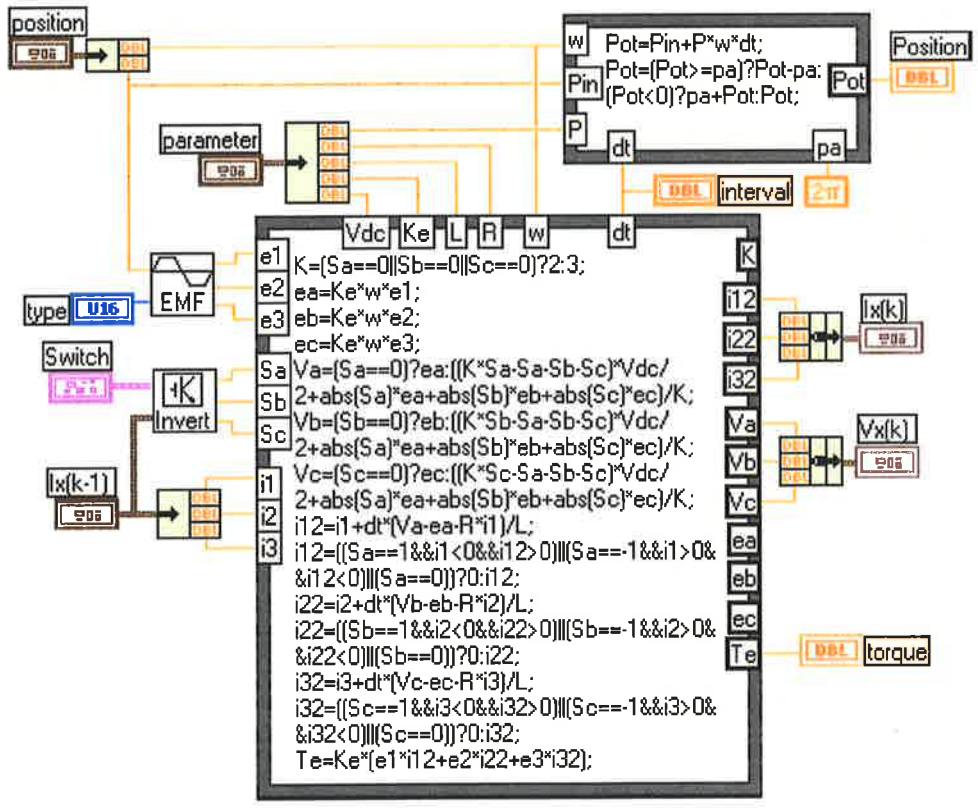

Figure 4.4 Block diagram of the three-phase PMAC motor VI

motor (which includes the number of pole pair, the phase resistance, the phase equivalent inductance, the back-EMF constant and the DC link voltage) and the calculation interval are the other two inputs in this VI. In order to set the initial values at the top-level VI, the former step values of the currents and the rotor position are also provided as inputs to the "*motor*" VI. An input signal named "*mode*" is defined to select the trapezoidal or the sinusoidal PMAC motor. The outputs of the "*motor*" VI include the phase currents, the phase voltages, the torque and the rotor position, which can be used to display the simulation results and also to simulate the sensorless scheme that will be performed in Chapter 5.

4.3.2 Virtual Instrument of the Current Controller

Similar to the practical motor drive system, the "*control*" VI is implemented here as the current controller of the motor drive VI. As discussed in Section 2.4.4, the purpose of the "*control*" VI is to force the "actual" phase currents to track the reference currents by generating suitable switching signals. As stated previous chapters, the trapezoidal and the sinusoidal PMAC motors require rectangular and sinusoidal excitation currents respectively. However, from the control point of view, an identical current controller can be accommodated in both excitation types. The only difference is that the motors need rectangular or sinusoidal current reference signals. Therefore, the first function of the "*control*" VI is to generate the three-phase current reference signals. The reference current waveforms can be either ideal sine waveforms or piecewise rectangular waveforms. The below equations show such ideal reference signals of phase A:

$$i_a^* = I_m \sin(\theta_e) \tag{4.29}$$

$$i_a^* = \begin{cases} 0 & 0 < \theta_e \le \dfrac{\pi}{6} \\ I_m & \dfrac{\pi}{6} < \theta_e \le \dfrac{5\pi}{6} \\ 0 & \dfrac{5\pi}{6} < \theta_e \le \dfrac{7\pi}{6} \\ -I_m & \dfrac{7\pi}{6} < \theta_e \le \dfrac{11\pi}{6} \\ 0 & \dfrac{11\pi}{6} < \theta_e \le 2\pi \end{cases} \tag{4.30}$$

where I_m is the amplitude of the reference phase current.

The three-phase reference current generator can be programmed as a sub-VI, which has three input terminals and one output. The input terminals include the rotor position signal, current command, and the mode that is used to select either rectangular or sinusoidal reference current. The output is the required reference current of one phase. Since the sub-VI of such implementation is simple, the block diagram is not given here. Three icons of the sub-VI should be used to generate three-phase reference currents in the "*control*" VI. In this module, the position signal is shifted 120^o electrical for each phase.

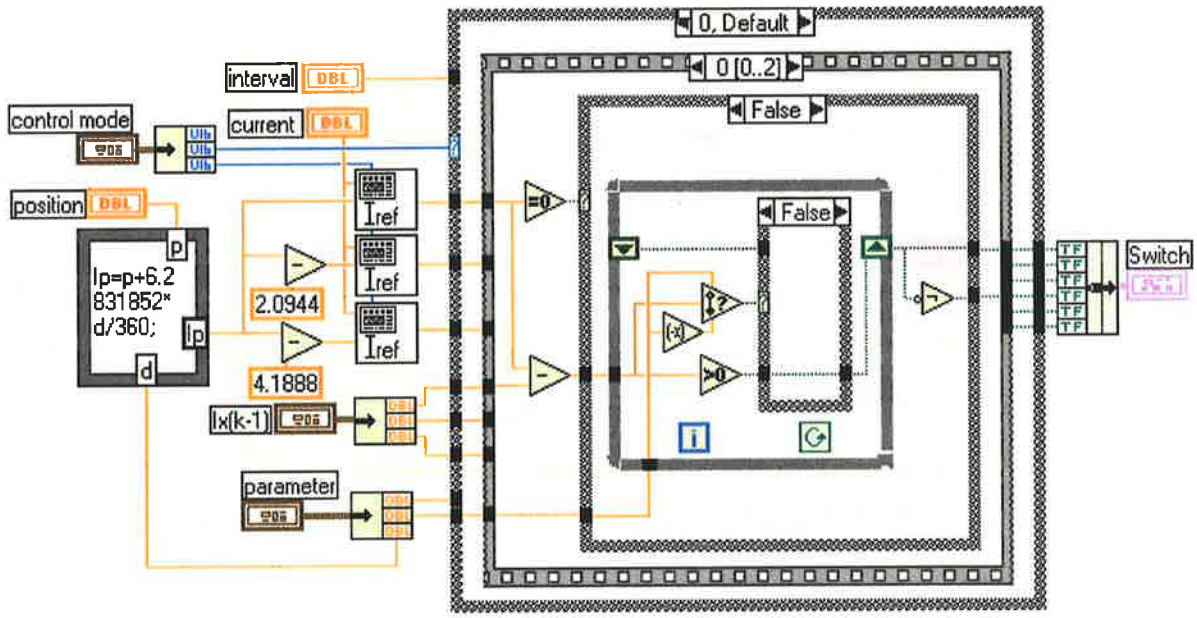

Figure 4.5 Block diagram of the current controller Simulation VI

Similar to the Section 2.4.4, only two commonly used current control schemes, Hysteresis Current Controller and the PWM Current Controller, are implemented here. The figure 4.5 shows the block diagram of the "*control*" sub-VI.

The "*control*" sub-VI has six inputs and one output. The rotor position and the amplitude value of the reference current are the two inputs that are used to generate the reference current signals. The phase current input is used as the current feedback signals for the controller (which simulate the current transducers as used in the practical system). The parameters of the controller (including modulation frequency for the PWM controller, the bandwidth for the hysteresis controller, and the phase shifting angle) and the time step are the other two inputs. In order to distinguish the types of motor and the current controller, two "*mode*" input signals are also utilized. The output is the switching signals, which are used to control the PMAC motor VI.

4.3.3 Virtual Instrument of the Steady State Operation

Figure 4.6 shows the block diagram of the VI that is designed to simulate the steady-state operation of the PMAC motor drive. The two icons "*control*" and "*motor*" in this figure represent the current controller VI and the PMAC motor VI respectively. There are three "*waveform graphs*" in this block diagram, which are used to display the phase currents, the phase voltages, and the electromagnetic torque.

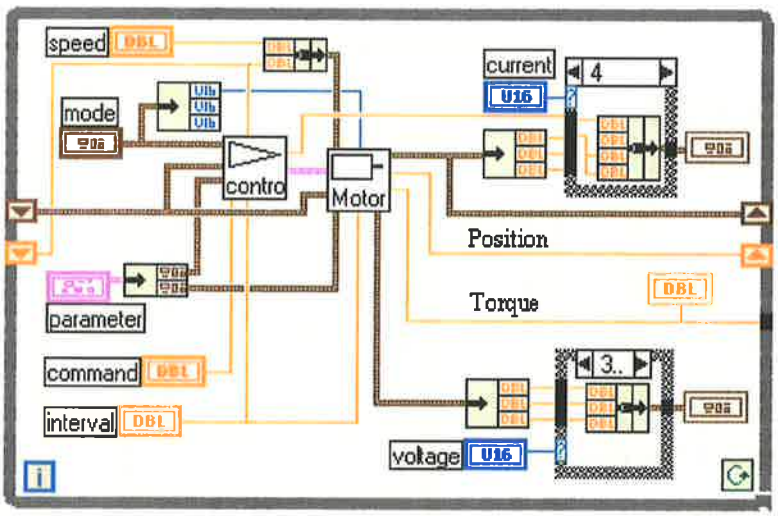

Figure 4.6 Block diagram of the steady-state operation simulation VI

Figure 4.7 shows the Front Panel of the block diagram described above. Single phase or all three-phase currents and voltages can be displayed on the Front Panel by using the control box provided. There are several parameter input controls and three output displays on the Front Panel. The input parameters are classified into three groups. The first group is the motor parameters, which include the number of pole pairs, the winding resistance R, the equivalent winding inductance L, the back-EMF constant k_e, and the DC link voltage of the inverter. The second group contains the current controller's parameters, which are the modulation frequency of the PWM Current Controller, the hysteresis bandwidth of the Hysteresis Current Controller and the phase advance/delay angle of the current command. The third group is called the "*mode*" parameters, which are used to select the type of the back-EMF (trapezoidal or sinusoidal), the wave shape of the reference current (rectangular or sinusoidal), and finally the type of the current controller (hysteresis or PWM). In addition to the above parameters, the motorÆs angular speed, the command current and the time step also need to be set in the steady-state simulation VI. The three displays are used to show the

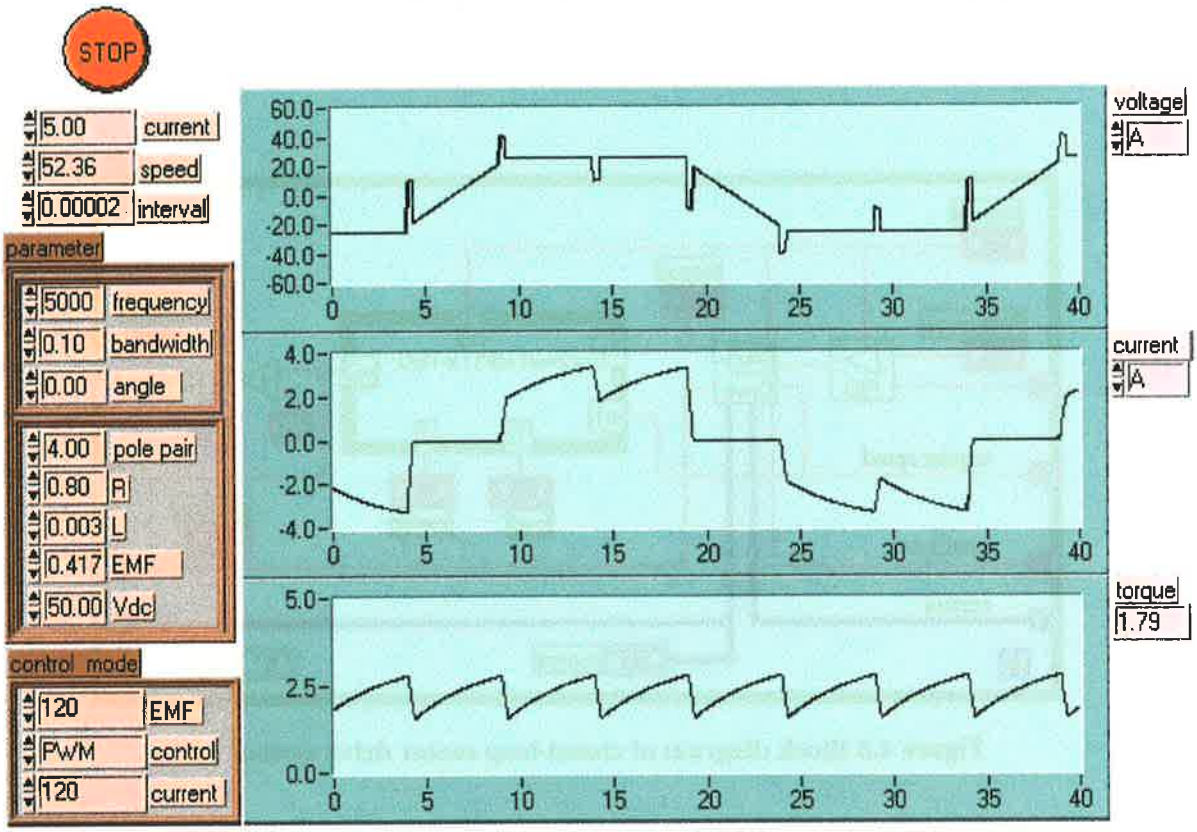

Figure 4.7 Front Panel of the steady-state operation simulation VI

simulation waveforms of the phase voltages, the phase currents, and the electromagnetic torque.

4.3.4 Virtual Instrument of the Dynamic State Operation

In order to simulate the transient performance of the PMAC motor drive while maintaining the simplicity of the structure, the VI shown in Figure 4.6 is integrated into a "*drive*" sub-VI that has five inputs and three outputs. The inputs of this sub-VI are the current command, the angular speed, the rotor position, the currents and the time step. The outputs include the torque, the rotor position and the currents. The principal purpose of these inputs and the outputs of the rotor position and the currents is to set the initial values.

The output of the motor drive is the torque that causes the load to rotate at a speed. To achieve the dynamic simulation, two additional components were implemented. The first component is the motion equation (as given in Equation (4.20)). In most motor drive applications, the motor speed has to be controlled using a closed-loop speed controller. Figure 4.8 shows the block diagram of the closed-loop PMAC motor drive system VI. In this figure, the speed controller is shown as an icon, which contains the algorithm of a PI

regulator. The output of the speed controller icon is the command current of the motor drive icon. The motor speed is fed back to the speed controller and is compared with the reference speed.

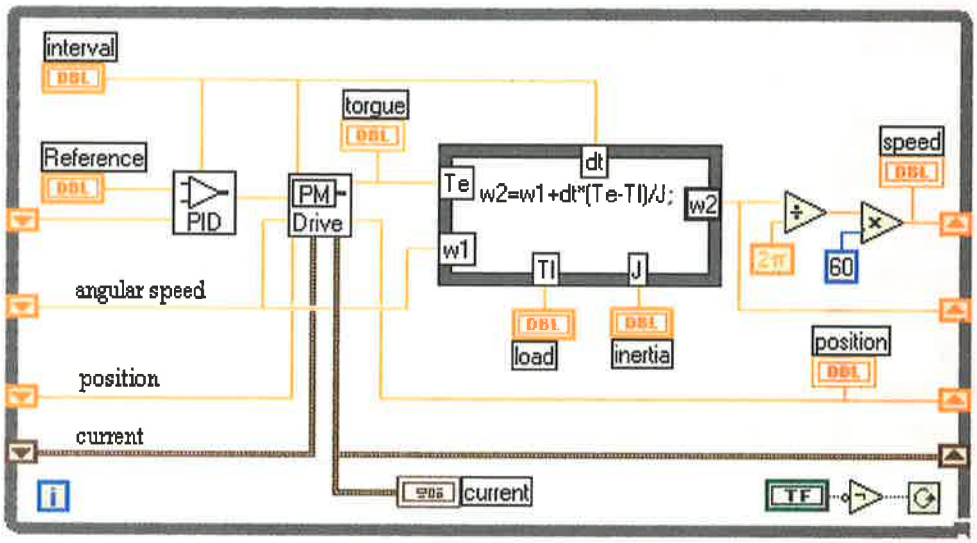

Figure 4.8 Block diagram of closed-loop motor drive system VI

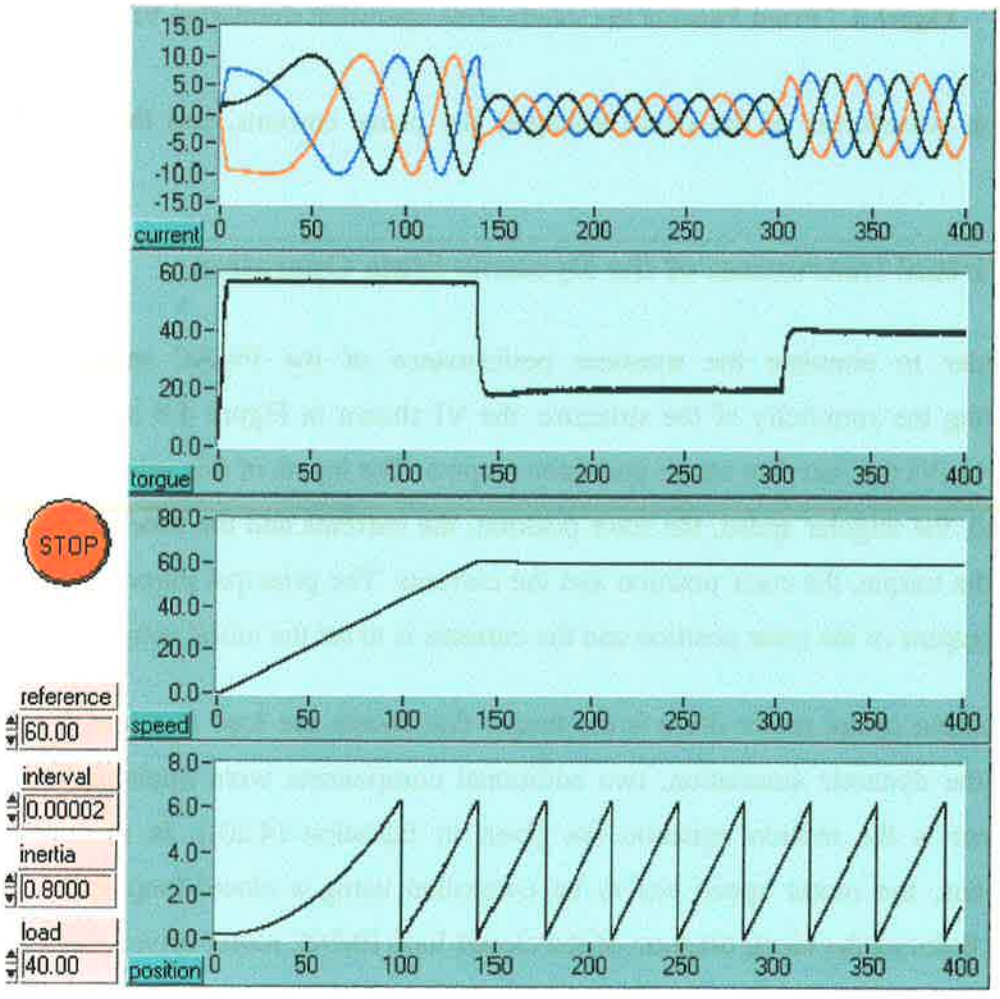

Figure 4.9 Front Panel of the dynamic state operation VI

Figure 4.9 shows the Front Panel of the closed-loop drive system VI. To run the dynamic simulation VI, five simulation parameters (reference speed, calculation interval, motor inertial and load torque) have to be defined on the control boxes of the Front Panel. Four graphs on the Front Panel are used to display the simulation results of the phase currents, the electromagnetic torque, the motor speed, and the rotor position.

4.4 Simulation Results

The results presented in this section were specifically chosen to understand some of the typical operations of the PMAC motor drive, and to demonstrate the validity and reliability of the simulation model. In addition, the tests are carried out to obtain some confidence to simulate the rotor position sensorless operation and the phase current reconstruction techniques that are described in the later chapters of the thesis.

The simulation results for both steady state and transient operations are given in this section. In the steady-state tests, the waveforms of the phase currents, the phase voltages, and the electromagnetic torque were displayed. In the transient tests, however, the waveforms of the phase current, the electromagnetic torque, the rotor speed and the rotor position. To demonstrate the capability of the simulation model, two different types of PMAC motors are simulated in this section. The trapezoidal and sinusoidal PM motor parameters used in the simulation are given in Table 4.1 and Table 4.2 respectively.

Table 4.1 The parameters of the trapezoidal PMAC motor

Back emf constant, k_e	0.417 V/rad/s
Moment of inertia, J	0.0008 kgm^2
Number of pole pairs, N_p	4
Winding resistance, R	0.8 Ω
Equivalent winding inductance, L	3.12 mH

Table 4.2 The parameters of the sinusoidal PMAC motor

Back-EMF constant, k_e	3.785 V/rad/s
Moment of inertia, J	0.08 kgm^2
Number of pole pairs, N_p	28
Winding resistance, R	6.4 Ω
Equivalent winding inductance, L	44.5 mH

4.4.1 Simulation Results Under Steady-State Operation

Firstly, the "drive" VI was used to simulate the steady-state operation of the trapezoidal PMAC motor. Figure 4.10 shows a set of simulation results. In this operating mode, the DC link voltage was set to 50V, the motor was rotating at a speed of 300 rpm and the command current was 5A. There was no phase advance or delay angle in this test. The PWM current controller at modulation frequency of 5KHz was also defined in the test.

Figure 4.10 shows the instantaneous waveforms of the voltage and the current of phase A and the electromagnetic torque of the motor. As seen in the figure, when the current is zero, the phase voltage is equal to the back-EMF voltage of the phase. However, when the phase (phase A here) conducts current, the phase voltage swings between $+V_{dc}/2$ and $-V_{dc}/2$. Due to the winding inductance, the commutation between two phases lasts a finite time, in which all three phases conduct current. Therefore, during the commutation period the phase voltage is either $\pm 2V_{dc}/3$ or $\pm V_{dc}/3$. For this reason, the phase current cannot follow the rectangular reference current closely.

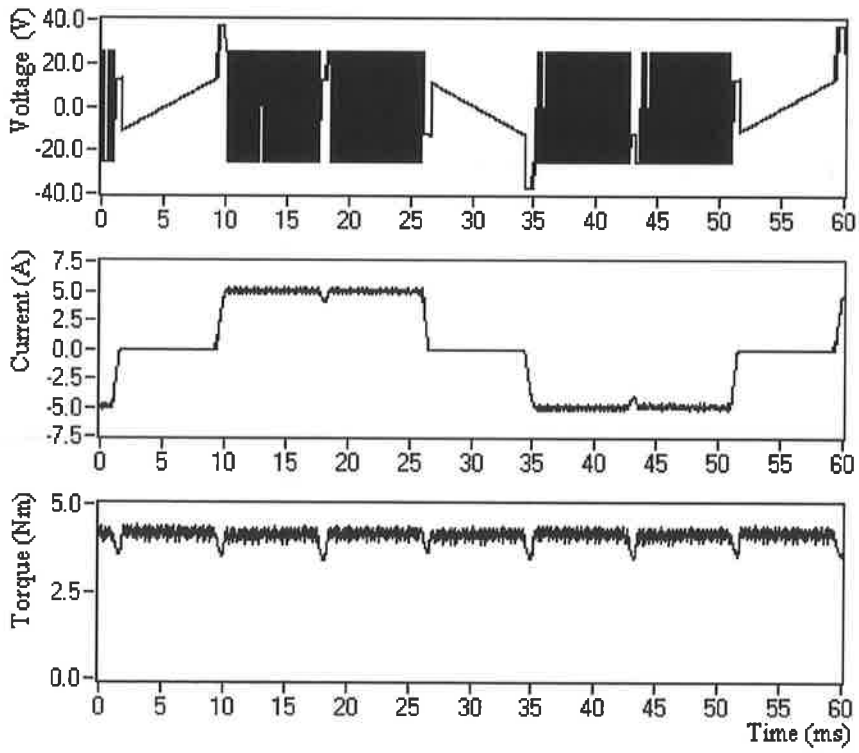

Figure 4.10 Simulations results of the trapezoidal PMAC motor under the steady-state operation conditions: 300 rpm. V_{dc}=50V, PWM Current Controller at a frequency of 5KHz, $I_{m(ref)}$ = 5A, no phase advance or delay angle.

However, outside the commutation time, the phase current can track the command current closely and has less current ripple, resulting less ripple on the electromagnetic torque. Within the commutation period, because the back-EMF of outgoing phase has to drive its current down while the back-EMF of the incoming phase has to oppose to the current build-up, the decay time of the current of the off-going phase is shorter than the rise time of the incoming phase current. The sum of these two currents is slightly smaller than the amplitude of the command current. Such smaller current sum causes relatively larger torque ripples during the commutation period, which occurs every 60^0 electrical degrees. This is a major disadvantage of trapezoidal PMAC motor drives.

In Figure 4.11, another simulation result is given, in which the desired speed of the motor was changed from 300rpm to 500 rpm but all other settings were unchanged. As shown, since the amplitude of the back-EMF voltages is proportional to the rotor speed, the effective voltage of the motor phase at a higher speed becomes insufficient to force the current to reach to the command current. Therefore, no current control is achieved under this operating condition. In this mode of operation, the phase current is limited by the net voltage across the

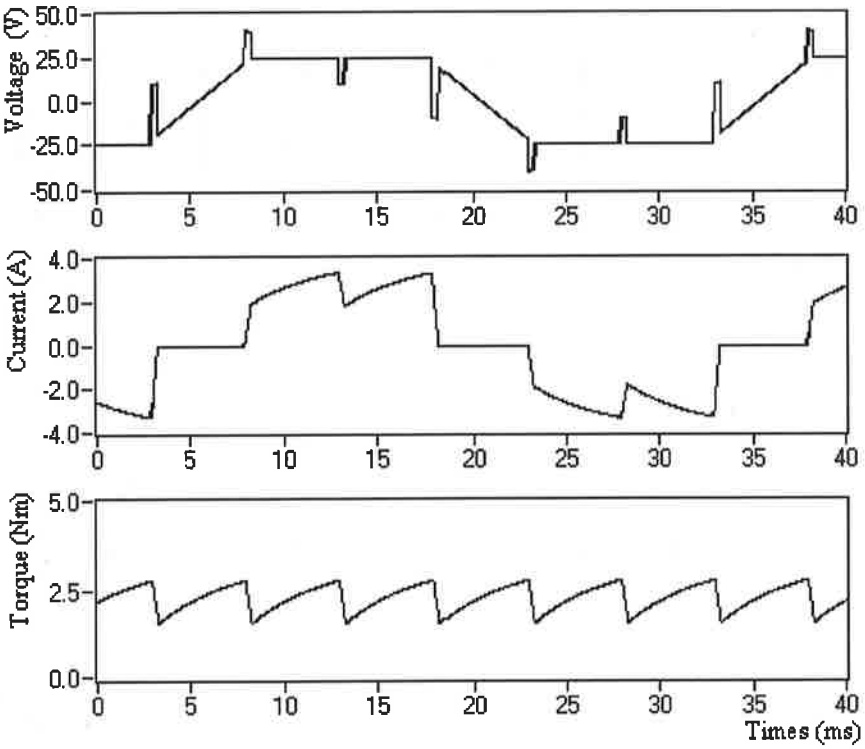

Figure 4.11 Simulations results of the trapezoidal PMAC motor under the steady-state operation conditions: 500 rpm. V_{dc}=50V, PWM Current Controller at a frequency of 5KHz, $I_{m(ref)}$ = 5A, no phase advance or delay angle.

two conducting windings, which is the difference between the DC link voltage and the instantaneous line-to-line back-EMF voltage. As a result of the large current ripple, the produced electromagnetic torque has large ripples. This mode of operation of the motor drive is known as the high-speed operation without current control.

In most applications, such torque ripples tend to be less troublesome due to the effective low-pass filtering action of the rotor inertia at high-speed range. However, the low torque value in this mode reduces the ability of the motor to drive a load. If this occurs, the phase advancing technique that is mentioned in Chapter 2 is used to restore some degree of torque production in the high-speed range.

Figure 4.12 shows the simulation results under the identical operating conditions as in Figure 4.11 but with a 30^0 phase advance angle. As seen in the figure, the phase advancing increases the current value before it is limited by the back-EMF. Although the torque ripples increase in this mode of operation, a high current value is achieved which increases the average torque.

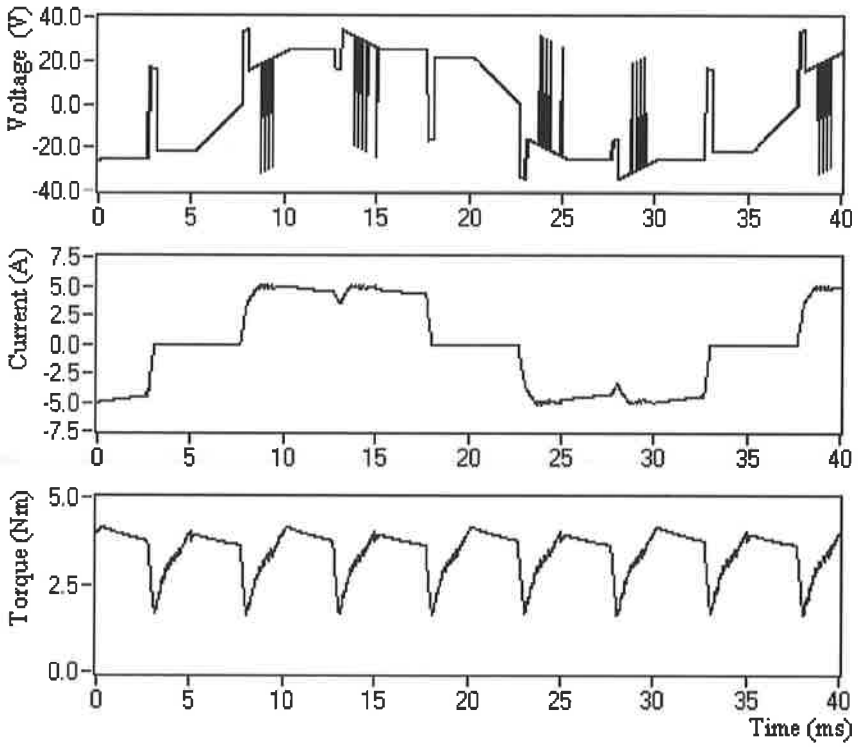

Figure 4.12 Simulations results of the trapezoidal PMAC motor under the steady-state operation conditions: 500 rpm. V_{dc}=50V, PWM Current Controller at a frequency of 5KHz, $I_{m(ref)}$ = 5A, 30^0 phase advance angle.

After resetting the motor parameters using the practical motor parameters given in Table 4.2, the "drive" VI was used to simulate the steady-state operation of the sinusoidal PMAC motor.

A set of simulation results are shown in Figure 4.13 under the steady-state operating condition. In this test, DC link voltage was 150V, the motor was running a speed of 80 rpm, and the magnitude of the command current was 5A. In addition, there was no phase advance or delay angle, and modulation frequency of the PWM controller was 5KHz.

Since all three phases conduct current at any time in the sinusoidal PM motors, depending upon the switching states the phase voltages can be either $\pm 2V_{dc}/3$ or $\pm V_{dc}/3$. A good sinusoidal current waveform can be produced in this operating mode. As a result, the developed electromagnetic torque has less torque ripples, which makes the sinusoidal PMAC motors a good candidate in servo motor applications.

Similar to the trapezoidal PMAC motor drive, when the motor speed increases, the available phase voltage decreases, which limits the current change. Therefore, the motor

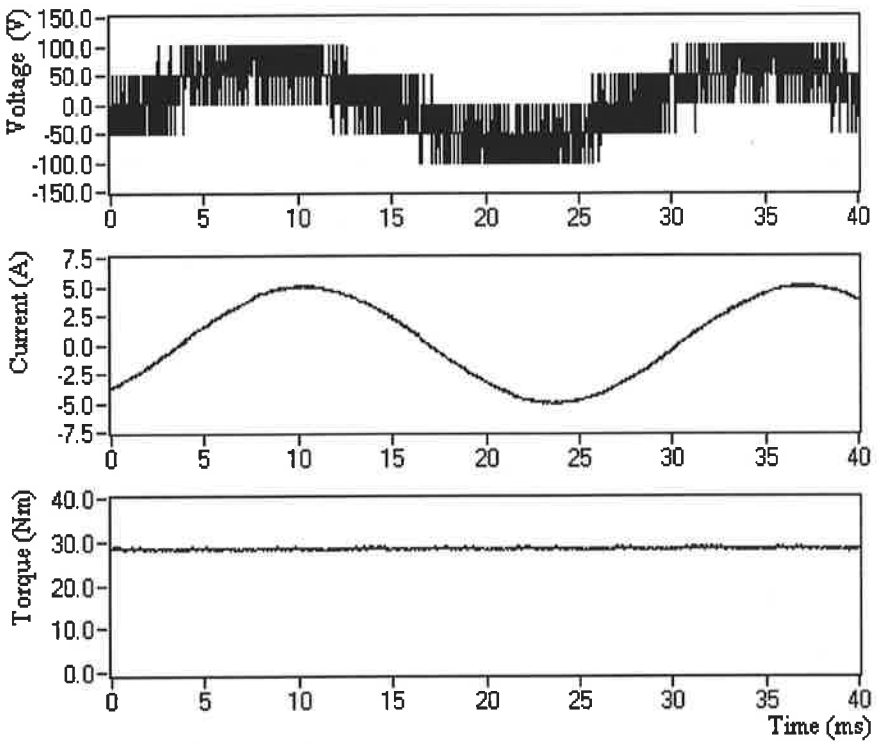

Figure 4.13 Simulations results of the sinusoidal PMAC motor under the steady-state operation conditions: 80 rpm. V_{dc}=150V, PWM current controller at a frequency of 5KHz, $I_{m(ref)}$ = 5A, no phase advance or delay angle.

current may not track the command current at certain speeds of the motor. Figure 4.14 shows the simulation results at high-speed operation. In this test, the parameters of the motor drive were kept same as in Figure 4.13. However, the speed reference was altered from 80rpm to 140rpm. As seen from Figure 4.14, the current waveform is not a good sinusoidal waveform and its amplitude less than the previous case. As a result, the generated electromagnetic torque is reduced and has significant torque ripple.

By advancing the current phase, it is possible to restore the current waveform as sinusoidal and enhance the current amplitude if the advance angle is properly selected [12]. In addition, the same technique can also be used to compensate the reduction on the torque value. Figure 4.15 displays a set of simulation results considering a 30^0 phase advance angle in the controller. As seen from the figure, the produced torque was restored in some extent and the torque ripple was reduced significantly at high-speed operation. However, it should be noted here that, due to the potential demagnetisation in the surface PMAC motors, the phase advancing has a limited speed range.

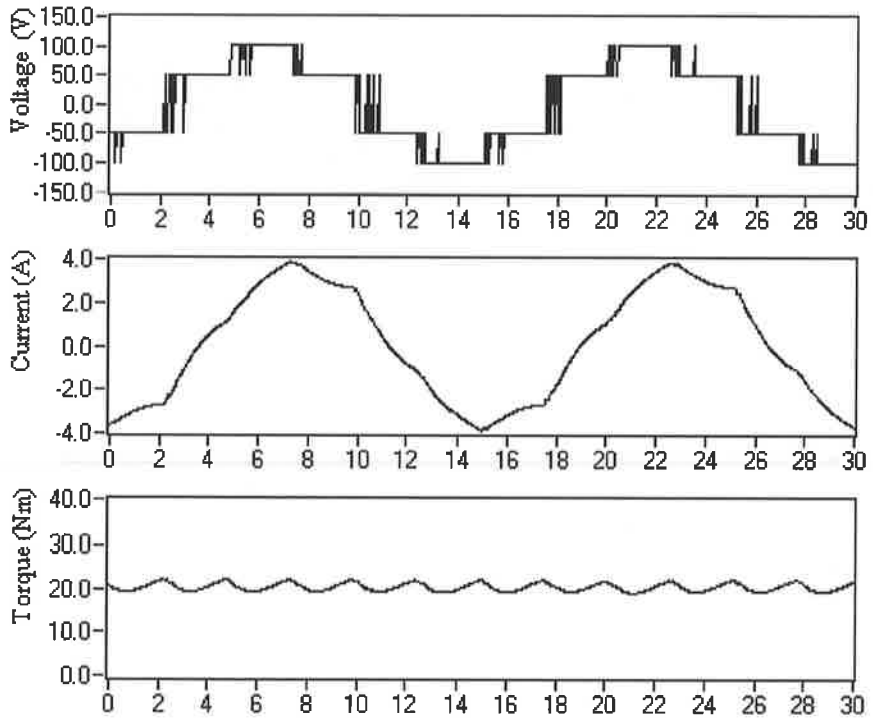

Figure 4.14 Simulations results of the sinusoidal PMAC motor under the steady-state operation conditions: 140 rpm. V_{dc}=150V, PWM current controller at a frequency of 5KHz, $I_{m(ref)}$ = 5A, no phase advance or delay angle.

4.4.2 Simulation Results in Closed-Loop Operation

As an example of the simulation of closed-loop operation, the dynamic performances of the PMAC motors are examined in this section. Figure 4.16 illustrates the simulation results obtained under the closed-loop operation of the trapezoidal PMAC motor drive. In this test, the motor accelerated from standstill up to a constant speed of 500 rpm at a constant DC link voltage of 50V. The maximum current level was 10A, which was set in the VI of the speed controller. The figure shows the waveforms of three-phase currents, the electromagnetic torque, the rotor speed, and the rotor position.

As can be seen from the figure that, the actual currents can track the command currents initially due to the low back-EMF. However, when the speed increases the actual currents gradually lose the ability to follow the command currents and the current profile diverts from the desired shape, and as a result the electromagnetic torque was reduced. After the speed reaches the reference value, 500rpm, the closed-loop drive system also reaches the steady-state operation. It should be noted here that if the torque reduces to the load value before the

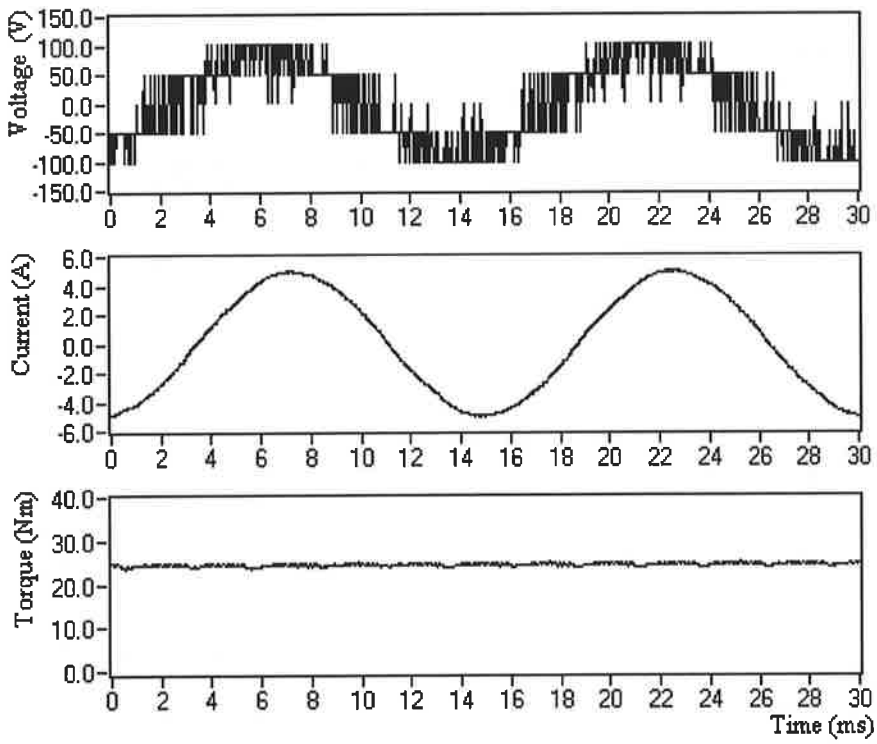

Figure 4.15 Simulations results of the sinusoidal PMAC motor under the steady-state operation conditions: 140 rpm. V_{dc}=150V, PWM current controller at a frequency of 5KHz, $I_{m(ref)}$ = 5A, 30^0 phase advance angle.

speed reaches to the desired value, the rotor speed couldn't reach the reference speed.

The transient simulation tests were also done for the sinusoidal PMAC motor and the results are given in Figure 4.17. The DC link voltage was 150V and the maximum current level was 10 A in this test. As seen from the figure, the motor accelerates from standstill up to a constant speed of 107.14 rpm (which corresponds to a frequency of 50Hz). Similar to the previous simulation results, the actual currents can track the command currents initially but lose this ability gradually when the speed increases. Within the period of no current control, the electromagnetic torque reduces significantly and possesses large torque ripple. When the motor speed reaches the reference value, the output of the speed regulator (that is the amplitude of current command) decreases, which is suitable for the light load. Hence, due to the reduction on the command current, the actual current can track the reference current and produce a good sinusoidal current waveform and a smooth electromagnetic torque.

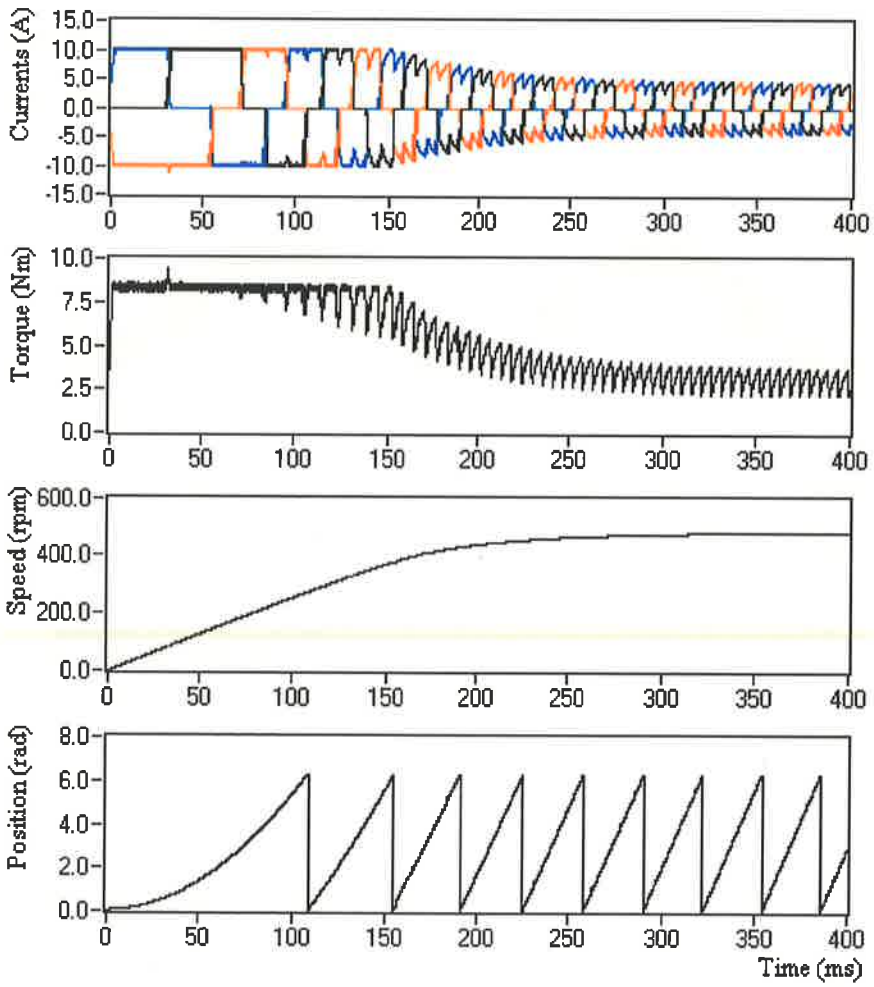

Figure 4.16 Transient simulation results of the trapezoidal PMAC motor under a closed-loop speed control: V_{dc}=50V, PWM current controller at a frequency of 5KHz, $I_{max(ref)}$ = 10A, J=0.02Nm^2, T_l =3Nm, and no phase advance angle.

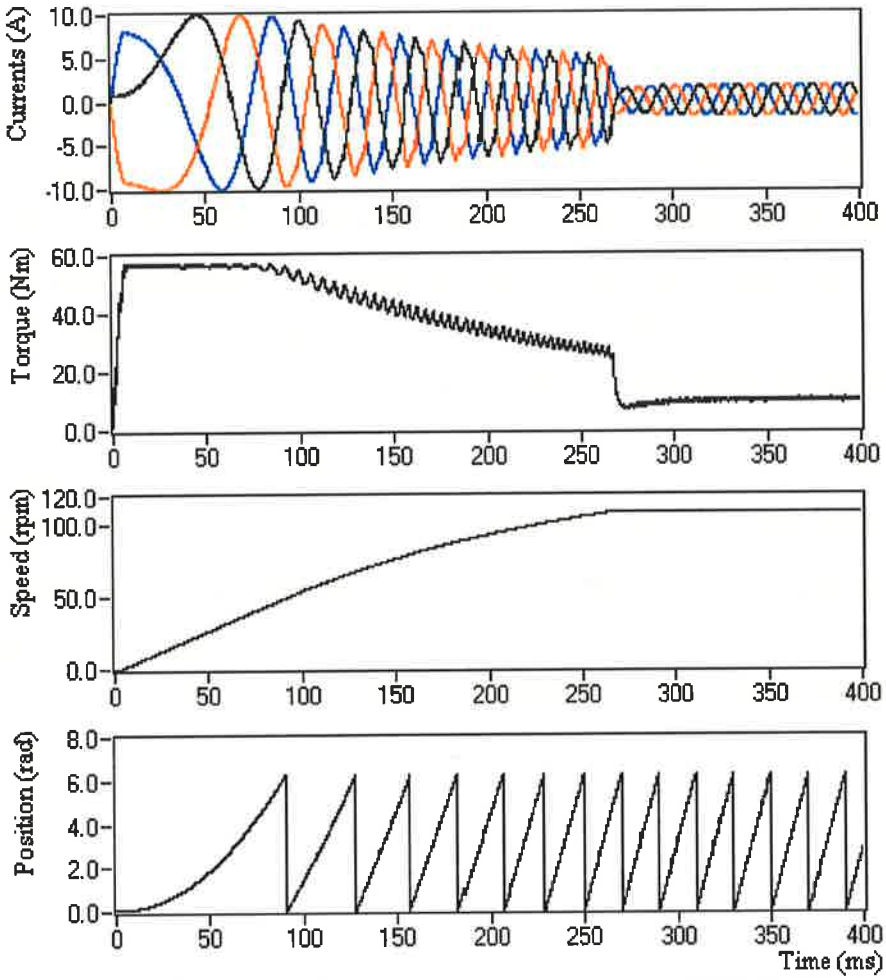

Figure 4.17 Transient simulation results of the sinusoidal PMAC motor under a closed-loop speed control: V_{dc}=150V, PWM current controller at a frequency of 5KHz, $I_{max(ref)}$ = 10A, J=0.8Nm^2, T_l =10Nm, and no phase advance angle.

As mentioned before, adding a suitable advance angle, some of the reduction in torque, which is due to the no current control operation mode, can be recovered. However no results are provided here to demonstrate the improvement on the dynamic performances of the PMAC motor drives.

4.5 Conclusions

As demonstrated in this Chapter, the computer simulation is a very useful tool to analyze the behavior of the PMAC motor drives. To accomplish a good simulation study, the most vital step is the establishment of an accurate simulation model of the complete motor drive, which is difficult to achieve due to the limitations on the accurate model of the motor and the inverter circuit. A simplified general-purpose simulation model is developed in this Chapter, which can be used for both trapezoidal and sinusoidal PMAC motor drives. The model is

formulated entirely in the natural three-phase reference frame that makes the direct comparison of the simulation and the experimental results possible.

The chapter demonstrated that the complex simulation structure that exist in the trapezoidal and sinusoidal PMAC motor drives can be simplified by using the graphical programming language LabVIEW. The simulation structure in LabVIEW also provided easy debugging and a user-friendly interface. The simulation tool developed here provides an accurate analysis tool for the PMAC motor drives under a wide range of operating conditions, including the steady state and the dynamic conditions.

Although the experimental results were not provided in this chapter, the simulation results provided a very good match with the real-time test results obtained using the practical motor drive implemented, described in the successive chapters. As stated previously, the simulation model of the drive is also utilized to study the various control algorithms and the parameter estimation techniques for the position estimation and the current reconstruction.

Chapter 5
Rotor Position Estimation

5.1 Introduction

One of the most active areas of research in PMAC motor controls has been the investigation of new techniques for eliminating the rotor position sensor that is required for self-synchronisation.

Elimination of the shaft-mounted position sensor is a very desirable objective in many applications since such sensor is often one of the most expensive and fragile components in the entire drive system. After the elimination of the direct sensor, a form of indirect rotor position detection technique should be accommodated to meet the requirement of self-synchronisation control for the PMAC motor drive. The expected benefits of the indirect rotor position sensing technique are: elimination of the electrical connections of sensors, reduction in size and inertia, absence of maintenance, lack of susceptibility to the environmental factors, and increase of reliability. In addition, when absolute rotor position sensors are considered, operating at zero and low speeds are also desirable features in the indirect rotor position detection techniques.

As discussed in Chapter 3, a number of indirect rotor position detection techniques were proposed in the literatures for the PMAC motor drives, which were broadly classified in three groups. For trapezoidal PMAC motors, the most common approach to detect rotor position is to extract the rotor position information from the back-EMF waveform of the unexcited phase. However, the back-EMF voltages of the PMAC motor are too low to be sensed at low speed range. In addition, the method is affected significantly from the switching transients of the phases that conduct currents. Therefore, such position detection techniques are not suitable at low-speed operation and require an open-loop special starting strategy to start the motor from standstill.

The indirect position detection techniques for sinusoidal PMAC motors are mainly based on the estimation methods that usually utilise the phase voltages and currents of the motor. By using these quantities, the rotor position can be determined using a state observer, Kalman

filtering technique, or by direct calculations. However, these techniques are computationally intensive, and they may generate large rotor position error due to the quantisation and truncation errors, and measurement inaccuracies. Moreover, the variation of motor parameters due to temperature and saturation significantly affects the estimated rotor position data. Furthermore, the estimation techniques suffer at low speed operation, which is mainly due to the drift that occurs in the integral functions used. All the problems mentioned here limit the use of position estimation methods in the practical PMAC motor drive.

In the interior PM motor with rotor saliency, the rotor position information can be indirectly detected using the inductance variations with position. However, the direct calculation of the inductance is very sensitive to the parameter variations in the motor. To avoid this, the rotor position information can be obtained using the analysis of high frequency test signals that is injected to the motor windings. This technique is not dependent upon the rotor speed, and can operate at very low speeds including standstill. However, these techniques are not suitable for the non-salient PMAC motors, such as surface permanent magnet motors, because of the absence of the rotor saliency.

The purpose of this chapter is to overcome some of the problems of the previous methods and to propose a novel indirect rotor position detection technique that is suitable for both trapezoidal and sinusoidal PMAC motor drives. In the novel method presented in this Chapter, three phase flux linkage increments are directly calculated from measured phase currents and voltages, without integration being required. The integration is required in the calculation of flux linkage and is the main source of the estimation error in the previous techniques. Then, the increments of flux linkage and the back-EMF functions of the motor are utilized to derive a single rotor position increment. Finally, the corresponding rotor position information can be calculated by integrating the rotor position increment. The back-EMF functions used in the calculation are generated from the estimated rotor position that forms an internal closed loop in such estimation scheme. By this way, the integration existed the flux linkage calculations is transferred to the position calculation, that is, from outside to inside of the closed loop. With the help of a phase-locked loop (PLL) algorithm, the internal closed loop can correct position drift that may be caused by the motor parameter deviations and/or the measurement inaccuracies.

As will be demonstrated in the results section of this chapter, the novel indirect rotor position detection technique can estimate rotor position information over wide speed range,

and has robustness with respect to the motor parameter variations and the measurement errors in the system. In addition, the proposed estimation scheme has less mathematical computations, which made the real time implementation of the position sensorless control possible.

The theoretical basis of the new rotor position estimation scheme is detailed in Section 5.2. In this section, the possible approaches to derive rotor position information using the mathematical model of the PMAC motor are discussed. In an ideal surface PM motor, the principal approach to obtain the rotor position is to analyse the flux linkage established by PM. In this section, the limitations of previous position estimation methods are discussed and a novel position estimation scheme is described in detail.

To study the new position estimation scheme described, the simulation VI developed in Chapter 4 is utilized in Section 5.3. Several simulation results under different operation conditions are given in this section to demonstrate the feasibility and reliability of the new position sensorless technique, which is suitable for both the sinusoidal and the trapezoidal PMAC motors.

One of the major limitations of the previous position estimation methods is their dependence to the motor parameter variations and the measurement inaccuracies. In Section 5.4, the position estimation errors caused by the parameter variations and the measurement errors are analysed. The robustness of the new rotor position algorithm is discussed and the limitations are highlighted in the section. A "prediction-rectification" algorithm is also presented to improve the robustness of the proposed method.

To demonstrate the validity and reliability of the proposed rotor position estimation algorithm and its suitability in a practical motor drive, a DSP based PMAC motor drive system was implemented and explained in Section 5.5. In this section, the motor drive was controlled using a conventional position sensor, an encoder, and the real data gathered using a LabVIEW based data acquisition system. This arrangement allowed us to verify the algorithm using the real data and the actual motor position without influencing the operation of the conventional motor drive.

In Section 5.6, the shaft-mounted encoder was replaced with the estimated rotor position and a closed-loop position sensorless control was achieved. The section provides the details of the hardware and the software used and presents a wide range of experimental results to

demonstrate the capabilities of the position sensorless PMAC motor driver system. Section 5.7 summarize the features of the new method and draws some conclusions.

5.2 Principle of the Position Estimation

5.2.1 Position Estimation in an Ideal PMAC Motor

As discussed in Chapter 4, under the ideal conditions, a three-phase star-connected PMAC motor can be modelled by a star-connected three-phase lumped parameter network consisting of a winding resistance, an equivalent winding inductance, and a back-EMF source per phase, all connected in series. The voltage equations of this model were given in Equation 4.1. Substituting the total flux linkages in Equation 4.2 into the voltage equations, the voltage equations of the PMAC motor can be rewritten as:

$$\begin{bmatrix} v_a \\ v_b \\ v_c \end{bmatrix} = \begin{bmatrix} R & 0 & 0 \\ 0 & R & 0 \\ 0 & 0 & R \end{bmatrix} \begin{bmatrix} i_a \\ i_b \\ i_c \end{bmatrix} + \frac{d}{dt}\left(\begin{bmatrix} L_a & M_{ab} & M_{ac} \\ M_{ba} & L_b & M_{bc} \\ M_{ca} & M_{cb} & L_c \end{bmatrix} \begin{bmatrix} i_a \\ i_b \\ i_c \end{bmatrix} \right) + \frac{d}{dt} \begin{bmatrix} \psi_{pma} \\ \psi_{pmb} \\ \psi_{pmc} \end{bmatrix} \tag{5.1}$$

In general, the self-inductances of each phase and the mutual inductances between two phases are the functions of the rotor position as given in Equation 4.3 and 4.4. The flux linkages established by permanent magnet are also functions of the rotor position. Their derivatives with respect to time are the back-EMF voltages induced in each phase winding when rotor rotates. The back-EMF waveforms are usually sinusoidal or trapezoidal as given in Equations 4.8 or 4.9.

In the above voltage equations, the three-phase currents and voltages can be measured directly. Therefore, it can be concluded from the above expression that there are two possible approaches to obtain the rotor position information. One of the approaches is to derive the rotor position information using the relationship between the self-inductances and the mutual inductances. A number of rotor position estimation methods based on this relationship were proposed as discussed in Section 3.2.5. However, such method is not suitable if the motor is a surface PM motor. The second approach is based on the relationship between the rotor position and the flux linkages of the permanent magnets or the back-EMF voltages, which were discussed earlier in Section 3.3.

It should be noted that various other approaches are also possible to derive the rotor position information using more complicated motor models that may consider the magnetic saturation [82,83] or harmonics caused by stator slotting [84]. However, such methods are too complicated to be used in the practical motor drives.

5.2.2 Flux Linkage or Back-EMF Estimation Approach

As discussed above, under the ideal conditions, the only rotor position estimation method suitable for the surface PM motor is based on the relationship between the rotor position and the magnet flux linkages or the back-EMF voltages. The most conventional method to derive the position from this relationship is to estimate the back-EMF using the voltage equation of the motor. Recalling Equation 4.13 and rearranging it for a single phase,

$$e = v - Ri - L\frac{di}{dt} \tag{5.2}$$

As can be seen in the above equation, the back-EMF waveform can be reconstructed by solving this equation, which then can be used to obtain the rotor position. However, this method is very sensitive to the parameter variations and the measurement noises. In addition, the back-EMF is proportional to the angular speed of the motor. This makes the estimation of the back EMF difficult at low or zero speeds.

An alternative method for estimation of the position is to estimate the flux linkage by integrating the phase voltage minus the voltage drop across the winding resistance. Then the total flux linkage of a single phase may be given by:

$$\psi = \int (v - Ri)dt \tag{5.3}$$

Due to the constant equivalent winding inductance in the surface PM motors, the flux linkage established by PM can be given by:

$$\psi_{pm} = \psi - L\,i = \int (v - Ri)dt - L\,i \tag{5.4}$$

If the PM flux linkage is estimated from the above equation, the rotor position information can easily be derived. Since the flux linkage is independent of the angular speed, this method has been demonstrated in the literature that it works well over a wide range of speed. Due to the presence of the integration algorithm, however, various errors become particularly

detrimental at low speeds, such as measurement noises, DC offsets, quantisation and truncation errors of digital approximation, and parameter variations. All these errors cause integration drift and pose a significant problem in the estimate algorithms. Several improvements have been reported in the literatures to reduce the effect of these errors on the integration, such as the compensation of integration offset [22], the estimation correction with a current closed-loop control [24], and the replacement of the integration by a low-pass filter [85].

In order to improve the accuracy of the flux linkage estimation, various other complex schemes have also been proposed, which are know as observer-based methods [86,87]. These methods estimate the internal state vectors, such as the flux linkages, by manipulating the mathematical model of the PMAC motor, and then derive the rotor position information from these estimations. One major advantage of such scheme is the stabilization of the integration algorithm of the flux linkage estimation. However, the parameter variations and the measurement inaccuracies still deteriorate the rotor position estimation since such observers are heavily dependent upon the motor parameters.

5.2.3 Incremental Algorithm

From above discussions, it can be seen that the rotor position derivation method based on the relationship between rotor position and flux linkages or back-EMF voltages has two major problems: the method is sensitive to motor parameter variations, and there is a low speed problem caused by integration drift.

To overcome these problems and to develop a simple and practical technique, a novel rotor position estimation scheme is proposed here. In this new scheme, the calculation of the flux linkage using a digital integrator is replaced with the direct calculation of the flux linkage increment using the voltage equations of the PMAC motor. In addition, the back-EMF voltages are disassembled as the product of angular speed and the unit back-EMF functions, so that the estimation of back-EMF functions becomes independent of the angular speed. In order to obtain a general estimation algorithm for both trapezoidal and sinusoidal PMAC motors, the stationary three-phase mathematical model of the PMAC motor (as given in Section 4.2) is used. In the voltage equations of the surface PM motor (Equation 4.13), the back-EMF voltage of each phase winding is the function of the rotor's angular speed and the rotor position. The three-phase back-EMF can be expressed in matrix form as follow:

$$\begin{bmatrix} e_a \\ e_b \\ e_c \end{bmatrix} = k_e \omega_r \begin{bmatrix} e_1(\theta_e) \\ e_2(\theta_e) \\ e_3(\theta_e) \end{bmatrix} = \frac{k_e}{N_p} \cdot \frac{d\theta_e}{dt} \begin{bmatrix} e_1(\theta_e) \\ e_2(\theta_e) \\ e_3(\theta_e) \end{bmatrix} \tag{5.5}$$

where k_e is the back EMF constant, $e_1(\theta_e)$, $e_2(\theta_e)$ and $e_3(\theta_e)$ are unit back EMF functions with respect to the rotor position θ_e, N_p is the number of pole pairs, and ω_r is the angular speed.

Substituting Equation 5.5 into the voltage equation (Equation 4.13), the voltage equation can be rewritten as:

$$\begin{bmatrix} v_a \\ v_b \\ v_c \end{bmatrix} = \begin{bmatrix} R & 0 & 0 \\ 0 & R & 0 \\ 0 & 0 & R \end{bmatrix} \begin{bmatrix} i_a \\ i_b \\ i_c \end{bmatrix} + \begin{bmatrix} L & 0 & 0 \\ 0 & L & 0 \\ 0 & 0 & L \end{bmatrix} \frac{d}{dt} \begin{bmatrix} i_a \\ i_b \\ i_c \end{bmatrix} + \frac{k_e}{N_p} \cdot \frac{d\theta_e}{dt} \begin{bmatrix} e_1(\theta_e) \\ e_2(\theta_e) \\ e_3(\theta_e) \end{bmatrix} \tag{5.6}$$

As can be seen in the above equation, if the sampling frequency is high enough in a practical system, the rotor position increment within one sample cycle can be derived, which is given in a discrete form below:

$$\begin{aligned} \Delta\theta_{ae} &= \frac{N_p}{k_e} \cdot \frac{(v_a - Ri_a).\Delta t - L\Delta i_a}{e_1(\theta_e)} = \frac{N_p}{k_e} \cdot \frac{\Delta\psi_a}{e_1(\theta_e)} \\ \Delta\theta_{be} &= \frac{N_p}{k_e} \cdot \frac{(v_b - Ri_b).\Delta t - L\Delta i_b}{e_2(\theta_e)} = \frac{N}{k_e} \cdot \frac{\Delta\psi_b}{e_2(\theta_e)} \\ \Delta\theta_{ce} &= \frac{N_p}{k_e} \cdot \frac{(v_c - Ri_c).\Delta t - L\Delta i_c}{e_3(\theta_e)} = \frac{N_p}{k_e} \cdot \frac{\Delta\psi_c}{e_3(\theta_e)} \end{aligned} \tag{5.7}$$

where Δt is the sampling interval, Δi_1, Δi_2 and Δi_3 are the three-phase current increments between the samples, and $\Delta\Psi_a$, $\Delta\Psi_b$ and $\Delta\Psi_c$ are the three-phase flux linkage increments within the sampling interval, which are given as:

$$\begin{aligned} \Delta\psi_a &= (v_a - R\,i_a).\Delta t - L\Delta i_a \\ \Delta\psi_b &= (v_b - R\,i_b).\Delta t - L\Delta i_b \\ \Delta\psi_c &= (v_c - R\,i_c).\Delta t - L\Delta i_c \end{aligned} \tag{5.8}$$

Theoretically, each motor phase should produce identical rotor position increments ($\Delta\theta_{ae} = \Delta\theta_{be} = \Delta\theta_{ce}$). In practice, however, any estimation error could cause them slightly

different from each other. Therefore, the simplest method to obtain single rotor position increment estimation is to calculate the average value of the three rotor position increments,

$$\Delta\theta_e = \frac{\Delta\theta_{ae} + \Delta\theta_{be} + \Delta\theta_{ce}}{3} \tag{5.9}$$

In addition, assuming that the previous value of the rotor position estimation is known, the rotor position can be estimated by:

$$\theta_e(k) = \theta_e(k-1) + \Delta\theta_e \tag{5.10}$$

where, the notation k is an integer representing the estimation of the discrete data at the kth instant of time.

5.2.4 Basic Algorithm for the Position Estimation

As can be seen in Equation 5.7, since back EMF function of each phase becomes zero at the corresponding rotor pole, the rotor position increment estimation of this phase produces infinitely high value. However, the remaining two phases can provide more accurate estimation at this position. This means that each phase has its optimal sensing region, where the rotor position increment estimation is more realistic. Although Equation 5.9 can be used to calculate the single value of the rotor position increment, the three rotor position increment estimations should be weighted or limited reference to their optimal sensing region. However, the simple weighting or limiting causes the loss of the rotor position information and the reduction of the accuracy of the position estimation.

In order to fully utilize the optimal sensing region of each phase and to improve the position estimation, Equation 5.7 can be rewritten in the format given below:

$$\begin{aligned}
\Delta\theta_e \cdot e_1(\theta_e) &= \frac{N_p}{k_e} \cdot [(v_a - R\,i_a).\Delta t - L\Delta i_a] = \frac{N_p}{k_e} \cdot \Delta\psi_a \\
\Delta\theta_e \cdot e_2(\theta_e) &= \frac{N_p}{k_e} \cdot [(v_b - R\,i_b).\Delta t - L\Delta i_b] = \frac{N_p}{k_e} \cdot \Delta\psi_b \\
\Delta\theta_e \cdot e_3(\theta_e) &= \frac{N_p}{k_e} \cdot [(v_c - R\,i_c).\Delta t - L\Delta i_c] = \frac{N_p}{k_e} \cdot \Delta\psi_c
\end{aligned} \tag{5.11}$$

Let us consider the sinusoidal PMAC motor first. This means that the back EMF functions of the motor are three-phase symmetrical sinusoidal functions, which can be given as:

$$
\begin{aligned}
e_1(\theta_e) &= \sin(\theta_e) \\
e_2(\theta_e) &= \sin(\theta_e + 2\pi/3) \\
e_3(\theta_e) &= \sin(\theta_e - 2\pi/3)
\end{aligned}
\tag{5.12}
$$

If each back-EMF function is squared and then added together,

$$
e_1^2(\theta_e) + e_2^2(\theta_e) + e_3^2(\theta_e) = 1.5 \tag{5.13}
$$

Based on this assumption, if both sides of Equation 5.11 are multiplied by $e_1(\theta_e)$, $e_2(\theta_e)$ and $e_3(\theta_e)$ respectively and the resulting three equations are added up, a convenient equation for the calculation of the single rotor position increment can be derived as:

$$
\Delta\theta_e = \frac{N_p}{1.5k_e} \cdot \left[\Delta\psi_a\, e_1(\theta_e) + \Delta\psi_b\, e_2(\theta_e) + \Delta\psi_c\, e_3(\theta_e)\right] \tag{5.14}
$$

For the PMAC motor without sinusoidal back EMF profiles, however, the left hand side of Equation 5.13 is not equal to 1.5. However, under normal condition, it is possible to demonstrate that the left hand side of Equation (5.13) is greater than zero.

A general algorithm for the rotor position increment estimation can be given as:

$$
\Delta\theta_e = \frac{N_p}{k_e} \cdot \frac{\Delta\psi_a\, e_1(\theta_e) + \Delta\psi_b\, e_2(\theta_e) + \Delta\psi_c\, e_3(\theta_e)}{e_1^2(\theta_e) + e_2^2(\theta_e) + e_3^2(\theta_e)} \tag{5.15}
$$

This equation will be called the basic algorithm 1 of the rotor position increment estimation. It can be said that under the ideal conditions, using the equations (5.8) and (5.10), this algorithm can estimate the rotor position value of the PMAC motor accurately. However, the parameter variations and the measurement errors that exist in the practical motor drive influence the rotor position estimation significantly. This is because the basic algorithm 1 has no auto correction feature built in, which will be discussed later. Therefore, the basic algorithm 1 alone cannot be used in the practical PMAC motor drive.

An alternative rotor position increment algorithm will be described below, which take the parameter variations and the measurement errors into account. To achieve this, let us multiply both sides of Equation 5.11 by $e_2(\theta_e)$, $e_3(\theta_e)$ and $e_1(\theta_e)$ respectively, and then sum all three equations. Then a new expression for the rotor position increment can be obtained as:

$$\Delta\theta_e = \frac{N_p}{k_e} \cdot \frac{\Delta\psi_a e_2(\theta_e) + \Delta\psi_b e_3(\theta_e) + \Delta\psi_c e_1(\theta_e)}{e_1(\theta_e)e_2(\theta_e) + e_2(\theta_e)e_3(\theta_e) + e_3(\theta_e)e_1(\theta_e)} \tag{5.16}$$

This equation will be called the basic algorithm 2 of the rotor position increment estimation, which accommodates the optimum regions for the accurate position estimation that can be used in the practical motor drives. A block diagram of the estimation algorithm is shown in Figure 5.1.

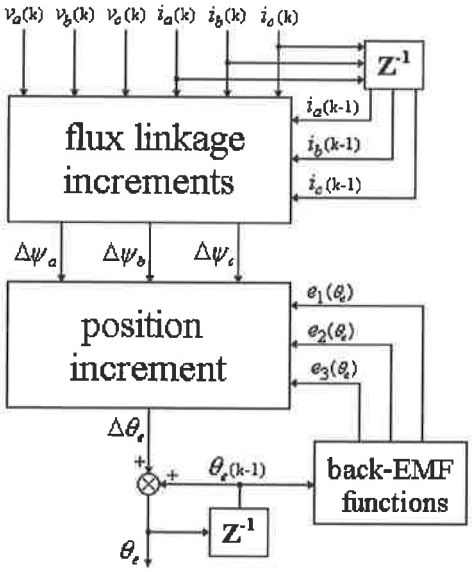

Figure 5.1 Block diagram of the position estimator

As can be seen in the figure, Equation 5.8 is used to calculate flux linkage increments using the measured phase currents and voltages. Then, the flux linkage increments and the back EMF functions are utilized to determine the rotor position increment using Equation 5.16. Finally, the rotor position information is estimated by using Equation 5.10.

It should be noted here that the back-EMF functions indicated in the block diagram are generated using their waveform functions (such as in Equation 5.12) and the estimated rotor position signal, which is feed back to the calculation of the rotor position increment. This structure forms an internal close loop. In comparison with the other rotor position estimation methods, the novel algorithm presented here has four principal advantages.

Firstly, the algorithm is simple, which makes it very practical to be used in a DSP based motor control system. As can be seen in Equation (5.8), (5.10) and (5.16), very few operation instructions are required to implement the algorithm for the rotor position estimation, which uses the measured currents and voltages of the motor drive.

Secondly, the algorithm is independent of the shape of back-EMF voltages; hence, it is suitable for both sinusoidal and trapezoidal PMAC motors, including any other PMAC motors with non-ideal back-EMF waveforms. To implement non-ideal back EMF waveforms in the algorithm, the options are to use a look up table or to use a Fourier series of the waveform.

Thirdly, the calculations of the flux linkage increments do not include any integration function; hence the drift associated with the digital integration has been avoided. Although a simple integration algorithm still exists in the position calculation (Equation 5.10), the internal closed loop produced by the back-EMF function feedbacks can stabilize the position integration, hence correct the position drift, which is the most important feature of the novel incremental algorithm. In other words, the method moves the integration loop from the flux linkage calculations to the position calculation stage. As a result, the problem of integration drift is solved by an internal closed loop correction. Furthermore, this internal correction loop improves the robustness of the rotor position estimation, which is highly influenced by the parameter variations and the measurement inaccuracies. Section 5.4 will provide more detailed discussions about the robustness of the position estimation algorithm and proposes a method for improvement.

Finally, the basic algorithm 2 does not support the reversal of the direction of the rotation. When the motor rotates in the positive direction, the rotor position increment must be positive, while the negative rotation must have negative rotor position increment. Therefore, if the motor rotates in the negative direction, the rotor position increment should be based on:

$$\Delta\theta_e = \frac{N_p}{k_e} \cdot \frac{\Delta\psi_a e_3(\theta_e) + \Delta\psi_b e_1(\theta_e) + \Delta\psi_c e_2(\theta_e)}{e_1(\theta_e)e_2(\theta_e) + e_2(\theta_e)e_3(\theta_e) + e_3(\theta_e)e_1(\theta_e)} \tag{5.17}$$

Theoretically, the choice between the two algorithms for the direction reversal is based on Equation 5.16 and 5.17. In the practical position sensorless motor drive, however, the rotor speed is also estimated using the estimated rotor position. When the rotor speed approaches zero, the error in the rotor speed estimation may cause incorrect selection of the algorithms and as a result disturbs the position estimation.

5.3 Computer Simulation

As stated in the previous chapter, a computer simulation is a very useful tool to investigate the behaviour of a proposed control algorithm before it is implemented in a practical system, which allows the user to test any extreme operation condition that may even not be possible to realize in the real drive. In this section, the general simulation VI of the PMAC motor developed in Chapter 4 is also used to simulate the rotor position algorithm proposed in Section 5.2, and various simulation results are provided to show the validity of the new position sensorless technique.

5.3.1 Simulation VI of the Rotor Position Estimation

The block diagram of the sub-VI for the rotor position estimation is shown in Figure 5.2, which utilizes the equation (5.8), (5.10) and (5.16). Two input terminals of the sub-VI receive the data of the phase currents and the phase voltages that are generated from the simulation model of the PMAC motor drive. The estimated rotor position and its derivative (used to estimate the rotor speed) are the outputs in the VI. As an incremental algorithm, the former value of the rotor position is also an input to the sub-VI. The back-EMF functions are generated from the former value of the rotor position, which use the back-EMF function sub-VI as shown in Figure 4.2. As stated in the previous chapter, the back-EMF functions can be selected using the input terminal, "mode", which allows the user to study different types of PMAC motors in the position estimation. The motor parameters and the time step are also the

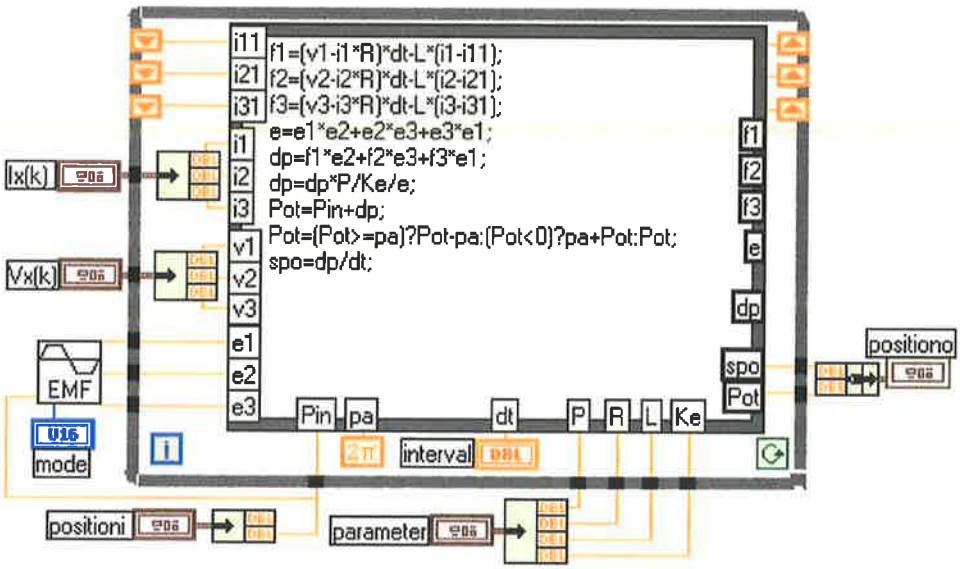

Figure 5.2 Block diagram of the rotor position estimator VI

inputs to the rotor position estimator sub-VI.

The icon of the rotor position estimator sub-VI "position" is used in the block diagram of the motor drive VI as shown in Figure 5.3, which allows the user to simulate the proposed rotor position algorithm under open-loop operation. The sub-VI "degree" utilized in the block diagram converts the unit of the rotor position from radian to degree, and calculates the error between the measured and the estimated rotor positions. There are four graph outputs as shown in the block diagram, which are designed to display the simulated waveforms of the phase currents, the measured rotor position, the estimated rotor position and the position error on the front panel.

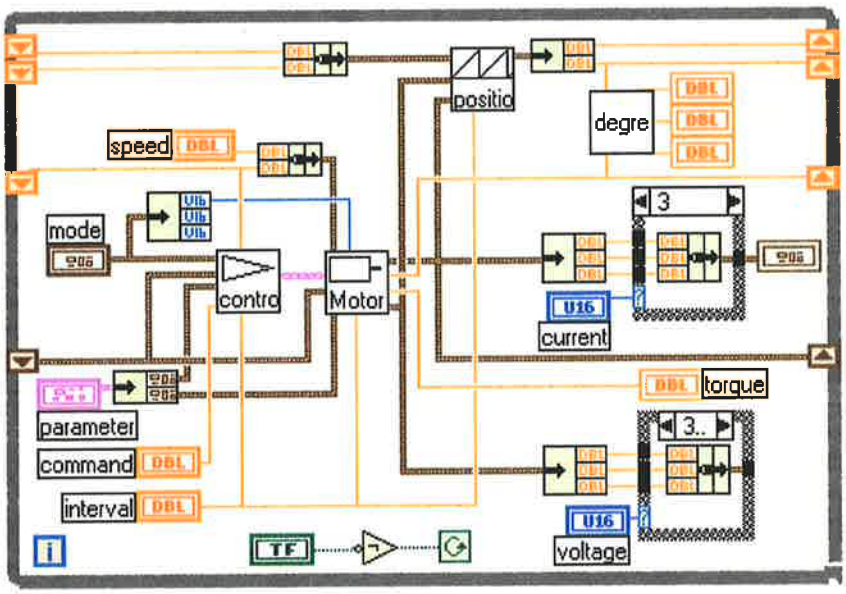

Figure 5.3 Block diagram of the position estimation simulation VI

5.3.2 Simulation Results of the Steady State Operation

In the simulation studies of the position estimation, two sets of motor parameters are used which were given in Table 4.1 (for the trapezoidal PMAC motor) and Table 4.2 (for the sinusoidal PMAC motor) of Chapter 4.

Figure 5.4 shows the simulation results of the rotor position estimation for the sinusoidal PMAC motor. The results are given while the motor drive was operating: under steady state, at 50Hz, the DC link voltage of 150V, and the command current of 2.5A. The current controller used in this test was PWM at a modulation frequency of 5KHz. The figure given illustrates the waveforms of a phase current, the measured (or actual) rotor position (M-position), the estimated rotor position (E-position) and the position error. As demonstrated in

the figure, the proposed rotor position estimation algorithm can estimate the rotor position accurately. Under the ideal conditions, the error (due to the calculation delay in the simulation) between the measured and the estimated rotor position is very small (about 0.2 degree), which indicates that the estimated rotor position signal can replace the measured signal as a position feedback.

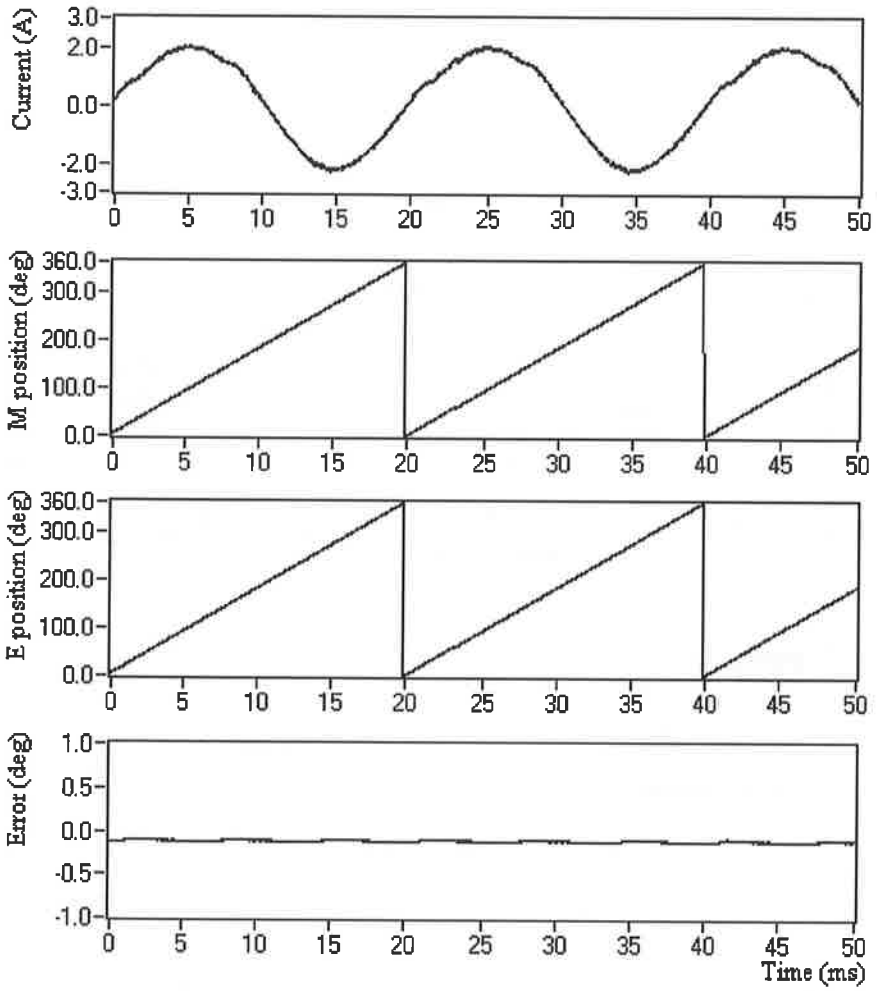

Figure 5.4 Simulation results of the rotor position estimation for the sinusoidal PMAC motor: f =50Hz,V_{dc}=150V, PWM current controller at a frequency of 5KHz, $I_{max(ref)}$ = 2.5A.

Figure 5.5 shows the simulation results of the rotor position estimation of the sinusoidal PMAC motor under the similar operating conditions as in Figure 5.4, but under a very low operating speed, 1Hz (2.14rpm). It can be seen that the proposed rotor position estimation algorithm can also estimate the rotor position signal accurately in very low speed range. Although a very small delay (about 0.2 degree) has been observed between the estimated and the actual rotor position, this is considered negligible and not to influence the correct operation of the motor drive.

These simulation results demonstrate that the proposed rotor position estimation algorithm is capable of operating in a wide range of speed in the PMAC motor drives.

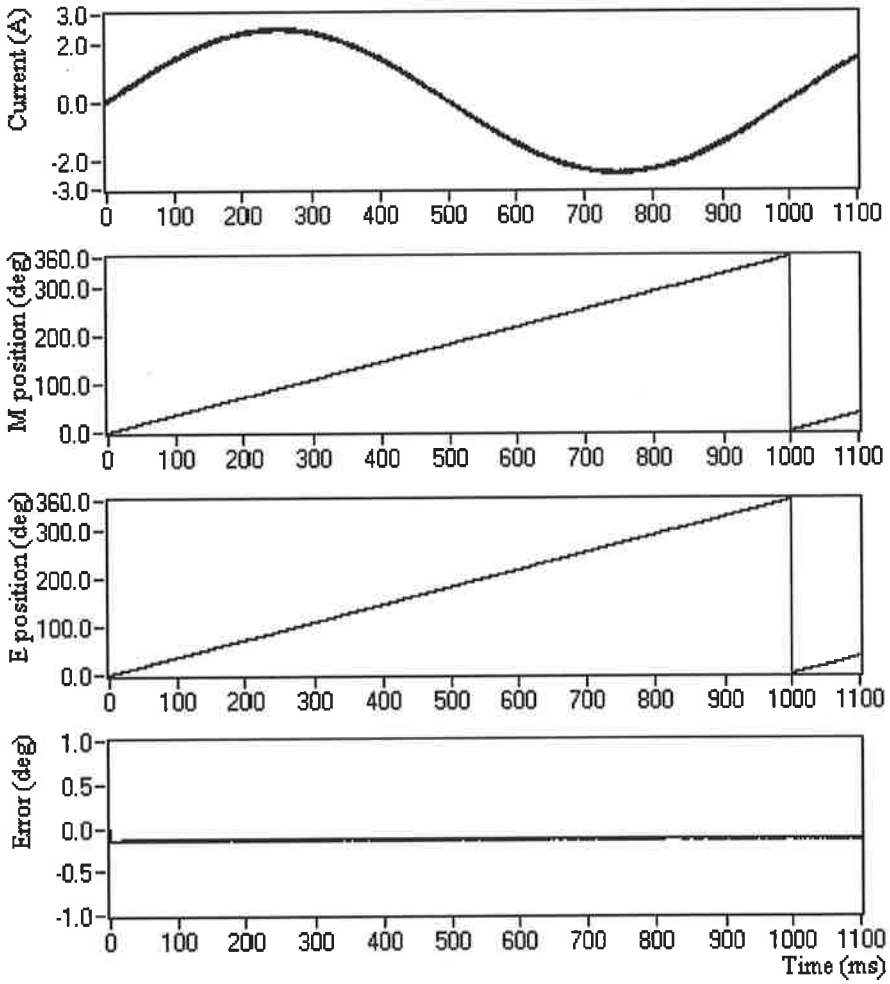

Figure 5.5 Simulation results of the rotor position estimation for the sinusoidal PMAC motor: f =1Hz,V_{dc}=150V, PWM current controller at a frequency of 5KHz, $I_{max(ref)}$ = 2.5A.

The above simulation studies were also repeated for the trapezoidal PMAC motor drive while the reference current was in rectangular shape. The identical position estimation algorithm was used in this study while the back-EMF function was "trapezoidal". The simulation results of the rotor position estimation at high-speed operation are given in Figure 5.6. The operating settings were: a DC link voltage of 70V, a speed of 50Hz, the PWM current controller at a modulation frequency of 5KHz and a command current of 2.5A.

Figure 5.6 displays the waveforms of one phase current, the measured rotor position, the estimated rotor position and the position error. In this high-speed operation without the current control, the simulation results demonstrate that the proposed algorithm can accurately estimate the rotor position in the trapezoidal PMAC motor drive. Although the position error

in this mode of operation is greater than that of in Figure 5.5 it is still small enough not to influence the correct operation of the motor drive. The reason of the greater position error is that the estimation algorithm is sensitive to the current increments as can be seen in Equation 5.8. The position error is due to the fast change in the phase currents during the commutation intervals causing a larger error in the estimated position. It should be noted here that this increase in the position error would be targeted later and corrected by the auto correctional action.

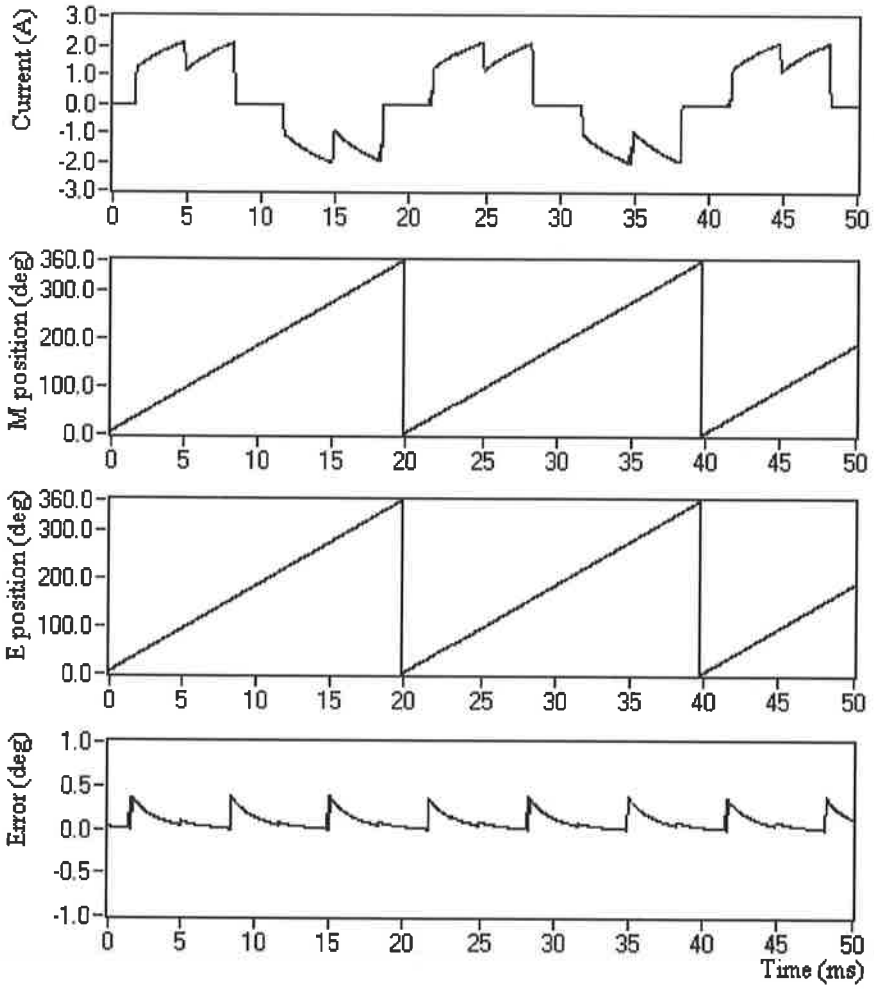

Figure 5.6 Simulation results of the rotor position estimation for the trapezoidal PMAC motor: f =50Hz,V_{dc}=70V, PWM current controller at a frequency of 5KHz, $I_{max(ref)}$ = 2.5A.

Figure 5.7 shows the rotor position estimation in the trapezoidal PMAC motor drive operating at a frequency of 1Hz. Again, a very small position error was observed in this operating mode. Therefore, it can be concluded that the proposed rotor position estimation algorithm can generate position data in a wide range of operating speed, which can be used in the sinusoidal as well as in the trapezoidal PMAC motor drives.

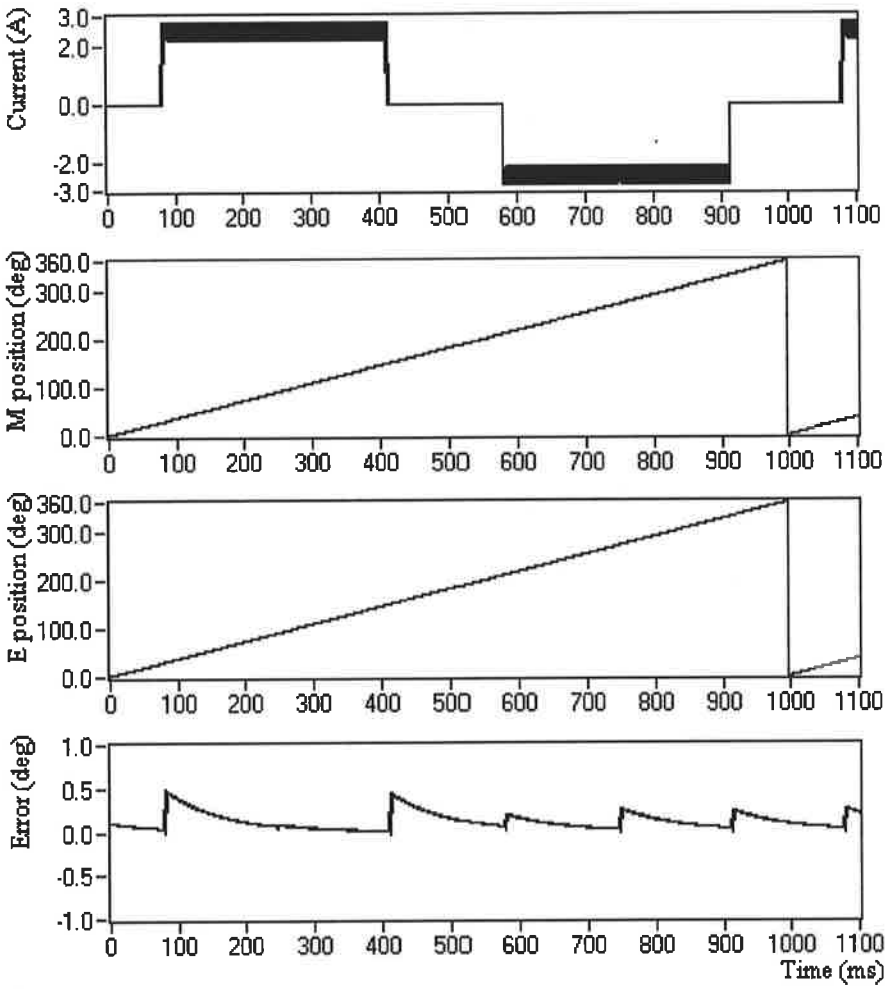

Figure 5.7 Simulation results of the rotor position estimation for the trapezoidal PMAC motor: f =1Hz,V_{dc}=70V, PWM current controller at a frequency of 5KHz, $I_{max(ref)}$ = 2.5A.

5.3.3 Position Sensorless PMAC Drive System

In the simulation tests given above, the estimated rotor position signal is only used to compare with the actual rotor position signal. In this section, we will simulate the operation of the position sensorless motor drive while the estimated position was the primary position sensor in the closed loop control.

The block diagram of the position sensorless drive system is shown in Figure 5.8. This control system consists of five blocks: position estimator, speed observer, speed regulator, current command generator and current controller. The position estimator calculates the rotor position signal using the measured three-phase currents and voltages, and feeds back to the current command generator to implement self-synchronized control. Meanwhile, the

estimated rotor position data is also used to obtain the rotor speed using the speed observer, which is then used in closed loop speed control.

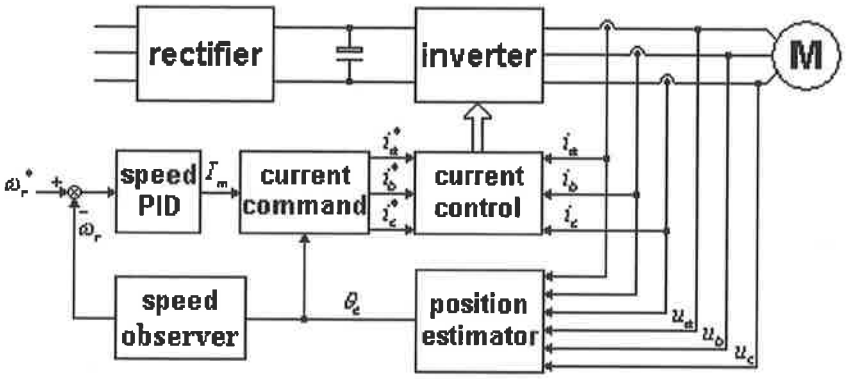

Figure 5.8 Block diagram of the complete position sensorless drive

Theoretically, the derivative of the rotor position is the motor speed, that is,

$$\omega_e = \frac{\Delta\theta_e}{\Delta t} \tag{5.18}$$

In a practical position sensorless drive system, however, the rotor position increment $\Delta\theta_e$ is estimated using the measured voltages and currents, which always contain some noises. Such noises may produce error in the rotor position increment $\Delta\theta_e$, which is amplified by the derivative function. Therefore, the use of filter is necessary in the estimation of the rotor speed from the rotor position data.

Although a low-pass digital filter can be used to achieve filtering noisy signals, but the dynamic performance of such filter in highly noisy environment is found insufficient [23]. The block diagram of the speed observer used in this study is shown in Figure 5.9, which can be divided into two principal sections: the open-loop system model and the feedback loop. The latter loop is necessary to ensure the correct operation at high precision estimation and

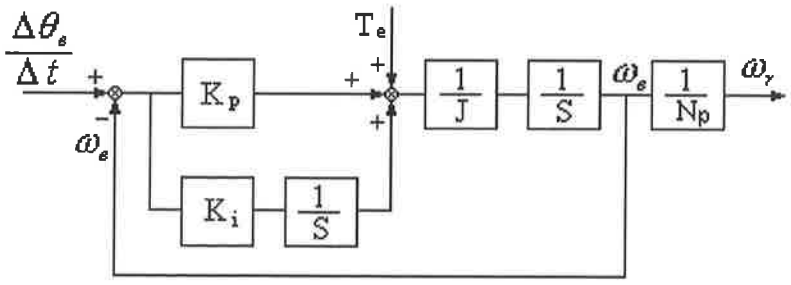

Figure 5.9 Block diagram of the speed observer

operation under parameter variations. As shown in the figure, the feedback signal (estimated electrical angular speed ω_e) is subtracted from the derivative of the rotor position to generate the speed error. The PI regulator is used to ensure a good dynamic and steady performance in the observer. The electromagnetic torque used in the observer is estimated using the measured three-phase currents that are based on Equation 4.18.

Using the angular speed estimated from the speed observer, a closed-loop speed control is implemented using an ordinary PI speed regulator with a limiter as shown in Figure 5.8. Output of the speed PI is usually considered as the torque command of the motor drive. In a surface PM motor, the torque is proportional to the amplitude of the excitation currents, assuming that the currents are in phase with the rotor position. Therefore, the torque command is directly used as the amplitude of the current command, which is then used to generate the required sinusoidal or rectangular reference currents. Finally, the current controller (hysteresis or PWM) forces the actual three-phase currents to follow the reference currents.

5.3.4 Dynamic Simulation Results

Based on the block diagram of the position sensorless drive system shown in Figure 5.8, another simulation VI is designed to test the dynamic performance of the position sensorless PMAC motor drive. The block diagram of this VI is similar to the VI shown in Figure 5.3. The only difference is that the rotor position signal used in the current control icon is obtained from the rotor position estimator icon. In addition, the speed observer icon was added into the block diagram in Figure 4.8 and the observed speed was used as the speed feedback in the dynamic simulation VI.

Firstly, the dynamic simulation study was carried out using the sinusoidal PMAC motor. The results are shown in Figure 5.10, which has the following operating settings: a DC link voltage of 250V, a maximum command current of 10A, a moment of inertia of 0.8Nm^2, a load torque of 10Nm, and under the PWM current controller at a modulation frequency of 5KHz. In the simulation study, the motor was accelerated from standstill up to a constant speed of 70 rpm, and the speed was reduced down to zero and then it was accelerated in reverse direction up to a constant speed of -70 rpm. Figure 5.10 shows the waveforms of the three-phase currents, the observed rotor speed, the estimated rotor position, and the position

error. As seen in the figure, the estimated rotor position signal is accurate enough over the entire operating speed range, which makes the position estimation practical.

The simulation VI was also used to study the dynamic performance of the trapezoidal PMAC motor. Figure 5.11 shows the simulation results of the three-phase currents, the rotor speed, the estimated rotor position, and the position error. The setting of the simulations under this operating condition were: a DC link voltage of 70V, a maximum command current of 10A, a moment of inertia of $0.02Nm^2$, a load torque of 2Nm, and the PWM current controller at a modulation frequency of 5KHz. Similar to the previous test condition, the motor again accelerates from standstill up to a constant speed of 600 rpm, and then stops and accelerates in the reverse direction up to a constant speed of -600 rpm. The simulation results demonstrate that the proposed position sensorless technique is also suitable for the trapezoidal PMAC motor drive.

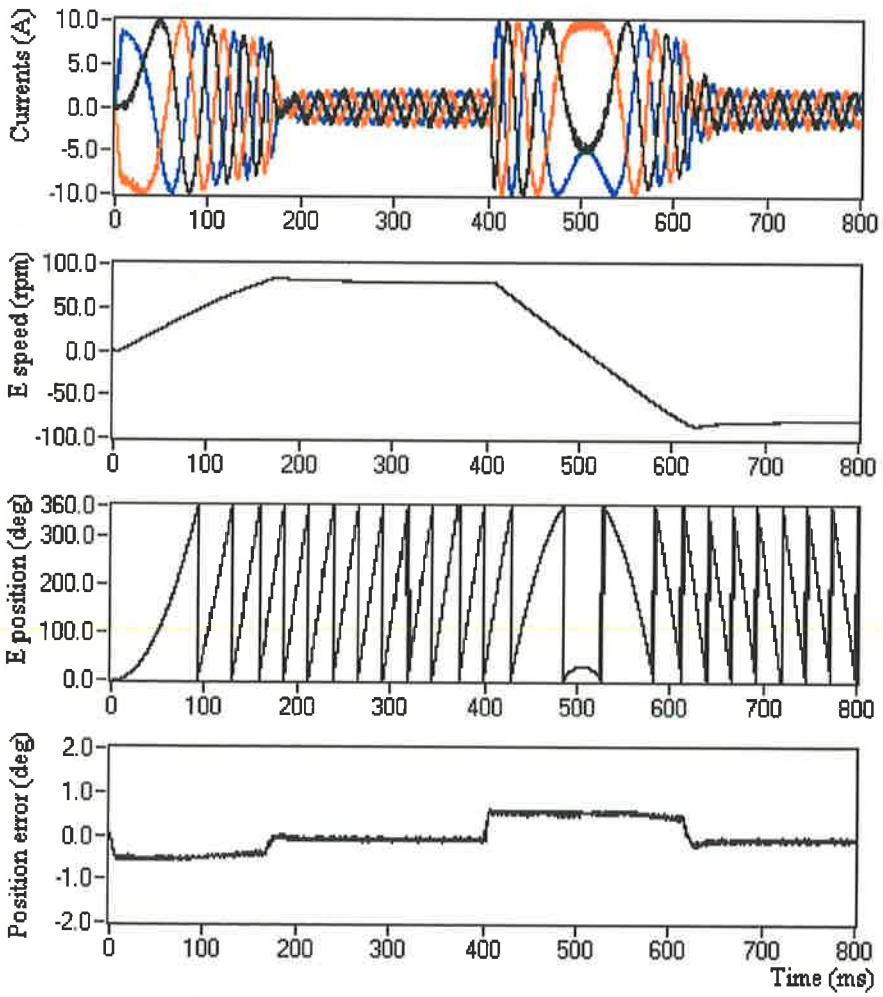

Figure 5.10 Simulation results of the position sensorless control of the sinusoidal PMAC motor drive: V_{dc}=250V, PWM current controller at frequency of 5KHz, $I_{max(ref)}$ = 10A, J=0.8Nm^2, T_l =10Nm.

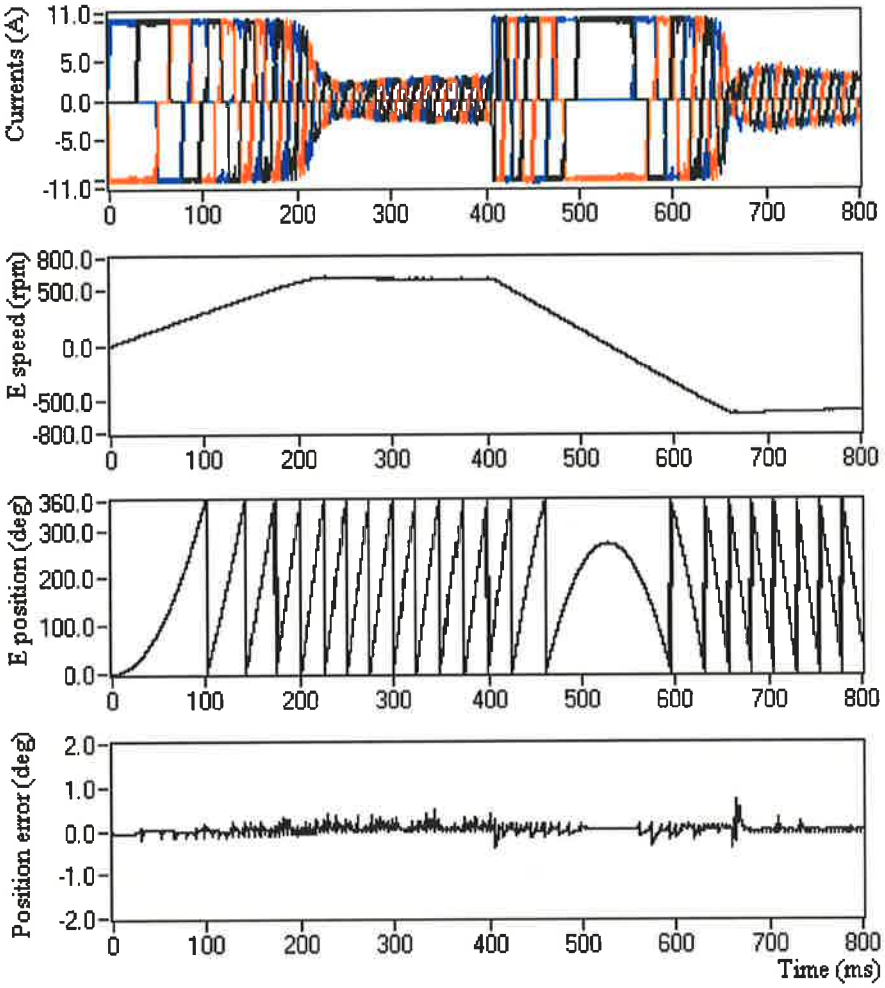

Figure 5.11 Simulation results of the position sensorless control of the trapezoidal PMAC motor drive: V_{dc}=70V, PWM current controller at a frequency of 5KHz, $I_{max(ref)}$ = 10A, J=0.02Nm^2, T_l =3Nm.

5.4 Robustness Analysis and Algorithm Improvement

As demonstrated in the simulation results, the proposed rotor position estimation algorithm can produce accurate rotor position data under the ideal conditions. In a practical drive system, however, the parameters of the motor vary significantly for various reasons, such as temperatures and magnetic saturations. In addition, there are no ideal measurement circuits in practice. The practical measurement circuits are affected from electrical noisy environments. Since the rotor position algorithm is based on a series of calculations that utilize the motor parameters, the phase currents and voltages, the parameter deviations and the measurement inaccuracies should be considered in the real-time motor drive systems, which directly affect the reliability and the robustness of the control algorithm. In this section, the robustness of the position estimation algorithm against the above-mentioned errors and

noises will be discussed, and suggested improvements will be explained to achieve a higher robustness.

5.4.1 Error and Noise Analyses

In a practical motor driver system, the major possible errors and noises include:

a) **Parameter variations:** variations of phase winding resistance, back-EMF constant, and equivalent inductance, which are primarily due to the temperature variation or the magnetic saturation;

b) **Measurement errors:** are due to the offset errors and scaling errors of the current and the voltage sensors or the signal conditioning amplifiers;

c) **Measurement noises:** are due to the electromagnetic interference in the measuring circuits and signal cables etc.

In a practical motor drive system, the parameters are non-linear functions of time and temperature or various other operating conditions. Since the measurement errors and noises are related to the power electronics systems, the associated software and the operation environments, it is different or maybe impossible to quantify accurately. However, it is useful to analyse the rotor position estimation error caused by the parameter and measurement errors. With such analysis, the features of the rotor position estimation errors caused by each source of the errors can fully be understood, and the knowledge gained may be utilized to improve the rotor position estimation algorithm to achieve higher robustness.

According to the classifications of the errors, the total position increment error due to the various parameters and the measurement errors can be expressed as:

$$\delta\theta_e = \delta\theta_{eR} + \delta\theta_{eKe} + \delta\theta_{eL} + \delta\theta_{eio} + \delta\theta_{evo} + \delta\theta_{eia} + \delta\theta_{eva} + \delta\theta_{e\mu} \tag{5.19}$$

where, $\delta\theta_e$ is total position increment error, and

$\delta\theta_{eR} = \dfrac{N_p \Delta R I_m \Delta t}{k_e}$ is the error due to the winding resistance variation of ΔR;

$\delta\theta_{eke} = \frac{\Delta k_e}{k_e}\Delta\theta_e$ is the error due to the back-EMF constant variation of Δk_e;

$\delta\theta_{eL} = \sqrt{3}\frac{N_p \Delta L\, I_m \Delta t}{k_e}$ is the error due to the equivalent inductance variation of ΔL;

$\delta\theta_{eio} = -\frac{3}{4}\frac{N_p R\,\Delta t}{k_e}[\delta I_a e_2(\theta_e) + \delta I_b e_3(\theta_e) + \delta I_c e_1(\theta_e)]$ is the error due to the current measurement offsets of δI_a, δI_b, and δI_c in each phase;

$\delta\theta_{evo} = \frac{3}{4}\frac{N_p\,\Delta t}{k_e}[\delta V_a e_2(\theta_e) + \delta V_b e_3(\theta_e) + \delta V_c e_1(\theta_e)]$ is error due to the voltage measurement offsets of δV_a, δV_b, and δV_c in each phase;

$\delta\theta_{eia} = (1+\sqrt{3})\frac{N_p R\,\delta\, I_m \Delta t}{k_e}$ is the error due to the current amplitude error of δI_m;

$\delta\theta_{eva} = 2\frac{N_p \delta V_m \Delta t}{k_e}\cos(\varphi + \pi/3)$ is the error due to the voltage amplitude error of δV_m;

$\delta\theta_{e\mu} = -\frac{3}{4}\frac{N_p \Delta t}{k_e}[\mu_a e_2(\theta_e) + \mu_b e_3(\theta_e) + \mu_c e_1(\theta_e)]$ is the error due to the measurement noises of μ_a, μ_b, and μ_c in each phase.

In the derivation of the total position increment error, it is assumed that the back-EMF functions are sinusoidal and the phase currents are in phase with the corresponding back-EMFs. The principal purpose of the error formula is to understand the fundamental features of each position increment error and to find possible strategies to eliminate or reduce their influence on the rotor position estimation in a practical position sensorless motor drive system. The detail derivations of the above formulas are given in Appendix C.

First, let us study the position increment error caused by the winding resistance variation. From the above expression, it can be seen that the error is proportional to the amplitude of the phase currents I_m. For a constant load current, the position increment error is also constant and independent from the motor speed, so that the error can cause significant influence on the rotor position estimation when motor is running at low speed range.

The position increment error caused by back-EMF variation, however, is proportional to the estimated value of the rotor position increment. This means that the error is proportional to the motor speed and the influence of the error on rotor position estimation reduces if the motor speed decreases. At zero speed, no error is caused by the back-EMF variation. Therefore, the error caused by the back-EMF variation is easier to compensate than the error caused by the other factors.

Let us now consider the expression of the position increment error caused by the equivalent inductance variation. Such error has similar feature as in the resistance variation, which is proportional to the amplitude of the phase currents and may effect the rotor position estimation significantly, specifically at low speed operation. In addition, the error caused by equivalent inductance variation has another feature, which will be discussed later in the section of the algorithm improvement.

The position increment errors caused by the current and the voltage measurement offsets have the same effect, which are normally sinusoidal functions of the rotor position and not constant, even at steady state. Their amplitudes are proportional to the sum of three-phase sinusoidal offsets and independent from the motor speed and the load current. If the offset values of three phases are same, the position increment error will be zero. In order to reduce these errors, therefore, the three-phase offsets should be set as equal as possible, and ideally they should be set to zero.

However, the position increment errors caused by the amplitude measurement errors have different features than that of the offsets. It can be seen form the expression of the position increment errors caused by current amplitude measurement errors that such errors are similar to the combination of the errors that were due to the winding resistance and the equivalent inductance variations.

The position increment errors caused by the voltage amplitude measurement errors are independent of the motor speed and the load current, but they are related to the power factor

angle φ of the motor. Therefore, these errors have serious influence on the rotor position estimation, specifically at dynamic state.

The position increment error caused by the measurement noises has the same feature as the measurement offsets. If the noises in three phases are same, the position increment error becomes zero.

5.4.2 Robustness Analysis

As discussed above, the parameter variations and the measurement errors cause an error on the estimated incremental position. If such error is not eliminated or corrected, it may accumulate over a time period, such as an integration time period, and causes catastrophic failures in the motor drive, such as loosing synchronism. Therefore, a position error correction has to be integrated into the position estimation algorithm. This section will provide the basics of the correctional action and will discuss its robustness.

It can be assumed that if the back-EMF functions of the PMAC motor are sinusoidal and the motor is excited by the sinusoidal currents, the flux linkage increments should be sinusoidal functions that can be given as:

$$\begin{aligned} \Delta\psi_a &= \Delta\psi_m \sin\theta_e^* \\ \Delta\psi_b &= \Delta\psi_m \sin(\theta_e^* - 2\pi/3) \\ \Delta\psi_c &= \Delta\psi_m \sin(\theta_e^* + 2\pi/3) \end{aligned} \tag{5.20}$$

where, $\Delta\psi_m$ is the amplitude of the flux linkage increments; θ_e^* is the phase angle of the flux linkage increments.

Under the ideal conditions, the value of the position increment estimated from Equation 5.16 only depend on the amplitude of the flux linkage increments. However, disturbances may appear in the position increment, which are mainly due to the parameter variations and/or the measurement errors. When the position increment error is feedback to the back-EMF functions through the internal closed loop, it causes a phase difference between the flux linkage increments and the back-EMF functions.

Let us now assume that the flux linkage increments have a phase angle of θ_e^*, which reflect the actual rotor position value, the estimated rotor position increment based on the basic algorithm 2 can be rewritten as:

$$\Delta\theta_e = \frac{N_p}{k_e}\cdot\frac{\Delta\psi_m\left[\sin\theta_e^*\sin(\theta_e-2\pi/3)+\sin(\theta_e^*-2\pi/3)\sin(\theta_e+2\pi/3)+\sin(\theta_e^*+2\pi/3)\sin\theta_e\right]}{\sin\theta_e\sin(\theta_e-2\pi/3)+\sin(\theta_e-2\pi/3)\sin(\theta_e+2\pi/3)+\sin(\theta_e+2\pi/3)\sin\theta_e}$$
$$=\frac{2N_p\Delta\psi_m}{k_e}\cos(\theta_e^*-\theta_e-\pi/3) \qquad (5.21)$$

In order to explain the robustness of the basic algorithm 2 by comparing with the basic algorithm 1, the estimated rotor position increment based on basic algorithm 1 can also be rewritten under the identical assumptions,

$$\Delta\theta_e = \frac{N_p}{k_e}\cdot\frac{\Delta\psi_m\left[\sin\theta_e^*\sin\theta_e+\sin(\theta_e^*+2\pi/3)\sin(\theta_e+2\pi/3)+\sin(\theta_e^*-2\pi/3)\sin(\theta_e-2\pi/3)\right]}{\sin\theta_e\sin\theta_e+\sin(\theta_e+2\pi/3)\sin(\theta_e+2\pi/3)+\sin(\theta_e-2\pi/3)\sin(\theta_e-2\pi/3)}$$
$$=\frac{N_p\Delta\psi_m}{k_e}\cos(\theta_e^*-\theta_e) \qquad (5.22)$$

Equation 5.21 and 5.22 are plotted in Figure 5.12. Under the ideal conditions, the estimated rotor position θ_e should be equal to the phase angle θ_e^* of the flux linkage increments ($\theta_e^*=\theta_e$) and the estimated rotor position increment is directly proportional to the amplitude of the flux linkage increments. If an error causes the estimated rotor position to differ from the phase angle of flux linkage increments, the difference is fed back by the internal closed-loop through the back-EMF functions, and the next step value of the position increment estimation is corrected within a range.

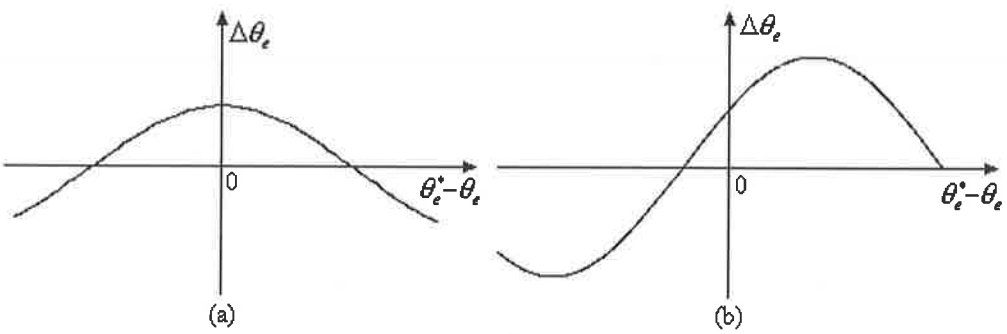

Figure 5.12 Auto-correctional action: (a) Algorithm 1, (b) Algorithm 2

For example, if the estimated rotor position leads the phase angle of the flux linkage increments ($\theta_e^*<\theta_e$), as seen from Figure 5.12, the phase difference produced by the feedback reduces the new estimated value of the position increment both in the basic

algorithm 1 and 2. As a result, further advance of the new rotor position estimation is limited. Conversely, if the estimated rotor position lags the phase angle of the flux linkage increments ($\theta_e^* > \theta_e$), the basic algorithms 1 and 2 have different modified results. For the basic algorithm 1, the phase difference also reduces the new estimated value of the position increment, which forces the new rotor position estimation to delay further and to accumulate the phase difference (as can be observed in Figure 5.12 (a)). While, the basic algorithms 2 increases the new estimated value of the position increment by the help of the phase difference (as can be observed in Figure 5.12 (b)). Therefore, further delay on the new rotor position estimation is limited. Hence, the rotor position estimation shift due to the parameter deviations or the measurement inaccuracies can be limited within an acceptable range by the basic algorithm 2. This is the principle of the auto-correctional action, in which the basic algorithm 2 corrects the integration shift utilizing the internal closed loop.

As discussed above, since the basic algorithm 1 has no auto-correctional ability in one direction of the phase difference, the rotor position increment errors caused by the parameter deviations and the measurement errors will be accumulated by the integration, which significantly influence the accuracy of the estimated rotor position. Therefore, the basic algorithm 1 is not suitable to be used in the practical motor drive system. Now on in the thesis, we will use "the basic algorithm" to indicate "the basic algorithm 2".

A qualitative analysis of the auto-correctional action of the basic position estimation algorithm has been explained above. To demonstrate the analysis about the robustness of the algorithm and provide some quantitative results, several simulation studies were performed, and some results were given for the sinusoidal PMAC motor drive.

Figure 5.13 shows three simulation results of the position error, which were obtained under the steady-state operation condition using the basic algorithm. The drive settings in the VI were: a DC link voltage of 150V, the PWM current controller operating at a modulation frequency of 5KHz, a command current of 2.5A, and a operating speed of 25Hz.

If all the parameters in the position estimator are identical to that of the simulation model of the motor, the rotor position can be accurately estimated using the basic algorithm. If the parameters (the winding resistance, the back-EMF constant, and the equivalent inductance) of the motor vary ±20% artificially, the position estimation produces some static errors, but the errors are not accumulated and can be limited within 2-3% of one electrical cycle, 360^0,

by the basic algorithm that accommodates the auto-correctional action using the internal closed loop.

The position estimation errors have the same feature as the position increment errors, which are described in Section 5.4.1. It can be seen in the figure that the values of the negative errors are slightly greater than the positive errors. This is because the basic algorithm has different auto-correctional ability for the positive and the negative errors, which can be observed in Figure 5.12(b).

The auto-correctional ability of the basic algorithm is based on the phase difference between the estimated rotor position and the phase angle of flux linkage increments. The variations of the equivalent inductances not only produce the position increment error but also affect the phase angle of the flux linkage increments. Therefore, the auto-correctional ability for the equivalent inductance variations is weaker than the other parameter variations. This is the primary reason of the noises produced on the position estimation due to the equivalent inductance variations.

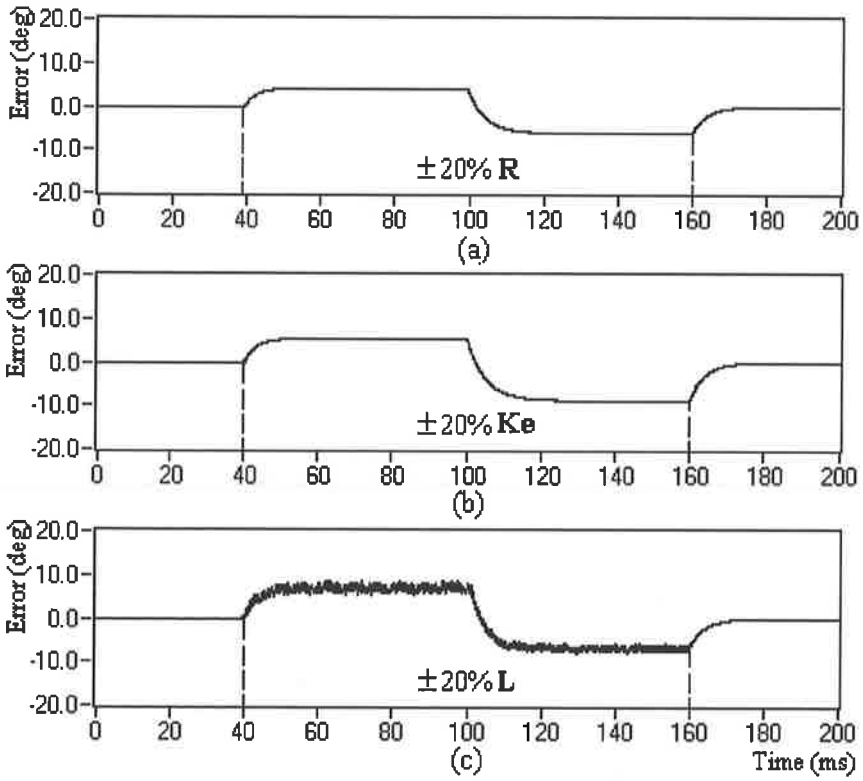

Figure 5.13 Simulation results of the position estimation errors for the basic algorithm with the sinusoidal PMAC motor parameters: f=25Hz, V_{dc}=150V, PWM current controller at a frequency of 5KHz, I_m =2.5A. (a) Winding resistance varies ±20%; (b) Back-EMF constant varies ±20%; (c) Equivalent inductance varies ±20%.

Under the identical simulation settings, the results of the position estimation errors are displayed in Figure 5.14, which considers that the current measurements are inaccurate. Figure 5.14(a) shows the position estimation errors due to a current measurement offset of 10%. As illustrated in the figure, within the time interval of 0-100ms, the offsets introduced to all three phases are identically, so that the position estimation error is nearly equal to zero, as in the qualitative analysis of the position increment error given in Section 5.4.1. If the offsets introduced are different in three phases (starting at 100ms in the figure), the position estimation error cannot accumulate. However, it varies as a sinusoidal function with respect to the rotor position.

Figure 5.14(b) shows the position errors due to a current amplitude error of ±10%. As can be demonstrated by the qualitative analysis on the position increment error, the position error due to the current amplitude error has the same effect as in the parameter variations. Some static errors appear on the position estimation, which can be limited within 2-3% one electrical cycle, 360^0, by the basic algorithm. If the current measurements contain 10% noise,

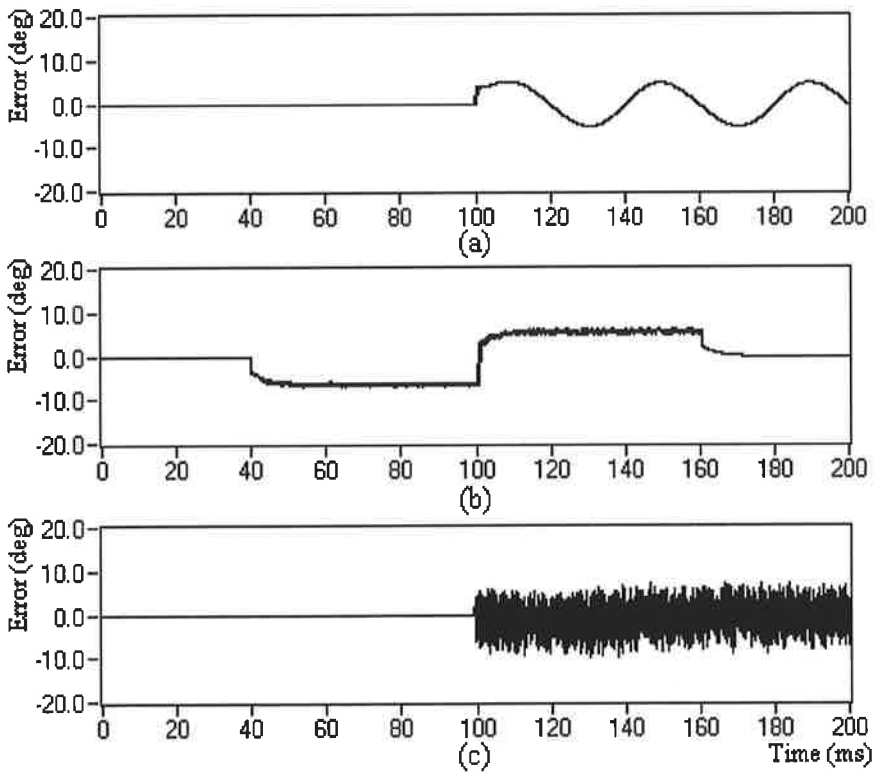

Figure 5.14 Simulation results of the position estimation errors for the basic algorithm with the sinusoidal PMAC motor parameters and operation conditions: f=25Hz, V_{dc}=150V, PWM Current Controller with frequency of 5KHz, I_m=2.5A. (a) Current measurement offset of 10%; (b) Current amplitude error of ±10%; (c) 10% measurement noises in current.

the simulation results are shown in Figure 5.14 (c). Similarly, the injected noises of three phases are identical until 100ms. Hence the position estimation error is nearly equal to zero. As demonstrated in the figure, at 100ms, different level of random noises are injected into each phase current. The result indicates that relatively larger random errors appear on the position estimation since the algorithm is sensitive to the current variations. However, the position estimation errors are limited to 3% one electrical cycle, 360^0, by the basic algorithm, which is an acceptable level in the practical motor drive systems.

Similarly, when the voltage measurements are inaccurate, the simulation results of the position estimation errors are shown in Figure 5.15. Figure 5.15(a) shows the position error due to a voltage measurement offset of 10%. Since the offsets introduced are same in all three phases until 100ms, the position estimation error is nearly equal to zero, which can be confirmed by the qualitative analysis on the position increment error. However, the position estimation error varies as a sinusoidal function with respect to the rotor position if the offsets introduced are different, which occurs after 100ms on the figure.

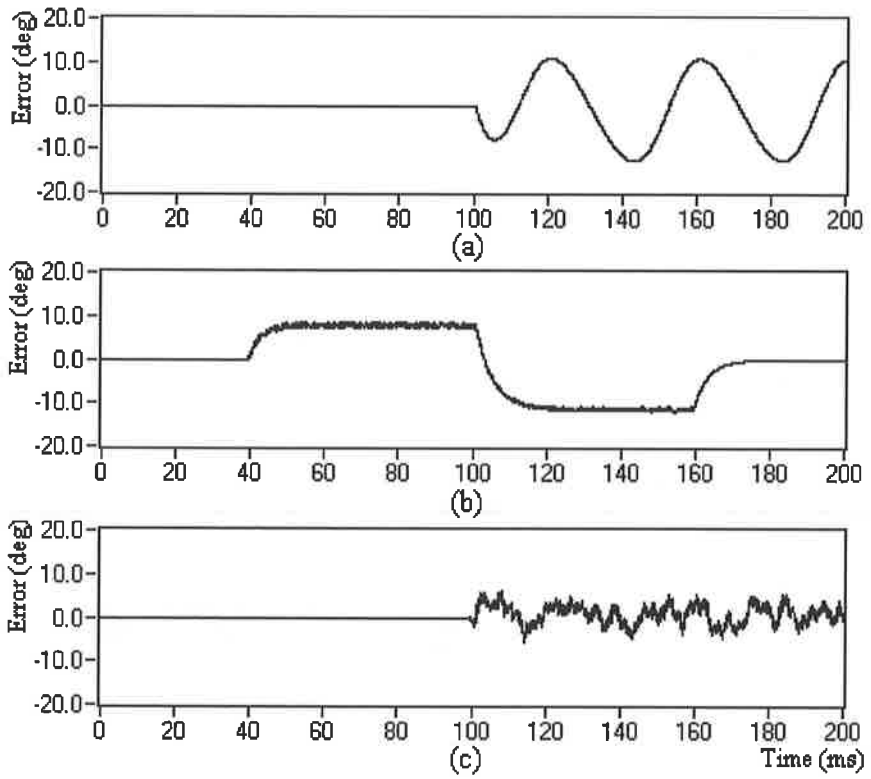

Figure 5.15 Simulation results of position estimation errors for the basic algorithm with the sinusoidal PMAC motor parameters: f=50Hz, V_{dc}=150V, PWM current controller at a frequency of 5KHz, I_m =2.5A. (a) Voltage measurement offset of 10%; (b) Voltage amplitude error of ±10%; (c) 50% measurement noises in voltage.

When the position errors of the voltage measurement offset are compared with the current measurement offset, an increase can be observed. This is due to the fact that, the amplitude values of the flux linkage increments mainly depend on the voltage amplitude. Therefore, it desirable to have equal voltage offsets in the practical motor drive.

If the voltage amplitude has ±10% error, the simulation result of the position estimation error is given in Figure 5.15(b). This error has the same feature as in the current amplitude error. In a practical motor derive fed from an inverter, the voltages of the motor are a series of high-frequency PWM voltage pulses, so that the measurements of such voltages include higher noises. In Figure 5.15 (c), the simulation result of the position estimation error is given under an injected voltage noise of 50%. Again, it can be observed from the figure that the position estimation error is nearly equal to zero if the injected noises are equal in all three phases. However, a large position error appears on the position estimation under the unequal measurement noises.

Using the simulation results and the discussions given above, it can be concluded that the basic algorithm can limit the position estimation errors, which may be caused by the parameter deviations and the measurement inaccuracies. In other words, the basic algorithm possesses robustness with respect to the parameter deviations and the measurement inaccuracies up to a level. In addition, it can be said that this feature of the estimation algorithm increases the reliability of the motor drive due to the insusceptibility to the environmental factors.

However, a degree of static position estimation error is present in the simulation results, which cannot be eliminated by the basic algorithm. Moreover, since the auto-correctional ability depends on the phase difference between the flux linkage increments and the back-EMF functions, the auto-correctional action is weaker if the motor speed slows down. At very low speed range, the auto-correctional action may be not strong enough to correct the static position estimation errors, and the errors may be accumulated. Therefore, the basic algorithm may not be suitable at very low speed operation; hence an algorithm improvement is required, which will be studied in the following section.

5.4.3 Algorithm Improvement

As stated above, the static errors are acceptable at high-speed operation of the motor drive. However, the static errors may be accumulated at low speeds by the integration mainly due to

the poor auto-correctional ability of the algorithm. This is more observable when the estimated rotor position lags the flux linkage increments. Therefore, to eliminate the impact of such errors at low speeds, a form of algorithm improvement is required.

To achieve this, let us analyse the basic algorithm again. The auto-correctional ability is based on the phase difference between the phase angle of the flux linkage increments and the estimated rotor position. Therefore, to improve the algorithm's performance, a form of phase-locked loop (PLL) method can be integrated into the position estimation algorithm. In addition, the back-EMF functions of a PMAC motor are assumed sinusoidal here. As mentioned before, the flux linkage increments are sinusoidal functions but have different phases angles from the back-EMF functions. Based on the principle of PLL, the three-phase flux linkage increments and three-phase back-EMF functions are considered as vectors. By using the vector product, the phase difference between the two quantities can be given approximately as [88]:

$$\begin{aligned}\left\|\Delta\vec{\psi}\times\vec{e}\right\| &= \Delta\psi_a e_2(\theta_e)+\Delta\psi_b e_3(\theta_e)+\Delta\psi_c e_1(\theta_e)-\Delta\psi_a e_3(\theta_e)-\Delta\psi_b e_1(\theta_e)-\Delta\psi_c e_2(\theta_e)\\ &= \frac{3\sqrt{3}}{2}\psi_m \sin(\theta_e^*-\theta_e)\approx\frac{3\sqrt{3}}{2}\psi_m(\theta_e^*-\theta_e)\end{aligned} \tag{5.23}$$

Using the above equation in the PLL, the phase difference between the phase angle of the flux linkage increments and the estimated rotor position can be estimated. Then, the result is utilizes to compensate the position incremental errors. With this method, a significant improvement on the rotor position estimation algorithm is achieved, and the block diagram of this improved algorithm is shown in Figure 5.16.

In this improved algorithm, the basic algorithm is unchanged, which still predict the next step rotor position value. If there are any parameter deviations or measurement inaccuracies in the system, the predicted value will have a static error. Therefore, the back-EMF functions generated by the predicted rotor position will have different phase angle from that of the flux linkage increments. The PLL added to the algorithm calculates the phase difference between the predicted rotor position and the phase angle of the flux linkage increments, which is then used to compensate the predicted rotor position in the consecutive step. Therefore, the improved rotor position estimation algorithm is called "prediction-rectification" method.

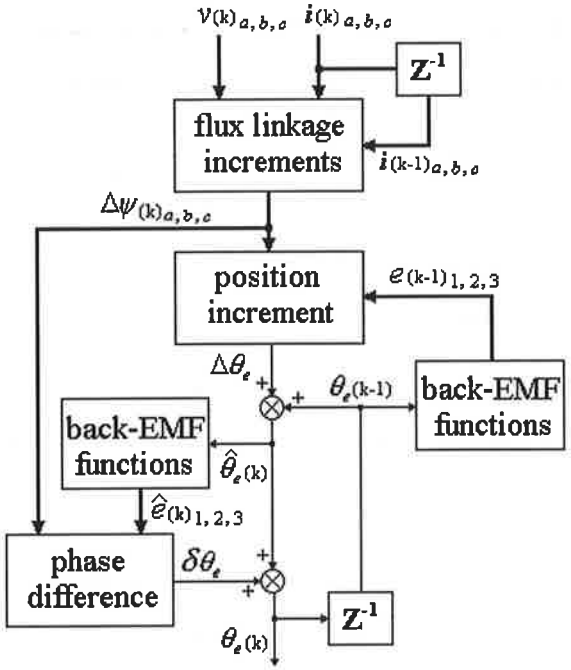

Figure 5.16 Block diagram of the improved position estimation algorithm

In the block diagram of the improved algorithm in Figure 5.16, $\hat{\theta}_{e(k)}$ is the predicted rotor position, and its value is calculated by the basic algorithm. The symbols $\hat{e}_{1(k)}, \hat{e}_{2(k)}, \hat{e}_{3(k)}$ are the predicted back-EMF functions that are generated by the predicted rotor position, which are different than the back-EMF functions used in the calculation of the predicted rotor position. Based on Equation 5.23, the predicted back-EMF functions and the flux linkage increments are used to estimate the phase difference $\delta\theta_e$ in the PLL algorithm.

5.4.4 Simulation Results to Demonstrate the Algorithm Improvement

To demonstrate the effectiveness of the algorithm improvement, extensive simulation studies were performed and the results were compared with the basic algorithm, which were given in the previous sections.

Figure 5.17 illustrates three simulation results of the position errors obtained using the improved algorithm. The settings used in the simulation VI were identical to the settings used in Figure 5.13. In the simulation tests, the indicated motor parameters are artificially varied and the position errors were calculated.

The results indicate that some estimation noises are observable in the improved algorithm even when all of the parameters in the position estimator are identical with that of the

simulation model of the motor, but these are negligible. The static position estimation errors caused by the winding resistance or the back-EMF constant variations are almost eliminated using the improved algorithm, which make the operation of the drive at low speed range possible.

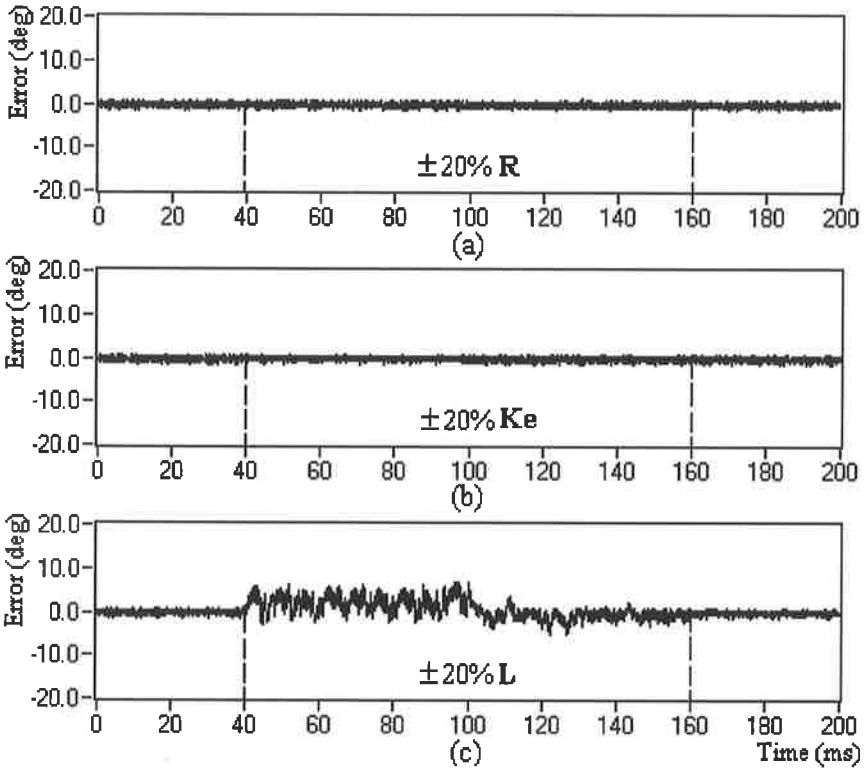

Figure 5.17 Simulation results of the position estimation errors for the improved algorithm with the sinusoidal PMAC motor parameters: f=25Hz, V_{dc}=150V, PWM current controller at a frequency of 5KHz, I_m=2.5A. (a) Winding resistances vary ±20%; (b) Back-EMF constant varies ±20%; (c) Equivalent inductances vary ±20%.

However, the improved algorithm cannot eliminate the position estimation errors caused by the equivalent inductance variations. This is because the improvement of the algorithm is based on the PLL technique. Since the variations of the equivalent inductance can affect the phase of the flux linkage increments, the estimated phase of the flux linkage increments may different from the actual value if the equivalent inductance deviates from the actual value. Therefore, the PLL cannot produce accurate values to rectify the rotor position estimations. However, this is not a serious limitation in a practical motor drive. In a practical non-salient PMAC motor, the equivalent winding inductance is more stable than the other parameters under normal operation conditions, which provide more accurate position estimation. However, it is recommended that the equivalent inductance value in the position estimator

should be identified accurately in order to minimize the position estimation errors in the practical drive.

The simulation results of position estimation errors are shown on Figure 5.18 when current measurements are inaccurate, which has the same operation conditions as described in Figure 5.14. Figure 5.18(a) shows the position error due to a current measurement offset of 10%. Similar to the previous studies, first the values of the offsets were set identical in all three phases (0-100ms), which generated a position estimation error that is nearly equal to zero. After 100 ms, unequal offset values were introduced to the three phases, which generated position estimation error that varies as a sinusoidal function with respect to the rotor position. When compared with the results presented in Figure 5.14, it can be concluded that the improved algorithm cannot reduce the estimated position errors resulting from the current measurement offsets. This is because the shape of the position increment errors that is sinusoidal. The PLL compensation cannot eliminate sinusoidal errors. Therefore, in order to minimize the position estimation errors in the practical motor drive, it is recommended to calibrate the three-phase current measurements accurately.

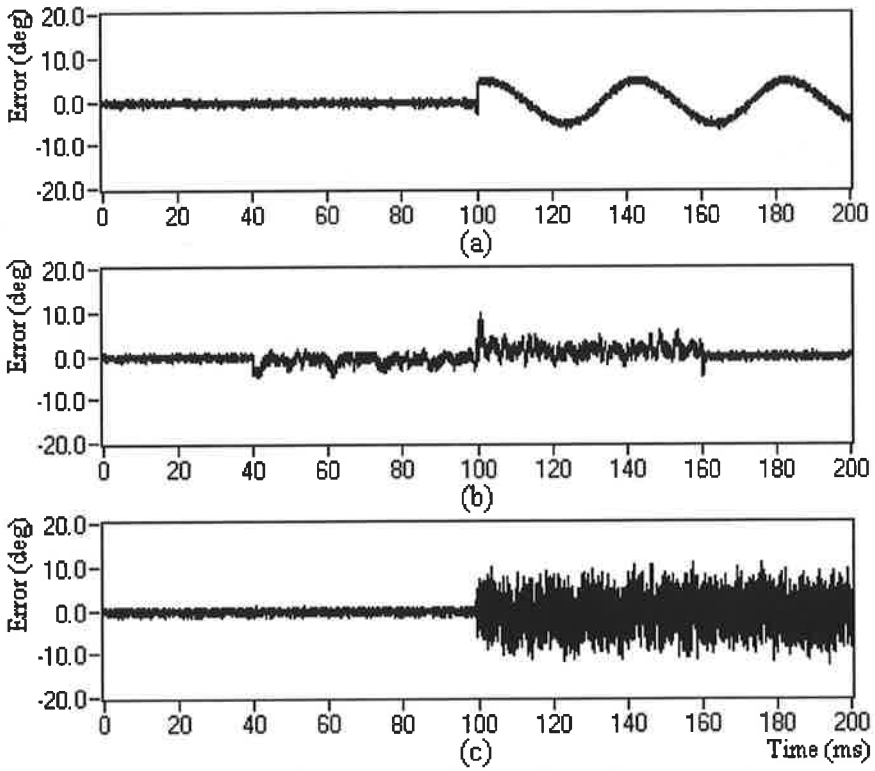

Figure 5.18 Simulation results of the position estimation errors for the improved algorithm using the sinusoidal PMAC motor drive parameters: f=25Hz, V_{dc}=150V, PWM current controller at a frequency of 5KHz, I_m =2.5A. (a) Current measurement offset of 10%; (b) Current amplitude error of ±10%; (c) 10% measurement noises in current.

Figure 5.18(b) shows the position estimation error of the improved algorithm, which is due to a current amplitude error of ±10%. It can be seen in the figure that the position estimation errors can be significantly reduced by the improved algorithm,, but some small estimation noises are present. Such improvement makes the algorithm very suitable at low speed operation.

When the current measurements contain 10% noise, the simulation results of the improved algorithm are given in Figure 5.18(c). This result shows that the random error occurred on the position estimation is significant. Again, since the basic algorithm is sensitive to the current variations, the PLL rectifier has no capability to compensate the random position errors. However, the errors due to the current measurement noise can be limited to the acceptable levels to be used in the practical applications.

Figure 5.19 displays another test results, when the voltage measurements are inaccurate. Figure 5.19(a) shows the position error of the improved algorithm, which is due to a voltage measurement offset of 10%. Like the position estimation error of the current measurement

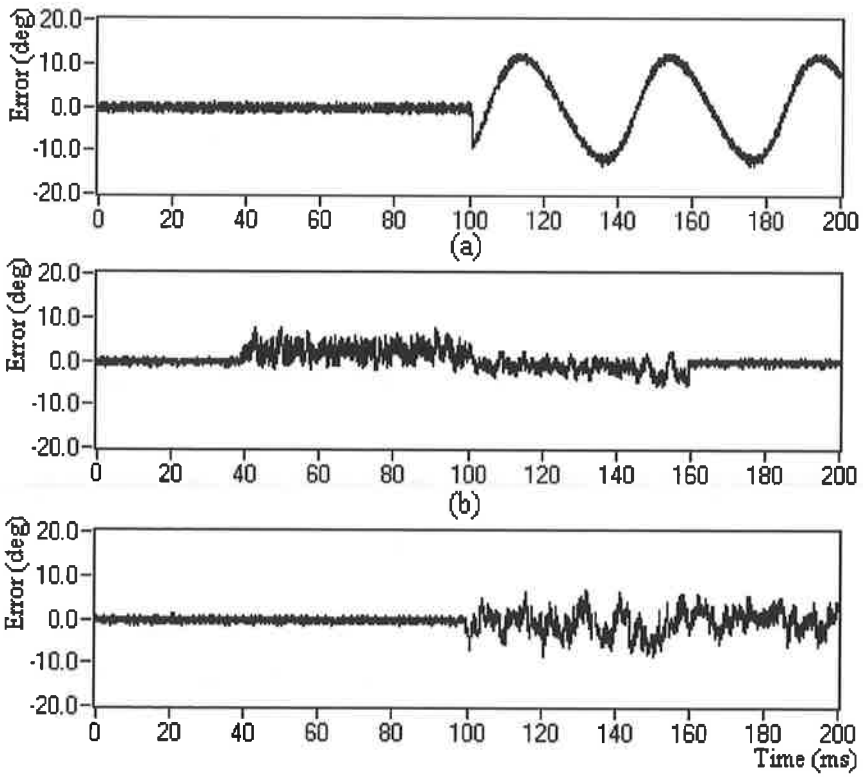

Figure 5.19 Simulation results of the position estimation errors for the improved algorithm using the sinusoidal PMAC motor drive parameters: f=25Hz, V_{dc}=150V, PWM current controller with frequency of 5KHz, I_m =2.5A. (a) Voltage measurement offset of 10%; (b) Voltage amplitude error of ±10%; (c) 50% measurement noises in voltage.

offsets, the improved algorithm cannot eliminate the estimated position errors that are due to the varying voltage measurement offsets.

It should be noted here that the three-phase voltages can be constructed using the switching signals and the DC link voltage of the inverter as will be described in Chapter 6. The reconstructed phase voltages can make the associated offsets identical for all three phases. Therefore, the reconstructed three-phase voltages can eliminate the position estimation error due to the voltage measurement offsets.

When the measured voltage amplitude has ±10% error, the simulation result of the position estimation error is shown in Figure 5.19(b). Comparing with the previous results given in Figure 5.15, it can be seen that the position estimation error was reduced significantly using the improved algorithm.

Similarly, when 50% measurement noise is added to the voltage measurements, the simulation result of the position estimation error is shown in the Figure 5.19(c). As seen in the figure, different random noises in each phase (after 100ms) can produce similar error results before the algorithm improvement. This demonstrates that the improved algorithm cannot compensate the random position errors caused by the large voltage measurement noises.

From the above tests and discussions, it can be concluded that the improved algorithm can reduce the position estimation errors caused by the parameter variations (winding resistance, back-EMF constant and equivalent inductance) and the measurement amplitude errors. In other types of identified errors, however, no significant reductions in the position error have been observed comparing to the basic algorithm. It was demonstrated that the position errors caused by the measurement offsets cannot be corrected neither basic nor improved algorithms. However, they can be reduced significantly by careful calibrations of the measuring devices.

In any practical system, a certain degree of measurement noises are inevitable. However, their impacts on the position estimation are limited with the improved algorithm. In addition, the random position errors are not accumulated by the integration of the rotor position calculation.

In the high-speed operation, the improved algorithm has no advantage over the basic algorithm in the noisy measurement environments. In the slow operating speeds, however, the improved algorithm can achieve higher robustness. It was found that the auto-correction

ability of the basic algorithm is poor at slow speeds, and the static position errors accumulates over time and generates completely wrong position estimation. With the help of PLL algorithm, however, the improved algorithm can reduce the static position estimation errors and have excellent correction ability even at very slow speeds.

The influence of the winding resistance variation on the position estimation is significant specifically at slower speeds. To demonstrate the ability of the improved algorithm, a simulation result is given in Figure 5.20 while the motor running at 0.5Hz. In this test, the winding resistance of the motor was reduced 20%. As can be seen in the figure, the improved algorithm can handle such resistance changes and can generate very low position error.

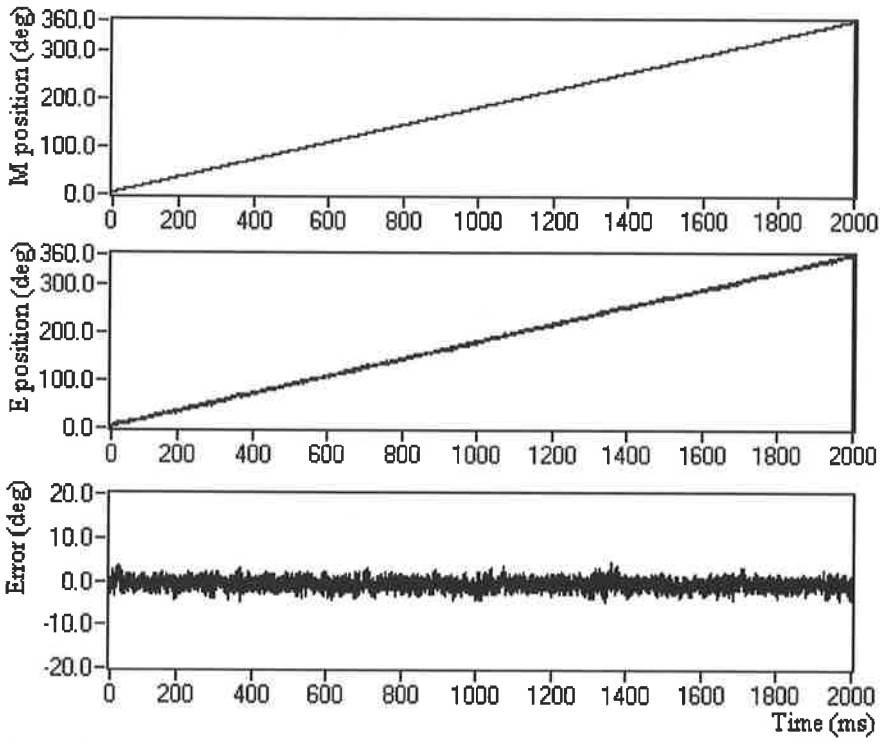

Figure 5.20. Simulation results under a low speed operation using the improved algorithm while the winding resistance is 20% less: f=0.5Hz, V_{dc}=150V, PWM current controller at a frequency of 5KHz, I_m=2.5A.

Although the simulation studies presented here use the sinusoidal PMAC motor under the sinusoidal current excitation, the similar studies can be done on the trapezoidal PMAC motor under the rectangular current excitation. However, it will be reported here that the improvements not be effective in the trapezoidal PMAC motors. This is due to the fact that the operation of the auto-correctional action and the PLL based improved algorithm depends upon the phase difference between the estimated rotor position and the phase angle of the flux linkage increment. In the trapezoidal PMAC motor with the rectangular excitation, the

variation of the phase angle is not constant and cannot be measured easily due to the non-sinusoidal waveform of the flux linkage increment. Therefore, under such operating condition, unstable phase angle variation will cause unstable operation of the algorithms developed. This may cause fluctuations on the rotor position estimation whenever the currents commutate under the parameter variations and the measurement errors. Moreover, the PLL algorithm amplifies these fluctuations and degrades the accuracy of the position estimation.

Figure 5.21 and 5.22 show two sets of simulation results using the trapezoidal PMAC motor in the simulation model and operating with the rectangular current excitation. In Figure 5.21, rotor position estimation errors due to 20% parameter variations are given, which allows direct comparison between the basic and the improved algorithms. As seen in the figures, there are similar correctional actions on the parameter variations for the rectangular excitations, but some fluctuations occur on the position estimation values as the discussions above. The static position estimation errors can be reduced by the improved algorithm even under the rectangular current excitation, but some high fluctuations were occurred on the position estimation values. It could be concluded that the large-scale fluctuations on the position estimation error may be due to the improved algorithm itself, specifically due to the equivalent inductance deviation.

Figure 5.22 illustrates the test results while the current and the voltage measurements are in error, an amplitude error of ±10%. As seen in the figure, the rectangular current excitation

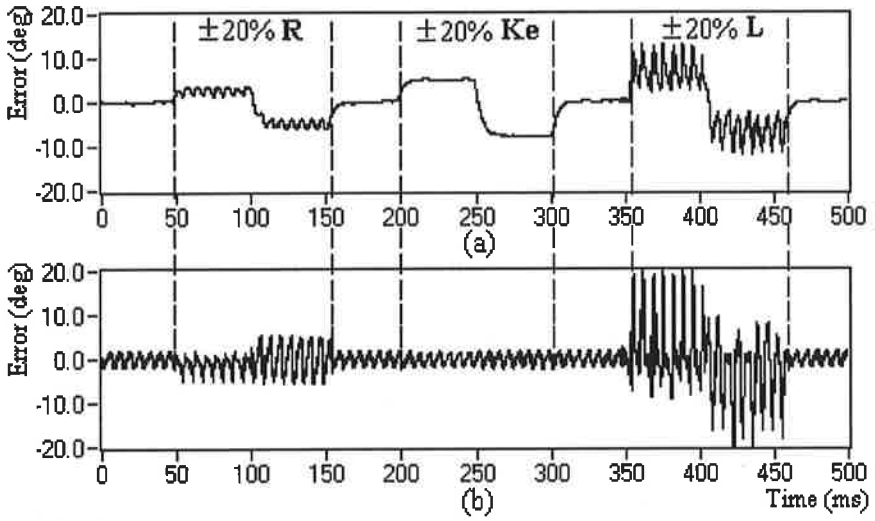

Figure 5.21 Simulation results of the position estimation errors due to 20% parameter variations in the PMAC motor: rectangular current excitation, f=25Hz, V_{dc}=150V, PWM current controller at a frequency of 5KHz, I_m =2.5A. (a) Basic algorithm; (b) Improved algorithm.

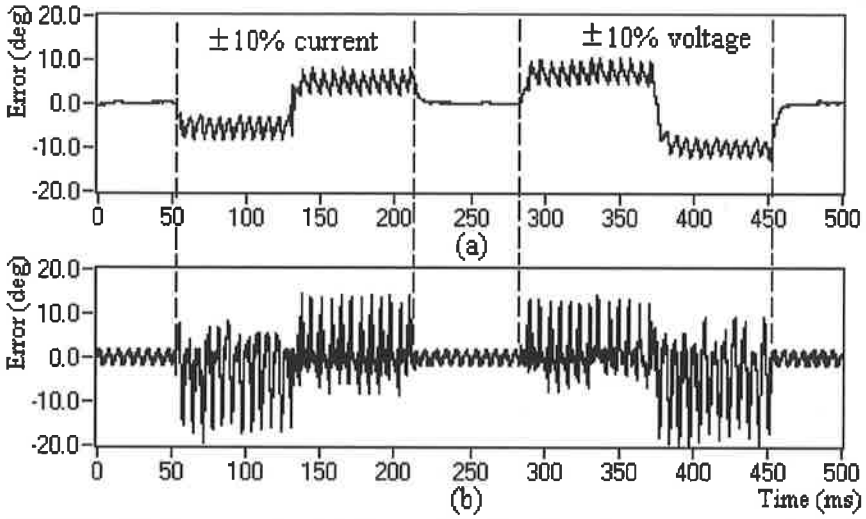

Figure 5.22 Simulation results of the position estimation errors due to the 10% measurement errors in the PMAC motor drive: rectangular current excitation, f=25Hz, V_{dc}=150V, PWM current controller at a frequency of 5KHz, I_m =2.5A. (a) Basic algorithm; (b) Improved algorithm.

causes fluctuations on the rotor position estimation. Although the improved algorithm can reduces the static position estimation errors, which were due to the measurement amplitude errors, the fluctuations caused by the non-sinusoidal waveforms are amplified. Therefore, the improved position estimation algorithm is not recommended for the trapezoidal PMAC motor drive with rectangular current excitations.

5.5 Experimental Results

To test the validity of the proposed rotor position estimation algorithms and the position sensorless technique, a complete PMAC motor drive was implemented. In the motor driver, an IRMDAC3 3-Phase 460VAC 3HP Motor Drive Board (International Rectifiers) was used as a power electronics converter circuit, and an ADMC 300 DSP-based Motor Controller (Analog Devices) was used as a controller where all the real-time control algorithms, including the position estimation routines, were implemented. A two channel incremental encoder for the position verification, and three high bandwidth voltage and two high bandwidth current transducers are accommodated in the control loop. The PMAC motor used in the setup was a sinusoidal PMAC motor. The motor parameters were given in table 4.2. Although the motor has sinusoidal back-EMF waveforms, the motor was excited both with the sinusoidal and the rectangular current waveforms to demonstrate the flexibility of the proposed method. More detail descriptions about the hardware of the motor drive system can be found in Appendix A.

5.5.1 Open-Loop Operation

Using the simulation studies, the position estimation algorithms were examined. However, the quantities consider in the position estimation routine as measured data differ significantly from the real data in a practical drive system. In order to test the position estimation algorithms suitable for actual acquisition data and demonstrate the robustness with the real data, the first stage experiments are designed as open loop experiments. In the open loop experiments, the motor drive is synchronously controlled with the actual measured rotor position signal from the shaft mounted encode. A standard PWM current controller with a PWM frequency of 5KHz is used to control motor currents through the inverter switches. In addition, a Lab VIEW based data acquisition system was established to sample the real data of the motor drive at a sampling frequency of 100KHz, which allowed off-line data procession and comparison. The hardware and software descriptions of this data acquisition system are given in Appendix B.

When the motor drive is running, the instantaneous values of the three-phase currents and voltages of the motor drive were sampled by the data acquisition system. Then, this real data were used to estimate the rotor position of the motor using the LabVIEW based position estimation algorithms that were described earlier. In order to verify the estimated rotor position, the measured rotor position signal that was available in the conventional controller were converted into the analogue signals by the serial DAC converter on the connector board of the ADMC 300 DSP-based Motor Controller. This analogue rotor position signals were also sampled simultaneously by the data acquisition system. Finally, the estimated rotor position was compared with the actual measured position, which provided us a direct comparison environment to check the quality of the position estimation. It should be highlighted here that the measured rotor position has also a degree of inaccuracy, but in this study it is used as an absolute reference position.

Two open-loop experiments were performed to test the validity and robustness of the position estimation algorithms. In the first experiment, the motor was excited by sinusoidal currents and operated at a steady-state speed of 53.5 rpm (about 25Hz). In each test, three-phase voltages and currents, and the actual rotor position signals were sampled simultaneously by the data acquisition system. Then, the sampled data of three-phase voltages and currents are used to estimate the rotor position. In order to demonstrate the

robustness of the position estimation algorithms, the measured voltages and currents and the relevant motor parameters were modified as indicated in the figures.

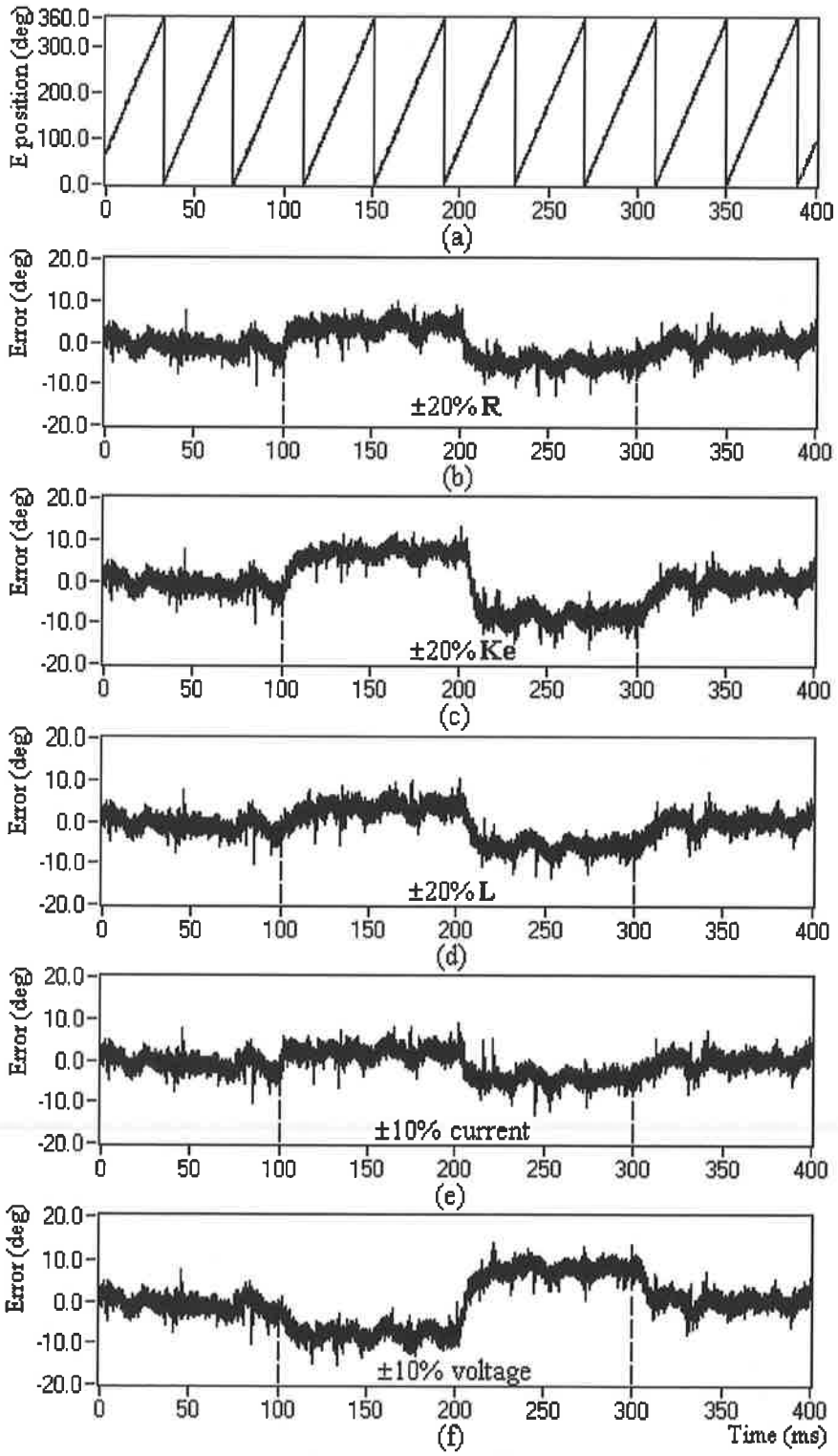

Figure 5.23. Robustness test of the basic algorithm using the measured data: (a) estimated position; (b) resistance variation of ±20%; (c) back-EMF constant variation of ±20%; (d) inductance variation of ±20%; (e) current amplitude error of ±10%; (f) voltage amplitude error of ±10%.

Figure 5.23 shows the experimental results of the estimated rotor position (a) and the position error graphs using the basic algorithm in the position estimator. In these tests the motor parameters (winding resistance, back-EMF constant, and equivalent inductance) were

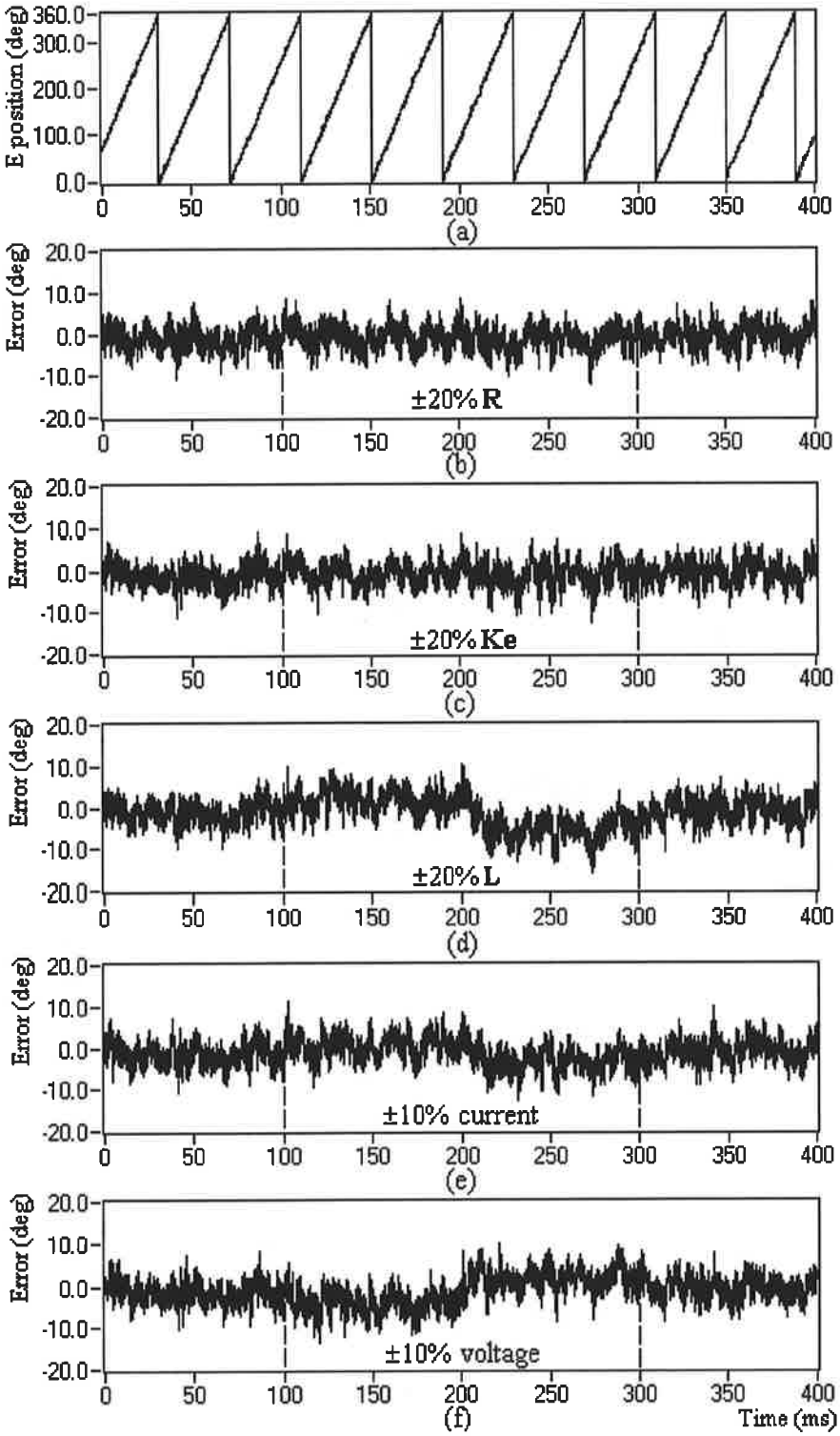

Figure 5.24. Robustness test of the improved algorithm using the measured data: (a) estimated position; (b) resistance variation of ±20%; (c) back-EMF constant variation of ±20%; (d) inductance variation of ±20%; (e) current amplitude error of ±10%; (f) voltage amplitude error of ±10%.

changed ±20%, and the measured data (voltages and currents) were altered ±10% artificially.

From Figure 5.23(a), it can be seen that the basic algorithm can estimate the rotor position accurately using the measured real data of the three-phase voltages and the currents. When

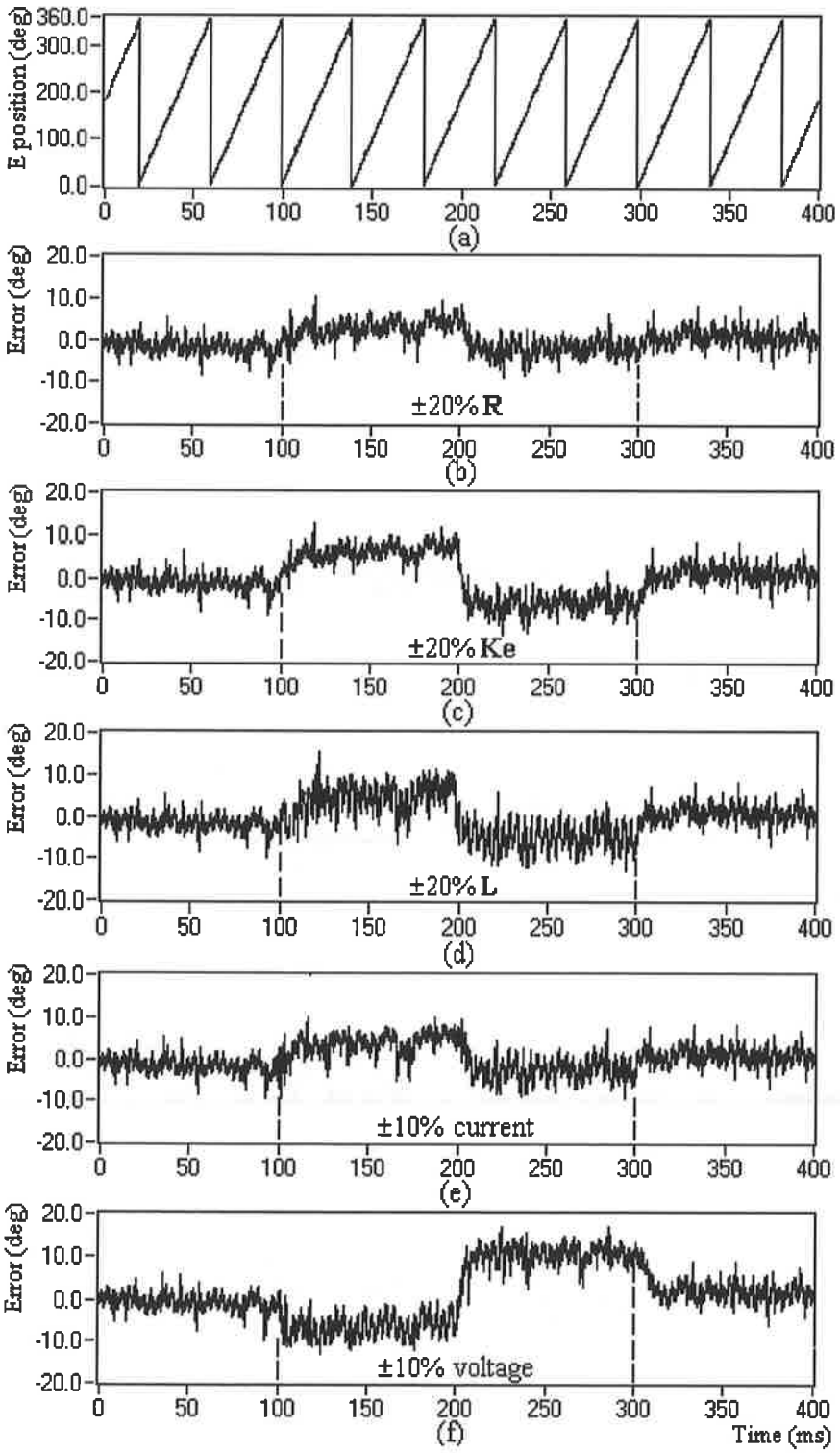

Figure 5.25. Robustness of the rectangular excitations: (a) estimated position; (b) resistance variation of ±20%; (c) back-EMF constant variation of ±20%; (d) inductance variation of ±20%; (e) current amplitude error of ±10%; (f) voltage amplitude error of ±10%.

the motor parameters were altered, however, some static position estimation errors occurred but were limited by the auto-correctional action of the algorithm within an acceptable range. This indicates that the basic position estimation algorithm has robustness with respect to the motor parameter variations and the measurement inaccuracies as studied in the simulation results. It should be noted here that the original measured voltages, the currents and the rotor position were assumed to be error-free, which is not a correct assumption in any real-time measurement system. The position error in this test is within 3-4%, which is similar to the simulation tests demonstrated earlier using the random noise injection. From these results, it can be concluded that the features of the insusceptibility to the environmental factors of the basic position estimation algorithm can increase the reliability and robustness of the position sensorless motor drive, and the estimated rotor position data is accurate enough to replace with the position sensor.

The acquired data in the previous test were reused in Figure 5.24 that performed the improved algorithm in the position estimation. As demonstrated in the figure, although the improved algorithm produces larger estimation noises, the static errors caused by the parameter deviations or the measurement inaccuracies are smaller than that of in the basic algorithm, and low speed operation of the drive is improved. Although larger scale estimation noises exist in the improved algorithm, the noises do not cause more interference on the position sensorless control in a real time motor drive system. This is because the difference of interruption frequencies of the current controller and the position estimator, which will be discussed in next section.

A second test was performed while the same motor was excited with the rectangular currents. The operating speed of the motor was again 53.5 rpm, and similar data set as described in Figure 5.23 was acquired. Figure 5.25 displays the results of this test using the basic position estimation algorithm. Similarly, in order to demonstrate the robustness of the proposed method, a degree of synthetic errors were introduced on the original motor parameters and the measured data. The results indicate that the position estimation is accurate even under the extreme noise condition, and the proposed position estimation algorithm is also suitable for the rectangular current excitation.

The table given below, table 5.1, summarizes the average position estimation errors due to the parameter variations and measurement inaccuracies in each test. It should be noted that the errors are not constant but affected by the operation conditions, such as speed and load.

Table 5.1 Summery of average errors in the open loop tests

Introduced parameter error	Average position estimation error	
	Basic algorithm	Improved algorithm
Resistance, ± 20%	5 degrees	0 degrees
Back-EMF constant, ± 20%	9 degrees	0 degrees
Inductance, ± 20%	7 degrees	5 degrees
Current, ±10%	6 degrees	3 degrees
Voltage, ±10%	8 degrees	4 degrees

5.5.2 Closed-Loop Position Sensorless Motor Drive

To implement a complete position sensorless motor drive, the identical hardware used in the open loop experiments is used. However, this time the encoder was excluded from the control loop, but utilized to verify the estimated rotor position in real time. It should be emphasised here that this new experimental setup could experience the impact of the estimated rotor position.

Figure 5.26 illustrates the complete block diagram of the position sensorless PMAC motor drive system, where the position estimator replaces the shaft-mounted encoder. Since the DSP used in this study has only five A/D converter channels, only three-phase voltages and two-phase currents are measured in real time. The third phase current that is required in the algorithm is calculated from two of the measured phase currents since the motor was star

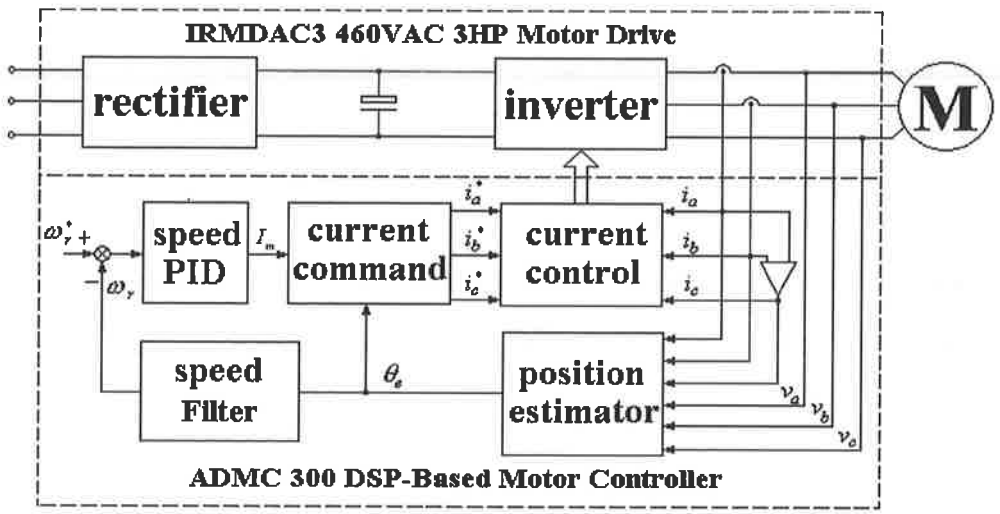

Figure 5.26 Block diagram of the position sensorless PMAC motor drive

connected.

In the closed-loop position sensorless drive, for the sinusoidal excitation, the measured voltages and currents are used to estimate the rotor position of the motor with the improved algorithm. In the rectangular current excitation however, the basic algorithm was accommodated in the rotor position estimation. In both types of current excitation, the estimated rotor position was used as an indirect rotor position data. The estimated rotor position information was also used to determine the motor speed after filtering. The speed estimation method used in the closed-loop system was described in Section 5.3.3.

The speed controller used in the position sensorless motor drive system is a standard PI controller. In the PMAC motor drives, the output of the speed controller is usually considered as the torque command. For the non-salient sinusoidal PMAC motor, if the currents waveforms are in phase with the rotor position, the electromagnetic torque is proportional to the amplitude of the excitation currents. Therefore, the amplitude of current commands can be taken as the torque command.

In the sinusoidal current excitation, a lookup table of a sinusoidal function (also used as the back-EMF function) was programmed inside the DSP chip as the reference current generator, which generates three-phase reference currents using the estimated rotor position and the output of the speed controller. Finally, these three-phase reference currents are compared with the measured three-phase currents and the results are used as the duty cycle signals to generate the three-phase PWM signals to be used in the inverter switching.

In the rectangular current excitation, however, some of the special functions of the PWM block on the DSP chip were used to generate the required switching patterns. In these patterns, only two inverter legs are switched on a given time, which means that two of the inverter legs have identical duty cycles. For example, it is possible to turn ON the high-side power device of Phase A and the low-side power device of Phase B at the same time. Meanwhile, the third inverter leg (Phase C in this example) should be disabled for a number of PWM cycles. In the normal operation, each inverter leg is disabled for certain number of periods of time, which is implemented by changing the value of the PWMSEG register according to the rotor position signals. Since the other two enabled inverter legs have identical duty cycles, they are operate as a DC PWM. Based on these switching patterns, no three-phase reference current generators are required, but the command current amplitude is directly used as the reference signal to compare with one phase measured current. The

compared result is used as the duty cycle of two enabled phases, which are also determined by the estimated rotor position data. Using the PWM signals, three-phase rectangular excitation currents can be produced through the inverter circuit. In the motor controller, the amplitudes of the currents depend on the current command, and the frequency of the rectangular currents is controlled by the rotor position signals.

As known in a digital motion control system, the duty cycle value can only be updated once in each PWM cycle (or twice if the double update PWM mode is used). In the conventional PMAC motor controller using a position sensor, there is only one interruption service routine to implement the entire control algorithm, which has the same frequency as the PWM.

In the position sensorless motor controller using the proposed position estimation algorithms, however, the position sensorless algorithm requires high bandwidth voltage measurements. Therefore, two different interruption service routines are required in such system. One of the routines is used to estimate rotor position signals, and the second one is used to implement the conventional motor control algorithm. This is because the voltage of one phase has 6 possible values in each PWM cycle when three-phases are excited with currents. Detailed discussions on this issue will be given in Chapter 6. Therefore, in order to sample the values of the phase voltage accurately, the A/D converter should have a higher sample rate than the PWM frequency.

On the other hand, it should be emphasised here that the proposed rotor position estimation method is a form of incremental algorithm and the accuracy of the position estimation is directly proportional to the sampling frequency. Therefore, a separate interruption service routine (separate than the other parts of the control algorithm) should be used in the rotor position estimator. The experiences indicate that the frequency of the interruption service routine should be at least 6 times of the PWM frequency.

The highest possible sampling rate of the A/D converter used in this study is 31.5KHz. Therefore, the frequency of PWM and motor control interruption service routine for the speed and current controllers is selected as 5208Hz. The sampling rate of the A/D converter has 6 times of the PWM frequency, which is used to implement the rotor position estimator interruption service routine. Since the estimated rotor position values are used only once in the motor control interruption service routine per PWM cycle, the six estimated rotor position values within this PWM cycle can be averaged or filtered in the real time system. Therefore,

the estimation noises were reduced using the filter and better estimation was achieved, which ensured the successful implementation of the closed loop position sensorless control.

For the display purpose, the serial DAC on the ADMC300 Connector Board was used to convert internal data of the estimated rotor position and the speed data into the analogue signals. Meanwhile, the actual rotor position signal from the shaft mounted encoder was also measured by the DSP, but it was only used to convert into the analogue signal aimed to compare with the estimated rotor position in the real time system. In this way, the experiment results were displayed on the oscilloscope screen or sampled by the data acquisition system.

5.4.3 Starting Strategy Used in the Position Sensorless Motor Drive

In most of the position sensorless techniques presented in the literatures, since there is no rotor position data available at stall, they are not self-starting. Therefore, a special starting strategy should be accommodated in the controller until the position algorithm generates an accurate estimation of the rotor position. Since the rotor position is required for the correct

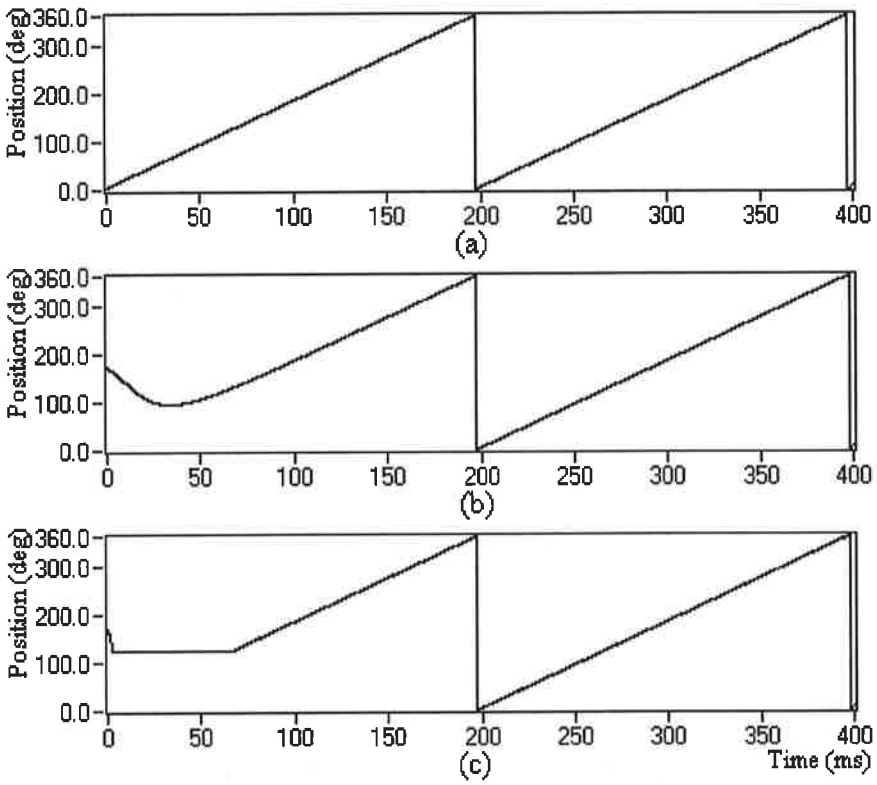

Figure 5.27 Simulation results of the position estimation demonstrating the starting procedure: the sinusoidal PMAC motor, f=5Hz, V_{dc}=150V, PWM current controller at a frequency of 5KHz, I_m =2.5A. (a) Actual rotor position; (b) Estimated rotor position using the basic algorithm; (c) Estimated rotor position using the improved algorithm.

current commutation of the motor, the starting strategy plays a very important role in the real time position sensorless motor drives.

As discussed in Section 4.2, the initial rotor position information cannot be determined in the non-salient PMAC motors using the inductance variations. Therefore, the starting method used in such motor drives are based on the open loop starting, where arbitrarily excitation of two or three stator windings utilized to bring the rotor to a known position.

The Initial value of the rotor position is also required in the position estimation proposed in this thesis. How to determine the initial position value and whether a wrong initial value could cause the position estimation catastrophic failure are the questions that need to be answered before the estimated rotor positions are used to implement closed loop synchronous control in real time.

As discussed in Section 5.4, the adaptive feature of the algorithm not only responds to the parameter variations and the measurement errors but also corrects the initial position value. This is mainly due to the auto-correctional action that is based on the phase difference between the estimated rotor position and the phase angle of the flux linkage increments. For

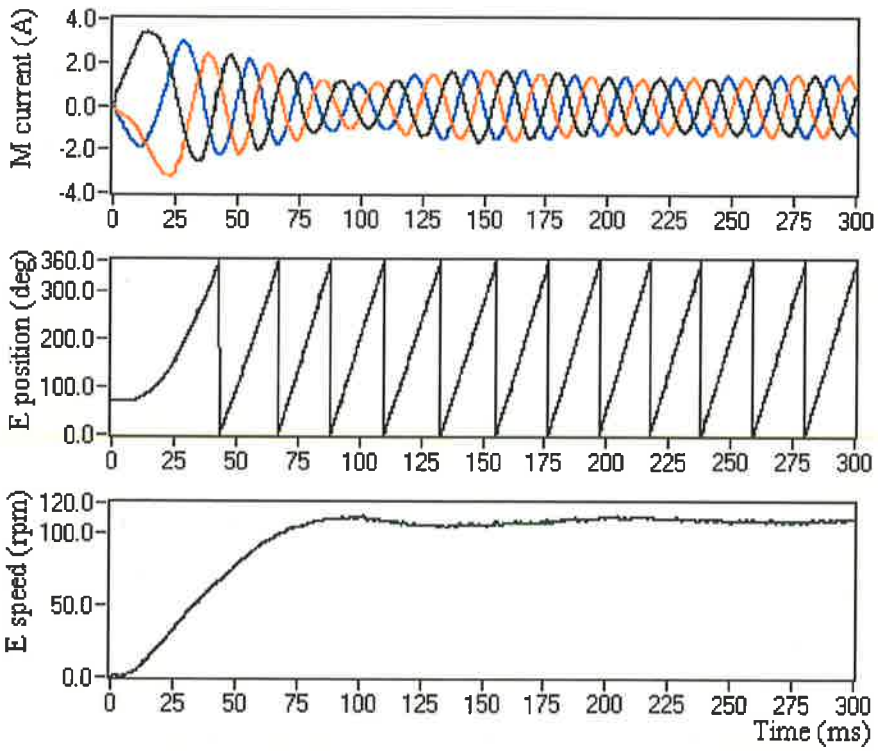

Figure 5.28 Real time experimental results of the starting procedure of the position sensorless motor drive with the best initial position value. (a) Measured three-phase currents; (b) Estimated rotor position; (c) Estimated rotor speed.

example, if the predetermined initial position is different from the actual rotor position, the phase difference between the initial rotor position and the phase angle of the flux linkage increments is fed back through the internal loop of the algorithm. Using this phase difference, the robust algorithm corrects the rotor position increment and updates the rotor position value, and after several sampling cycles, the estimated rotor position converges to the actual value.

Figure 5.27 shows the simulation results of the auto-correction procedure. At start, it is assumed that the initial value in the position estimator is different from the actual position value, which was selected randomly. As seen in the figure, after the algorithm executes the position estimation routines, the position error is gradually reduced by the auto-correctional action of the algorithms, and within an electrical cycle, the estimated rotor position converges to the actual value. It was also tested that both the basic algorithm and the improved algorithm have similar convergence time.

Using the above studies, it can be said that, the proposed position sensorless technique can be used to start the PMAC motor from standstill in real time. This implies that the position estimation algorithm can predict the rotor position from a random initial value (such as zero). If the estimated rotor position is used as the position feedback in the controller, the motor

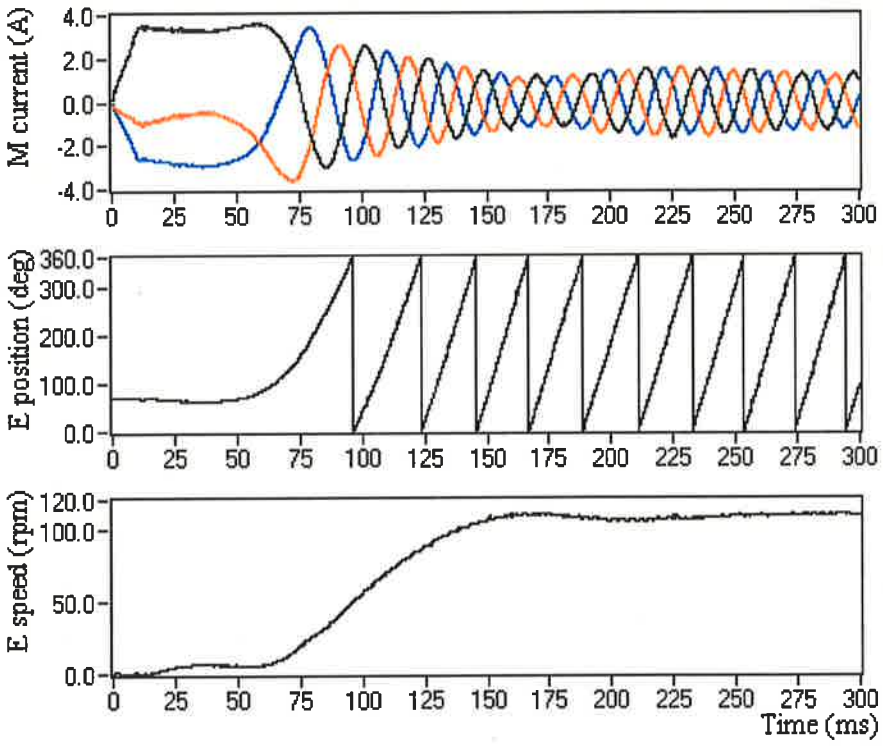

Figure 5.29 Real time experimental result of the starting procedure of the position sensorless motor drive with the worst initial position value. (a) Measured three-phase currents; (b) Estimated rotor position; (c) Estimated rotor speed.

may produce lower or even negative electromagnetic torque initially, which may affect the starting performance of the motor drive. However, the estimated position can converge to the actual position within the first electrical cycle and can be used in the real motor drive.

Figure 5.28 displays a set of real time experimental results demonstrating the starting performance of the position sensorless motor drive, which was obtained when the initial rotor position was very close to the actual position. In the test, the measured three-phase currents, the estimated rotor position and the rotor speed indicate that the position sensorless motor drive can start easily and can achieve a high dynamic performance.

A second real-time test was also performed under the identical experimental conditions but this time with completely different initial rotor position. The result given Figure 5.29 demonstrates that the motor drive can start smoothly without the help of any special starting strategy. Although the starting performance is slower and has lower dynamic performance than the previous test, this is still acceptable, which makes the technique practical.

Comparing with the previous open-loop starting strategies, the starting method proposed here has a shorter starting time and a higher dynamic performance. The previous open loop starting methods require the motor to run in the open-loop mode until the speed of the motor reaches to a certain value, at which the rotor position can be estimated accurately. In addition, the switching to closed-loop position sensorless control may not be smooth. While, it was demonstrated that the proposed position sensorless technique can start the PMAC motor directly from standstill, and it was observed that the starting procedure is smooth.

5.4.4 Real-Time Experimental Results

To demonstrate the effectiveness of the position sensorless technique, a number of real time experiments have been performed over a wide range of operating conditions, such as steady state and transient state, with and without the current control, and with sinusoidal or rectangular current excitation. These experimental results demonstrated the performances of the real time position sensorless PMAC motor drive system and indicated the feasibility of the realization of the new position sensorless technique that can be used in the practical applications.

Firstly, the PMAC test motor is excited with the sinusoidal currents, and the measured three-phase voltages and currents are used to estimate the rotor position and the speed using the improved algorithm in the DSP-based controller. The estimated position and the speed are

used as the feedbacks to implement the closed loop position sensorless control. As demonstrated, the real time motor drive can start from zero speed smoothly and operates in the entire speed range and operating conditions.

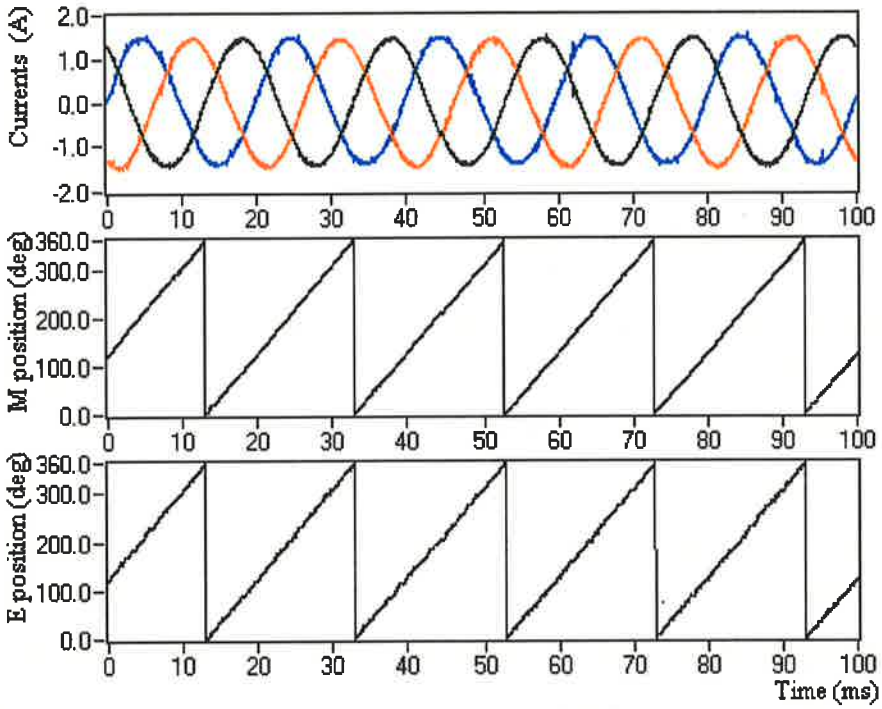

Figure 5.30. High-speed operation of the real position sensorless motor drive with sinusoidal excitation: three-phase current, measured rotor position and estimated rotor position.

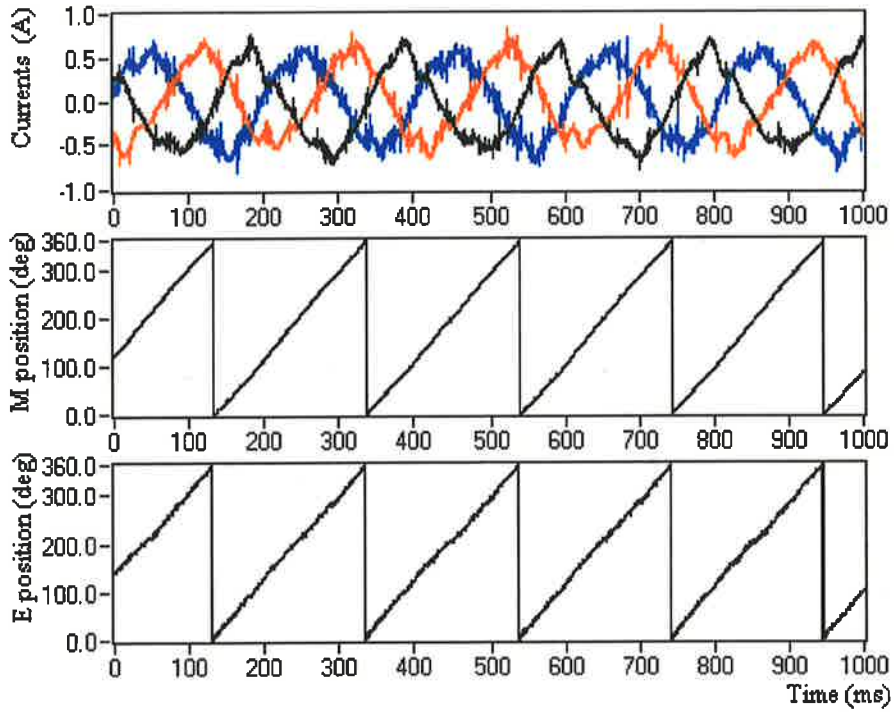

Figure 5.31. Low-speed operation of the real position sensorless motor drive: three-phase current, measured rotor position and estimated rotor position.

Figure 5.30 shows a steady-state experimental result at a speed of 107rpm (about 50Hz). The measured three-phase currents, the actual rotor position (only to verify the calculated values) and the estimated rotor position are given in the figure. As seen in the position waveforms, the discrepancy between the estimated and the measured position data is negligible. In addition, the actual phase current waveforms are very close to the desired waveforms (sinusoidal), which were generated using the estimated rotor position data. These results indicate that the position sensorless motor drive system can run steadily at high-speeds and has a good steady-state performance.

Figure 5.31 illustrates the test results while the motor is operating at a slow steady-state speed, 10.7rpm (about 5Hz). It can be seen from the figure that the estimated rotor position is very close to the actual position even at slow speeds. This demonstrates that the real position sensorless motor drive can operate over a wide speed range. However, significant distortions were observed on the actual phase currents. The main reason for this is the small mechanical at low speed range. This is due to the fact that the loading arrangement used in the test setup is not capable of generating higher loads. It should be reported here a second PMAC machine was used to load the test motor via a three-phase resistive load bank. In addition, since the motor under test has 28 pole pairs, it was found difficult to obtain a desirable current

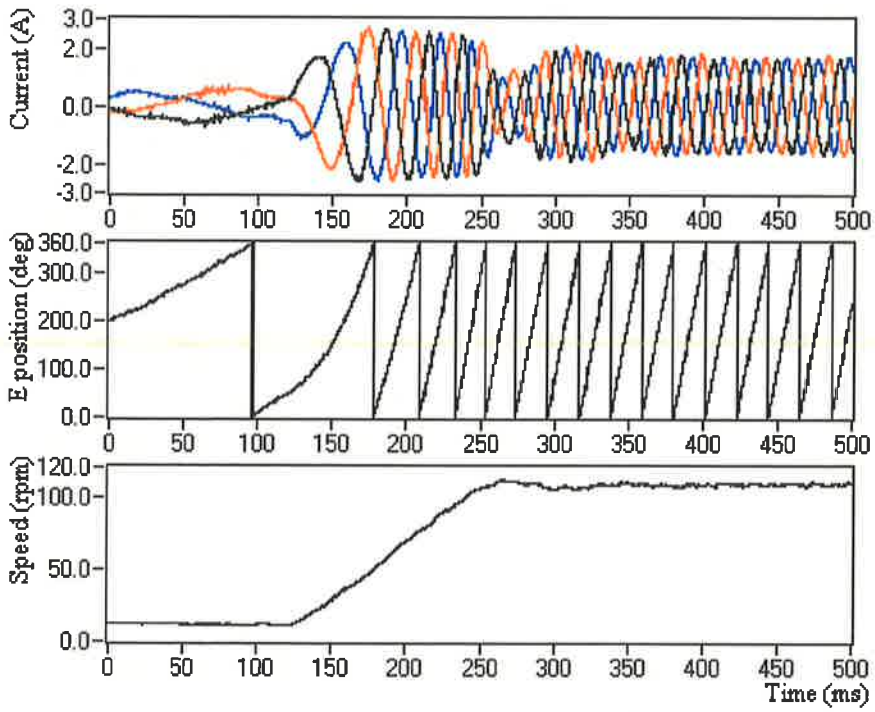

Figure 5.32. Dynamic performance of the real position sensorless motor drive: three-phase currents, measured rotor position and estimated rotor speed.

regulation in the real motor drive.

A dynamic experimental study was also performed in the test setup and the results were given in Figure 5.32. In this experiment, the closed-loop position sensorless motor drive was

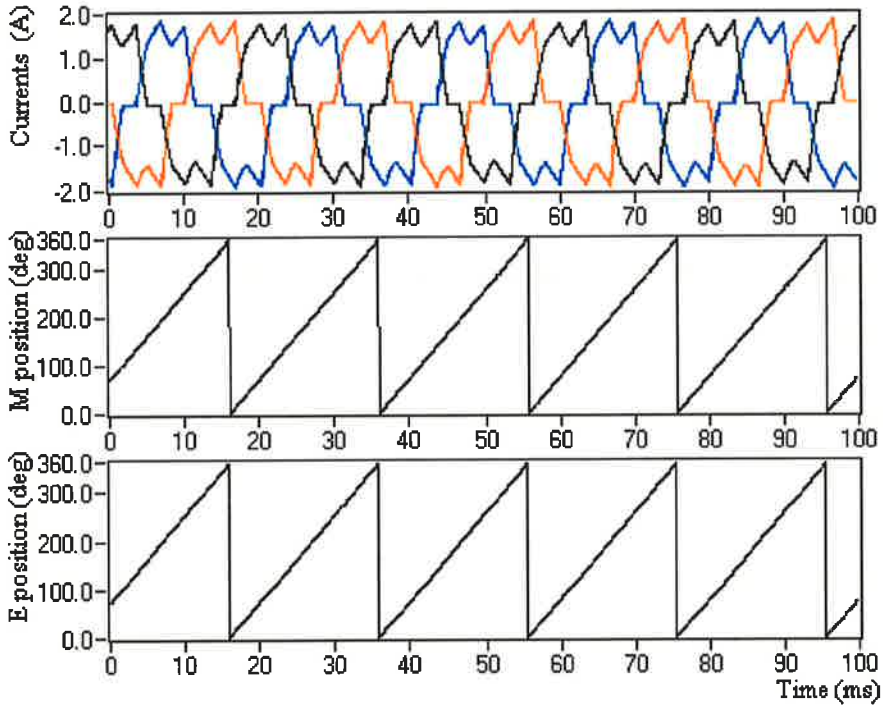

Figure 5.33 High-speed operation without current control of the real position sensorless motor drive under rectangular excitation: three-phase current, measured rotor position and estimated rotor position.

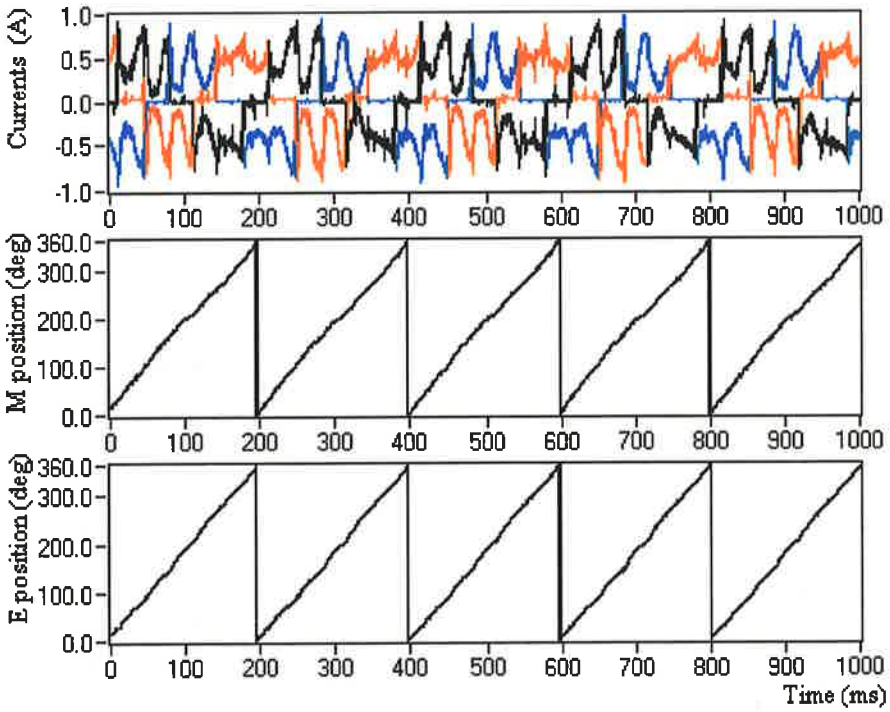

Figure 5.34 Low-speed operation with current control of the real position sensorless motor drive under rectangular excitation: three-phase current, measured rotor position and estimated rotor position.

accelerated from 10.7rpm to 107rpm. The transient waveforms of the three-phase currents, the estimated rotor position and the rotor speed are given in the figure. The results indicate that the improved algorithm can estimate the rotor position accurately even under dynamic conditions, and the real position sensorless motor drive can demonstrate a high dynamic performance as achieved in a conventional motor drive using a direct position sensor.

A second group of steady-state experiments was performed when the motor is excited with rectangular currents and the rotor position and speed were estimated using the basic algorithm via the DSP-based controller. The position sensorless motor drive system can directly start smoothly from standstill and can run under entire speed range and different operation conditions.

Figure 5.33 shows the test results of the position sensorless motor drive running at steady state speed of 107rpm. The waveforms of measured and estimated rotor positions given on the figure show the good agreement between them and demonstrate the good steady-state operation performances. In addition, the waveforms of measured three-phase currents indicate that the motor drive is running at high speed without current control mode, and the current are accurately synchronous with the rotor position that makes the system run stably at the operation condition.

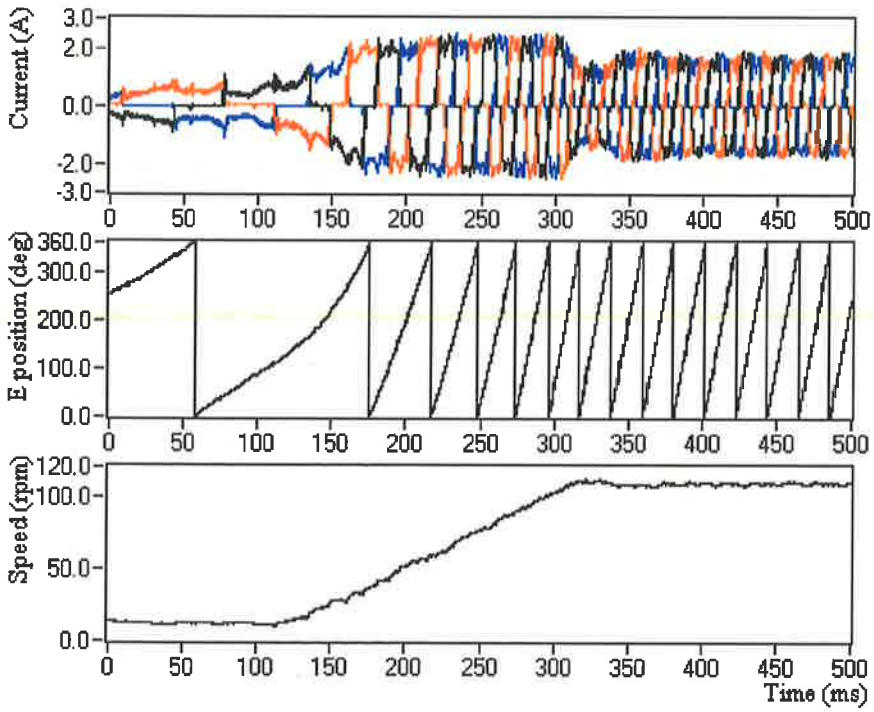

Figure 5.35. Dynamic performance of the real position sensorless motor drive with rectangular excitation: three-phase currents, measured rotor position and estimated rotor speed.

When the speed is slow down to 10.7rpm, the similar experiment results are shown in Figure 5.34. As demonstrated, the estimated rotor position of the closed-loop motor drive is in good agreement with the measured rotor position. However, the shape of the actual phase current is far from ideal, rectangular waveform. This is due to the low mechanical load at the low speed, which makes the effective voltage across the motor winding small.

The dynamic experimental results of the PMAC motor with the rectangular current excitation are shown in Figure 5.35. In this transient study, the position sensorless motor drive accelerates from 10.7rpm to 107rpm. The results indicate that the basic algorithm can estimate the rotor position accurately even under the dynamic conditions.

5.6 Conclusions

This chapter proposed a novel position sensorless technique for both the sinusoidal and trapezoidal PMAC motors. Although the principles of the position estimation algorithm were developed and explained for the motors without any rotor saliency, the method is also applicable to the motors with saliency. It should be emphasised here that the position sensing is much easier in the motors with rotor saliency using the variations of the inductance with position.

One of the possible solutions to estimate the rotor position in the PMAC motors without saliency is based on the relationship between the rotor position and the flux linkages of the permanent magnets. Using the measured phase voltages and the currents, the conventional position estimation algorithms usually calculate the flux linkages by an integration method and derive the rotor position information from these flux linkages. As a result of the integration, these algorithms suffer from the motor parameter variations and the measurement inaccuracies, which cause integration drift and pose significant problems in the rotor position estimation, specifically at the low speeds of the motor. In this novel algorithm, however, the integration routine is eliminated but three phase flux linkage increments are utilized. In the method, the back-EMF voltages were disassembled into the product of the angular speed and unity back-EMF functions with respect to the rotor position. Using the flux linkage increments and the back-EMF functions, the novel algorithm calculates the rotor position increment, which is then integrated to determine the rotor position.

The back-EMF functions used in the calculation of the rotor position increment are generated using the estimated rotor position, which forms an internal closed loop in the

algorithm. In this new arrangement, the integration is transferred from the flux linkage calculation stage to the position calculation state, which forms an internal closed-loop. In addition, by accommodating an auto-correctional algorithm (basic algorithm 2), this internal closed-loop corrects the position drift caused by the motor parameter deviations or the measurement inaccuracies.

The new algorithm estimates the rotor position increment using the motor model and the measured voltages and currents, which all, in the real systems, deviates from the initial values and may be in error. The parameter deviations and the measurement inaccuracies cause a degree of position errors, which were studied in detail. As demonstrated, using the phase difference between the flux linkage increments and the back-EMF functions, the auto-correctional algorithm can limit the position drift within an acceptable range of 3-4% under normal parameter variations and the measurement inaccuracies. This conclusion is drawn from the simulation results and from the open-loop experiments using the real-data. Therefore, it was concluded that the new position sensorless method can estimate the rotor position accurately and displays a degree of robustness.

However, some static errors on the estimated position were observed in the practical motor drive, and it was experienced that the auto-correction ability of the basic algorithm is directly proportional to the motor speed, which creates problems specifically at slower speeds. This is due to the fact that the static errors are accumulated by the integration due to the poor auto-correction ability. In order to make the algorithm resistant to the static errors, the original algorithm was improved using a PLL, which was demonstrated to be very effective using the simulation results as well as the real-time data in an open-loop system. Therefore, the improved algorithm has higher robustness and has the ability to operate the proposed sensorless motor drive over a wider speed range.

Another important feature of the novel position sensorless technique is that the algorithm is independent of the back-EMF waveform, and is suitable for both the sinusoidal and the trapezoidal PMAC motors, as well as for the motors with non-ideal back-EMF waveforms.

The simulation and the experimental results provided in the chapter demonstrated that the new position estimation algorithm is also suitable for the rectangular current excitations. Since the incremental algorithm is sensitive to the current increment, the transient variation of the phase currents during the commutations cause much higher dynamic position estimation errors in the motors with rectangular current excitation. However, such higher

errors can be limited by the auto correction action in the algorithm developed. The accuracy of the position estimation and robustness of the motor drive were also demonstrated in this section.

In the improved algorithm, however, the PLL algorithm depends on the phase difference between the estimated rotor position and the phase angle of the flux linkage increment. The unstable phase angle changes due to the non-sinusoidal waveforms of flux linkage increment and the back-EMF functions can cause unstable position correction action. As a result, the rotor position estimation may fluctuate during the current commutation, and the PLL algorithm may amplify the fluctuations and degrade the accuracy of the position estimation. Therefore, the improved algorithm is not recommended to the trapezoidal PMAC motor with rectangular excitation.

The third and the most important feature of the new position sensorless technique is that the position estimation algorithm proposed is simple and mathematically less intensive, which makes the real-time implementation possible. This was demonstrated by the implementation accommodating a commercially available motor control DSP.

In the digital motion control system, it is worth noting that the position estimation should be implemented using a separate interruption service routine in the DSP that is due to the requirement of high bandwidth voltage measurements. The experiences indicated that the frequency of the interruption service routine should be at least six times of the PWM frequency. In this way, six estimated rotor position values in each PWM cycle could be averaged to filter some of the estimation related noises mainly caused by the measurement noises.

In the real-time motor drive, the estimated rotor position is used directly in the closed loop controller, which effectively an indirect position sensing method not utilizing a shaft mounted conventional position sensor. The speed feedback signal was also estimated from the estimated rotor position for the closed loop speed control. Moreover, it was demonstrated that the position sensorless motor drive can smoothly start from standstill and can operate in entire speed range and in different operating conditions. The real time experimental results demonstrated that the position sensorless motor driver system has a good static and dynamic performance under the practical operating conditions. In addition, the high robustness makes the proposed sensorless technique suitable for the practical applications.

It should be noted here that all the real time results presented here were based on the PMAC motor with sinusoidal back-EMF. The research mainly was focused on the position estimation and the sensorless control, and not on the current controller. In the practical motor drives, the actual phase currents are not as good as the simulation results, specifically at the low speed operation and with the rectangular excitation in the current control mode. To improve the performance of the motor drive, especially the dynamic performance, the current controller should be carefully designed in the practical motor drive, and the measuring sensors must be calibrated carefully.

In addition, the practical motor used in this research has 28 pole pairs and the test setup had a slight mechanical problem, which made the demonstration of the motor operating at much lower speed impossible, such as running at 1Hz.

Chapter 6

Phase Current Reconstruction

6.1 Introduction

In addition to the rotor position information, three-phase current signals are also required in the control of most PMAC motor drive systems. In the motor drives, the phase current signals are used as feedbacks to implement the closed loop current control [89,90], and are also used in the rotor position estimation schemes. In some applications that require rapid torque response and high performance operation, the phase current signals can also be used for the direct torque control [91-94]. Although direct measurements of the three-phase current using three current sensors are the most effective method to achieve this goal, using three current sensors is an expensive solution in many low-cost motor drive applications.

Recently, significant number of studies has been reported to eliminate or to minimise the number of current sensors used in the PMAC motor drives. As mentioned in Section 2.5, three-phase current values of a PMAC motor can be reconstructed from the DC link current measurement that requires a single current sensor. However, the previous schemes have some drawbacks, specifically if the reconstructed currents are going to be used in the fast acting closed loop current controller or in the rotor position estimation. In addition, the previous techniques are too sensitive to the measurement noise and the motor parameter variations.

This chapter proposes a novel method for the reconstruction of the three-phase currents using the DC link current measurement. The method is not restricted to one type of current excitation, and therefore can be used in the sinusoidal as well as in the rectangular current excited PMAC motor drives. The method is based on an adaptive state observer, which uses the mathematic model of a PMAC motor drive to estimate the three-phase currents. Then, the DC link current is reconstructed from the estimated three-phase currents as the output of the observer. This output is compared with the measured DC link current and using an adaptive scheme regulates the error. Finally, the regulated result is utilized to compensate the DC link voltage that is used in the phase current estimation. It was found that due to the symmetry of

the three phases, this DC link voltage compensation could correct the estimated three-phase currents and force them to follow actual winding currents in real-time.

The new phase current reconstruction technique can estimate the three-phase winding currents accurately under different operating conditions. The estimated phase currents have high dynamic performances that make them suitable for the fast acting closed-loop current controller and rotor position estimation. As will be demonstrated later in this chapter, the reconstructed phase currents are not sensitive to the parameter variations of the motor and the measurement noises on the DC link current sensing with the help of the adaptive scheme.

The reconstruction of the three-phase currents from the DC link measurement requires a good understanding of the relationship between the phase currents and the DC link current of the inverter. In Section 6.2, all possible operating modes of a three-phase inverter are discussed, and the basis of the novel approach is presented. Some experimental results are also given in this Section to demonstrate the accuracy of the analysis and the reconstructed DC link current.

The detailed descriptions of the adaptive current observer are introduced in section 6.3. In Section 6.4, the reconstructed phase currents are used to replace the phase current measurements as the feedback signals in the closed-loop current control system. The section also presents the details of the hardware and software used, and displays a number of experimental results to verify the validity of the motor drive using a single current sensor on the DC link. Section 6.5 draws some conclusions and summarizes the features of the phase current reconstruction technique.

6.2 Reconstruction of the DC Link Current

The knowledge of the DC link current in a PWM inverter-fed AC motor drive is important. This is partly because it improves the general understanding of the inverter operation and allows the filter capacitors to be specified satisfactorily, but it can also be used for system protection, efficiency optimisation and state identification [69, 95, 96]. Several approaches have been proposed to analysis the DC link current in the PWM inverter motor drive. However, it was found that most of the available approaches are unnecessarily complicated or impractical for a modern drive system, which uses the space vector PWM schemes [97-99].

For the reconstruction of the three-phase currents utilizing the DC link current measurement, the primary requirement is to understand the relationship between the three-phase currents and the DC link current of the inverter. As required in the proposed method, the DC link current should be reconstructed using the motor model-based estimated three-phase currents, which becomes the output of the current observer that generates the three-phase currents. The proposed method also requires a direct comparison between the reconstructed DC link current and the measured DC link current, and demands a good understanding about all possible operating modes of the three-phase inverter and all possible states of the switches used in the inverter.

6.2.1 Operation Modes of an Inverter

A three-phase voltage source inverter and a three-phase PMAC motor load is shown in Figure 6.1. The inverter consists of six power switches and six freewheeling diodes. In the figure, I_{dc} is the instantaneous DC link current; i_a, i_b and i_c are the instantaneous three phase currents. The positive directions of the phase currents are indicated using the arrow signs. In the inverter, the DC link voltage V_{dc} is assumed to be constant, and the mid-point of the DC link voltage is defined as the reference point. Hence, the voltages of the positive supply rail and negative supply rail are assumed to swing between $+V_{dc}/2$ and $-V_{dc}/2$.

Our principal aim here is to establish the relationships among the DC link current, the phase winding current and the device switching modes. To simplify this, it is assumed that the power devices are ideal: both on-state losses and switching times are negligible, and there are no recovery effects of the freewheeling diodes and no effects of the snubber circuits. Based on these assumptions, it can be said that the conduction states of the devices solely depend on the switching signals and the current directions only.

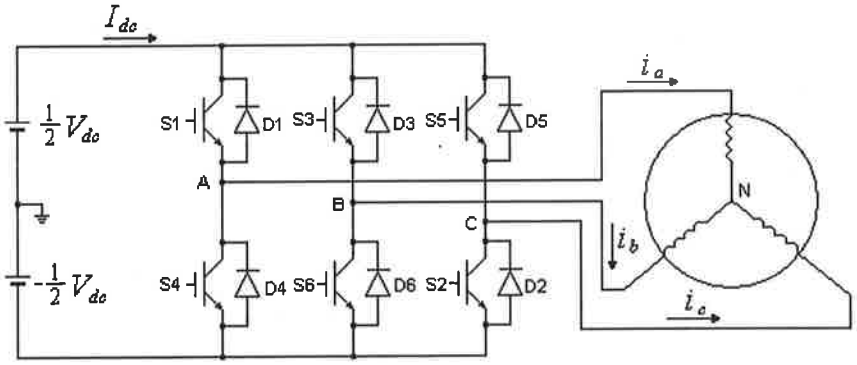

Figure 6.1 Three-phase inverter with the motor load

To develop the main aim, let us assume that one of the power switches on upper DC rail receives a switching on signal and the current direction of this phase is positive, the power switch turns on and the positive current flows through the switch and the corresponding motor winding. However, if the direction of the phase current is negative, even though the power switch experiences an on signal, the power switch does not conduct the current, but the current flows via the freewheeling diode on the upper DC rail of this phase. This is because the conduction condition of the diode only depends on the direction of the current.

According to above principle, several different operating modes of one phase (say phase A) can be summarized as follow:

- When $i_a = 0$, if power switch S_1 experiences on signal, S_1 conducts a current and the direction of the current is positive; if power switch S_4 experiences on signal, S_4 conducts a current and the direction of the current is negative; if the two power switches experience off signals, nothing happens in this phase and none of the four power devices conduct current.

- When $i_a > 0$, if power switch S_1 experiences on signal, S_1 conducts the current; otherwise the current flows via diode D_1 (whether the power switch S_4 experiences on signal or not).

- When $i_a < 0$, if power switch S_4 experiences on signal, S_4 conducts the current; otherwise the current flows via diode D_4 (whether the power switch S_1 experiences on signal or not).

It should be noted here that the two power switches linked to one phase must not experience on signals simultaneously under the normal operation conditions that is guaranteed by the dead time in the inverter. Therefore, we can assume that only one of the power devices linked to the phase can conduct current at any time and there are four different operating modes in a phase.

Under the normal operating conditions, two or three phase windings of the three-phase motor should conduct current. When two of the three phase windings conduct current, it flows via two of the twelve power devices (six power switches and six free wheeling diodes) in the inverter. If all three-phase windings conduct currents, the currents flow via three of the power devices, one in each phase. Therefore, when all possible conduction modes are

considered, a total of seventy-two possible operating modes can be identified in the three-phase inverter, which is listed in Table 6.1.

The operating modes in Table 6.1 can be classified into twelve different groups. In the groups of 1 to 4, only two of the three-phase windings conduct current at the same time. If the phase current flows via two power switches on each phase leg, the operating modes are in the group 1. In this case, the DC link current is positive (flows from positive rail of the supply to the negative rail) and equal to the phase winding current. When two power switches are turned off at the same time in an inductive motor load, the phase current continue to flow via two freewheeling diodes. The DC link current is also equal to the phase current but flows from the negative rail of the supply to the positive rail. This case belongs to the operating modes of the group 2. If only one of the two power switches is turned off from the group 1, the operating modes appear in the group 3 or 4. In this case, the phase current does not flow via either the positive or the negative rail but circulates around the inverter bridge, that is, the

Table 6.1 Operation modes and DC link current of a three-phase inverter

Group No.	Conducting Devices	Switch States			DC Link current	
		Sa	Sb	Sc	Value	Sign
1	S1, S6	1	-1	0	$i_a=-i_b$	+
	S1, S2	1	0	-1	$i_a=-i_c$	
	S3, S4	-1	1	0	$i_b=-i_a$	
	S3, S2	0	1	-1	$i_b=-i_c$	
	S5, S4	-1	0	1	$i_c=-i_a$	
	S5, S6	0	-1	1	$i_c=-i_b$	
2	D6, D1	1	-1	0	$i_a=-i_b$	-
	D2, D1	1	0	-1	$i_a=-i_c$	
	D4, D3	-1	1	0	$i_b=-i_a$	
	D2, D3	0	1	-1	$i_b=-i_c$	
	D4, D5	-1	0	1	$i_c=-i_a$	
	D6, D5	0	-1	1	$i_c=-i_b$	
3	S1, D3	1	1	0	$i_a+i_b=0$	0
	D4, S6	-1	-1	0	$i_a+i_b=0$	
	S1, D5	1	0	1	$i_a+i_c=0$	
	D4, S2	-1	0	-1	$i_a+i_c=0$	
	S3, D5	0	1	1	$i_b+i_c=0$	
	D6, S2	0	-1	-1	$i_b+i_c=0$	
4	S3, D1	1	1	0	$i_a+i_b=0$	0
	D6, S4	-1	-1	0	$i_a+i_b=0$	
	S5, D1	1	0	1	$i_a+i_c=0$	
	D2, S4	-1	0	-1	$i_a+i_c=0$	
	S5, D3	0	1	1	$i_b+i_c=0$	
	D2, S6	0	-1	-1	$i_b+i_c=0$	
5	S1, S6, S2	1	-1	-1	$i_a=-i_b-i_c$	+
	S1, S3, S2	1	1	-1	$i_a+i_b=-i_c$	
	S1, S6, S5	1	-1	1	$i_a+i_c=-i_b$	
	S4, S3, S2	-1	1	-1	$i_b=-i_a-i_c$	
	S4, S3, S5	-1	1	1	$i_b+i_c=-i_a$	
	S4, S6, S5	-1	-1	1	$i_c=-i_a-i_b$	
6	D1, D6, D2	1	-1	-1	$i_a=-i_b-i_c$	-
	D1, D3, D2	1	1	-1	$i_a+i_b=-i_c$	
	D1, D6, D5	1	-1	1	$i_a+i_c=-i_b$	
	D4, D3, D2	-1	1	-1	$i_b=-i_a-i_c$	
	D4, D3, D5	-1	1	1	$i_b+i_c=-i_a$	
	D4, D6, D5	-1	-1	1	$i_c=-i_a-i_b$	

Group No.	Conducting Devices	Switch States			DC Link current	
		Sa	Sb	Sc	Value	Sign
7	S1, S6, D2	1	-1	-1	$i_a=-i_b-i_c$	+
	S1, D3, S2	1	1	-1	$i_a+i_b=-i_c$	
	D1, S6, S5	1	-1	1	$i_a+i_c=-i_b$	
	D4, S3, S2	-1	1	-1	$i_b=-i_a-i_c$	
	S4, S3, D5	-1	1	1	$i_b+i_c=-i_a$	
	S4, D6, S5	-1	-1	1	$i_c=-i_a-i_b$	
8	S1, D6, S2	1	-1	-1	$i_a=-i_b-i_c$	+
	D1, S3, S2	1	1	-1	$i_a+i_b=-i_c$	
	S1, S6, D5	1	-1	1	$i_a+i_c=-i_b$	
	S4, S3, D2	-1	1	-1	$i_b=-i_a-i_c$	
	S4, D3, S5	-1	1	1	$i_b+i_c=-i_a$	
	D4, S6, S5	-1	-1	1	$i_c=-i_a-i_b$	
9	D1, D6, S2	1	-1	-1	$i_a=-i_b-i_c$	-
	D1, S3, D2	1	1	-1	$i_a+i_b=-i_c$	
	S1, D6, D5	1	-1	1	$i_a+i_c=-i_b$	
	S4, D3, D2	-1	1	-1	$i_b=-i_a-i_c$	
	D4, D3, S5	-1	1	1	$i_b+i_c=-i_a$	
	D4, S6, D5	-1	-1	1	$i_c=-i_a-i_b$	
10	D1, S6, D2	1	-1	-1	$i_a=-i_b-i_c$	-
	S1, D3, D2	1	1	-1	$i_a+i_b=-i_c$	
	D1, D6, S5	1	-1	1	$i_a+i_c=-i_b$	
	D4, D3, S2	-1	1	-1	$i_b=-i_a-i_c$	
	D4, S3, D5	-1	1	1	$i_b+i_c=-i_a$	
	S4, D6, D5	-1	-1	1	$i_c=-i_a-i_b$	
11	S1, S3, D5	1	1	1	$i_a+i_b+i_c=0$	0
	S1, D3, S5	1	1	1	$i_a+i_b+i_c=0$	
	D1, S3, S5	1	1	1	$i_a+i_b+i_c=0$	
	S4, S6, D2	-1	-1	-1	$i_a+i_b+i_c=0$	
	S4, D6, S2	-1	-1	-1	$i_a+i_b+i_c=0$	
	D4, S6, S2	-1	-1	-1	$i_a+i_b+i_c=0$	
12	S1, D3, D5	1	1	1	$i_a+i_b+i_c=0$	0
	D1, S3, D5	1	1	1	$i_a+i_b+i_c=0$	
	D1, D3, S5	1	1	1	$i_a+i_b+i_c=0$	
	S4, D6, D2	-1	-1	-1	$i_a+i_b+i_c=0$	
	D4, S6, D2	-1	-1	-1	$i_a+i_b+i_c=0$	
	D4, D6, S2	-1	-1	-1	$i_a+i_b+i_c=0$	

DC link current is equal to zero.

If all of the three-phase windings conduct currents at the same time, the possible operating modes are included in the groups 5 to 12. When three power switches, one in each phase, carry the winding currents at the same time, the operating modes are in the group 5. In this case, the DC link current is positive and is equal to one of the winding currents or the sum of the other two winding currents.

Using the operating modes of the group 5, it can be said that if one of the three power switches is turned off, the operating modes appears in the group 7, 8 or 11 that depends upon which power switch is turned off. In the group 7 and 8, the DC link current is still positive and is equal to one of the winding currents or the sum of the other two winding currents. In addition, since the winding currents circulate around the inverter bridge in the group 11, the DC link current is equal to zero.

If two of the three power switches are switched off in the group 5, the operating modes appear in the group 9, 10 or 12. In the group 9 and 10, the DC link current is negative and also equal to one of the winding currents or the sum of the other two winding currents. However, in the group 12, the winding currents circulate inside the inverter bridge and the DC link current is equal to zero. When all of the three power switches are turned off together, the operating modes are in the group 6. In this mode, the winding currents flow through the three freewheeling diodes. The DC link current in the group 6 is negative and is equal to one of the winding currents or the sum of the other two winding currents.

In Table 6.1, the values and the signs of the DC link current are also listed. Using the above descriptions, the currents can be classified under three separate cases. In the first case, the DC link current is positive and its value is equal to one of the winding currents or the sum of the other two winding currents. The sign of the DC link current can be used to indicate the direction of the energy flow. Therefore, in the first case, the energy flow is from the supply to the inverter. In the second case, the winding currents circulate around the inverter bridge and the DC link current is equal to zero. The zero DC link current indicates that there is no energy output from the inverter. In the third case, the DC link current is negative but its value is also equal one of the winding currents or the sum of the other two winding currents. The negative sign of the DC link current indicate the energy is feedback from the motor to the inverter.

6.2.2 Switch States

Table 6.1 lists all the possible operating modes of a three-phase inverter. The DC link current can accurately be reconstructed from three-phase currents according to this table. However, this approach is too complicated for a real time system, which will be simplified in the following discussions.

Using the explanations given in the previous section, it can be conclude that any two conducting devices (power switch and freewheeling diode) in the same leg of the inverter can generate the same terminal voltage for the corresponding phase. For example, if the current of phase A flows via the power switch S_1 or via the freewheeling diode D_1, the terminal voltage of phase A is equal to $+V_{dc}/2$. Inversely, if the switch S_4 or the diode D_4 carries the current, the voltage of terminal A will be $-V_{dc}/2$. Therefore, a pair of power switch and freewheeling diode can be considered as a bi-directional mechanical switch that has different conduction conditions in either direction. The positive conduction via a power switch depends on both the switching signal and the direction of the phase current, while the negative conduction via a freewheeling diode depends on the direction of the phase current only.

It should be noted here that above discussions are based on the assumption of the ideal power devices used in the inverter circuit. If on-state voltage drops of the power devices are considered, the terminal voltage of the phase will be a "bit" different when either the power switch or the freewheeling diode conducts the current [100,101].

In the PMAC motor with sinusoidal current excitation, since all three-phase windings carry currents at any instant, one of the two switches of a phase must be closed. Based on this feature, a conventional analysis approach is that the two switches of a phase can be represented by a state variable S_p. Here the subscript p denotes the phases a, b and c. Hence, if the positive DC rail switch of phase p is closed, S_p=1, and if the negative DC rail switch of phase p is closed, S_p= 0. Using these representations, a total of eight switch states can be defined in the three-phase inverter, which can be represented by the space voltage vectors S_a, S_b, and S_c, which have the values (0,0,0), (0,0,1), ..., (1,1,1).

Since the DC link currents flowing via the positive or the negative supply rail have the same value but opposite direction, only the positive rail DC link current is considered here. It is easy to see from Figure 6.1 that the DC link current flowing through the positive supply

rail is equal to the sum of the currents via three positive DC rail switches. Moreover, since the current of the positive DC rail switch of one phase is equal to the winding current of this phase, the instantaneous DC link current can easily be expressed as the sum of the three inverter switch currents [97]:

$$I_{dc} = i_a \cdot S_a + i_b \cdot S_b + i_c \cdot S_c \tag{6.1}$$

However, this approach is not suitable for a PMAC motor with rectangular current excitation since only two of three phases conduct current at a time, and the current of the third phase is equal to zero. The zero current implies that the two switches in this phase are in off state and the terminal voltage of the phase only depends on the back EMF voltage of the motor. Therefore, the switch states of the third phase cannot be represented by a state variable using only two states: 0,1.

In the three-phase inverter, there are two independent switches on each phase, which can be turned off but cannot be turned on at the same time. Therefore, a state variable, S_p with three different states can be defined to represent the states of the two switches of this phase: if the upper switch of phase p is closed S_p=1, if the lower switch of phase p is closed S_p=-1, and if both switches are open S_p=0.

Using the above descriptions, it can be concluded that there are twenty-seven possible switch states in the three-phase inverter. However, since at least two of the three-phase windings should conduct currents at a given instant, only twenty switch states are defined under the normal operating conditions. Therefore, if we only consider the switch states (not the actual power devices), 72 operating modes listed in Table 1 can be reduced to 20 different switch states that are given in Table 2.

As shown in Table 6.2, 20 switch states are divided into three groups. In the Group 1, all three-phase windings conduct current at the same time and the phase current flow via the DC link. Moreover, only two of the three-phase windings conduct current at the same time in Group 2 and the phase currents also flow via DC link. The twelve switch states in Group 1 and Group 2 are all active states and one phase current can be derived from the DC link current. However, in Group 3, two or three phase windings conduct current, and the winding currents circulate inside the inverter bridge and do not flow through either the positive or the negative rail, that is, the DC link current is equal to zero. For this reason, these states are usually called zero states.

Table 6.2 Switch states of a three-phase inverter

Group No.	Switch States			DC Link current	Comment
	Sa	Sb	Sc		
1	1	-1	0	$i_a=-i_b$	three phases conduct current
	1	0	-1	$i_a=-i_c$	
	-1	1	0	$i_b=-i_a$	
	0	1	-1	$i_b=-i_c$	
	-1	0	1	$i_c=-i_a$	
	0	-1	1	$i_c=-i_b$	
2	1	-1	-1	$i_a=-i_b-i_c$	two phases conduct current
	1	1	-1	$i_a+i_b=-i_c$	
	1	-1	1	$i_a+i_c=-i_b$	
	-1	1	-1	$i_b=-i_a-i_c$	
	-1	1	1	$i_b+i_c=-i_a$	
	-1	-1	1	$i_c=-i_a-i_b$	
3	1	1	0	$i_a+i_b=0$	zero states
	-1	-1	0	$i_a+i_b=0$	
	1	0	1	$i_a+i_c=0$	
	-1	0	-1	$i_a+i_c=0$	
	0	1	1	$i_b+i_c=0$	
	0	-1	-1	$i_b+i_c=0$	
	1	1	1	$i_a+i_b+i_c=0$	
	-1	-1	-1	$i_a+i_b+i_c=0$	

Since the DC link currents flowing via the positive or the negative supply rail have the same value but opposite polarity, the DC link current can be calculated using the half value of the total current, that is, the sum of the three-phase currents flowing via either the positive or the negative supply rail. Moreover, one phase current flowing via either the positive or the negative supply rail can also be expressed as I_p*S_p. Therefore, the instantaneous DC link current can be given as:

$$I_{dc} = (i_a \cdot S_a + i_b \cdot S_b + i_c \cdot S_c)/2 \tag{6.2}$$

The above equation represents the relationship between the DC link current and the three phase currents using the new analysis approach. One of the advantages of this relationship is that the new approach is suitable for both in two-phase and in three-phase conducting modes. In addition, when this equation is used to reconstruct the DC link current from the three-phase current measurements, the average action involved in the equation can reduce the error, which may be due to the unequal gain constants and the DC offsets in the current sensors.

It should be emphasised here that in the case of three phases conducting currents, the switching signals cannot be directly used as the switch state variables. The main reason of this is that a "dead time" is inevitably required in the actual inverter to protect the power

devices being short-circuited across the power supply. During the period of the dead time, two of the power switches in one phase are both turned off. In this mode, the winding current is carried by a freewheeling diode, and therefore the switch state in the main circuit of the inverter is not the same as the switching signals in the control circuit.

As stated earlier, the switch states can be determined using the switching signals and the directions of the phase currents. As an example, the switch states of phase A are given in Table 6.3. As seen in the table, if the current of phase A is positive, the switch state S_a depends on the switching signal of the power switch S_1. Conversely, if the current of phase A is negative, the switch state S_a depends on the switching signal of the power switch S_4. When the current of phase A is equal to zero, the switch state S_a depends on both the switching signals of the power switch S_1 and S_4. Similar switch state tables can be easily reproduced for phase B and C.

Table 6.3 Switch state variable

phase current	switching signal	S_a
$i_a > 0$	$S_1 = 1$	1
	$S_1 = 0$	-1
$i_a < 0$	$S_4 = 1$	-1
	$S_4 = 0$	1
$i_a = 0$	$S_1 = 1$	1
	$S_4 = 1$	-1
	$S_1 = S_4 = 0$	0

6.2.3 Analysis of the DC Link Current

Using Equation 6.2 and Table 6.3, the DC link current of the three-phase inverter can be reconstructed from the three-phase currents. The waveform of the DC link current depends on the three-phase current waveforms and the modulation strategies used in the inverter. This section discusses the DC link current waveform under normal PWM operation conditions aiming to produce sinusoidal or rectangular excitation currents.

In the trapezoidal PMAC motor, double polar modulation is normally used to produce the required rectangular excitation currents. With the double polar modulation, two power switches, one in each phase that conducts the current, are turned on and off together. In one

phase, when the power switch on the upper leg is turned on, the power switch on the lower leg must be turned off, vice versa. For example, if phase A and phase B conduct the current, the power switches S_1 and S_6 (or S_4 and S_3) are turned on or off together. When S_1 and S_6 are on, S_1 and S_6 are off. Conversely, when S_1 and S_6 are off, S_1 and S_6 are on.

In order to understand the characteristics of the DC link current, Figure 6.2 presents some simulation results for the trapezoidal PMAC motor. The figure shows the waveforms of the three-phase currents, the DC link current, and an zoomed DC link current under the double polar modulation strategy. The time period between 9 to 20 ms in the zoomed figure is used as an example to explain the characteristics. In the period of phase A and C conducting current, the power switches S_1 and S_2 are turned on or off together. When they are turned on, the phase current flows via the power switches S_1 and S_2, and the DC link current is positive and is equal to the phase current. When the switches are turned off, the phase current flows via the freewheeling diodes D_4 and D_5, and the DC link current also is equal to the value of the phase current, but its direction is negative. Consequently, only two different values of the DC link current occur in each PWM cycle, which are normally one positive and one negative. The double polar pulse of the DC link current has the frequency of the PWM frequency. For

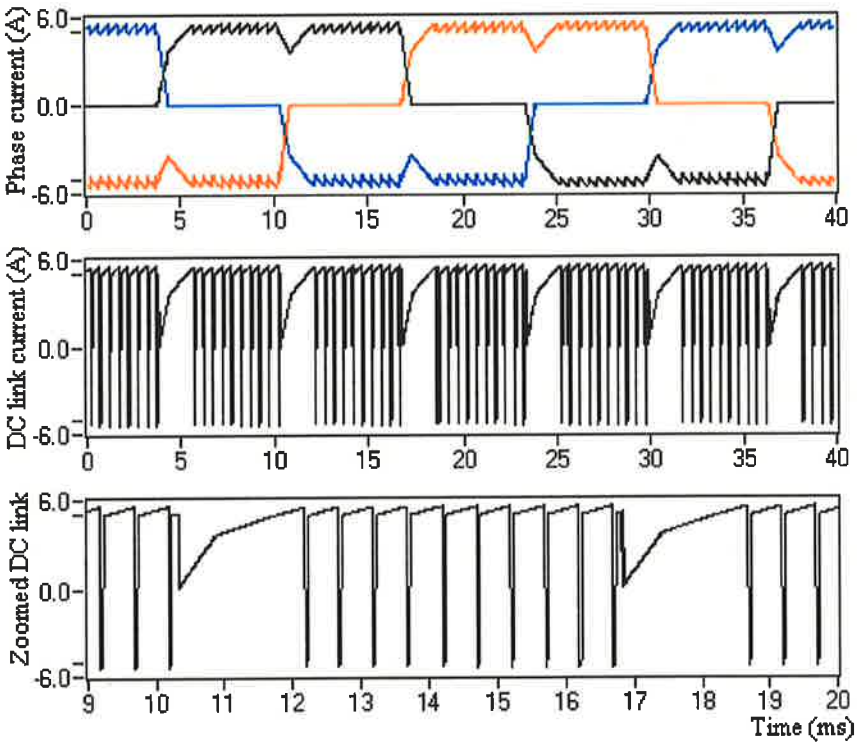

Figure 6.2 Simulated waveforms for the trapezoidal PMAC motor: three-phase currents, DC link current, and a portion of DC link current (between 9-20 ms).

an inductive load, the "dead time" used to protect power switches from short circuit has no effect on the DC link current waveform.

During the commutation period between phase A and B, two power switches of phase A are turned off completely, and the power switches S_3 and S_2 are turned on or off together. Therefore, the current of phase A freely decays to zero via freewheeling diode D_4, and the current of phase B gradually builds up and enter into a time period where phase B and C conducts current. In this commutation period, the power switches S_3 and S_2 are turned on in most of the time, and the DC link current is equal to the current of phase B and gradually increases from zero to a desired level. If S_3 and S_2 are turned off, the DC link current is equal to the current of phase C, which has a negative value during this commutation period.

In the sinusoidal PMAC motor, several PWM modulation strategies are normally used, such as SPWM, space vector modulation, and closed-loop current control. Since the DC link current waveform in the closed-loop current control strategy is closely related to the motor parameters and the operating conditions, and the space vector modulation are more complicated, the normal SPWM strategy is used here as an example to explain the DC link current waveform of the sinusoidal PMAC motor. In SPWM, the standard three-phase sinusoidal reference signals are used to compare with a triangular carrier signal. If the reference signal of one phase is more positive than the carrier signal, the upper leg power switch of the phase is turned on, and the related lower leg power switch is turned off, and a positive voltage is applied to the phase. Similarly, if the reference signal is more negative than the carrier signal, the upper power switch is turned off, and the lower power switch is turned on, and a negative voltage is applied to the corresponding phase.

Figure 6.3 illustrates a set of simulation results obtained from the sinusoidal PMAC motor that is controlled by using the normal SPWM strategy. In order to see the characteristics of the DC link current clearly, the waveforms of three-phase currents, the DC link current, and an zoomed graph of the DC link current together with the waveforms of the SPWM strategy are given in the figure. Reference to the figure of the SPWM strategy, it can be said that the switch states of the inverter in one PWM cycle within the zoomed period should be:

$$(-1,-1,-1) \rightarrow (1,-1,-1) \rightarrow (1,1,-1) \rightarrow (1,1,1) \rightarrow (1,1,-1) \rightarrow (1,-1,-1) \rightarrow (-1,-1,-1)$$

The switch states of (-1,-1,-1) and (1,1,1) are the zero states, and the DC link current is equal to zero at these states. Using Table 6.2, it can be seen that the DC link current of the

switch state (1,-1,-1) is equal to the current of phase A, and at the switch state (1,1,-1), the DC link current is equal to minus of the current of phase C. As can be seen on the zoomed DC link current graphs, the DC link current reaches to zero value twice in each PWM cycle due to the zero states.

At the beginning of the zoomed period, the switch state (1,-1,-1) lasts longer period of time, so that the DC link current is equal to the current of phase A twice during most of the time in each PWM cycle. The short duration of the switch state (1,1,-1) causes the DC link current to be equal to minus the current of phase C, again twice per PWM cycle. Since the motor is an inductive load and the current has a phase delay reference to the voltage (that is equivalent to the reference signal of the SPWM strategy), the positive current of phase C causes negative current pulse on the DC link at the beginning of the zoomed graph. After this period, the duration of the switch state (1,-1,-1) gradually gets smaller and the duration of the

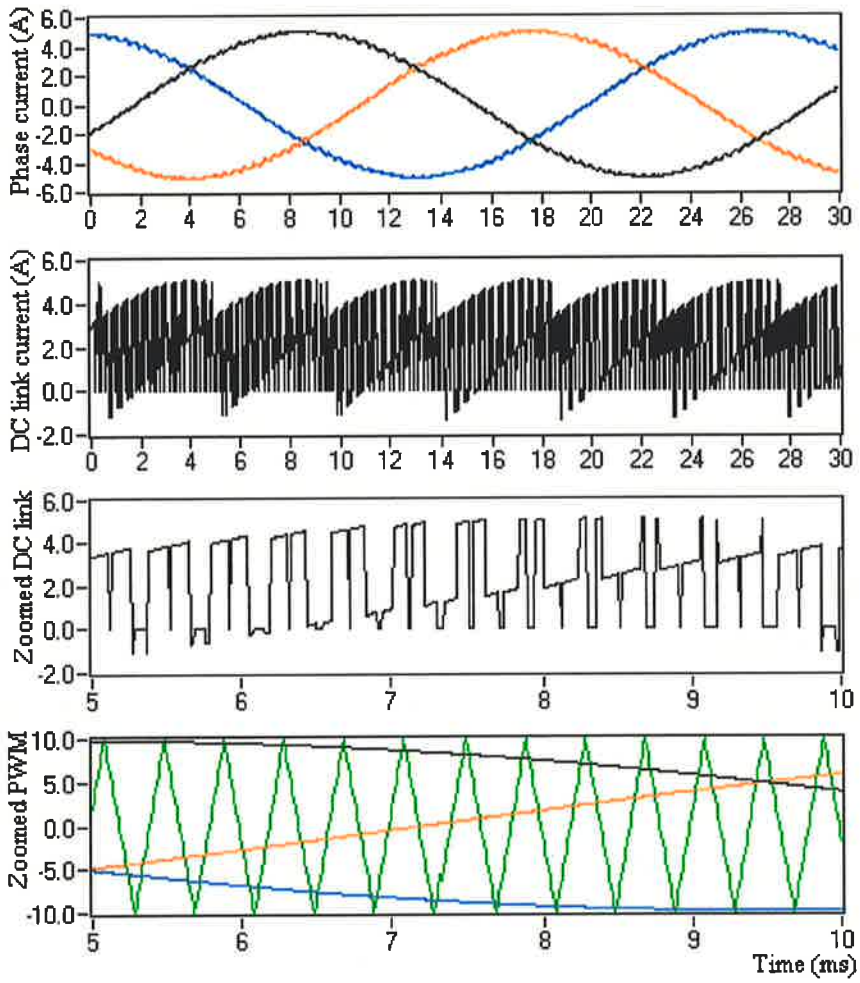

Figure 6.3 Simulation waveforms of the sinusoidal PMAC motor: three-phase currents, DC link current, zoomed DC link current, and zoomed SPWM strategy.

switch state (1, 1,-1) gradually gets larger. After the reference signal of phase B is more positive than that of phase A, the switch state (1,-1,-1) does not exist, and the DC link current is not equal to the current of phase A any more. At the same time, the duration of switch state (1, 1,-1) in one PWM cycle reaches to a maximum, so that the DC link current is equal to minus the phase C current in each PWM cycle most of the time.

From the simulation results, it can be seen that the DC link current contains pulses twice the PWM frequency. Assuming that the phase currents are constant within the PWM cycle, the DC link current becomes symmetrical in the first and the second half-cycle of the PWM. In fact, there are three values of the current in each half PWM cycle. One of the values is equal to zero that correspondence to the zero state. Two of the active states emerging in the half cycle cause the values of the other two DC link currents to be equal to one of the phase currents. However, if the duty cycles of the two phases are similar, one of the active states may appear too short, which may prevent the measurement of the DC link current. In addition, if the duty cycles of all three phases are similar, the DC link current pulse becomes too narrow, which may not be detected. Therefore, due to the irregular profile of the DC link current, the values of the DC link current have to be sampled accurately, which can be done using an expensive data acquisition hardware or using an over sampling technique to sample every possible values of the DC link current.

6.2.4 Experimental Results

To verify the simulation results and the current reconstruction method, the PMAC motor drive system as described in Chapter 5 was used. The sinusoidal PMAC motor was energised through the IRMDAC3 3-Phase 460VAC 3HP Motor Drive Board, which was controlled by the ADMC 300 DSP-based motor controller accommodating the conventional control approach. The standard PWM strategies at a PWM frequency of 5KHz were used to generate the desired sinusoidal or the rectangular excitation currents, which aimed to demonstrate the flexibility of the proposed DC link current reconstruction method. In addition, the data acquisition system based on Lab VIEW was used to sample the real data simultaneously. The sampling frequency of the acquisition system was set to 100kHz. The details of the data acquisition software were provided in Appendix B.

When the motor drive was running, the data acquisition system sampled the three-phase currents and the DC link current using the current sensors and the switching signals from

DSP based motor controller. Figure 6.4 gives the real-time DC link current and the corresponding switching signals, which were captured using the data acquisition system.

Using a LabVIEW VI that was based on Equation 6.2, the real data of the three-phase currents and the switching signals were utilized to reconstruct the DC link current. The reconstructed and the measured DC link currents were given in Figure 6.5, which covers the sinusoidal current excitation as well as the rectangular current excitation. As demonstrated in the figure, the DC link currents reconstructed using the measured three phase currents and the inverter-switching signals are in very good match with the measured waveforms. However, some transient spikes are observed on the measured waveforms, which may be due to the proximity effects of the power switches and the finite recovery time of the freewheeling diodes and the power switches. In a practical inverter, the " dead time" used to protect the power switches, which may also cause some negative spikes if the duty cycles of two phases are almost same [97].

However, the reconstructed DC link current is only used as the output of the current observer in here. These current spikes may be seen as some noises on the DC link current measurement.

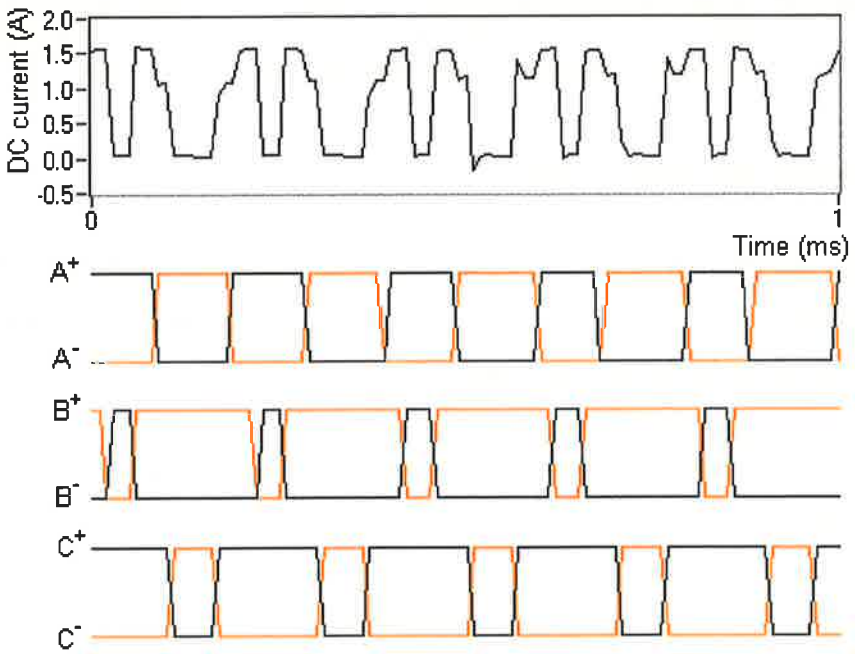

Figure 6.4 DC link current and corresponding switching signals

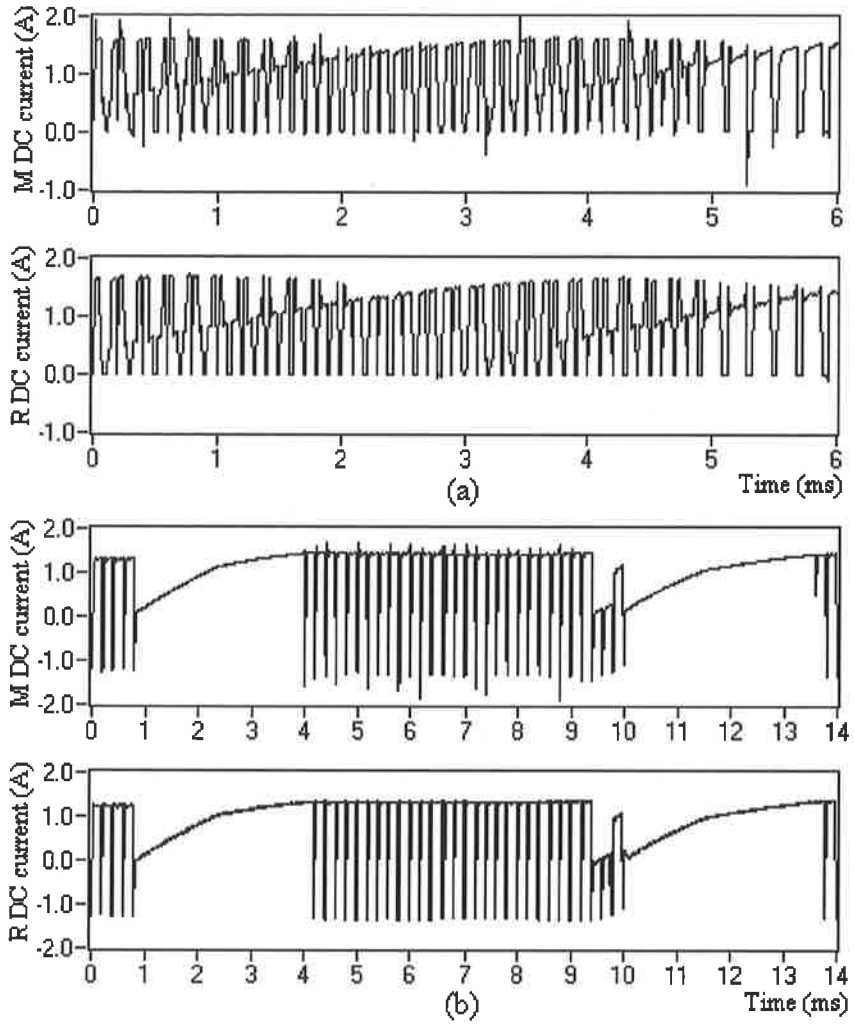

Figure 6.5 A portion of the measured (M) and the reconstructed (R) DC link currents of the test motor drive: (a) Sinusoidal excitation current, (b) Rectangular excitation current.

6.3 Phase Current Reconstruction

In many cases, the internal states of a plant cannot be measured easily, but the states may be required to control the plant. State observers deal with such problems by deducing the internal states from the external measurements.

The state observer is based on an accurate model of the plant, which has the same input signals as the plant itself. Plant and model outputs are compared and the error is fed back to the model, so that the model behaviour is corrected. Since the internal states of the model can be monitored directly, the model states may be expected to reflect the states of the plant.

Since the mathematical model of the PMAC motor drive is adequately known, therefore, the general principle of the state observer explained above may be applied to estimate the three-phase currents of the motor drive by using the DC link current measurement.

6.3.1 Current Observer

Figure 6.6 shows the block diagram of the phase current observer system. In the figure, the dotted line block "observer" is the phase current observer of the PMAC motor drive, which consists of five main blocks. Phase Voltages block reconstructs the three-phase voltages of the motor using the switching signals and the measured DC link voltage. The phase currents of the motor are estimated using the voltage equations that are the outputs of the Phase Voltages. The block named DC Link Current reconstructs the DC link current of the motor drive using the estimated phase currents that are the output of the current observer. Then the reconstructed DC link current is compared with the measured DC link current and the result is regulated using an adaptive scheme. Finally, the regulated result is used to compensate the DC link voltage, which is used to correct the estimated phase currents and force them to follow the actual currents of the motor.

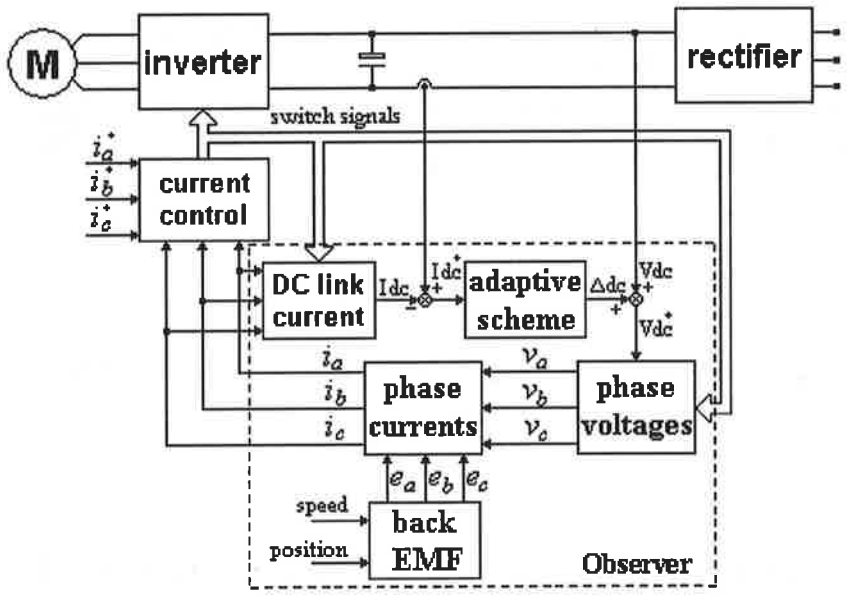

Figure 6.6 Block diagram of the phase current observer system

In this observer, the DC link current reconstruction has been discussed in Section 6.2 and the model of the PMAC motor drive was described in Section 4.2. The other parts of the observer will be described below.

6.3.2 Phase Voltage Reconstruction

The principle of the three-phase voltage reconstruction is relatively simple concept. Similar to the simulation model used in Chapter 4, three-phase voltages of the real motor drive system can be reconstructed using the DC link voltage and the switching signals. It should be noted here that in the motor with the rectangular excitation current, the back EMF voltages of the motor are also required in the reconstruction. A number of experimental results are given here, which are compared with the measured three-phase voltages to demonstrate the validity of the reconstruction approach proposed.

Apart from the three-phase currents, the DC link current and the switching signals, the DC link voltage and three-phase voltages of the motor drive were also sampled simultaneously in the tests. As mentioned in Section 4.2.3, when the motor is excited with the rectangular

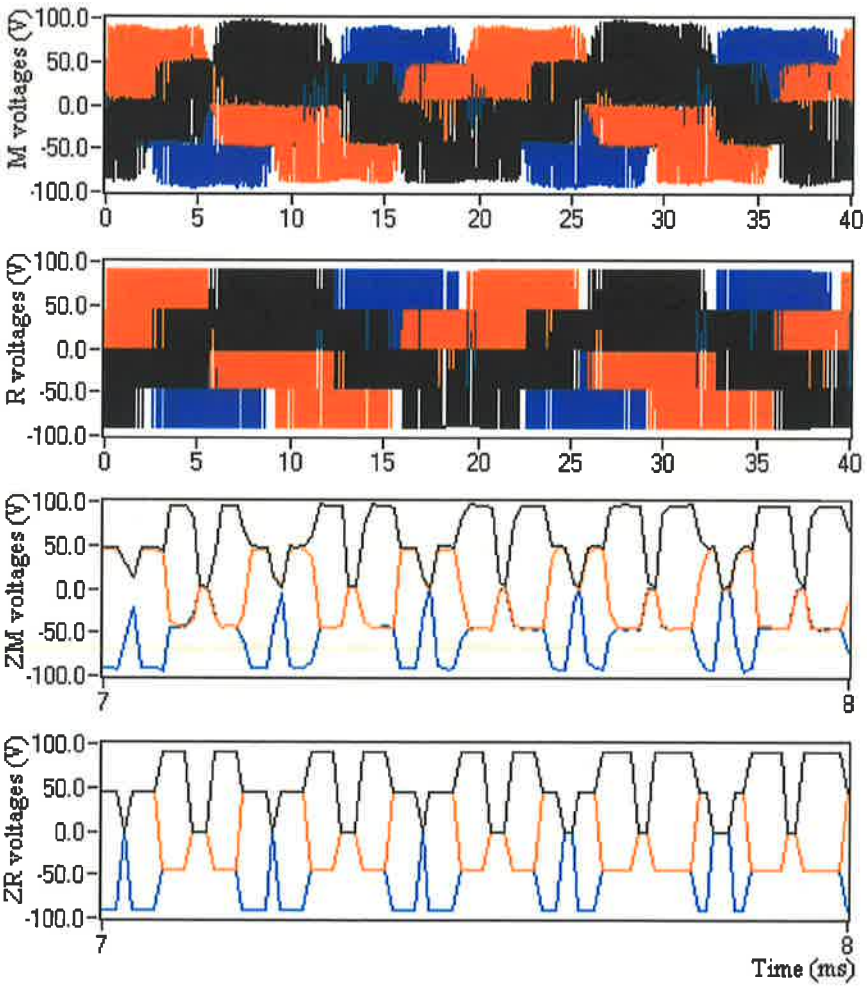

Figure 6.7 Measured (M), reconstructed (R), zoomed measured (ZM) and zoomed reconstructed (ZR) three phase voltages of the test motor under the sinusoidal current excitation.

currents, the three-phase voltage reconstruction technique requires the back EMF voltages. The back EMF voltages of the motor depend on the rotor position and the speed. Therefore, the measured three-phase currents and the voltages are used to estimate the required rotor position and the speed first (which is based on the technique proposed in Chapter 5). Then, the measured DC link voltage and the switching signals, together with the rotor position and the speed, are used to reconstruct the three-phase voltages that were based on Equation (4.25) or (4.26). Finally, the reconstructed results are compared with the measured three-phase voltages as given in the figures.

Figure 6.7 displays a number of measured and reconstructed waveforms when the motor was excited with sinusoidal currents. Since the phase voltages depends upon the DC link voltage and the switching signals only for the sinusoidal excitation, the reconstruction of the voltages are easy. It can be seen in the figure that the reconstructed phase voltages are very

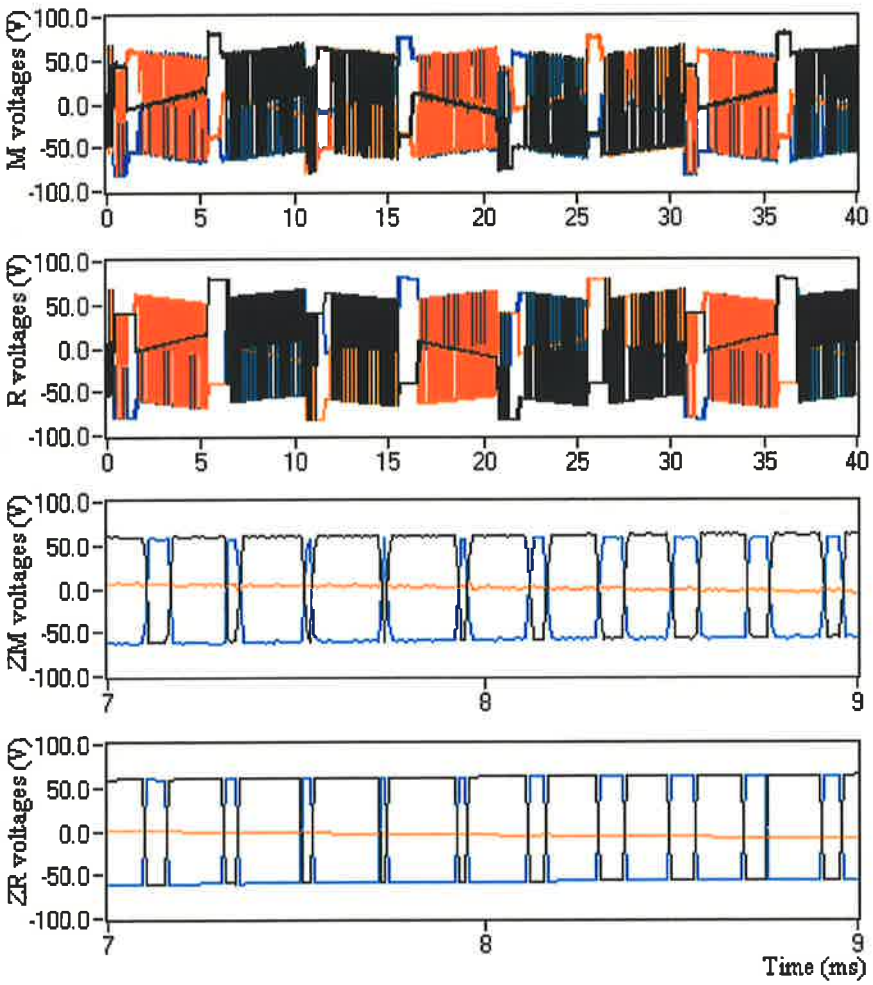

Figure 6.8 Measured (M), reconstructed (R), zoomed measured (ZM) and zoomed reconstructed (ZR) three phase voltages of the test motor under the rectangular current excitation.

close to the measured waveforms. In addition, when the zoomed waveforms were examined, it can be seen that the phase voltage contains pulses twice the PWM frequency, which is similar to the DC link current. A close examination of the voltage waveform also indicates that it is symmetrical in the first and in the second half-cycle of the PWM and has three values in each half PWM cycle: 0, $\pm\frac{1}{3}V_{dc}$ and $\pm\frac{2}{3}V_{dc}$. Therefore, to sample the voltages in a real time system, the A/D converter should have the scan rate of at least six times of the PWM frequency.

A second test was also performed under the rectangular current excitation of the motor drive, and the corresponding waveforms are shown in Figure 6.8. Again, there is a good agreement between the measured phase voltages and the reconstructed phase voltages. However, as stated earlier, in this current excitation mode the phase voltages depend upon the DC link voltage, the switching signals, the rotor position and the rotor speed. In addition, the state of a zero current in a phase is an important condition in the reconstruction of the phase voltages. In the practical system, if one phase current reaches to zero caused by the current measurement noises, the voltage reconstruction may produce incorrect results. These features indicate that the phase voltage reconstruction in the rectangular current excitation is more complicated and may be not suitable in some applications. Further discussions about these features will be given in the subsequent chapter.

Similar to the results given in Figure 6.7, it can be seen clearly in the zoomed waveforms of Figure 6.8 that the phase voltage usually has two possible values in each PWM cycle when three-phases are excited with the rectangular currents. Therefore, the sample of the voltage in a real time system requires a relatively lower scan rate.

6.3.3 Adaptive Scheme

Under the ideal conditions, the estimated three-phase currents using the mathematical model of the motor should be equal to the actual phase currents. In practice, however, there are always some discrepancies between the model established and the actual motor drive. In addition, the parameters of the motor may vary with the operating condition and the environmental factors. Therefore, it is desirable to have a correction routine in the observer system.

If three-phase currents are considered to be independent from each other, the phase currents are not observable when all three phases conduct current at the same time [58].

However, the three phases of the PMAC motor is symmetrical. If the control strategies for each phase are also symmetrical, the three-phase currents of the motor will be dependent and symmetrical. Therefore, it can be assumed that any changes in the operating and environmental conditions will have the same impact on each phase. Therefore, a variation on a phase current can be used to predict the variations on the other phase currents with the help of the operating conditions.

Furthermore, the DC link current is a combination of three-phase currents and is equal to one phase current during any active switch state. In fact, the error between the measured and the reconstructed DC link currents is the phase current error. Therefore, the DC link current error can be applied to correct the estimated three-phase currents at the instant considered. For example, when the DC link current is equal to the current of phase A, the error between the measured and the reconstructed DC link currents is equal to the error between the actual and the estimated currents of phase A. Hence, the error can directly be feedback to correct the phase A current estimation as in a linear observer. However, phase B and phase C have different operating conditions at this instant. Therefore, the error should be modified to represent the real operating condition first, and then it can be used to correct the phase B and the phase C current estimations as well.

In order to achieve a common modification method for all three phases of the motor drive, a novel correction algorithm is presented here. In the proposed algorithm, the DC link current error is not fed back directly to correct any phase current estimation as in the linear observer. Instead, it is used to compensate the DC link voltage. Then, the compensated value is modified by the switch states of each phase, and is fed back to correct the current estimations. To eliminate the effects of the measurement noise in the practical system, a proportional and integral adaptive scheme is used to regulate the DC link current error, and the result is applied to compensate the DC link voltage in the current observer, which is given by,

$$V_{dc}^{*} = V_{dc} + K_p \varepsilon_{dc} + K_i \int_0^t \varepsilon_{dc} dt \tag{6.3}$$

where $\varepsilon_{dc} = I_{dc}^{*} - I_{dc}$, is the error between the measured and the reconstructed DC link currents, V_{dc} is the measured DC link voltage, V_{dc}^{*} is the corrected DC link voltage, K_p and K_i are the constants of the PI current regulator respectively.

As seen from the discussions in Section 6.2.3, the DC link current is a current pulse with six values in each PWM cycle (or two values in the rectangular current excitation) and not all switch states are active. At zero-states, the phase currents circulate within the inverter bridge and the DC link current is equal to zero. The measured value of DC link current at zero-states cannot reflect any phase current and cannot be used as a valid feedback signal. In addition, some active switch states may be too short in a practical system for the DC link current. The feature of the DC link current indicates that some DC link current values are not measurable and measured zero values are not valid as the feedback signal.

As seen in Figure 6.2 and Figure 6.3, fortunately, at least one valid DC link current value, which is equal to one of the phase currents, is measurable in each PWM cycle under the normal operating conditions. Therefore, the phase current estimations can be corrected at least once per PWM cycle.

In the practical drive system, however, more complicated hardware and software are required to sample the valid DC link current value in each PWM cycle due to the irregular waveforms. An alternative approach is to use over sampling technique, that is, to sample every possible DC link current values as fast as possible at the highest acquisition frequency. In this way, all DC link current measurements are fed back to the adaptive correction algorithm, which force the reconstructed DC link current to follow the measured DC link current. Since the observer and the actual inverter use the identical switching control signals, and due to the symmetry of the motor windings, the estimated three-phase currents also follow the actual phase currents, even though their parameters may not be identical.

Since the DC link current is equal to zero at zero-states, the phase current observer can be seen as an open loop estimator and the estimated three-phase currents may not be corrected at these instants. By using the DC link current reconstruction formula in Equation 6.2, however, the zero DC link current feedback at zero-states can correct the balance of the three-phase estimated currents, that is, to force the sum of the three-phase estimated currents equal to zero. This is very important for the phase current estimation in the star connected motor.

6.3.4 Off Line Experimental results

To verify the validity of the proposed phase current reconstruction method, the practical PMAC motor drive implemented earlier was also used here. Similarly, when the motor drive is running, the three-phase currents and voltages of the motor, the DC link current, the DC

link voltage of the inverter, and the switching signals from the DSP controller were acquired simultaneously at an acquisition frequency of 100KHz. All of the acquired real data were saved in a file to be used for the off-line testing.

The phase current reconstruction simulation used here has the similar block diagram as the three-phase PMAC motor VI given in Figure 4.4. The rotor position and the speed are not directly measured but estimated from the acquired data of the three-phase currents and the voltages based on the position sensorless technique explained in Chapter 5. The data of the DC link voltage and the switching signals, as well as the back-EMF voltages generated from the rotor position and the rotor speed are utilized to reconstruct the three-phase voltages and to estimate the three-phase currents. The DC link current is reconstructed from the estimated phase currents as the output of the current observer. This output is compared with the measured DC link current data, and the error between them is regulated by the adaptive

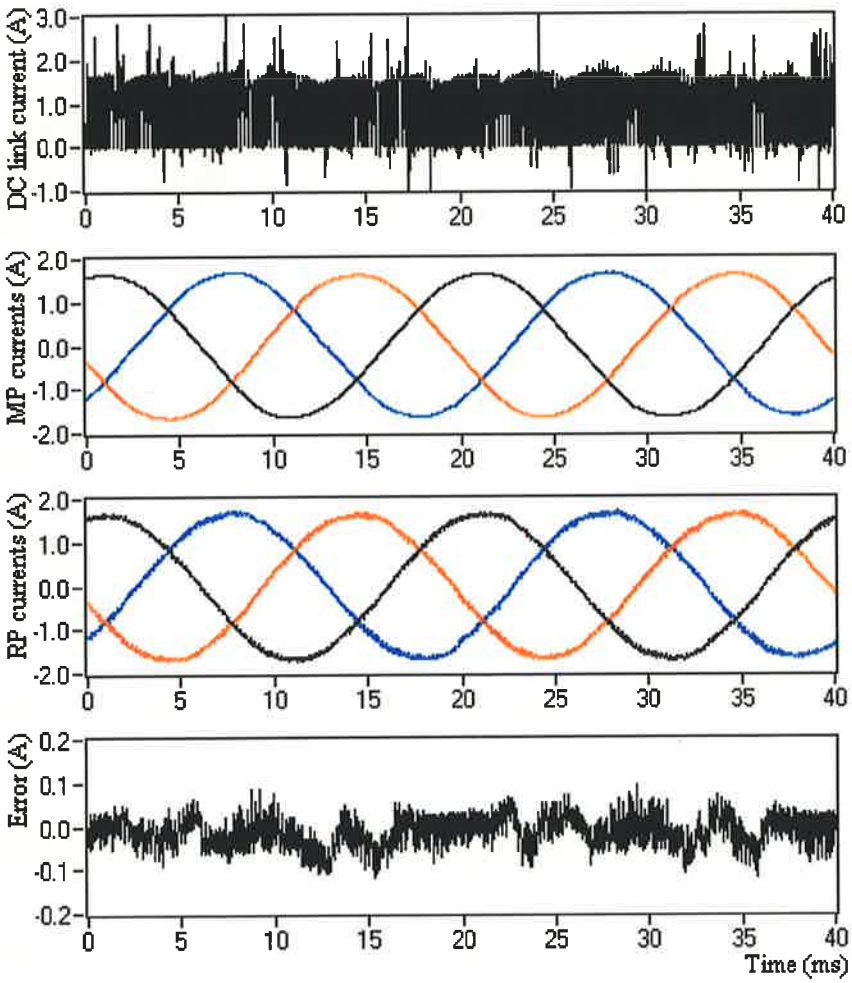

Figure 6.9 Off line experimental results for the sinusoidal PMAC motor excited by the sinusoidal current and operating at 50Hz: DC link current, measured phase (MP) current, reconstructed phase (RP) current, and current error of phase A.

algorithm. Finally, the regulation result is fed back to compensate the DC link voltage and to achieve adaptive correction for the estimation of the phase currents.

Several tests at different operating conditions were performed to reconstruct the three-phase currents using the measured switching signals and the DC link current and voltage. In these tests, the reconstructed values were compared with the measured currents to demonstrate the capability of the phase current reconstruction method proposed.

Figure 6.9 shows the experimental results when the motor was running at a speed of 50Hz and was excited by the sinusoidal currents. In order to visualise the quality of the reconstruction, the figure provides a number of waveforms, including the measured DC link current, the measured three-phase currents, the reconstructed phase current and the current error of phase A. Figure 6.10 provides similar test results but at a speed of 20 Hz. It can be seen from these two figures that the proposed method can reconstruct the phase currents

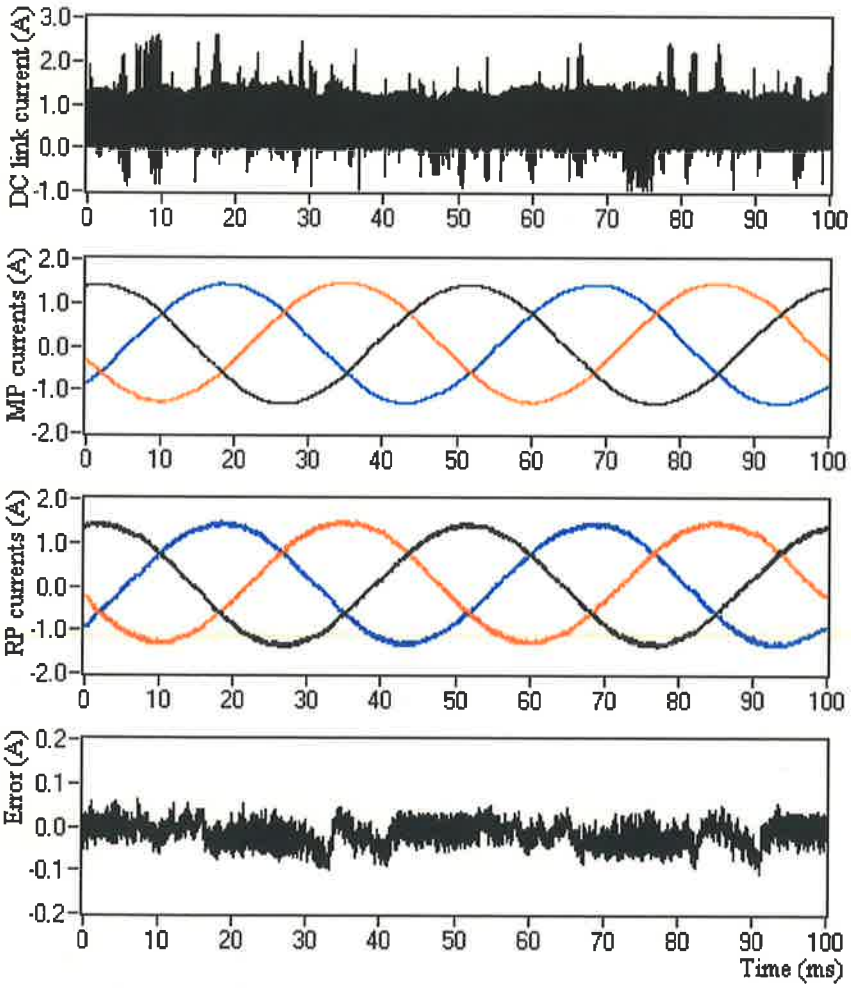

Figure 6.10 Off line experimental results for the sinusoidal PMAC motor excited by the sinusoidal current and operating at 20Hz: DC link current, measured phase (MP) current, reconstructed phase (RP) current, and current error of phase A.

accurately and the current errors are negligible. This demonstrates that the adaptive observer is a possible solution for the three-phase current reconstruction utilizing only one current sensor on the DC link. The results demonstrate that the reconstructed phase currents can be used as the feedback signals to implement the current closed loop control. From the figures, it also can be seen that the current error is larger at the intersection point of the two-phase currents. This is because the near equal duty cycles of the two-phase currents at the intersection point. Therefore, the shape of the DC link current is very narrow in these regions, which makes the accurate detection of the data difficult.

Similarly, when the test motor was excited with the rectangular currents, the experimental results were given in Figure 6.11 and Figure 6.12. In Figure 6.11, the motor drive was running at high speed, 50Hz and without current control. Figure 6.12 present the test results

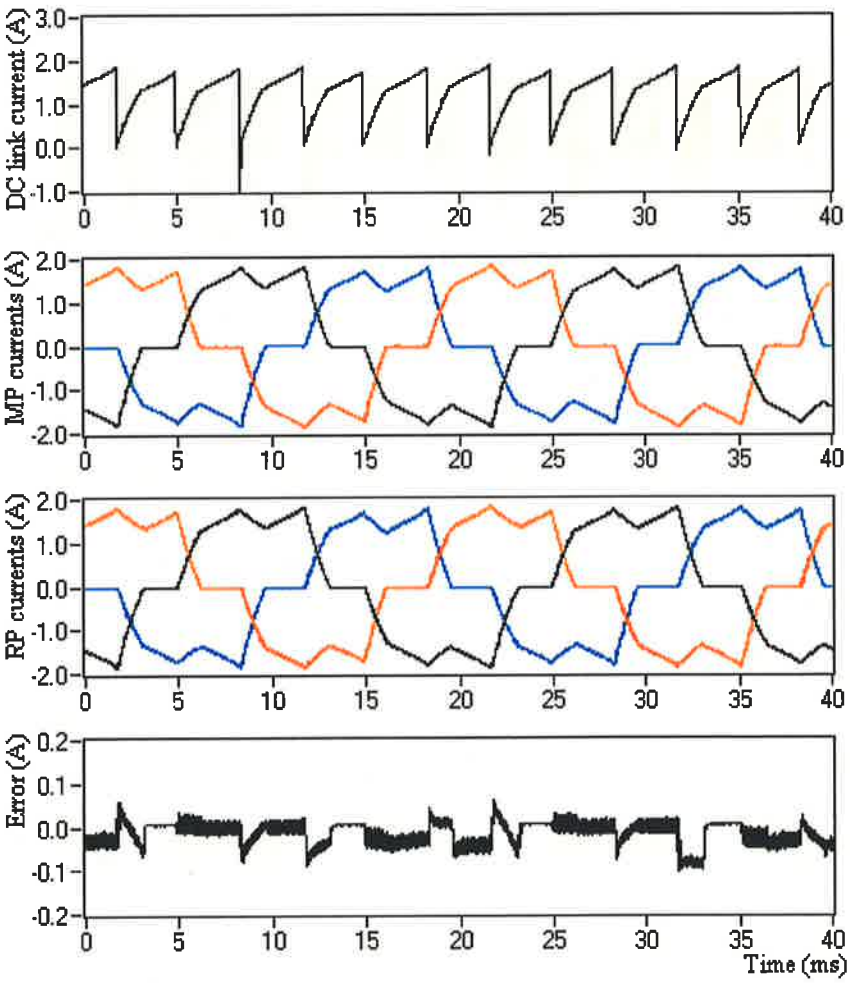

Figure 6.11 Off line experimental results of the sinusoidal PMAC motor excited by the rectangular current operating at 50Hz without current control: DC link current, measured phase (MP) current, reconstructed phase (RP) current, and error between measurement and reconstructed currents of phase A.

at a speed of 20Hz and with current control. It can be seen from these two figures that the proposed method can also reconstruct the phase currents in the trapezoidal PMAC motors. As discussed before, the adaptive observer method is based on the symmetry between the three phases of the motor. If the three phases are not symmetrical exactly, the errors during the commutation periods increase, which are observable in the figures given.

The phase current reconstruction method is based on an adaptive observer. As stated earlier, the motor parameters used in the observer may deviate from the actual values. Therefore, a number of tests were conducted to test the influence of the parameter variations on the phase current reconstructions. In these tests, the parameters of winding resistance, back EMF constant or equivalent inductance used in the observer was altered ±20%. The experiment results indicate that the parameter variations have little effect on the phase current

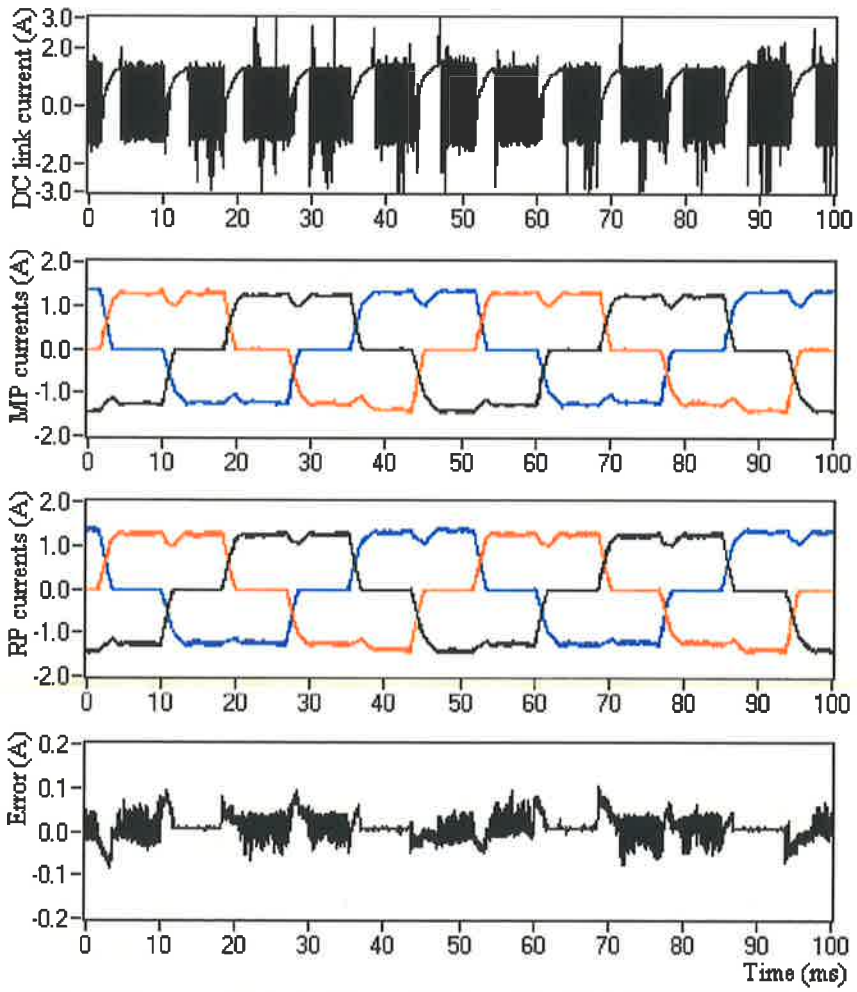

Figure 6.12 Off line experimental results for the sinusoidal PMAC motor excited by the sinusoidal current operating at 20Hz with current control: DC link current, measured phase (MP) current, reconstructed phase (RP) current, and current error of phase A.

reconstructions and the estimated phase currents can also follow actual phase currents accurately even under the faulty motor parameters. This means that the proposed reconstruction method has an adaptive ability for the parameter variation. Due to the similarity with above shown figures, the test results are not given here.

It should be emphasised that unlike the rotor position estimation that has the robustness against the measurement inaccuracies, the phase current reconstruction is fully depended on the DC link current measurement. Any measurement inaccuracies may deviate the reconstructed phase currents significantly from the real current. Therefore, it is important to ensure that the DC link current measurement is accurate to reduce the error in the reconstructed currents. However, it was demonstrated in this thesis that the proposed method is less sensitive to the spikes or other noises on the DC link current measurement. This is primarily because of the integration component of the adaptive scheme that eliminates the effects of the measurement noises.

6.4 Real-Time Implementation

In the previous subsections of this chapter, the proposed current reconstruction method was validated using a set of off-line experiments. This section, however, provides the real-time implementation details of the proposed technique while the technique was applied to the closed-loop current control of the motor drive. The principal purpose of this section is to demonstrate the feasibility of the method in the real motor drive. Some hardware and software issues are also discussed in the section.

6.4.1 Description of the Implemented System

Similar to the position sensorless control, the IRMDAC3 3-Phase 460VAC 3HP motor drive board and the ADMC 300 DSP-based motor controller and a single DC-link current sensor were used in the test setup. Figure 6.13 shows the block diagram of the system. As illustrated in the figure, two A/D converter channels of the DSP are used to measure the DC link current and the DC link voltage. In the tests, the encoder interface unit of the DSP is used to produce the measured rotor position and the speed information of the motor.

Since no internal register was available in the DSP chip to obtain the switching signal states, the switching signals used to control the inverter are connected to the digital input ports on the ADMC Connector Board using extra wires. Thus, the switching signals required

in the reconstructions of the DC link current and the phase voltages were obtained directly from the digital input ports.

For display and plotting purposes, the serial DAC on the ADMC connector board was used to convert the internal data to the analogue signals, such as the reconstructed three-phase currents, the measured DC link current and the rotor speed.

As mentioned before, the phase current reconstruction method fully depends on the DC link current measurement, and the actual DC link current is a high-frequency signal and has several values in each PWM cycle. To measure such high-bandwidth data, the sample rate of the A/D converter should be much higher than the PWM frequency. Similar to the position sensorless control, therefore, the software of the DSP to implement this single current sensor control should be separated into two interruption service routines with different interruption frequencies. One of the service routines is the PWM block, which implements the measurements of the rotor position and the speed, the speed regulation sub-routine, the current control sub-routine and the PWM output. This service routine is similar to the conventional control algorithm except the phase current signals that are not obtained from A/D converter but from an additional service routine. The additional service routine is used to implement the phase current reconstruction utilizing the switching signals, the measured DC link current and the voltage. The interruption frequency of the current reconstruction

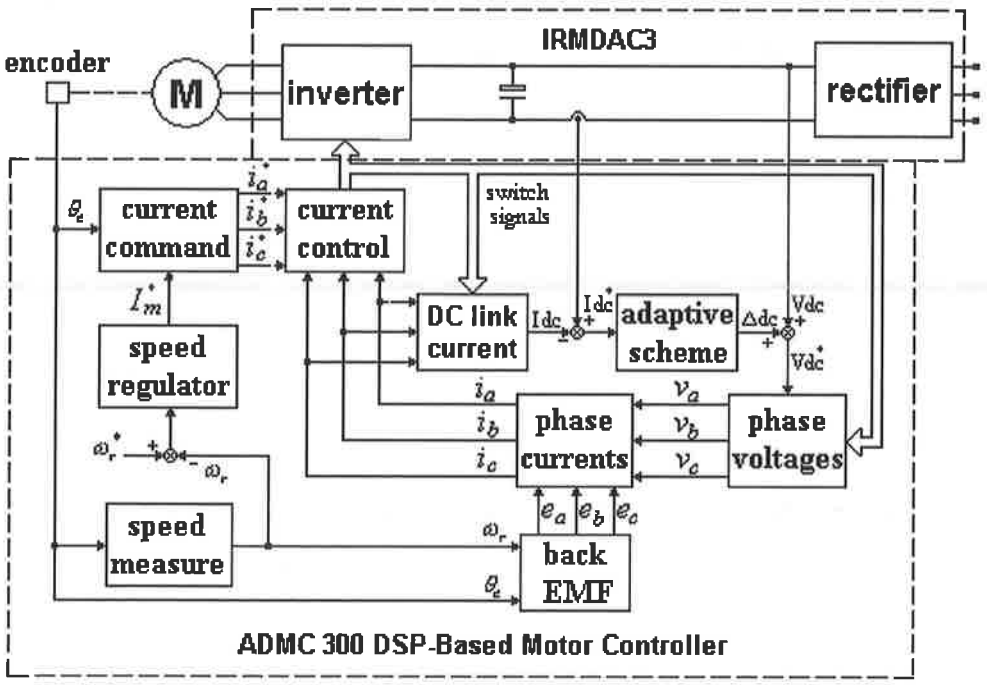

Figure 6.13 Block diagram of the drive system using a single current sensor.

routine is usually several times higher than that of in the PWM block. Since the reconstructed phase current values are only used in the current controller once per PWM cycle, the several reconstructed current values within this cycle can be averaged in the real time system. Like the position estimation in the real time system, this average filter can further eliminate the influence of the measurement noises on the DC link current and can achieve better reconstruction results.

In the standard sinusoidal PWM, there may be six valid DC link current values in each PWM cycle, and as explained before, some of these values may appear a very short period of time. Based on the features of the available hardware, the highest possible sample rate of the A/D converter is 31.5KHz. Therefore the PWM frequency of the system was selected as 1302Hz in order to achieve reasonable accuracy on the DC link current measurement. This means that the interruption frequency of the reconstruction service routine will be 24 times the PWM frequency, which was found sufficient to implement the single current sensor control in the sinusoidal current excitation mode.

In the rectangular current excitation, however, the special functions of the PWM block on the DSP chip are used to generate the required switching pattens, which have been detailed earlier in the section of position estimation method. Based on the switching patterns, only two different DC link current values may appear in each PWM cycle. Therefore, the sampling frequency of the DC link current measurement in the rectangular current excitation can be relatively lower than that of in the sinusoidal current excitation. In order to achieve a better performance in the rectangular current excitation, the interruption frequency of the reconstruction service routine again was set to the possible highest value of 31.5KHz. However, the PWM frequency was increased to 5208Hz in order to produce better modulation results, and the sample rate of the A/D converter was only 6 times the PWM frequency in the real time system.

6.4.2 Closed-Loop Experimental Results

To demonstrate closed-loop operation of the single current sensor control, a number of experimental results were obtained under a wide range of operating conditions, such as the steady state and the transient states, with and without the current control, and with sinusoidal or rectangular current excitation.

Figure 6.14 shows the steady-state experimental results of the single current sensor drive under the sinusoidal current excitation. The measured DC link current and the reconstructed three-phase currents are given in the figure for two different speeds (43 Hz in Figure (a) and 14 Hz in Figure (b)).

It can be seen from the figure that the reconstructed phase current waveforms in both operating modes can be utilised as the current feedbacks in the PMAC motor drive. Although there are some small ripples on the current waveforms, which is due to the low PWM frequency, the closed loop control using the reconstructed phase currents is stable and achieves high static performances. However, when the speed of the motor drive is reduced, such as lower than 10Hz, the experiments indicated that the single current sensor drive system becomes unstable. The principal reason for this is that the proposed reconstruction method is completely based on the DC link current measurement. At low operating

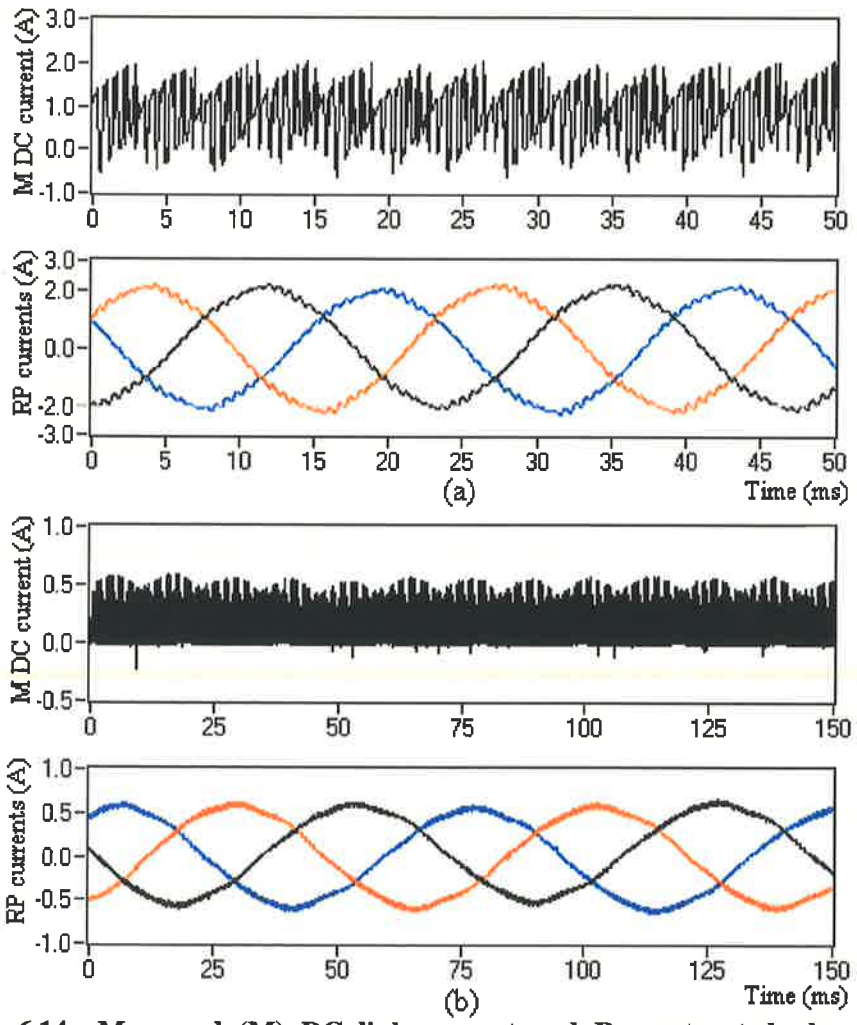

Figure 6.14 Measured (M) DC link current and Reconstructed phase (RP) current in the real-time drive system with sinusoidal current excitation: (a) High-speed operation without current control, (b) Low-speed operation with current control.

frequencies, the modulation index of the sinusoidal PWM is deeper, and the DC link current pulses are very narrow. Therefore, it is difficult to detect a valid value of the very short DC link current pulses using the available hardware at the highest sample frequency of 31.5KHz. If the DC link current measurement is less accurate, the phase current reconstruction becomes less reliable. An unreliable phase current feedback and a lower PWM frequency can make the motor drive system unstable. Therefore, to improve the performance of the reconstruction, a higher speed DSP with high performance A/D converter should be used as the controller, such as ADMC 501.

When the motor is excited with the rectangular current, the steady-state experimental results are shown in Figure 6.15. As seen in the figure, since the PWM frequency in the rectangular current excitation is much higher, no apparent small ripples appear on the current

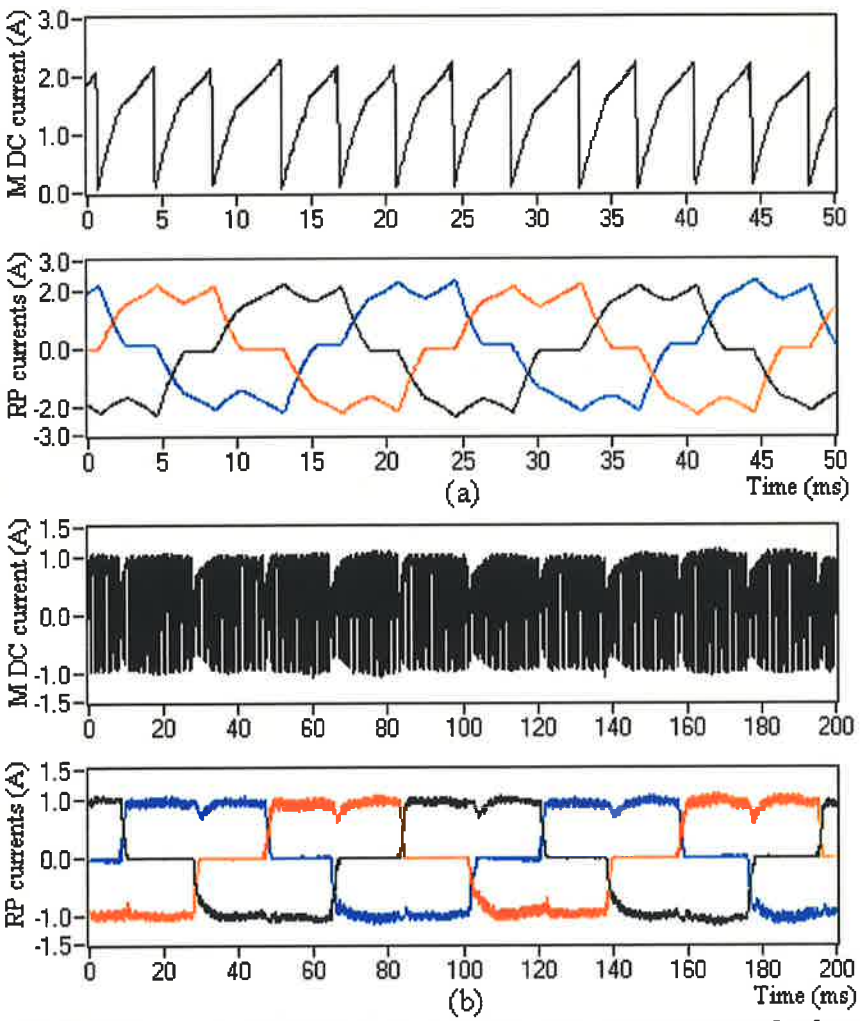

Figure 6.15 Measured (M) DC link current and Reconstructed phase (RP) current in the real-time drive system with rectangular current excitation: (a) High-speed operation without current control, 43Hz (b) Low-speed operation with current control, 9Hz.

waveforms as in the sinusoidal excitation. As seen in Figure 6.15a, since the DC link current can be detected accurately in the high-speed without current control operation, the reconstructed phase currents are good to be in the real time motor drive. When motor is excited with rectangular current, the single current sensor motor drive system can operate stably at lower speed than that of sinusoidal excitation. This is because the DC link current can still be accurately detected at low speed range when the special switching pattens are utilized to generate the rectangular excitation current.

As mentioned before, only two different DC link current values may exist in each PWM cycle when the motor current is under control, and the DC link current is a bipolar current pulse and has the same frequency as the PWM. When the motor speed decreases, the modulation index of the PWM is deeper. Similar to the bipolar modulation, however, the

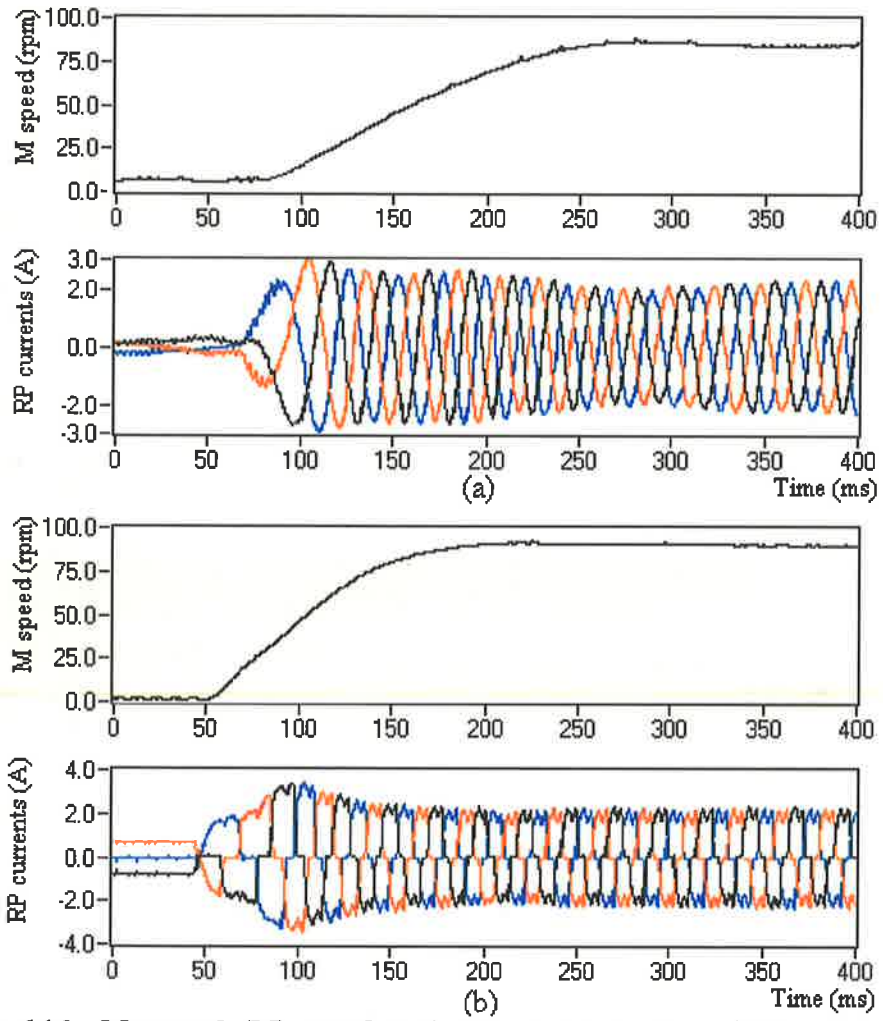

Figure 6.16 Measured (M) speed and reconstructed phase (RP) current in dynamic state of the real-time drive system: (a) With sinusoidal current excitation, (b) With rectangular current excitation.

deeper modulation index means that the duty cycle of PWM is about 50%. This duty cycle indicates that the two DC link current values can be detected accurately by the A/D converter. Therefore, the proposed phase current reconstruction method is suitable for the rectangular current excitation and can be used in a wide speed range.

Figure 6.16 shows a set of dynamic experimental results of the motor drive system operating using a single current sensor on the DC link. When the motor is excited with the sinusoidal currents, the dynamic waveforms of the measured rotor speed and the reconstructed three-phase currents are given in Figure 6.16a. In this test, the motor was accelerated from 8rpm to 80rpm, and a god dynamic performance was observed. Figure 6.16b shows the dynamic results when the motor was accelerated 4rpm to 85rpm using the rectangular current excitation. The results demonstrated that the proposed reconstruction method is also suitable for the rectangular current excitation, and good dynamic performances of the motor drive system can be achieved using a single current sensor.

6.5 Conclusions

The chapter proposed a novel three-phase current reconstruction technique for the PMAC motor drives, which utilised the DC link current measurement and the switching signals of the inverter. The technique is based on an adaptive current observer that effectively compares the reconstructed and the measured DC link currents and corrects the three-phase current estimates. The technique is suitable for both the sinusoidal and the rectangular current excited PMAC motors.

In the chapter, a comprehensive analysis was given to explain the relationships among the DC link current, the phase voltages and all possible switching states in the three-phase inverter that is connected to the PMAC motor. The analysis was also covered two different types of current excitations used in the PMAC motor control, rectangular or sinusoidal current excitation.

The experimental results demonstrated that the reconstructed three-phase currents can follow the actual winding currents accurately under different operating conditions and have small static errors and fast dynamic responses. Therefore the method is suitable for the practical applications, which can accommodate a single current sensor to implement a closed loop current control.

Since the phase current reconstruction technique is based on a state observer, the parameters of the motor are required in the estimation of the phase currents. With the help of adaptive scheme, however, divergences of the parameters have very small impact on the phase current reconstruction, that is, the reconstructed phase currents are not sensitive to the parameter variations. This feature indicates that the proposed phase current reconstruction technique has adaptive ability to the parameter variations. However, the phase current reconstruction is fully depended on the DC link current measurement. In order to implement a good system, a higher speed DSP controller with high performance A/D converter should be utilized to measure the DC link current as accurately as possible. Unlike the previous techniques, this novel method does not require complex hardware circuits and does not require any modification on the PWM signals, which may influence the actual output currents of the inverter and increase their harmonic components. Moreover, the integration action in the adaptive scheme and the average algorithm within one PWM cycle can eliminate the influences of the DC link current measurement noise. This means that the proposed reconstruction technique is not sensitive to the current spikes that inevitably appear on the DC link current measurements.

An inaccurate DC link current measurement may cause unreliable phase current reconstruction. Therefore when the motor is excited with sinusoidal currents, the reconstruction technique has limitations at very low speed range unless the hardware is improved. However, there is no such limitation when the motor is excited with thc rectangular current excitation.

The main purpose of this phase current reconstruction technique presented here is to reduce the number of current and voltage sensors used in the PMAC motor drives. Therefore, a position sensorless PMAC motor drive system with a minimum number of sensors can be realized, which will be discussed in the subsequent chapter, Chapter 7.

Chapter 7
PMAC Motor Drive with a Minimum Number of Sensors

7.1 Introduction

As discussed in Chapter 2, a PMAC motor has permanent magnets mounted on its rotor and polyphase excitation windings inserted in the stator that is similar to a conventional induction motor. When the rotor is rotating, the back-EMF voltages induced in the stator windings are AC. In order to produce a constant torque, the winding excitation currents should also be AC and should be synchronised with the back-EMF voltages. Therefore, the most fundamental requirement in the PMAC motor control is to know the rotor position information, which is required to generate the excitation currents and to implement self-synchronous control. In addition, the speed control may be necessary in many applications. To achieve this goal, a speed feedback signal is also required to implement the closed loop speed control. Furthermore, in some applications, such as PMAC servo motor drives, the torque control is required to achieve a high dynamic performance, which can easily be done by mapping it to the current control. The purpose of the current control is to force the actual phase currents to track the reference currents in the closed loop current controller, which can be achieved by measuring the three-phase currents.

It can be seen from the above explanations that a high performance PMAC motor drive requires a number of sensors to obtain the necessary feedback signals, the rotor position, the rotor speed, and the three-phase currents. All these quantities can be measured directly from the motor drive. However, using sensors increases the complexity and the cost of the drive while reducing it reliability. Therefore, the reduction of the number of sensors in the PMAC motor drives is considered in this chapter.

In a practical motor drive, the rotor speed data can be derived from the rotor position information, so that the speed sensor can be eliminated. In addition, if the motor is star-connected, the number of current sensors can be reduced to two since the third phase current can be derived easily using the other two-phase currents. Therefore, it may be sufficient to

use only three sensors (one position sensor, two phase current sensors) to implement a high performance motor drive.

Traditionally, the rotor position information is obtained directly from the motor shaft using some form of shaft-mounted position sensor. As studied in detail in Chapter 3, the elimination of the shaft-mounted position sensor is very desirable objective that can be realised by using a position sensorless technique. However, in order to estimate the rotor position accurately, most of the successful techniques require accurate measurement of the three-phase currents and the voltages in the motor drive, which means that five sensors are still required to implement the position sensorless PMAC motor drive. In these approaches, if the motor has sinusoidal back-EMF voltages and sinusoidal excitation currents, the number of voltage sensors can be reduced to two when two-phase reference frame is used in the position estimators. However, the number of sensors just to replace the shaft mounted position sensor remains high: two current and two voltage sensors.

Furthermore, the voltage and current measurements in the real drive require electrical isolation, which increases the sensor's cost significantly, while reducing the measurement accuracy due to the limited bandwidth of the practical sensors.

As stated previously, employing a minimum number of sensors in the PMAC motor drive is the primary aim in this chapter. The chapter discuses the feasibility of such aim and how to combine the previous sensor reduction techniques proposed and implemented in Chapter 5 and Chapter 6.

Section 7.2 reviews the reconstruction methods of the phase voltages and the currents in two different type PMAC motors: sinusoidal and trapezoidal PMAC motors. In Section 7.3, the fundamental requirements of rotor position estimation are revisited. Based on the position sensorless technique proposed and the reconstruction methods of the phase currents and the voltages, the PMAC motor drive system with a minimum number of sensors is explained in Section 7.4. Some open-loop experimental studies were presented in the same section to illustrate the features of the reconstructed values of the phase voltages and currents, and the estimated rotor position using these reconstructed values. The section also discusses the real time implementation issues and provides a wide range of closed-loop experimental results. These results demonstrate the feasibility of the PMAC motor drive utilizing a minimum number of sensors: two sensors if the DC link voltage is not constant or one DC link current sensor if the DC link voltage is constant. Section 7.5 draws some conclusions and

summarizes the features of the high performance PMAC motor control using the minimum number sensors.

7.2 Minimizing the Current and the Voltage Sensors

In most PMAC motor applications, the knowledge of the phase currents and the voltages is required to implement the closed-loop current control and to accommodate inverter and drive protection. In the position sensorless motor drive system, the phase current and voltage signals are also required to estimate the rotor position. As stated earlier, in order to minimize the number of sensors, the three-phase currents and voltages of the PMAC motor can be reconstructed using the DC link measurements and the switch states of the inverter.

7.2.1 Phase Voltage Reconstruction

When the PMAC motor is powered from the three-phase inverter, the three-phase voltages of the motor are closely related to the switch states of the inverter. As discussed in Chapter 4 and Chapter 6, the unified expression for the phase voltage reconstruction can be rewritten as:

$$v_p = \frac{1}{K}\left[\left(K \cdot S_p - S_a - S_b - S_c\right)\cdot\frac{V_{dc}}{2} + \left(|S_a|\cdot e_a + |S_b|\cdot e_b + |S_c|\cdot e_c\right)\right] \tag{7.1}$$

In the above expression, the switch states (S_a, S_b, S_c) depend on the switching signals of the inverter and the directions of the phase currents, and the DC link voltage, V_{dc} can easily be measured. However, the three-phase back EMF voltages (e_a, e_b, e_c) cannot be measured directly but can be estimated from the rotor position and the speed signals.

If the three-phase voltages used to estimate the rotor position and the speed are conversely reconstructed from the estimated rotor position and the speed, the motor drive control may not operate steadily and has low reliability against the changes in the operation conditions. If back EMF voltages of a PMAC motor are sinusoidal, fortunately, the sum of the three-phase back EMF voltages is equal to zero. When all three phases are excited with the currents, such as three-phase sinusoidal currents, there are only eight possible switch states, which makes the phase voltage reconstruction simple:

$$v_p = \left[S_p - \frac{1}{3}\left(S_a + S_b + S_c\right)\right]\cdot V_{dc}/2 = \frac{V_{dc}}{6}\left(3\cdot S_p - S_a - S_b - S_c\right) \tag{7.2}$$

This expression indicates that the phase voltages of the sinusoidal PMAC motor only depend on the DC link voltage and the switch states, which can be derived from the switching signals and using the directions of the phase currents that were given in Table 6.3.

In the standard sinusoidal PWM strategy, two switching signals in one phase of the inverter should have opposite sign at any time except the dead time. During the dead time, the two switching signals are equal to zero (to turn the power switches off), and the switch state of the relevant phase depends on the directions of the phase current. The existence of the dead time indicates that the switch states are different from the switching signals of the inverter. In a practical inverter, however, the dead time only lasts very short period of time. If the reconstructed phase voltages are only used in the current observer and in the rotor position estimator, the impact of the dead time on the reconstructed phase voltages can be ignored. Therefore, the phase voltages sometimes may be reconstructed simply using the switching signals in the sinusoidal current excited motor.

When the reconstructed phase voltages are used to estimate the rotor position and the speed of the motor, they bring additional benefits to the estimation. As mentioned before, the three-phase voltages of the inverter driven motor are high-frequency voltage pulses, and the measured phase voltages always contain some high-frequency measurement noises that are hard to filter. Some of the benefits of the reconstructed phase voltages are that the influence of the noise and the measurement DC offset in the position estimation are eliminated. This improves the accuracy of the rotor position estimation significantly.

However, it should be noted here that the reconstructed phase voltages might be different from the actual phase voltages specifically if the motor is running at very low speeds. If the DC link voltage remains constant, some of the voltage pulses become very narrow pulses when the motor speed slows down. In addition, at very low speed range, the dynamic voltage drops of the power devices may influence these narrow voltage pulses. However, the reconstruction method of the phase voltages implemented here assumes ideal power devices in the inverter. Therefore, the influences of the dynamic voltage drops of the power devices can make the reconstructed values far from ideal.

If the back EMF voltages of the PMAC motor are trapezoidal, however, the sum of the three-phase back EMF voltages is not equal to zero. In addition, the trapezoidal motor normally requires rectangular excitation currents. In this case, there are only two phases conducting the currents at a given time except the commutation periods. If only two of the

three phases conduct current, the voltage of unexcited phase is equal to the back-EMF voltage of that phase, that is,

$$If \quad S_p = 0, \quad v_p = e_p \tag{7.3}$$

If the phase voltage is reconstructed based on the above equation, the voltage depends on the rotor position and the speed signals only. Therefore, if there is an estimation error in the rotor position and the rotor speed, the reconstructed phase voltage will be affected from this error. This generates more error if the reconstructed phase voltage is again used to estimate the rotor position and the speed. Such positive feedback action, consequently, can make the position estimation incorrect causing significant vibration in the motor drive. Therefore, as will be demonstrated later, the voltage reconstruction technique to estimate the rotor position cannot easily be implemented in the trapezoidal PMAC motor drives.

7.2.2 Phase Current Reconstruction

In the position sensorless PMAC motor drive system, three-phase current signals are used in the estimation of the rotor position, as well as in the closed-loop current control.

When the motor is powered from an inverter, the three-phase currents of the motor are closely related to the DC link current of the inverter. As described in Chapter 6, this relationship was used to reconstruct the three-phase currents, which was based on an adaptive current observer. The method proposed used the mathematic model of the PMAC motor drive as a state observer. In the observer, the DC link current was constructed first using the estimated three-phase currents from the motor model. Then assuming a three-phase symmetry in the PMAC motor, the observer output compares the measured and the reconstructed DC link currents and produces some compensation on the DC link voltage that is used to reconstruct the three-phase voltages in the current observer. As demonstrated, such compensation can correct the estimated three-phase currents and force them to follow the actual winding currents under all operating conditions. Figure 7.1 redraws the portion of the current observer that was given earlier in Figure 6.6.

The experimental results given in Chapter 6 show that the current observer can reconstruct the three-phase currents of the PMAC motor accurately using the DC link measurements and the switching signals of the inverter. As also demonstrated, the reconstructed phase currents

have smaller static errors and faster dynamic responses and can be used as feedback signals to implement the closed loop current control in the PMAC motor drives.

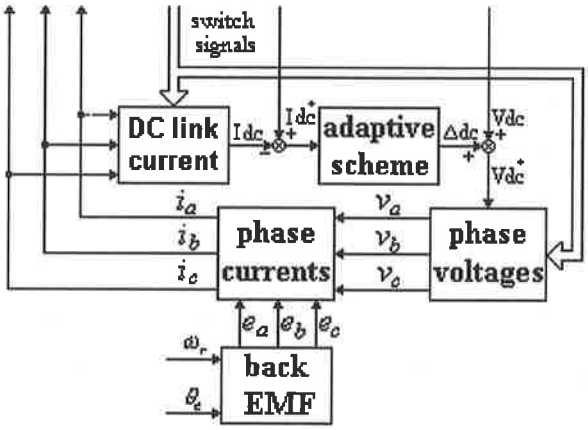

Figure 7.1. Block diagram of the current observer

Due to the sufficient accuracy in the reconstruction, the reconstructed phase currents can also be used in the rotor position estimation routine. When these reconstructed current are used in the actual drive, although some small fluctuations in the current waveforms are present, these can be considered as measurement noises that have a limited impact on the rotor position estimation.

When the parameters used in the current observer are different than the actual motor parameters, the reconstructed phase currents may have some small phase difference compared to the actual currents. However, the effect of the phase difference on the position estimation can be limited if the proposed robust position estimation algorithm is used. In addition, since the reconstruction is based on an ideal symmetrical mathematic model of the motor, the reconstructed three-phase currents have little or equal offset errors. The equal offset errors on three-phase current signals have no effect on the rotor position estimation as discussed in Section 5.4.2.

It should be noted here that the current reconstruction technique is based on the current observer that requires the back EMF voltages, which cannot be measured but were generated using the estimated rotor position and the speed. This means that the reconstructed phase currents and the estimated rotor position are interrelated. However, the back EMF voltages play a minor role in the current estimation as can be seen from the mathematic model. Moreover, the current observer is a closed loop adaptive observer. The modified DC link voltage can compensate the errors in the estimated back EMF voltages. Unlike the phase

voltage reconstruction in the trapezoidal PMAC motor, the reconstructed phase currents can still be used to estimate the rotor position and the speed even though their reconstruction is related to the back EMF voltages.

By using the phase current reconstruction technique proposed, the number of current sensors required in the PMAC motor drive system was reduced to a single sensor. As a result, the total number of sensors required in the motor drive was reduced to two sensors: one voltage sensor to measure the DC link voltage, and one current sensor to measure the DC link current. Furthermore, when the motor drive is supplied from a utility power line, the DC link voltage of a voltage source inverter may be assumed constant, which allow the elimination of the voltage sensor. In this case, only one current sensor is sufficient to implement the closed-loop PMAC motor drive.

7.3 Elimination the Rotor Position Sensor

As stated previously, the PMAC motor is a synchronous motor. Therefore, to control such motor, the rotor position information is required, which is utilised to generate the excitation currents that are in synchronism with the back-EMF voltages. Although shaft-mounted position sensors are used traditionally to obtain the rotor position, the proposed indirect position sensing method explained in the earlier chapters utilises the motor's voltages and currents to determine the rotor position.

When the previous position sensorless techniques are reviewed, it can be seen that minimisation of the sensors in the PMAC motor drives are difficult. For the methods of back-EMF sensing, the voltage sensors used to measure the back-EMF voltage on the unexcited phase cannot be eliminated or minimized. This implies that the position sensorless techniques cannot be used to implement a PMAC motor drive with a minimum number of sensors. In addition, most of the observer-based methods are computationally intensive and are sensitive to the errors that are present in the practical motor drives. Due to the reconstructed phase voltages and currents may be slightly different from actual values, the techniques sensitive to the differences are not suitable for the PMAC motor control with a minimum number of sensors. Furthermore, the current measurements play an important role in the position detection using the rotor saliency. If the reconstructed phase currents are used to replace the current measurements, much valuable information on the current waveforms can be lost. Therefore, the position sensorless techniques based on rotor saliency are also not suitable to minimize the number of sensors in the closed-loop control of PMAC motor drive.

In order to minimize the number of sensors in a PMAC motor control, the requirements of three-phase current and voltage information should be reconstructed from DC link measurements. Although the reconstructed values may be slightly different from actual phase currents and voltages, the position sensorless technique detailed in Chapter 5 has the robustness with respect to these differences. Therefore, the integration of the two techniques proposed in the previous chapters can minimize the number of sensors used in a PMAC motor drive.

Similar to the measurement errors, the reconstructed values may also have three types of errors, offset errors, scaling errors and noises. Using the proposed reconstruction methods, the offset errors of three-phase voltages and currents are nearly zero or equal each other. As mentioned before, the equal offset errors have no impact on the rotor position estimation. Although a possible larger scaling error caused by the reconstruction may generate a larger position estimation error, this will be limited by the auto-correctional action of the robust position estimation algorithm proposed. The other differences between reconstructed and actual values can be assumed as measurement noises, but the noises are mush smaller compared with other reconstruction methods. The smaller assumed measurement noises on reconstructed voltages and currents can produce smaller random position estimation errors, which could be filtered by the average action in the real time system.

Therefore, it can be concluded that the position estimation technique proposed in this thesis can use the reconstructed three-phase currents and voltages to estimate rotor position information accurately, which allows the significant reduction on the number sensors used.

7.4 Realization of the PMAC Motor Drive with a Minimum Number of Sensors

In this section, the integration of the previous estimation and reconstruction techniques are done, the integrated system was realized, and a number of experimental results were presented to demonstrate the feasibility of the implementation of the PMAC motor control using only two sensors.

7.4.1 Motor Drive System

Figure 7.2 shows the block diagram of the PMAC motor drive system that accommodates only two sensors: DC link current and voltage sensors. As stated earlier, a further reduction

of the sensors is possible if the DC link voltage remains constant during the operation of the motor drive, and its value is known in the drive model. As explained previously, the close relation between the reconstructed phase currents and the estimated rotor position does not influence the stability of the closed loop position sensorless control in the real time system.

Furthermore, it should be emphasised here that the phase voltages should be reconstructed twice in the integrated motor drive. First, in the current observer, the measured DC link voltage must be compensated by the adaptive scheme using the DC link current error and then can be used to reconstruct the modified phase voltages, which are used in the estimation of the phase currents. Second, the actual measured DC link voltage should be directly used to reconstruct the phase voltages that are required in the position estimation algorithm.

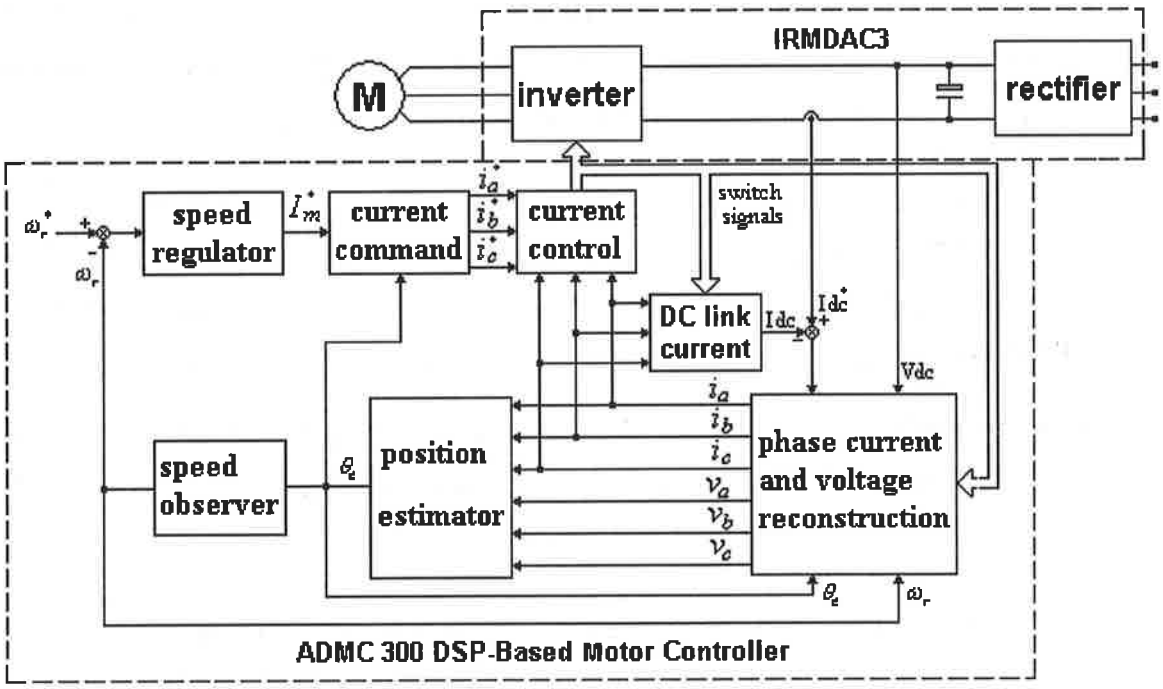

Figure 7.2 PMAC motor drive with a minimum number of sensors

Consequently, the speed observer uses the rotor position to estimate the angular speed signals, which is then used as the speed feedback to implement the closed loop speed control. The output of the speed regulator is defined as the amplitude of the current command. Together with the estimated rotor position signals, the amplitude is used to generate the required current reference signals, and the reconstructed phase currents are used as the current feedback signals.

7.4.2 Open-Loop Experimental Results

In the open-loop tests, the PMAC motor drive was controlled using the conventional control approach. The standard PWM strategies with a PWM frequency of 5KHz were used to generate the reference excitation currents. When the motor drive was running, the data acquisition system was used to sample various quantities simultaneously at a frequency of 100KHz. The measured quantities include three-phase voltages, two-phase currents, the DC link current and voltage, the measured rotor position and the switching signals of the inverter.

In this study, the acquired data of the switching signals, and the DC link current and the DC link voltage are utilized to reconstruct the three-phase voltages and currents, and then to estimate the rotor position. The off-line data processing was performed by a custom written software in LabVIEW. The reconstructed three-phase voltages and currents, and the estimated rotor position were plotted and compared with the measured values to demonstrate the feasibility of the PMAC motor control technique using two real sensors.

Figure 7.3 illustrates the open loop experiment results when the motor is excited by the sinusoidal currents and running at a steady-state speed of 53.5 rpm (about 25Hz). The figure shows the waveforms of measured (M) and estimated (E) rotor position, measured (MP) and reconstructed (RP) three-phase currents, and measured and reconstructed three-phase voltages. As demonstrated in the figures, the rotor position, the phase currents and voltages are accurately estimated, indicating that two of the measured values, the DC link voltage and current, can be used as the feedback signals to implement the PMAC motor control.

When the motor is excited with the rectangular currents at a steady-state speed of 53.5 rpm (about 25Hz), the open loop experiment results are given in Figure 7.4. Similarly, there is a good agreement between the measured and the reconstructed and estimated values. However, a close observation of these results indicate that the rotor position estimation and the reconstruction of phase voltages and currents are more sensitive to the measurement inaccuracies and the parameter variations, which is primarily due to the open loop reconstruction of the phase voltages. When the motor is excited with the rectangular currents, the phase voltages depend on the DC link voltage and the switching signals as well as the rotor position and the speed signals. While, the rotor position and speed signals are estimated from the reconstructed phase voltages and currents. If measurement inaccuracies and the parameter variations cause some estimation errors on the rotor position and the speed, the reconstructed phase voltage differ from the actual value. Using these inaccurate reconstructed

phase voltages in the estimation, more errors are generated on the rotor position and the speed. Therefore, it can be concluded that two sensors approach is more sensitive to the measurement inaccuracies and the parameter variations in the rectangular current excitation, which may cause instability in the real motor drive.

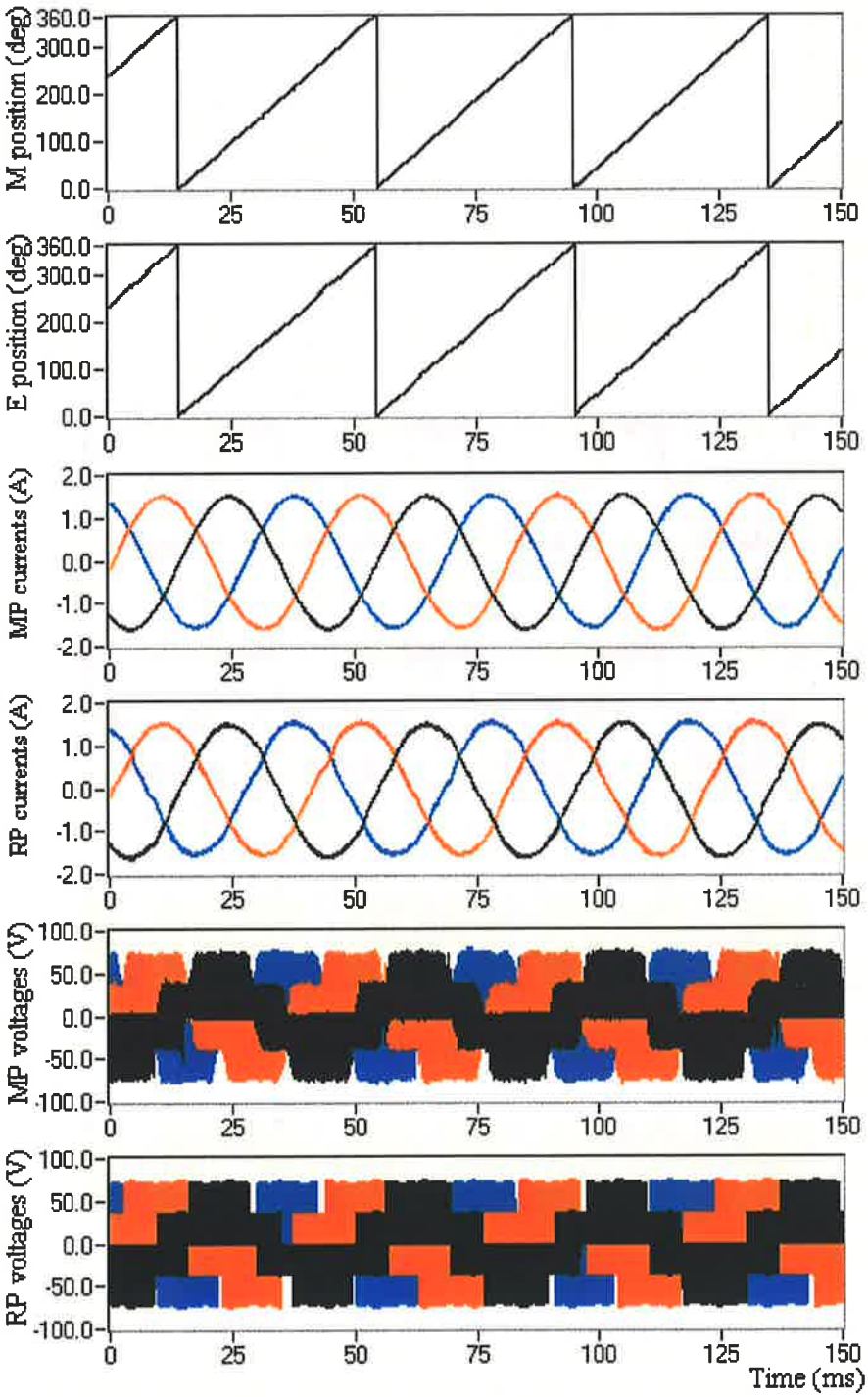

Figure 7.3 Open loop test results of the phase voltage and current reconstruction and the rotor position estimation under the sinusoidal current excitation at 25Hz.

In order to clearly indicate the test results of rotor position estimation and phase current reconstruction, Figure 7.5 show the errors of estimated rotor position and reconstructed phase current in the open loop test in the Figure 7.3 and Figure 7.4.

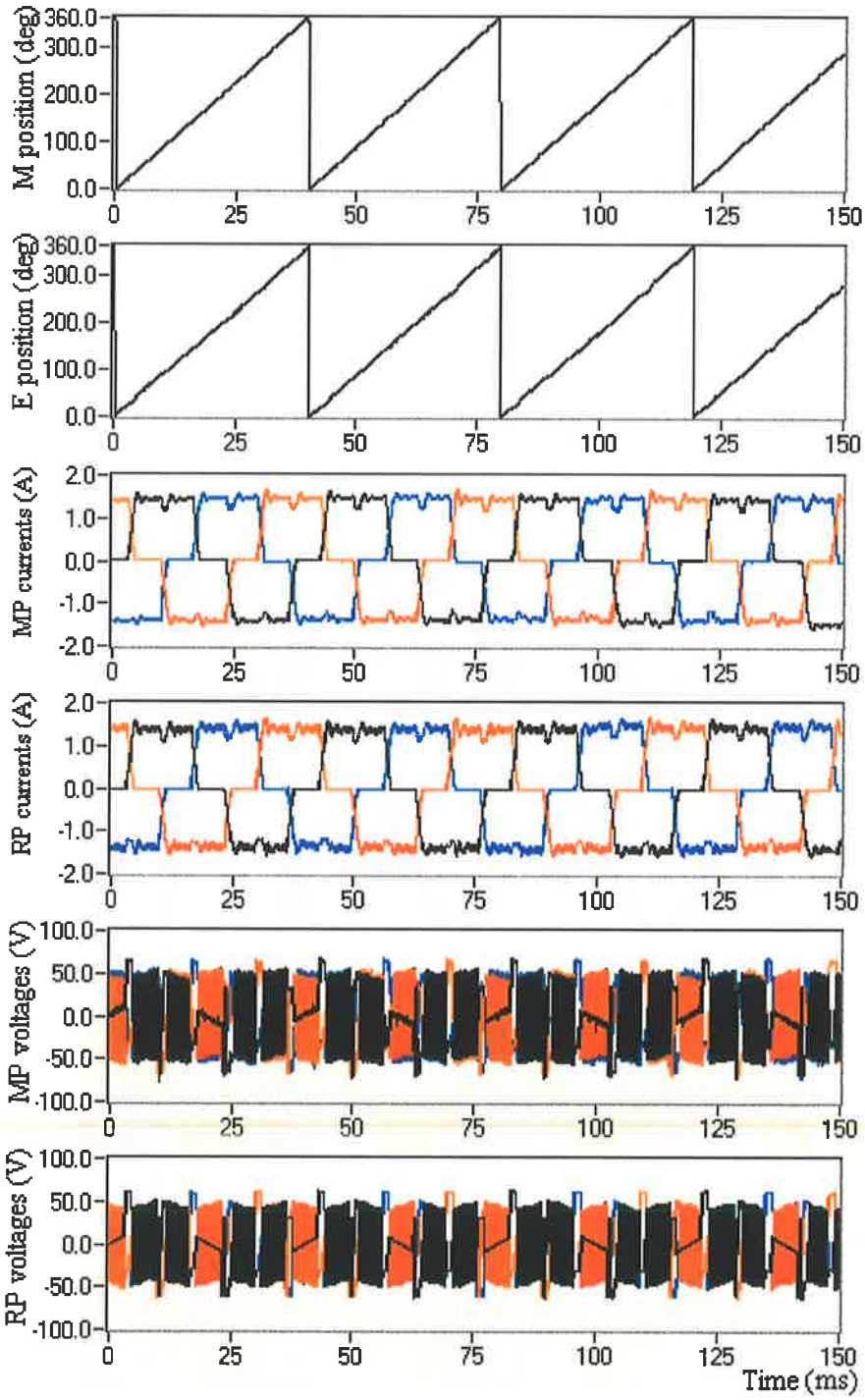

Figure 7.4 Open loop test results of the phase voltage and current reconstruction and the rotor position estimation under the rectangular excitation at 25Hz.

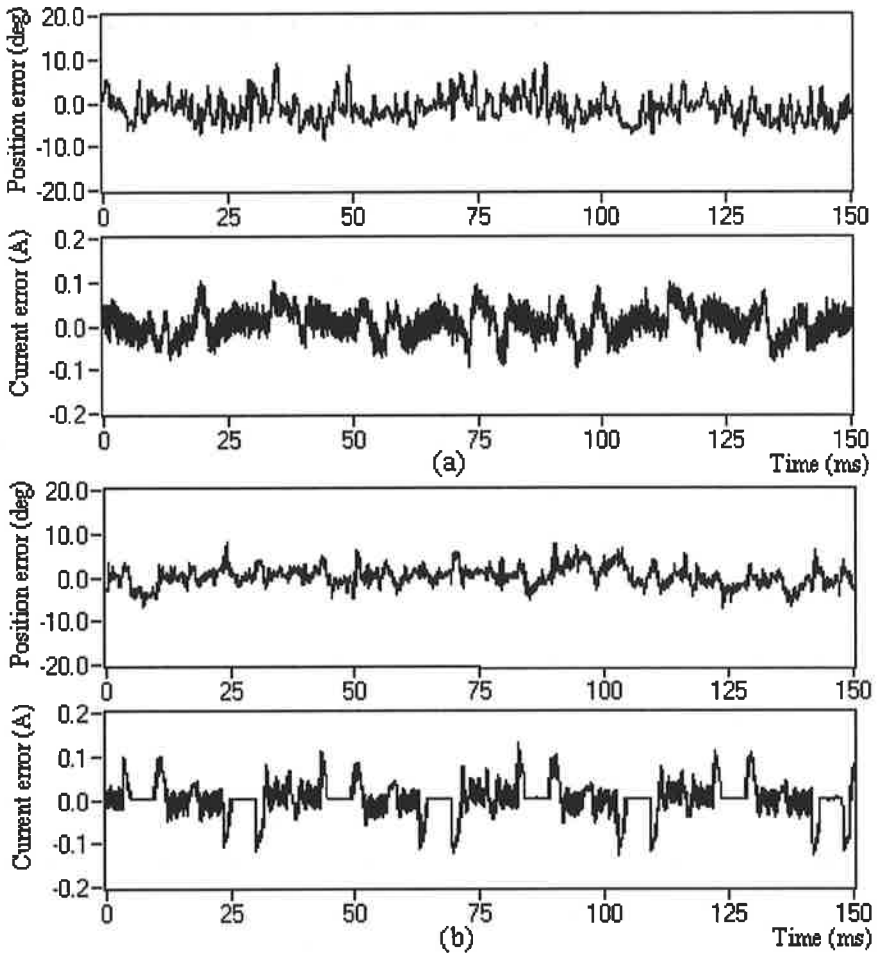

Figure 7.5 Estimated position errors and reconstructed phase current errors. (a) Open loop test in Figure 7.3; (b) Open loop test in Figure 7.4.

7.4.3 Real Time Implementation of the Closed Loop System

To implement the PMAC motor control with a minimum number of sensors in real time, the hardware described earlier was also used. However, only two A/D converter channels on the DSP based motor controller are utilized to measure the DC link current and voltage. In addition, the switching signals used to control the inverter are also connected to the digital input ports on the ADMC connector board using extra wires. The DSP read these digital signals as the switching signals required in the reconstruction of the DC link current and the phase voltages.

Again, the ADMC 300 DSP-based motor controller was the core processor in this study, where all the algorithms described above were implemented in real-time. However, the software of the implementation was separated into two interruption service routines at different interruption frequencies. One of the service routines, which has the same interruption frequency as the PWM frequency, performs the speed regulation, the current

control and the PWM output. The algorithm of this service routine is same as the conventional control except the phase current signals, the rotor position and the speed signals were not obtained via the A/D converters and but linked to the second service routine.

The second service routine performs the reconstruction of the three-phase currents and voltages, the estimation of the rotor position and the rotor speed observer. As mentioned in Chapter 6, the phase current reconstruction directly depends on the accuracy of the DC link current measurement. Therefore, the sample rate of A/D converter should be as high as possible in the real system The highest possible sample rate of the A/D converter of the ADMC 300 DSP-based motor controller is 31.5KHz. Based on this hardware limitation, we have selected the PWM frequency as 1302Hz that provided reasonable accuracy in the measurement of the DC link current. This means that the interruption frequency of the reconstruction and the estimation service routine is 24 times of the PWM frequency in the real time system, which allowed us to implement the PMAC motor control with two sensors.

According to the structure of the software implementation, the reconstruction and the estimation service routine perform 24 times in each PWM cycle, but the reconstructed phase current, the estimated rotor position and the speed values are updated once per PWM cycle.

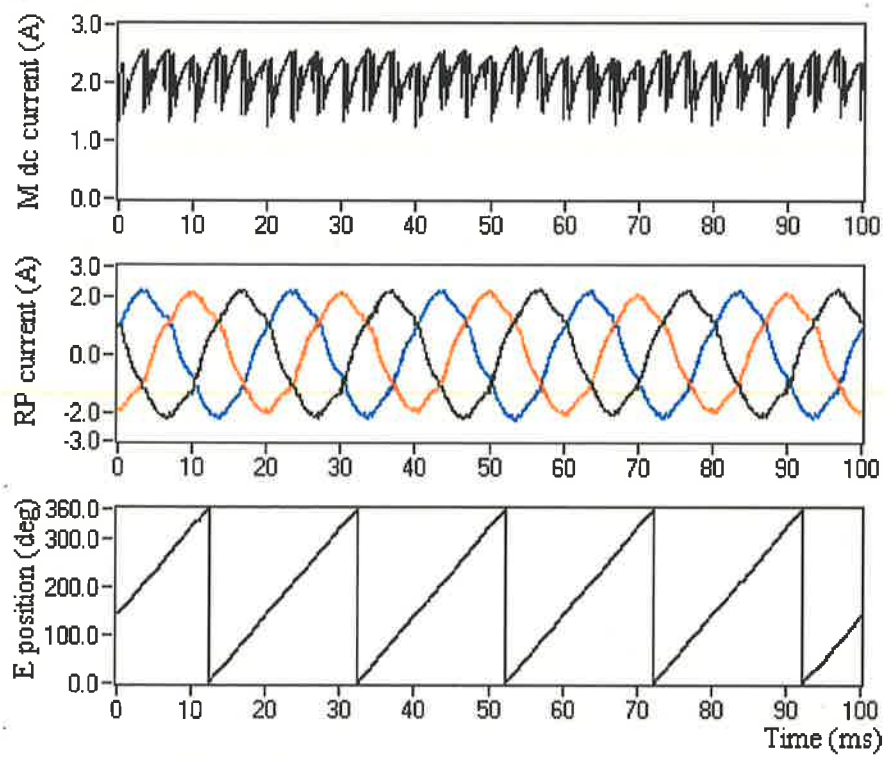

Figure 7.6 A steady-state experimental results using two sensors running at 50Hz: measured DC link current, reconstructed phase currents, and estimated rotor position.

Therefore, 24 reconstructed and estimated values within one cycle can be averaged or filtered, which may produce better results by reducing the fluctuations in the reconstructed three-phase currents and the random position estimation errors.

In the real time implementation of the PMAC motor control utilising two sensors can use the same starting strategy described earlier in the position sensorless control, that is, the motor drive can start directly from zero speed in real time without accommodating any special starting strategy. At beginning of the starting, the reconstruction algorithms predict the phase voltages and currents using the measured DC link current and the voltage, and the position estimation algorithm uses the reconstructed values to estimate the rotor position using a random initial value. Although this may generate wrong estimation, within one electrical cycle, the reconstructed phase currents and the estimated rotor position can converge to the actual values and can be used as the correct feedback signals in the closed loop system. Due to the large errors of the reconstructed phase currents and the estimated rotor position at start, the dynamic performance of the starting procedure of the motor drive is not as good as expected. However, it was observed during the tests that the motor drive can always start smoothly with this starting approach.

The first test result shown in Figure 7.6 illustrates the operation of the two sensor motor

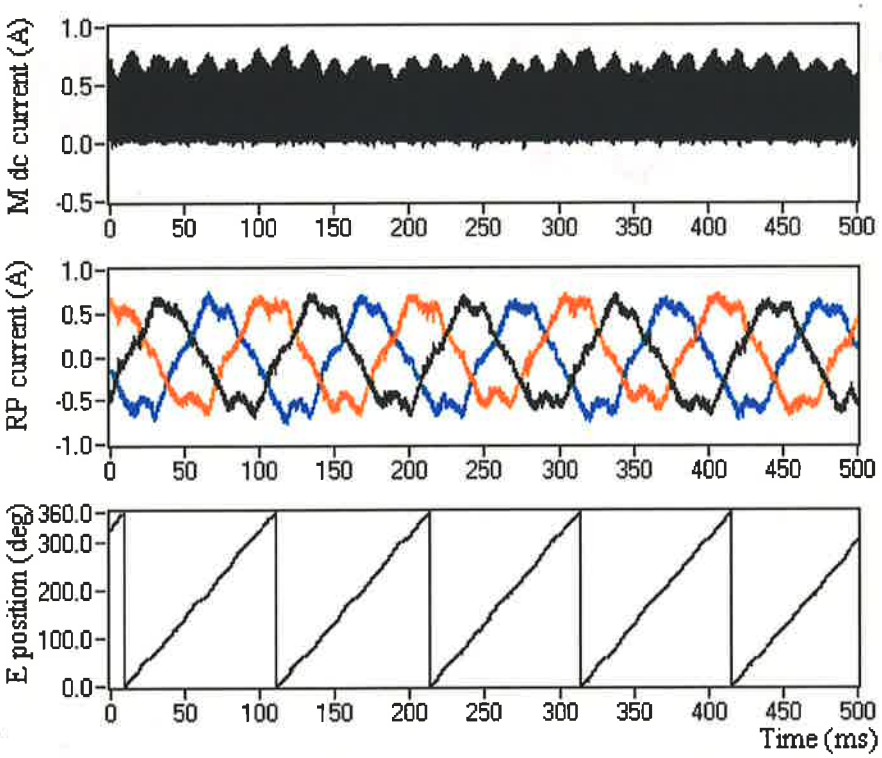

Figure 7.7 A steady-state experimental results using two sensors and running at 10Hz: measured DC link current, reconstructed phase currents, and estimated rotor position.

drive at a steady-state speed 107rpm. In the figure, the measured DC link current, the reconstructed three-phase currents, and the estimated rotor position are given. The test is repeated at a much lower operating speed of 21.4rpm and the results are presented in Figure 7.7. As demonstrated, the waveforms of the reconstructed three-phase currents and the rotor position are used as the feedback signals in the drive and the closed loop control was achieved in the motor drive.

Figure 7.8 shows an ultimate test result to demonstrate the dynamic performance of the motor drive operating in closed-loop and using only two sensors. The transient waveforms of the three-phase currents, the estimated rotor position and the speed are all given in the figure. In this test, the motor drive starts from standstill, accelerates and reaches to a steady-state speed of 107 rpm within 200ms. The results indicate that the motor drive can start directly from zero speed and also demonstrates a reasonable dynamic performance when uses the reconstructed phase currents in the current control loop and the estimated rotor position to generate the reference currents.

When the above results are compared with the test results presented in the position estimation chapter, the performances of the motor drive are not very accurate. In addition, it was found that the combined approach (two sensor approach) has a limited operating speed

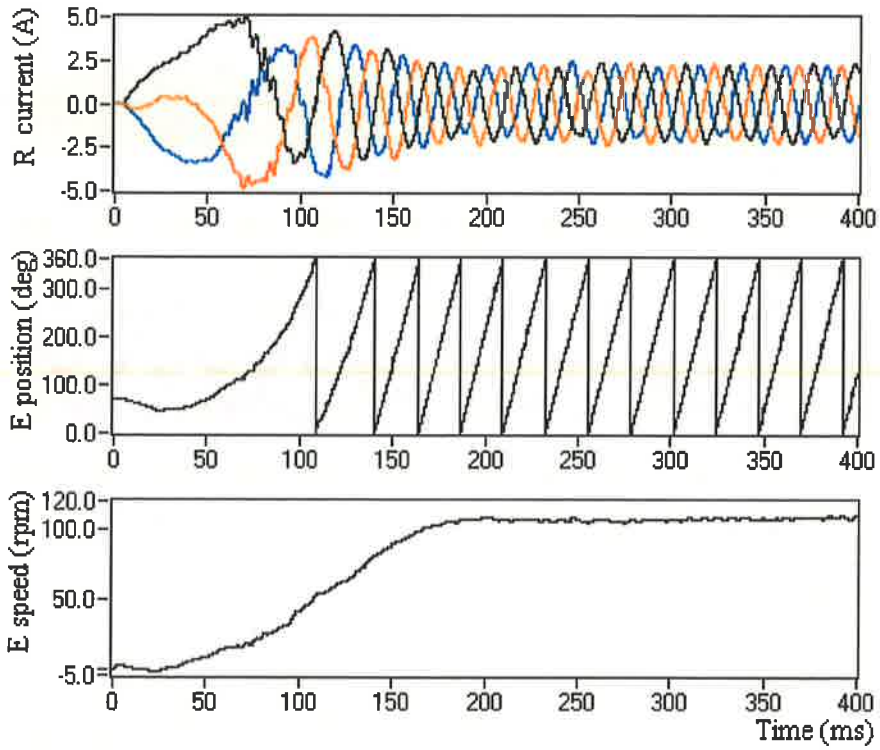

Figure 7.8 A dynamic test results of the motor drive using only two sensors: reconstructed phase currents, estimated rotor position, and estimated rotor speed.

range. Moreover, the actual current waveforms clearly reflect the increased errors in the rotor position estimation. The primary reason of such weaknesses is the limitation of the available hardware as described earlier. To improve the performance of the two-sensor motor drive, a higher speed DSP with higher performance A/D converters should be used, such as ADMC 501. In addition, the speed observer, the speed regulator and the current controller in the drive system should be carefully redesigned to reduce the execution time and some form of digital filtering should be accommodated in the estimation and in the reconstruction routines.

We also perform some experiments for rectangular current excitation. In the real time implementation, the interruption frequency of the service routine of current reconstruction and position estimation is still set the possible highest value of 31.5KHz, but the PWM frequency is selected as 5208Hz, which is similar to the one current sensor control. When we use the measured phase currents and rotor position as the feedback signals to implement closed loop control, it can be observed that the reconstructed phase currents and estimated rotor position have good waveforms and agreement with the measured values. If the reconstructed phase currents and estimated rotor position are used as the feedback signals, however, the motor drive cannot operate properly and motor system may vibrate when operation conditions are changed. In order to find out the major reason of this vibration, we modify the DSP program with several different options of feedback signals and perform the experiments. When we use the measured phase voltages and reconstructed phase currents to estimate rotor position, it is found that the motor drive can implement stable closed loop operation using the reconstructed phase currents and estimated rotor position as the feedback signals. The experiment results indicate that the reconstructed voltages do cause the vibration when the motor is excited with rectangular currents.

As mentioned before, when the rectangular currents excite the motor, the phase voltages depend on the DC link voltage, the switching signals, the rotor position and the speed. If the reconstructed phase voltages are used to estimate the rotor position and the speed, the phase voltage and the rotor position will be interdependent. In this case, if the estimated rotor position is inaccurate, which may be caused by the measurement errors or the parameter variations, the reconstructed phase voltage differs from the actual value. Inversely, the inaccurate reconstructed phase voltage can cause more errors in the estimation of the rotor position. Finally, if the estimated rotor position is completely different than the actual value, the motor drive does not rotate but oscillates back and forth. Therefore, it can be concluded that the open loop voltage reconstruction technique in the rectangular current excitation may

not give reliable constructed phase voltages, which also depend on the rotor position and the speed. Using the unreliable voltages to estimate the rotor position, the motor drive cannot reliably implement self-synchronization control with the estimated value. This implies that the motor control technique with a minimum number of sensors cannot be suitable for a trapezoidal PMAC motor.

7.5 Conclusions

The chapter discussed a possible solution for the sensor reduction in the PMAC motor drives. Normally, such motor drives require the rotor position, the speed, and the three-phase currents as feedback signals to implement the closed loop control. In order to minimize the number of sensors that are used to measure these signals, the position sensorless technique and the reconstruction methods for the phase currents and the voltages were combined.

As demonstrated in the chapter, the phase voltages of the inverter driven and sinusoidal current excited motor can easily be reconstructed using the DC link voltage and the switching states. If the motor is excited with the rectangular currents, however, the phase voltages not only depend on the DC link voltage and the switching signals but also related to the rotor position and the rotor speed. Therefore, if the rotor position and the speed data are not accurate enough, the reconstructed phase voltages become unreliable, hence not to be used in the position estimation.

Furthermore, it was demonstrated that the current observer described in the previous chapter is suitable for both the sinusoidal and the rectangular excitations, and therefore the reconstructed three-phase currents can be used as the feedback signals to implement the closed loop current control utilizing a single current sensor. However, in order to obtain accurate results, a higher speed DSP controller with high performance A/D converter should be utilized to measure the DC link current.

Although the phase currents as well as the phase voltages can be reconstructed from the DC link measurements, small reconstruction errors are inevitable, which is primarily due to the ideal motor model used. Therefore, if the reconstructed phase voltages and the phase currents are used to estimate the rotor position, the estimation algorithm must be robust with respect to the reconstruction errors. As demonstrated in Chapter 5, the position sensorless technique proposed has robustness with respect to the measurement inaccuracies. Therefore,

the reconstructed three-phase currents and the voltages can be used to estimate the rotor position in the PMAC motor drives.

By combining the proposed techniques for the position estimation and for the voltage/current reconstruction, the PMAC motor drive utilising only two sensors on the DC link (one for voltage and one for current measurement) were demonstrated. It was also explained that if the DC link voltage remains constant, the DC link voltage sensor can be eliminated and therefore only one current sensor can be used to achieve a closed loop control. In this case, the numerical value of the DC link voltage has to be provided to the reconstruction algorithms.

When the motor is excited with the sinusoidal currents, the estimated rotor position and the reconstructed phase currents can be used successfully in the closed loop control. The experiment al results demonstrated the feasibility of the implementation of the PMAC motor control using two sensors. When the motor is excited with the rectangular currents, however, the motor drive with two sensors cannot operate properly and the motor drive system may vibrate when the operating conditions were changed. This implies that the real-time trapezoidal PMAC motor control was not satisfactory by using two sensors. The primary reason of this limitation is due to the voltage reconstruction is related to the rotor position and speed signals when the motor is excited with rectangular currents.

Due to the limitation of the available hardware and low PWM frequency, the performances of the motor drive with only two sensors are not satisfied. It was suggested that to improve the performance of the motor drive, a higher speed DSP with high performance A/D converter should be accommodated in the controller, such as ADMC 501. In addition, the design of the speed observer, the speed regulator and the current controller in the drive system should be revisited, which may require further investigations.

It should be emphasized here that this research focused on the sensor minimization techniques only for the closed-loop control of the PMAC motor drive. To protect the motor drive against the potential faults, additional sensors may still be needed, but this is not covered in this study.

Chapter 8

General Conclusions and Suggestions for the Future Research

The brushless PM motors are doubly excited motors, which use permanent magnets on the rotor to provide the field excitation. This inside-out construction in the motor, compared with the conventional DC motors, brings a number of operational advantages. These include no excitation loss and higher efficiency due to the absence of field excitation system, higher torque or output power per volume. A better dynamic performance using high performance PM materials, the simplicity of the construction and the reduced maintenance are the other additional benefits of such motors. In addition, the absence of commutator and brushes reduces the motor length and the moment inertia, and as a result of these, brush friction and speed dependent current limitations are eliminated. Therefore, considerable improvements in dynamics of the motor are achieved, which make the motors a good candidate in AC servo drive applications.

However, the brushless configuration also means that an electronic switching converter has to be accommodated to perform the current commutation in the motor, which has similar function as the mechanical commutator/brushes. The electronic commutation circuit ensures that the motor phases are switched on and off with reference to the rotor position, in other words with reference to the back EMF voltages. Therefore, the brushless PM motors requires the position feedback to realise a self-synchronous control.

Conventionally, the PMAC motor drives use shaft-mounted position sensors, such as resolvers, absolute position encoders and Hall-Effect sensors, to measure the rotor position directly. However, these mechanical shaft-mounted position sensors have many drawbacks, such as greater installation and maintenance costs, a greater number of connections between the motor and the control circuits, sensitivity to the environmental factors, and the requirement for additional space for mounting the sensor. In addition, the position sensors are the most expensive and fragile components in the entire motor drive. Therefore, the elimination of the shaft-mounted position sensors is a very desirable objective in many applications.

A number of position sensor elimination, or indirect position detection, techniques have been proposed for the PMAC motor drives, which are broadly classified in three groups.

In the trapezoidal PMAC motors, the most common approach to detect rotor position is to extract the rotor position information indirectly from the back-EMF waveform of an unexcited phase. However, the back-EMF voltages of the PMAC motor are too low to be sensed at low speed range. In addition, the method is affected from the switching transients of the phases that conduct currents. Therefore, this kind of position detection techniques is not suitable for low-speed operation and a special starting strategy must be applied to start the motor from standstill.

The indirect position detection techniques for the sinusoidal PMAC motors are mainly based on the estimation methods using the phase voltages and the currents of the motor. In these techniques, the rotor position can be obtained by a state observer, or by Kalman filtering technique, or by direct calculations. However, the previous methods proposed in the literature are computationally intensive, and they generate inaccurate position estimation due to the motor parameter variations and the measurement inaccuracies that are present in any practical motor drive. Moreover, these techniques may suffer at low speed operation, which is mainly due to drift of the integral functions employed in the algorithms.

In the interior permanent magnet motor with rotor saliency, the rotor position can be indirectly detected using the position dependent inductance values. In addition, the rotor position information in such motors can be extracted from the responses of an injected high frequency test signal. These techniques are independent from the motor speed, hence can operate at very low speeds including standstill. However, such techniques are not suitable for the non-salient PMAC motors, such as surface permanent magnet motors.

In order to overcome the limitations of the previous techniques, this thesis proposes, develops and implements a novel indirect rotor position detection technique that is suitable for both the trapezoidal and the sinusoidal PMAC motor drives. In the novel method, three-phase flux linkage increments are calculated using the measured phase currents and the voltages. The proposed technique requires no integration routine, which is used in the previous methods to calculate the flux linkage and is the main source of the estimation errors. In the novel method, the back-EMF voltages are defined as the product of the angular speed and the unity back-EMF functions. Using the flux linkage increments and the back-EMF functions, the proposed algorithm can calculate a single rotor position increment, which also

has auto-correction ability against errors. Finally, the corresponding rotor position information is calculated by integrating the rotor position increment. The back-EMF functions used in the calculation are generated using the estimated rotor position that can form an internal closed loop in the algorithm. Therefore, the integration loop that usually exists in the calculation of the flux linkage and located outside the closed-loop is transferred to the position calculation level that is located inside the closed-loop. In addition, it was demonstrated that using a phase-locked loop (PLL) algorithm, the internal closed loop can correct the position drift that may be due to the motor parameter deviations and/or the measurement inaccuracies.

As stated, the parameter variations and the measurement inaccuracies are inevitable in the practical motor drive. Therefore, in this thesis special attention is given to the analysis of the parameter variations and the measurement inaccuracies and their impact on the rotor position estimation. A number of simulation studies and open loop experiments were done to study the novel indirect rotor position detection technique in detail. The robustness with respect to the parameter variations and the measurement inaccuracies were also studied, which demonstrated that the new algorithm can limit the position drift within an acceptable range of 2-3%.

Another important feature of the proposed position estimation method is that the algorithm has less mathematical computations, which made the real-time implementation possible using a DSP. In this research, all experimental results were obtained using a comprehensive test setup, which contains an IRMDAC3 3-Phase 460VAC 3HP motor drive board and an ADMC 300 DSP-based motor controller. The control, the reconstruction and the estimation software were all written in Assembly Language in the DSP.

In the real-time motor drive, the estimated rotor position was used to replace the position feedback signal, and the speed feedback signal was obtained from the estimated rotor position, which allowed us to develop a closed loop speed control. As demonstrated, the sensorless motor drive can start from standstill smoothly and operate in entire speed range and in different operating conditions. Moreover, the real time experimental results shown that the proposed position estimation method has good static and dynamic performances. Furthermore, the high robustness of the motor drive indicated that the new position sensorless technique is suitable to be used in the practical applications.

In order to continuously estimate the rotor position, most of the observer based position estimation algorithms require real-time three-phase currents and voltages. In addition, the three-phase currents are also used in the drive to implement the closed-loop current control. Although the direct measurements of the three-phase voltages and currents using separate sensors are the most effective method, this is an expensive solution.

Employing a minimum number of sensors, which increases the reliability of the system and reduces the drive cost, are desirable in many applications. This is the primary aim of this research.

As demonstrated, the three-phase voltages and currents of the PMAC motor can be reconstructed from the DC link measurements and the switch states of the inverter. This approach allowed us to investigate the sensor reduction concept further. When a motor is fed by a three-phase inverter, the terminal voltages of each phase can be either $\frac{1}{2}V_{dc}$ or $-\frac{1}{2}V_{dc}$, depending on the switch states of the phase in the inverter. However, the phase voltages are also related to the floating neutral voltage of a star connected motor, which is not constant but varies with the switch states and the back-EMF voltages. If the back EMF voltages of a PMAC motor are sinusoidal, the sum of the three-phase back EMF voltages is equal to zero. When all of three phases are excited with currents, such as sinusoidal currents, the phase voltages of the motor only depend on DC link voltage and the switch states, that is, the phase voltage will be 0, $\pm\frac{1}{3}V_{dc}$ or $\pm\frac{2}{3}V_{dc}$.

However, if the back EMF voltages of a PMAC motor are trapezoidal, the phase voltage reconstruction is more complicated since the phase voltages not only depend on the DC link voltage and the switch states, but also relate to the back-EMF voltages. Although the back-EMF voltages can be regenerated using the rotor position and the rotor speed data, the open loop regeneration may cause some instability in the drive, specifically when the reconstructed phase voltages are used in the rotor position estimation.

As verified, three-phase currents of the inverter driven motor are closely related to the DC link current of the inverter. Based on this relationship, it was concluded that the three-phase currents can be reconstructed using the DC link current measurement. When the rectangular currents excite the motor, the reconstruction is relatively easier since only two of the three phase windings conduct currents at a given time, and the value of the two-phase current is exactly equal to the DC link current but their directions depend on switching state of the

inverter. However, during current commutation periods, the reconstruction method does not work, which is due to the three-phase conduction during the commutation instants.

When the sinusoidal currents excite the motor, all three-phase windings carry currents at any instant. The three-phase current reconstruction using the DC link current measurement is still possible. When all of the three phases conduct current simultaneously, the inverter only has eight possible switching states: two zero-states and six active-states. During the six active states, one of the phase currents flows through the DC link. During the two zero-states, however, the phase currents circulate inside the inverter bridge, not passing through the DC link. Under the normal PWM mode, there are two possible active-states in each PWM cycle. Hence, the two-phase currents can be obtained from the DC link current measurement at two consecutive points. If the PWM frequency is high enough, the phase currents vary slightly over one PWM cycle. In this case, the values obtained can represent the two-phase currents within this cycle, and the third phase current can easily be calculated using the two values if the motor is star connected.

However, under certain operating conditions, either two active-states in one PWM cycle may last for a short period of time. Due to the finite switching time of the power devices, the dead times, and the delays in the electronic circuits, the actual phase current may not be visible on the DC link measurement. Although several different methods have been proposed in the literature to solve this problem, complicated hardware circuits are required to detect the values of the current at given instants. The measurement noise may also cause significant error in the reconstruction. In addition, the previous methods can obtain the average values of the phase currents within one or several PWM cycles using integration or averaging techniques. Therefore, the variations of the currents within one PWM cycle cannot be obtained, which is required in the fast acting closed loop current controller. Moreover, modified PWM signals in the previous methods may influence the actual output currents of the inverter and increase the total harmonic distortion and the switching losses.

In order to overcome some of the previous problems and to reconstruct the three-phase currents that are suitable for the position estimation as well as for the closed loop current control, this thesis also proposes and implements a novel three-phase current reconstruction technique, which is based on an adaptive current observer. The novel technique estimates the three-phase currents using the mathematical model of the PMAC motor drive. Using the estimated phase currents, a DC link current is reconstructed as the output of the current

observer. Then, the output is compared with the measured DC link current and the error is regulated by the adaptive scheme implemented. Finally, the regulated result is utilized to compensate the DC link voltage, which is then used in the phase current estimation. As demonstrated, using the symmetry of the three phases, it was shown that the DC link voltage compensation can correct the estimated three-phase currents and force them to follow the actual winding currents accurately, which were verified using off-line real data obtained from the test setup. As shown, the phase current reconstruction technique is suitable for both the trapezoidal and the sinusoidal PMAC motor drives. In addition, it was demonstrated that the current reconstruction technique has good dynamic performances that makes the replacement of the three-phase current measurements with a single DC current sensor possible.

By combining the indirect position detection and the phase current reconstruction techniques together, a practical PMAC motor drive was also established, which employed only two sensors (voltage and current) on the DC link. As stated in the thesis, if the DC link voltage remains constant, only the DC link current measurement is sufficient in the motor drive system. The three-phase voltages and currents required by the position estimation are reconstructed using the DC link current measurements and the switching signals of the inverter, and then the rotor position is estimated using the reconstructed values. When the sinusoidal currents excite the motor, the estimated rotor position and the reconstructed phase currents were used as feedback signals, and the closed loop control was to implement. The experimental results demonstrated the feasibility of the PMAC motor control using only two sensors. When the rectangular currents excite the motor, however, the real-time closed loop control was not successful as expected. As stated, the primary reason for this is the interdependent relationship between the reconstructed voltages and the rotor position when the rectangular currents excite the motor.

In the computer simulation, the position sensorless method proposed in this thesis can operate at a very low speed, such as 1Hz. However, this operating speed was not verified due to the limitations on the motor setup. Therefore, further research may be carried out to investigate and verify the very low speed operation capability. In addition, the instantaneous electromagnetic torque measurement can be utilised in the real tests to compare the conventional motor drive (employing the shaft mounted position sensor) with the closed-loop position sensorless drive.

As shown in the thesis, the sensorless motor drive can start from standstill. However, further studies may be required to improve the dynamic performance of the starting procedure. This may be done by accommodating a better initial position detection technique in the drive control.

In the implementation of the PMAC motor control using two sensors, the most important parameter is the DC link current measurement. To improve the measurement and to satisfy the requirements of the phase current reconstruction, the DC link current has to be measured as accurate as possible, which can be done considering a better current sensing hardware. Using a higher speed DSP and a high performance A/D converter in the motor controller, such as ADMC 501, may achieve this. Furthermore, the speed observer, the speed regulator and the current controller in the drive system may be redesigned to improve the position estimation and the reconstruction techniques further.

Appendix A
Hardware of the Motor Drive

A.1 IRMDAC3

The IRMDAC3 is a reference design kit for a 3HP AC motor drive, which works as an evaluation platform for IR2233 three-phase motor control IC and IRPT2062A power module. By connecting three-phase AC, drive signals, motor and hall sensors, user can also complete a motor drive system easily. Figure A.1 shows the circuit of the IRMDAC3, which consists of IRPT2062A power module, IR2233 three-phase motor control IC, and other accessory components [102].

The power module integrates all rectifiers, ultra-fast short circuit rated IGBTs, fast recovery commutation diodes, brake IGBT and other processing components needed for a 3HP motor drive. Semiconductor dice are mounted on a thermally efficient substrate and housed within a convenient, potted module. When connected to the host PCB, the power components become configured as a 3-phase input bridge rectifier, and IGBT inverter with current sensing shunt resistors. An NTC thermistor is bonded to the substrate to furnish the host PCB with accurate temperature reading. A galvanic ally isolated metal back plate provides excellent thermal coupling to an external heat sink, which is necessary for full load operation.

The IR2233 is high voltage, high-speed power MOSFET and IGBT driver with three independent high side and low side referenced output channels for 3-phase applications. Proprietary HVIC technology enables ruggedized monolithic construction. Logic inputs are compatible with CMOS or LSTTL outputs, down to 2.5V logic. An independent operational amplifier provides an analog feedback of bridge current via an external current sense resistor. A current trip function, which terminates all six outputs, can also be derived from this resistor. A shutdown function is available to terminate all six outputs. An open drain FAULT signal is provided to indicate that an over-current or under-voltage shutdown has occurred. Fault conditions are cleared with the FLT-CLR lead. The output drives feature a high pulse current buffer stage designed for minimum driver cross-conduction. Propagation delays are

matched to simplify use in high frequency applications. The floating channels can be used to drive N-channel power MOSFETs or IGBTs in the high side configuration, which operates up to 600 volts or 1200 volts.

The power module, motor control IC, and accessory components are all connected to a host PCB as a flexible power conversion system, primarily for interface with a 3HP Motor. An NTC thermistor connected on board is used to reduce inrush current for soft-start. Also on-board is a regulated low voltage power supply to provide bias for the IR2233 and other low voltage components. When connected to the power module, the unit is fully protected

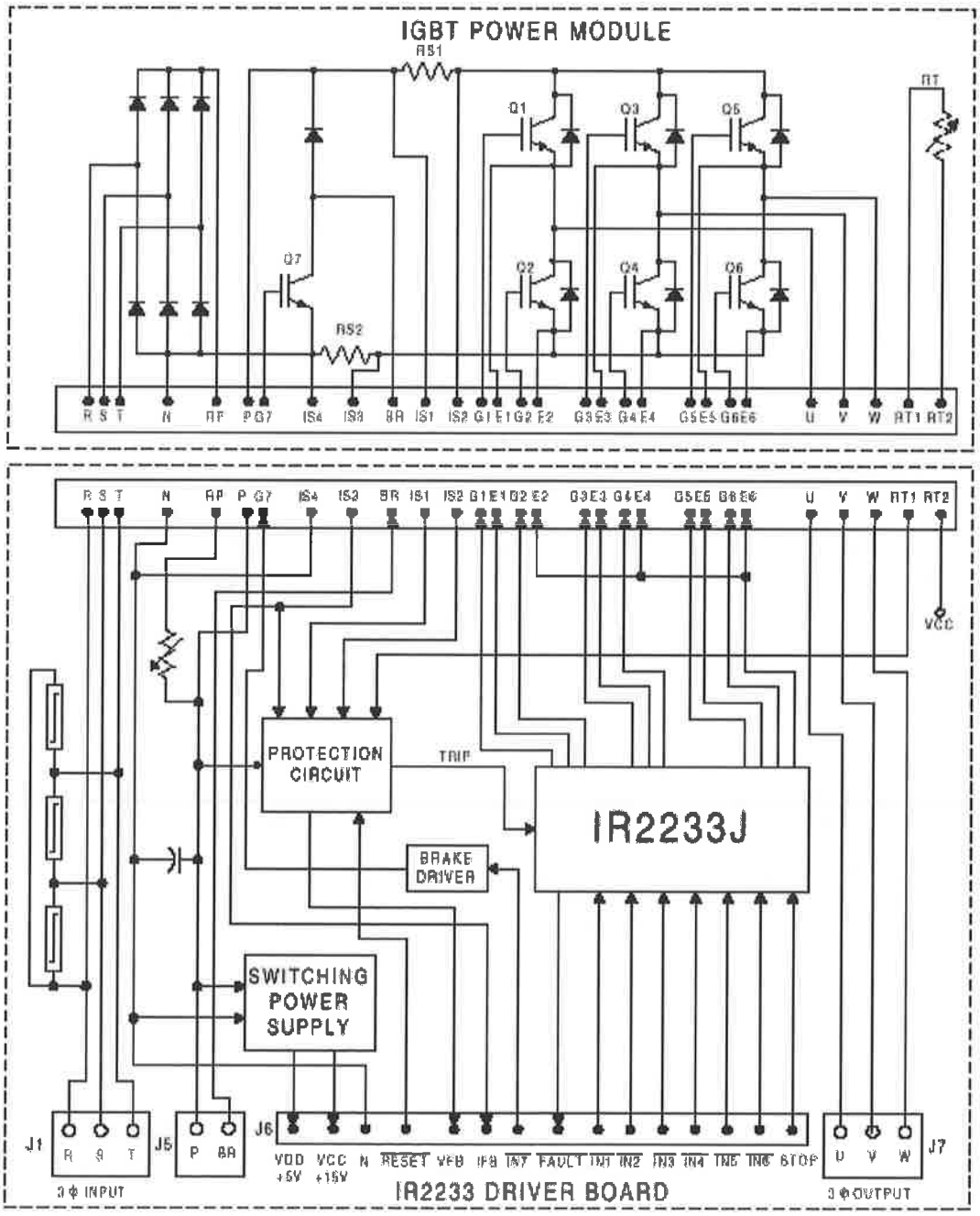

Figure A.1 Circuit of the IRMDAC3

against overcurrent and ground faults through DC bus voltage and current feedback. Over-temperature is guarded against through feedback from a thermistor embedded within the power module. A 16-pin single in line header connector is provided to interface control signals and two terminal blocks connect 3-phase AC inlet and output to the load. The user provides 5V CMOS / TTL level signals which are then processed by the IR2233 Control IC and delivered to the power module.

A.2 ADMC300

The ADMC300 is a single-chip DSP-based controller, suitable for high performance control of AC induction motors, permanent magnet synchronous motors and brushless DC motors. The ADMC300 integrates a 25 MIPS, fixed-point DSP core with a complete set of motor control peripherals that permits fast, efficient development of servo motor controllers [103].

The DSP core of the ADMC300 is the ADSP-2171, which is completely code compatible with the ADSP-2100 DSP family and combines three computational units, data address generators and a program sequencer. The computational units comprise an ALU, a multiplier/accumulator (MAC) and a barrel shifter. The ADSP-2171 adds new instructions for bit manipulation, multiplication (X squared), biased rounding and global interrupt masking. In addition, two flexible, double-buffered, bidirectional, synchronous serial ports are included in the ADMC300.

The ADMC300 provides 4K · 24-bit program memory RAM, 2K · 24-bit program memory ROM and 1K · 16-bit data memory RAM. The program and data memory RAM can be boot loaded through the serial port from either a serial SROM/ E2PROM, asynchronous (UART) connection, or synchronous connection. The program memory ROM includes a monitor that adds software debugging features through the serial port. In addition, a number of pre-programmed mathematical and motor control functions are included in the program memory ROM.

The motor control peripherals of the ADMC300 comprise a high performance, five channel ADC system that uses sigma-delta conversion technology offering a typical signal-to-noise ratio (SNR) of 76 dB, equivalent to 12 bits. In addition, a 16-bit center-based PWM generation unit can be used to produce high accuracy PWM signals with minimal processor overhead. The ADMC300 also contains a flexible encoder interface unit for position sensor

feedback, two auxiliary PWM outputs, twelve lines of digital I/O, a two-channel event capture system, a 16-bit watchdog timer, a 16-bit interval timer and a programmable interrupt controller that manages all peripheral interrupts.

A.3 Processor Board

The *ADMC300 PROCESSOR BOARD* is intended as a compact, highly-integrated evaluation and software development platform for the ADMC300 controller. The processor board permits access through a UART connection to the *Motion Control Debugger* software that operates under Windows 95™ or Windows NT™. The *Motion Control Debugger* is used to download executable code, examine the contents of registers, program memory and data memory, run executable modules, set breakpoints and enable single-step operation [104].

The processor board is designed for compact size so that all relevant input and output signals are brought to three connector headers underneath the board. The processor board contains the following features and components:

- The ADMC300 Single-Chip DSP-Based Controller.
- A 12 MHz crystal and associated capacitors to provide the CLKIN frequency.
- A power-on reset circuit based on the AD709 that is used to provide a reset signal to the ADMC300 and UART communications port. A push button is also provided to initiate a processor and system reset.
- A socket for a serial memory device (ROM or E2PROM) that may be used for serial boot loading on power up for stand alone operation.
- An isolated UART interface to the *Motion Control Debugger*. The signals are optically isolated from the remainder of the processor board. The AD7306 is used to drive the appropriate signals on the 9-way UART connector.
- An input power supply connector that accepts +5V, +15V, -15V and GND. The 5V is used to drive the digital circuits and the analog portion of the ADMC300. The +15V and -15V supplies are used for the analog interface circuits of the processor board.

- An on board 5V to 5V dc-dc converter that provides an isolated 5V supply for the UART interface circuit.

- Analog interface circuits that correctly offset the analog input signals to the ADC inputs of the ADMC300. Five independent analog interface circuits are included; one for each ADC channel of the ADMC300.

- An ADG408 eight-to-one line multiplexer that may be used to multiplex any one of eight analog inputs to the board into the ADC5 channel of the ADMC300.

- An on board precision 2.5V voltage reference using the AD780, that provides the input reference for the ADCs of the ADMC300. The reference voltage is also buffered and brought to the connector underneath the board.

- Jumpers that permit setting of the PWM polarity, enabling or disabling of the PWMTRIP input and enabling or disabling the serial memory device in the socket.

- Three socket blocks underneath the processor board that permit access to all of the input and output signals of interest. The three sockets comprise two digital sockets (IF1 and IF3) and one analog socket (IF2).

The *ADMC300 PROCESSOR BOARD* may operate in a stand-alone mode, where the user must supply only the appropriate power supply voltages and either a UART connection to the *Motion Control Debugger* or a suitable serial memory device. In this case, the user must provide suitable connectors to interface to the various input and output signals on the expansion connectors underneath the board. Alternatively, the processor board may be plugged into the *ADMC CONNECTOR BOARD*. The connector board provides easy access to all relevant input and output signals via appropriate connectors and terminal blocks. The connector board also provides an easy interface to the International Rectifier PowIRtrain™ modules to permit development of complete motor control solutions. In addition, the connector board adds new functionality including an 8-channel, 12-bit, serial DAC, a differential line receiver for interface to an incremental encoder with differential outputs, and a large prototype area for system expansion [105].

Appendix B
Data Acquisition System

In this research project, in order to implement open loop experiments or off line real data simulation, a data acquisition system is established to sample real data of a motor drive system. Using the off line real data, all of the algorithms can be simulated with a LabVIEW VI. The off line simulation results are more reliable than that of the simulation implemented with mathematic model. Figure B.1 shows the open loop experimental system. In this system, the motor drive is controlled by conventional method with a shaft mounted encode. When the motor drive is running, the data acquisition system samples all required data, which include three-phase currents and voltages, DC link current and voltage, and switching signals of the motor drive. Since the analog signals and digital signals have close relationship with time in the motor drive system, the data acquisition system should be able to sample all of the data synchronously.

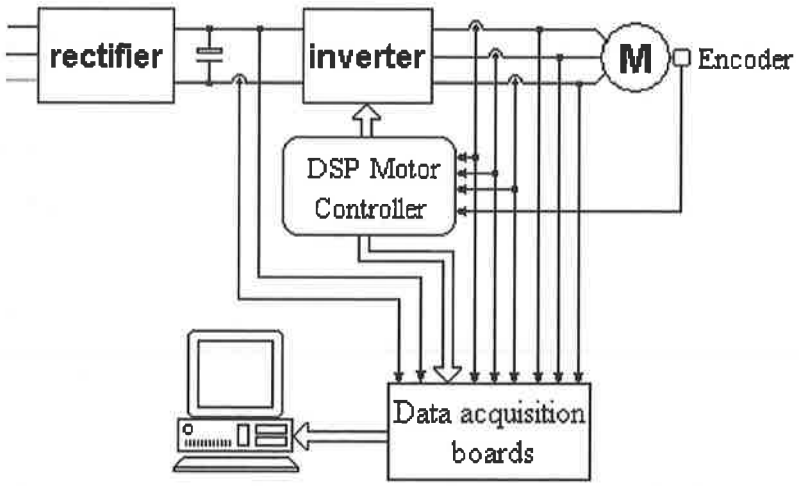

Figure B.1 Open loop experimental system

To satisfy these requirements, two National Instruments PCI-6110E boards and one PCI-6534 board, together with a personal computer, are used to compose hardware of the data acquisition system. All of the board should have their RTSI (Real-Time System Integration bus) lines connected together to synchronize the data acquisitions. On other hand, LabVIEW provides interactive graphics, a state-of-the-art user interface, and a powerful graphical

programming language and LabVIEW Data Acquisition VI Library, a series of VIs for using LabVIEW with National Instruments DAQ hardware, is included with LabVIEW. Therefore, LabVIEW is selected as the software to implement the data acquisitions.

B.1 PCI-6110E Board

PCI-6110E board uses E Series technology to deliver high performance and reliable data acquisition capabilities to meet a wide range of application requirements. The PCI-6110E board provides 5 MS/s simultaneously sampled, 12-bit performance at up to ±42V, with four different analog inputs. The PCI-6111E board also features analog and digital triggering capability, as well as two 16-bit analog outputs; two 24-bit, 20 MHz counter/timers; and eight lines of TTL-compatible digital I/O [106].

PCI-6110E board is a completely Plug and Play, switchless and jumperless data acquisition (DAQ) board for the PCI bus. This feature is made possible by the National Instruments MITE bus interface chip that connects the board to the PCI I/O bus. The MITE implements the PCI Local Bus Specification so that the interrupts and base memory addresses are all software configured. Therefore, the board is easily software-configured and calibrated.

The 6110E board uses the National Instruments DAQ-STC system-timing controller for time-related functions. The DAQ-STC consists of three timing groups that control analog input, analog output, and general-purpose counter/timer functions. These groups include a total of seven 24-bit and three 16-bit counters and a maximum timing resolution of 50 ns. The DAQ-STC makes possible such applications as buffered pulse generation, equivalent time sampling, and seamlessly changing the sampling rate. Often with DAQ boards, it is not easy to synchronize several measurement functions to a common trigger or timing event. The 6110E board has the Real-Time System Integration (RTSI) bus to solve this problem. The RTSI bus consists of RTSI bus interface and a ribbon cable to route timing and trigger signals between several functions on as many as five DAQ boards in a computer.

B.2 PCI-6534 Board

The PCI-6534 board is a high-speed, 32-bit, parallel digital I/O interface for PCI bus. It performs pattern I/O and high-speed data transfer using a wide range of handshaking protocols at speeds up to 80 Mbytes/s. The PCI-6534 delivers digital I/O coupled with large

on-board memory. It features user-defined power-up states, start and stop triggering, and pattern and change detection.

The 32 digital I/O lines are divided into four 8-bit ports. For pattern I/O or handshaking, the ports can be grouped into two 8-bit or 16-bit groups, or a single 32-bit group. Each I/O line is 5 V/TTL-compatible. When configured for standard output, each data line can sink or source 24 mA when set logic low or high, respectively. When configured as inputs, the 6534 data lines are diode-terminated to dampen line reflections.

When not using handshaking or group operations, each of the 32 I/O lines can be individually configured as input or output. You can also choose standard or wired-OR outputs. Wired-OR outputs sink 24 mA when logic low, but do not source current when logic high. Unlike standard outputs, two or more wired-OR outputs can drive a single line.

Pattern I/O is reading (data acquisition) or writing (waveform generation) digital data at a predetermined rate without wait states. When you want to communicate with a peripheral device using an exchange of signals to request and acknowledge each data transfer, the handshaking I/O mode could be used.

The PCI-6534 board has RTSI Bus to send and receive clock and trigger signals to and

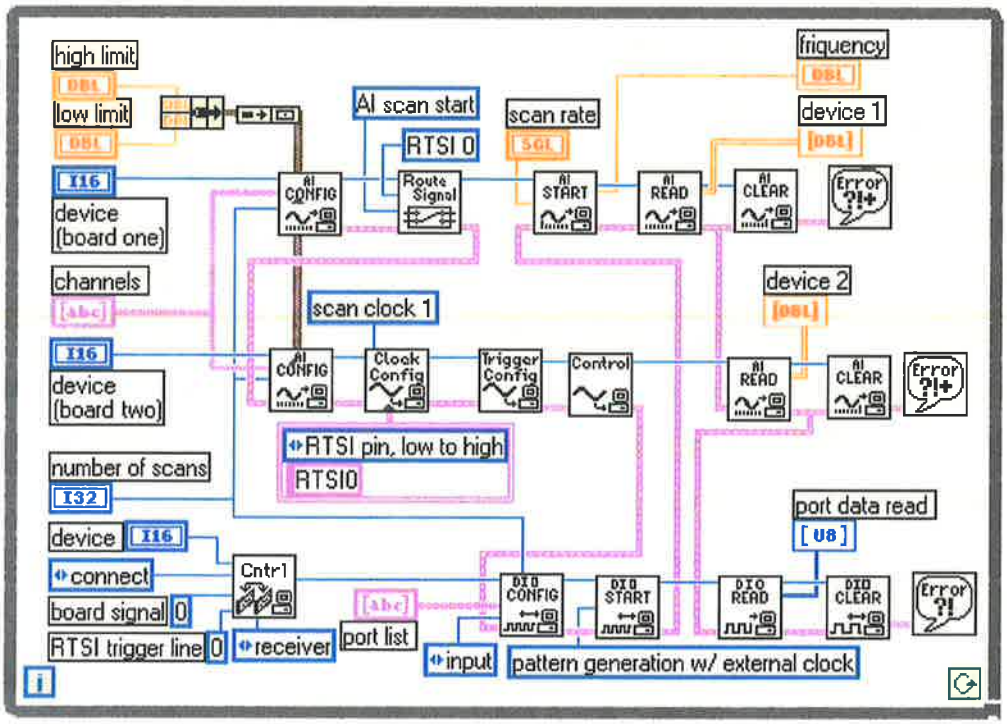

Figure B.2 Block diagram of synchronous data acquisition VI

from other boards in the system. Using these buses, you can create synchronized systems with large number of digital I/O lines, and systems in which digital I/O is synchronized with other types of input or output signals.

B.3 Software Structure

To implement synchronous acquisition of the analog and digital signals, LabVIEW is used to program the software. The data acquisition VI based on LabVIEW consist of two frames. The first one is the frame of data acquisition, and its block diagram is shown on Figure B.2. This frame initializes the three boards as eight analog inputs and one digital input port (8-bit). The signal of AI Scan Start is mapped to RTSI 0 and used as the synchronous signal of the three boards, so that all of the eight analog inputs and one digital input port can sample data synchronously. The sampled results are then directly transferred to another frame to process the data.

Figure B.3 shows the block diagram of the other frame, which is used to process the sampled data. The processions include input port calibration, data scaling, plotting waveforms and saving the data as a file.

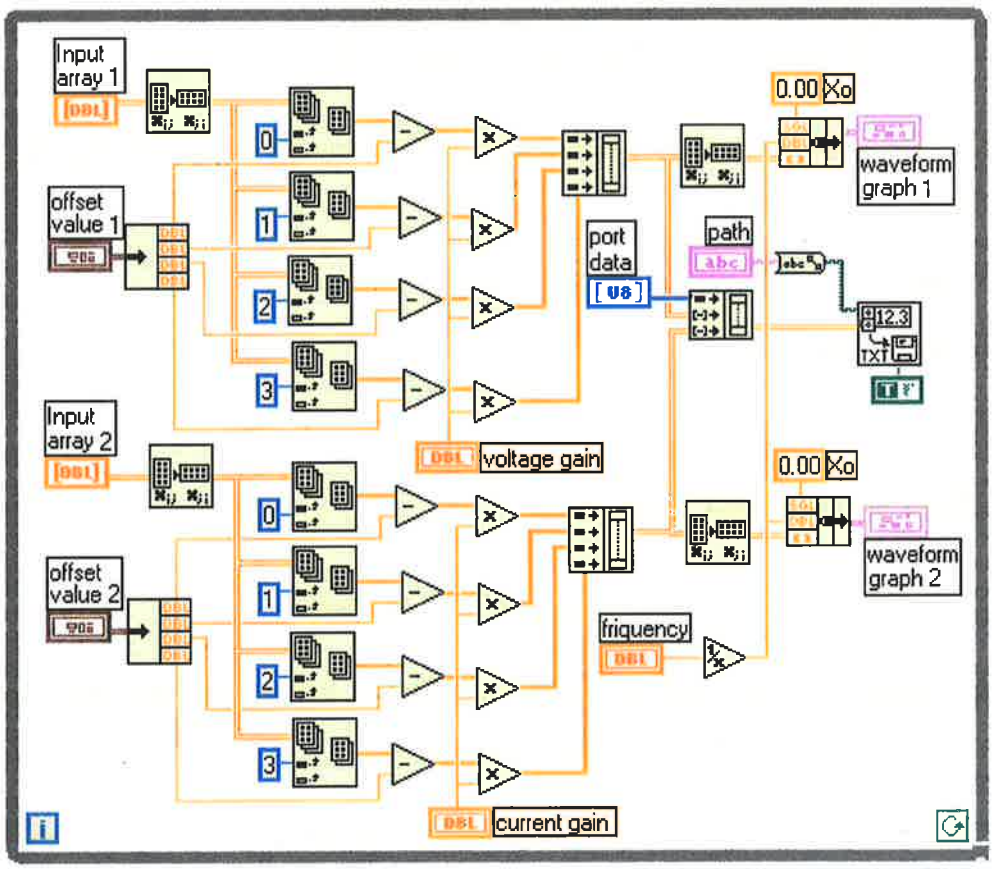

Figure B.3 Block diagram of data calibration, plotting and saving

Appendix C

Derivation of Position Estimation Errors

C.1 Equations of the Basic Rotor Position Algorithm

For ease to see the derivations in this appendix, the equations of the basic rotor position algorithm and other relative formulas are rewritten here.

The flux linkage increments of three phases are rewritten as,

$$\begin{aligned}\Delta\psi_a &= (\mathrm{v}_a - R\,i_a).\Delta t - L\Delta i_a \\ \Delta\psi_b &= (\mathrm{v}_b - R\,i_b).\Delta t - L\Delta i_b \\ \Delta\psi_c &= (\mathrm{v}_c - R\,i_c).\Delta t - L\Delta i_c\end{aligned} \tag{C.1}$$

The basic algorithm of position increment is re-shown as,

$$\Delta\theta_e = \frac{N_p}{k_e}\cdot\frac{\Delta\psi_a e_2(\theta_e)+\Delta\psi_b e_3(\theta_e)+\Delta\psi_c e_1(\theta_e)}{e_1(\theta_e)e_2(\theta_e)+e_2(\theta_e)e_3(\theta_e)+e_3(\theta_e)e_1(\theta_e)} \tag{C.2}$$

In the derivations, the back-EMF functions of a PMAC motor are assumed as sinusoidal functions, that is,

$$\begin{aligned}e_1(\theta_e) &= \sin(\theta_e) \\ e_2(\theta_e) &= \sin(\theta_e - 2\pi/3) \\ e_3(\theta_e) &= \sin(\theta_e + 2\pi/3)\end{aligned} \tag{C.3}$$

C.2 Position Increment Errors

In the derivations below, the following assumptions are made.

a) The motor has sinusoidal back-EMF waveforms, that is, the back-EMF functions are three-phase symmetry sinusoidal functions.

b) The three phases have the same parameter variations, that is, ΔR, Δk_e and ΔL are the same at the three phases.

c) Three-phase currents are synchronous exactly with the back-EMF functions and have ideal sinusoidal waveforms.

d) The sampling interval is short enough.

C.2.1 Resistance Variation

If the winding resistance of a PMAC motor varies ΔR, the three-phase flux increments calculated by Equation C.1 will produce some errors, which are shown as,

$$\begin{aligned}
\delta\psi_a &= \Delta R i_a \Delta t = \Delta R I_m e_1(\theta_e)\Delta t \\
\delta\psi_b &= \Delta R i_b \Delta t = \Delta R I_m e_2(\theta_e)\Delta t \\
\delta\psi_c &= \Delta R i_c \Delta t = \Delta R I_m e_3(\theta_e)\Delta t
\end{aligned} \tag{C.4}$$

where I_m is the amplitude of the phase currents.

Based on the basic position incremental algorithm of Equation C.2, therefore, the position increment error due to the variation of the winding resistance can be derived as,

$$\begin{aligned}
\delta\theta_{eR} &= \frac{N_p}{k_e} \cdot \frac{\delta\psi_a e_2(\theta_e) + \delta\psi_b e_3(\theta_e) + \delta\psi_c e_1(\theta_e)}{e_1(\theta_e)e_2(\theta_e) + e_2(\theta_e)e_3(\theta_e) + e_3(\theta_e)e_1(\theta_e)} \\
&= \frac{N_p}{k_e} \cdot \frac{\Delta R I_m \Delta t\left[e_1(\theta_e)e_2(\theta_e) + e_2(\theta_e)e_3(\theta_e) + e_3(\theta_e)e_1(\theta_e)\right]}{e_1(\theta_e)e_2(\theta_e) + e_2(\theta_e)e_3(\theta_e) + e_3(\theta_e)e_1(\theta_e)} \\
&= \frac{N_p \Delta R I_m \Delta t}{k_e}
\end{aligned} \tag{C.5}$$

C.2.2 Equivalent Inductance Variation

If the equivalent inductance of a PMAC motor varies ΔL, the three-phase flux increments calculated by Equation C.1 will produce some errors, which are shown as,

$$\begin{aligned}
\delta\psi_a &= \Delta L \Delta i_a = \Delta L \frac{di_a}{dt}\Delta t = \Delta L I_m e_1'(\theta_e)\Delta t \\
\delta\psi_b &= \Delta L \Delta i_b = \Delta L \frac{di_b}{dt}\Delta t = \Delta L I_m e_2'(\theta_e)\Delta t \\
\delta\psi_c &= \Delta L \Delta i_c = \Delta L \frac{di_c}{dt}\Delta t = \Delta L I_m e_3'(\theta_e)\Delta t
\end{aligned} \tag{C.6}$$

Based on the basic position incremental algorithm of Equation C.2 and substituting the three-phase back-EMF functions of Equation C.3, the position incremental error due to the variation of the equivalent inductance can be derived as,

$$\begin{aligned}\delta\theta_{eL} &= \frac{N_p}{k_e}\cdot\frac{\delta\psi_a e_2(\theta_e)+\delta\psi_b e_3(\theta_e)+\delta\psi_c e_1(\theta_e)}{e_1(\theta_e)e_2(\theta_e)+e_2(\theta_e)e_3(\theta_e)+e_3(\theta_e)e_1(\theta_e)}\\ &= \frac{N_p}{k_e}\cdot\frac{\Delta L\, I_m \Delta t\left[e_1'(\theta_e)e_2(\theta_e)+e_2'(\theta_e)e_3(\theta_e)+e_3'(\theta_e)e_1(\theta_e)\right]}{e_1(\theta_e)e_2(\theta_e)+e_2(\theta_e)e_3(\theta_e)+e_3(\theta_e)e_1(\theta_e)}\\ &= \sqrt{3}\frac{N_p \Delta L\, I_m \Delta t}{k_e}\end{aligned} \tag{C.7}$$

C.2.3 Back-EMF Constant Variation

The variation of the back-EMF constant of a PMAC motor does not cause any error in the three-phase flux increments calculations based on Equation C.1, but it still produce position incremental error when the basic position incremental algorithm of Equation C.2 is used. The position incremental error due to the back-EMF constant variation of Δk_e can be easily derived and shown as,

$$\delta\theta_{eke} = \frac{\Delta k_e}{k_e}\Delta\theta_e \tag{C.8}$$

C.2.4 Current Measurement Offset

Assuming current measurement offsets of the three-phase current sensors are constant value under all operation conditions, the three-phase flux increments errors caused by these offsets can be expressed as,

$$\begin{aligned}\delta\psi_a &= R\,\delta I_a\,\Delta t\\ \delta\psi_b &= R\,\delta I_b\,\Delta t\\ \delta\psi_c &= R\,\delta I_c\,\Delta t\end{aligned} \tag{C.9}$$

where δI_a, δI_b and δI_c are the current measurement offsets of three phases respectively.

Therefore, the position increment error caused by these offsets can be written as,

$$\begin{aligned}\delta\theta_{eio} &= \frac{N_p}{k_e}\cdot\frac{\delta\psi_a e_2(\theta_e)+\delta\psi_b e_3(\theta_e)+\delta\psi_c e_1(\theta_e)}{e_1(\theta_e)e_2(\theta_e)+e_2(\theta_e)e_3(\theta_e)+e_3(\theta_e)e_1(\theta_e)}\\ &= \frac{N_p}{k_e}\cdot\frac{R\Delta t\left[\delta I_a e_2(\theta_e)+\delta I_b e_3(\theta_e)+\delta I_c e_1(\theta_e)\right]}{e_1(\theta_e)e_2(\theta_e)+e_2(\theta_e)e_3(\theta_e)+e_3(\theta_e)e_1(\theta_e)}\\ &= -\frac{3}{4}\frac{N_p R\Delta t}{k_e}\left[\delta I_a e_2(\theta_e)+\delta I_b e_3(\theta_e)+\delta I_c e_1(\theta_e)\right]\end{aligned} \tag{C.10}$$

Unlike other errors above, the position increment error caused by the current measurement offsets is not constant even in steady state. It is a sinusoidal error and proportional to the summation of three sinusoidal offsets. If all the offsets of three phases are the same, the position increment error will be zero.

C.2.5 Voltage Measurement Offset

Similarly, if voltage measurement offsets of three-phase current sensors are assumed to have constant values under all operation conditions, the position increment error caused by these offsets will have the same feature as that of current offset but different expression, which is shown as,

$$\delta\theta_{evo} = \frac{3}{4}\frac{N_p\Delta t}{k_e}\left[\delta V_a e_2(\theta_e)+\delta V_b e_3(\theta_e)+\delta V_c e_1(\theta_e)\right] \tag{C.11}$$

where δV_a, δV_b and δV_c are the current measurement offsets of three phase respectively.

Also, the position increment error caused by the voltage measurement offsets is a sinusoidal error and will be zero when the offset values of all three phases are the same.

C.2.6 Amplitude Error of Current Measurement

When the gains of current sensors or their amplifiers have errors, the current measurement error caused by this gain will vary with measured current. This means that the current measurement error will also be a sinusoidal error for a sinusoidal current measurement. Assuming the gains of three phases are the same, therefore, the three-phase flux increments errors caused by this gain error can be expressed as,

$$\delta\psi_a = R\delta i_a \Delta t + L\frac{d\delta i_a}{dt}\Delta t = R\delta I_m e_1(\theta_e)\Delta t + L\delta I_m e_1'(\theta_e)\Delta t$$

$$\delta\psi_b = R\delta i_b \Delta t + L\frac{d\delta i_b}{dt}\Delta t = R\delta I_m e_2(\theta_e)\Delta t + L\delta I_m e_2'(\theta_e)\Delta t \quad \text{(C.12)}$$

$$\delta\psi_c = R\delta i_c \Delta t + L\frac{d\delta i_c}{dt}\Delta t = R\delta I_m e_3(\theta_e)\Delta t + L\delta I_m e_3'(\theta_e)\Delta t$$

where δI_m, is the amplitude error of current measurements.

Similar with the derivations of resistance and inductance variations, when substituting Equation C.12 into Equation C.2, the position increment errors caused by the current amplitude measurement errors can be derived as,

$$\delta\theta_{eia} = \frac{N_p R\delta I_m \Delta t}{k_e} + \sqrt{3}\frac{N_p R\delta I_m \Delta t}{k_e} = (1+\sqrt{3})\frac{N_p R\delta I_m \Delta t}{k_e} \quad \text{(C.13)}$$

It can be seen that the position increment errors caused by the current amplitude measurement errors is just like the combination of that of the resistance and inductance variations.

C.2.7 Amplitude Error of Voltage Measurement

Similar with the current amplitude error, when the gains of voltage sensors or their amplifiers have errors, the voltage measurement error caused by this gain will also vary with measured voltage. However, the three-phase voltages of a PMAC motor normally have a phase leading from their currents. The position increment errors caused by the voltage amplitude measurement errors will be quite different from that of the current measurement errors.

Assuming the gains of three phases are the same and the phase difference between voltage and current is constant as φ, if only fundamental harmonics are considered, the three-phase flux increments errors caused by the voltage amplitude errors can be given as,

$$\delta\psi_a = \delta v_a \Delta t = \delta V_m e_1(\theta_e + \varphi)\Delta t$$

$$\delta\psi_b = \delta v_b \Delta t = \delta V_m e_2(\theta_e + \varphi)\Delta t \quad \text{(C.14)}$$

$$\delta\psi_c = \delta v_c \Delta t = \delta V_m e_3(\theta_e + \varphi)\Delta t$$

where δV_m, is amplitude error of voltage measurements.

Therefore, the position increment error caused by the voltage amplitude errors can be derived as,

$$\begin{aligned}\delta\theta_{eva} &= \frac{N_p}{k_e}\cdot\frac{\delta\psi_a e_2(\theta_e)+\delta\psi_b e_3(\theta_e)+\delta\psi_c e_1(\theta_e)}{e_1(\theta_e)e_2(\theta_e)+e_2(\theta_e)e_3(\theta_e)+e_3(\theta_e)e_1(\theta_e)}\\ &= \frac{N_p}{k_e}\cdot\frac{\delta V_m\Delta t[e_1(\theta_e+\varphi)e_2(\theta_e)+e_2(\theta_e+\varphi)e_3(\theta_e)+e_3(\theta_e+\varphi)e_1(\theta_e)]}{e_1(\theta_e)e_2(\theta_e)+e_2(\theta_e)e_3(\theta_e)+e_3(\theta_e)e_1(\theta_e)}\\ &= 2\frac{N_p\delta V_m\Delta t}{k_e}\cos(\varphi+\pi/3)\end{aligned} \qquad (C.15)$$

As seen from above equation, the position increment errors caused by the voltage amplitude measurement errors is a function of the power factor of the motor.

C.2.8 Measurement Signal Noise

Assuming measurement noises is independent of the measured signals and the noises from current and voltage measurements are considered together, the three-phase flux increments errors caused by these noises can be expressed as,

$$\begin{aligned}\delta\psi_a &= \mu_a\Delta t\\ \delta\psi_b &= \mu_b\Delta t\\ \delta\psi_c &= \mu_c\Delta t\end{aligned} \qquad (C.16)$$

where μ_a, μ_b and μ_c are the measurement noises of three phase respectively.

Therefore, the position increment error caused by these noises can be written as,

$$\begin{aligned}\delta\theta_{e\mu} &= \frac{N_p}{k_e}\cdot\frac{\delta\psi_a e_2(\theta_e)+\delta\psi_b e_3(\theta_e)+\delta\psi_c e_1(\theta_e)}{e_1(\theta_e)e_2(\theta_e)+e_2(\theta_e)e_3(\theta_e)+e_3(\theta_e)e_1(\theta_e)}\\ &= \frac{N_p}{k_e}\cdot\frac{\Delta t[\mu_a e_2(\theta_e)+\mu_b e_3(\theta_e)+\mu_c e_1(\theta_e)]}{e_1(\theta_e)e_2(\theta_e)+e_2(\theta_e)e_3(\theta_e)+e_3(\theta_e)e_1(\theta_e)}\\ &= -\frac{3}{4}\frac{N_p\Delta t}{k_e}[\mu_a e_2(\theta_e)+\mu_b e_3(\theta_e)+\mu_c e_1(\theta_e)]\end{aligned} \qquad (C.17)$$

It can be seen that the position increment error caused by the measurement noises has the same feature as that of the measurement offsets. If all the noises in three-phase are the same, the position increment error will be zero.

Appendix D

Photographs of the Test Setup

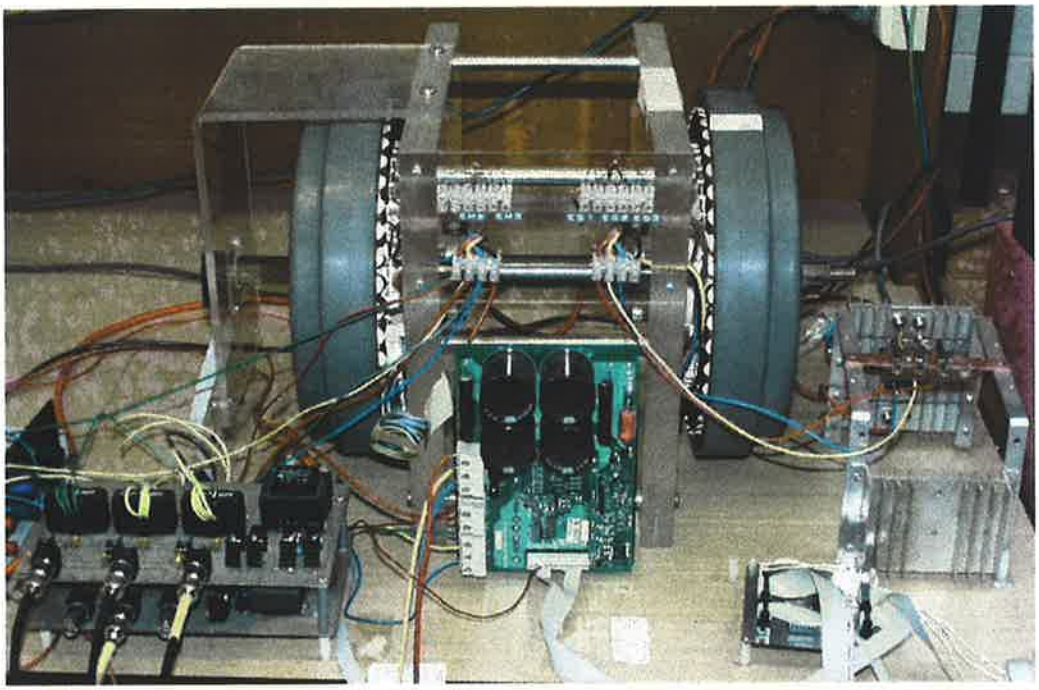

Photo D.1 The motor drive system

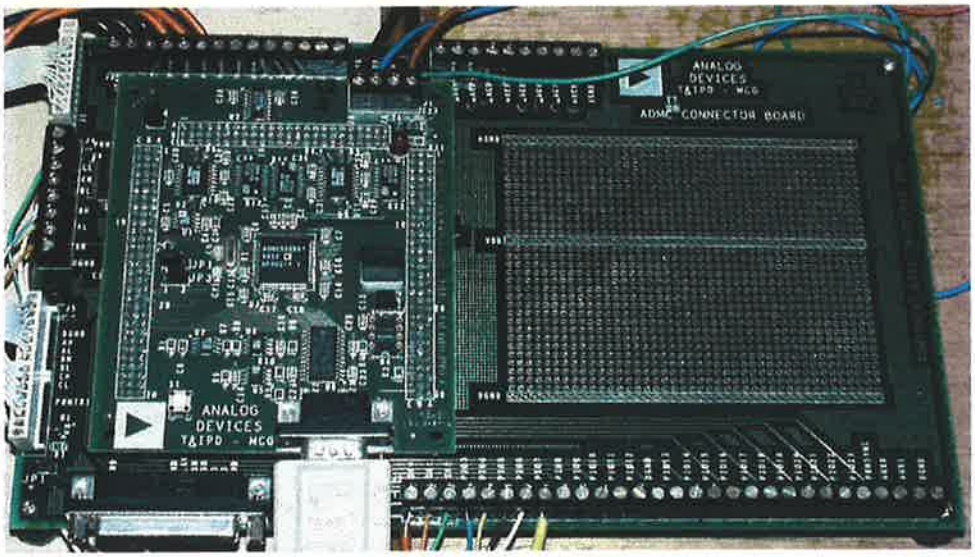

Photo D.2 ADMC300 DSP-based motor controller

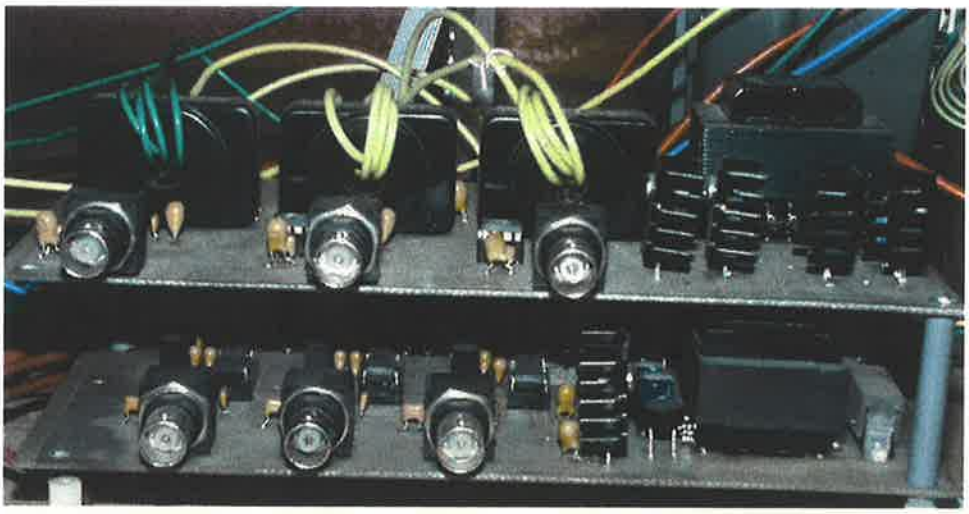

Photo D.3 Current and voltage transducers

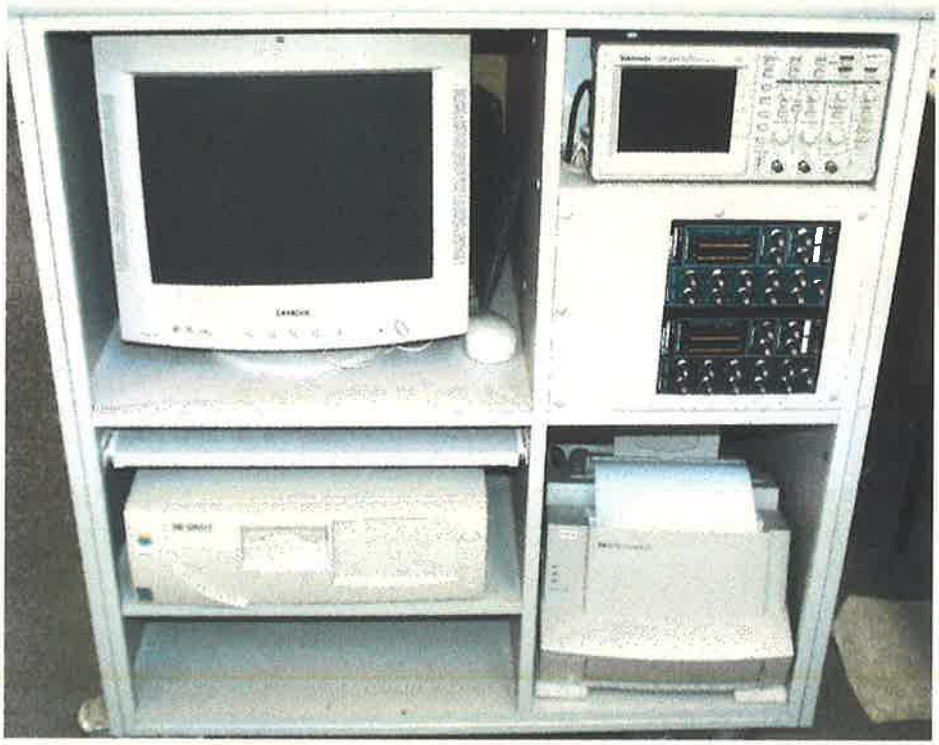

Photo D.4 The data acquisition system

REFERENCES

[1] Bose B. K., "Power Electronics and Variable Frequency Drives," IEEE Press, New York, 1996.

[2] Gieras J. F. and Wing M., "Permanent Magnet Motor Technology, " Marcel Dekker Inc., New York, 1997.

[3] Nasar S.A., Boldea I., et al, "Permanent Magnet, Reluctance and Self-Synchronous Motors, " CRC Press, Inc., 1993.

[4] Miller T. J. E., "Brushless Permanent-Magnet and Reluctance Motor Drives," Oxford University Press, New York, 1989.

[5] Ertugrul N., "Position Estimation and Performance Prediction for Permanent-Magnet Motor Drives, " PhD Thesis, University of Newcastle upon Tyne, UK, 1993.

[6] Becerra R.C., Ehsani M., and Jahns T.M., "Four-Quadrant Brushless ECM Drive with Integrated Current Regulation," IEEE Transactions on Industry Applications, Vol. 28, no. 4, pp. 833-841, July/August 1992.

[7] Brod D.M., and Novotny D.W., "Current Control of VSI-PWM Inverters," IEEE Transactions on Industry Applications, Vol. 21, no. 3, pp. 562-570, May/June 1985.

[8] Morimoto S., Takeda Y., et al., "Expansion of Operating Limits for MP Motor by Optimum Flux Weakening," IEEE Transactions on Industry Applications, Vol. 26, no. 5, pp. 866-871, September/October 1990.

[9] Bose B. K., "A High-Performance Inverter-Fed Drive System of an Interior PM Synchronous Machine," IEEE Transactions on Industry Applications, Vol. 24, no. 6, pp. 987-998, November/December 1988.

[10] Li T., and Slemon G.R., "Reduction of Cogging Torque in PM Motors," IEEE Transactions on Magnetics, Vol. 24, no. 6, pp. 2901-2903, 1988.

[11] Carlson, R., Lajoie-Mazenc M., and Fagundes J.C., "Analysis of Torque Ripple due to Phase Commutations in Brushless DC Machines," Conference Record of IEEE IAS Annual Meeting, pp. 287-292, 1990.

[12] Jahns, T.M., "Torque production in permanent magnet synchronous motor drives with trapezoidal electromotive force," IEEE Transactions on Industry applications, Vol. 20, No.4, pp. 803-813, July/august 1984.

[13] Jahns, T.M., "Flux weakening regime operation of an interior PM synchronous motor drive," IEEE Transactions on Industry applications, Vol. 23, No.4, pp. 681-689, July/august 1987.

[14] Jufer M., "self-Commutation of Brushless DC Motor Encoders," proceeding of the First European Power Electronics Conference, Brussels, PP. 3.275-3.280, 1985.

[15] Endo T., Tajima F. et al., "Microcomputer Controlled Brushless Motor without a Shaft Mounted Position Sensor," International Power Electronics Conference, Tokyo, pp. 1477-1486, 1983.

[16] Iizuka K., Uzuhashi H., et al., "Microcomputer Control for Sensorless Brushless Motor," IEEE Transactions on Industry Applications, Vol. 21, no. 3, pp. 595-601, May/June 1985.

[17] "Sensorless Spindle Motor Controller," Part ML4410, Advance Information, Microlinear Corporation, January 1990.

[18] Becerra R. C., Jahns T. M., and Ehsani M., "Four Quadrant Sensorless Brushless EMC Drive," IEEE Applied Power Electronics Conference and Exposition, pp. 202-209, 1991.

[19] Moreira J. C., "Indirect Sensing for Rotor Flux Position of Permanent Magnet AC Motors Operation Over a Wide Speed Range, " Conference Record of IEEE ISA Annual Meeting, pp. 401-407, 1994.

[20] Moreira J. C., "Indirect Sensing for Rotor Flux Position of Permanent Magnet AC Motors Operation Over a Wide Speed Range, " IEEE Transactions on Industry Applications, pp. 1394-1401, November/December, 1996.

[21] Ogasawara S. and Akagi H., "An Approach to Position Sensorless Drive for Brushless DC Motor, " IEEE Transactions on Industry Applications, pp. 928-933, September/October, 1991.

[22] Rusong. W., and Slemon G. R., "A Permanent Magnet Motor Drive Without a Shaft Sensor, " Conference Record of IEEE IAS Annual Meeting, pp. 553-558, 1990.

[23] Consoli A. Musumeci S., et al., "Sensorless Vector and Speed Control of Brushless Motor Drives, " IEEE Transactions on Industrial Electronics, pp. 91-96, February 1994.

[24] Ertugrul N. and Acarnley P. P., "A New Algorithm for Sensorless Operation of Permanent Magnet Motors, " IEEE Transactions on Industry Applications, Vol. 30, No.1, pp. 126-133, January/February 1994.

[25] French C. and Acarnley P. P., "Control of Permanent Magnet Motor Drives Using a New Position Estimation Technique, " IEEE Transactions on Industry Applications, Vol. 32, No.5, pp. 1089-1097, September/October 1996.

[26] Ostlund S. and Brokemper M., "Initial Rotor position Detection for an Integrated Pm Synchronous Motor Drive" Conference Record of IEEE Annual Meeting, pp.741-747, 1995.

[27] Min-Ho P., Hong-Hee L., "Sensorless Vector Control of Permanent Magnet Synchronous Motor Using Adaptive Identification, " IEEE IECON proceeding, pp 209-214, 1989.

[28] Matsui N. and Shigyo M., "Brushless DC Motor Control Without position and speed sensors, " IEEE Transactions on Industry Applications, Vol. 28, No.1, pp. 120-127, January/February 1992.

[29] Matsui N., "Sensorless PM Brushless DC Motor Drives, " IEEE Transactions on Industrial Electronics, Vol. 43, No.2, pp. 300-308, April 1996.

[30] Xue M. Y., Rahman M. F., Lim K.W., "Implementation of a New Sensorless Control Algorithm for a Permanent Magnet Synchronous Motor, " Australasian Universities Power Engineering Conference, pp. 91-96, 1997.

[31] Schroedl M., "Sensorless Control of Permanent Magnet Synchronous Motor, " Electric Machines and Power System, Vol. 22, pp. 173-185, 1994.

[32] Dhaouadi R., Mohan N., and Norum L., "Design and Implementation of an Extended Kalman Filter for the State Estimation of a Permanent Magnet Synchronous Motor, " IEEE Transactions on Power Electronics, Vol. 6, No.3, pp. 491-497, July 1991.

[33] Bolognani S., Oboe R., Ziglitto M. "Sensorless Full-Digital PMSM Drive With EKF Estimation of speed and Rotor Position" IEEE Transactions on Industrial Electronics, Vol. 46, No.1, pp. 184-191, February 1999.

[34] Jones L. A. and Lang J. H., "A State Observer for the Permanent Magnet Synchronous Motor," IEEE Transactions on Industrial Electronics, Vol. 36, No.3, pp. 374-382, August 1989.

[35] Tatematsu K., Hamada D., et al., "Sensorless Control for Permanent Synchronous Motor with Reduced Order Observer," Record of PESC, pp. 125-131, 1998.

[36] Kim J. S., Sul S. K., "High performance PMSM Drives Without Rotational Position Sensors Using Reduced Order Observer," Conference Record of IEEE IAS Annual Meeting, pp. 75-82, 1995.

[37] Kim J. S., Sul S. K., "New Approach for the Low-Speed Operation of PMAC Drive Without Rotation Position Sensors," IEEE Transactions on Power Electronics, Vol. 11, No.3, pp. 512-519, May 1996.

[38] Tomita M., Senjyu T., et al., "New Sensorless Control for Brushless DC Motor Using Disturbance Observers and Adaptive Velocity Estimations," IEEE Transactions on Industrial Electronics, Vol. 45, No.2, pp. 274-282, April 1998.

[39] Kulkarni A. B., and Ehsani M., "A Novel position Sensor Elimination Technique for the Interior Permanent Magnet Synchronous Motor Drive, " IEEE Transactions on Industry Applications, Vol. 28, No.1, pp. 144-150, January/February 1992.

[40] Ogasawara S., and Akagi H., "An Approach to Real-Time Position Estimation at Zero and Low Speed for a PM Motor Based on Saliency, " IEEE Transactions on Industry Applications, Vol. 34, No.1, pp. 163-168, January/February 1998.

[41] Ogasawara S., and Akagi H., "Implementation and Position Control Performance of a Position-Sensorless IPM Motor Drive System Based on Magnetic Saliency, " IEEE Transactions on Industry Applications, Vol. 34, No.4, pp. 806-812, July/August 1998.

[42] Aihara T., Toba A., et al., "Sensor-less Torque Control of Salient-Pole Synchronous Motor at Zero Speed Operation," IEEE APEC, pp. 715-720, 1997.

[43] Ogasawara S., and Akagi H. "Rotor Position Estimation Based on Magnetic Saliency of an IPM Motor," Conference Record of IEEE ISA Annual Meeting, pp. 460-466, 1998.

[44] Chuanyang W., and Longya X. "Investigation of a Practical Approach for Rotor Position Estimation of PM Machines without Rotor Saliency," Proceedings of IPEMC 2000, pp. 329-335, 2000, Beijin.

[45] Ribeiro L. A. S., Degner M. W., and Lorenz R. D., "Comparison of Carrier Signal Voltage and Current Injection for the Estimation of Flux Angle or Rotor Position, " Conference Record of IEEE ISA Annual Meeting, pp. 452-458, 1998.

[46] Corley M. J., and Lorenz R. D., "Rotor Position and Velocity Estimation for a Salient-Pole Permanent Magnet Synchronous Machine at Standstill and High Speeds, " IEEE Transactions on Industry Applications, Vol. 34, No.4, pp. 784-789, July/August 1998.

[47] Schroedl M. "Sensorless Control of AC Machines at Low Speed and Standstill Based on the INFORM Method," Conference Record of IEEE ISA Annual Meeting, pp. 270-277, 1996.

[48] Degner M. W., and Lorenz R. D., "Using Multiple Saliencies for the Estimation of Flux, Position, and Velocity in AC machine, " IEEE Transactions on Industry Applications, Vol. 34, No.5, pp. 1097-1104, September/October 1998.

[49] Wijenayake A. H., Bailey J. M., Naidu M. "A DSP-based Position Sensor Elimination Method With an On-line Parameter Identification Scheme For Permanent Magnet Synchronous Motor Drives," Conference Record of IEEE ISA Annual Meeting, pp. 207-215, 1995.

[50] Limei W., Qingding G., and Lorenz R. D., "Sensorless Control of Permanent Magnet Synchronous Motor," Proceedings of IPEMC 2000, pp. 329-335, 2000, Beijin.

[51] Cardoletti L. and Cassat L. "Sensorless Position and Speed Control of a Brushless DC Motor from Star-up to Nominal Speed," EPE Journal, Vol. 2, No. 1, pp. 25-34, March 1992.

[52] Matsui N., and Takesshita T., "A Novel Starting Method of Sensorless Salient-Pole Brushless Motor," Conference Record of IEEE ISA Annual Meeting, pp. 386-392, 1994.

[53] Kondo S., Takahashi A., and Nishida T., "Armature Current Locus Based Estimation Method of Rotor Position of Permanent Magnet Synchronous Motor Without Mechanical Sensor," Conference Record of IEEE ISA Annual Meeting, pp. 55-60, 1995.

[54] Noguchi T., Yamada K., et al., "Initial Rotor Position Estimation Method of Sensorless PM Synchronous Motor with No Sensitivity to Armature Resistance," IEEE Transactions on Industrial Electronics, Vol. 45, No.1, pp. 118-125, February 1998.

[55] Kavanagh R. C., Murphy J. M. D., and Egan M. G., "Innovative Current Sensing for Brushless DC Drives, " IEE PEVD Conference Publication, pp. 354-357, 1988.

[56] Tan H. and Ho S. L., "A novel single current sensor technique suitable for BLDCM drives, " Record of PEDS'99, July 1999, Hong Kong.

[57] Acarnley P. P. and Eng C., "Current measurement in three-phase Brushless DC drives, " IEE Proceedings-B, Vol. 140, No.1, pp. 71-79, January 1993.

[58] Acarnley P. P., "Observability Criteria for Winding Currents in Three-Phase Brushless DC Drives, " IEEE Transactions on Power Electronics, Vol. 8, No.3, pp. 264-270, July 1993.

[59] "Three phase current measurements using a single line resistor on the TMS320F240," Literature No: BPRA007, Texas Instruments Europe, May 1998.

[60] Green T.C. and Williams B.W., "Derivation of Motor Line-Current Waveforms from the DC-link Current of an Inverter, " IEE Proceedings-B, Vol. 136, No.4, pp. 196-204, July 1989.

[61] Green T.C. and Williams B.W., "Control of Induction Motor Using Phase Current Feedback Derived from the DC-link, " Proceeding of EPE'89, Vol. 3, pp. 1391-1396, 1989.

[62] Xue Y., Xu X., et al., "A Low Cost Stator Flux Oriented Voltage Source Variable Speed Drive," Proceedings of ASI'90, pp. 410-415, 1990.

[63] Xue Y., Xu X., et al., "A Stator Flux-oriented Voltage Source Variable-Speed Drive Based on DC Link Measurement," IEEE Transactions on Industry Application, Vol. 27, No.5, pp. 962-969, September/October 1991.

[64] Mognihan J. F., Kavanagh R. C., et al., "Indirect Phase Current Detection for Field Oriented Control of a Permanent magnet Synchronous Motor Drive, " Proceedings of EPE'91, Vol. 3, pp. 641-646, 1991.

[65] Pedersen J. K., Blaabjerg F., "An Ideal PWM-VSI Inverter Using only One Current Sensor in the DC-link, " Proceedings of PEVD'94, pp. 458-464, 1994.

[66] Riese M., "Phase Current Reconstruction of a Three-phase Voltage Source Inverter-fed Drive Using Sensor in the DC-link, " Proceedings of PCIM'96, pp. 95-101, 1996.

[67] Joo H. G., Kim C. G. et al., "Detection of three phase current in space-vector PWM inverters with only one DC link current sensor, " 0-7803-2775-6/96 $4.00 ©1996 IEEE.

[68] Blaabjerg F., Pedersen J. K., "A New Low-cost Fully Fault Protected PWM-VSI Inverter with True Phase-current Information, " Proceedings of IPEC`95, Vol. 2, pp. 984-991, 1995.

[69] Blaabjerg F., Pedersen J. K., et al., "Single Current Sensor Technique in the DC link of Three-phase PWM-VS Inverters: a Review and a Novel Solution," IEEE Transactions on Industry Application, Vol. 33, No.5, pp. 1241-1253, Sept/Oct, 1997.

[70] Woo C. L., Taeck K. L and Dong S. H., "Comparison of Single-Sensor Current Control in the DC Link for Three-Phase Voltage-Source PWM Converters," IEEE Transactions on Industrial Electronics, Vol. 48, No.3, pp. 491-505, June, 2001.

[71] Mognihan J. F., Bolognani S., et al., "Single Sensor Current Control of AC Servodrives Using Digital Signal Processors, " Proceedings of EPE'93, Vol. 4, pp. 415-421, 1993.

[72] Mognihan J. F., Kavanagh R. C., et al., "State Observer Based Indirect Current Detection for PM Synchronous Servo Drives, " Proceedings of ICEM'91, pp. 617-621, 1991.

[73] Slemon G.R., and Xian L., "Modeling and Design Optimization of Permanent Magnet Machines," Electric Machines and Power Systems, Vol. 20, pp. 71-92, 1992.

[74] Sebastian T., Slemon G.R., and Rahman M.A., "Modeling of Permanent Magnet Synchronous Motor," IEEE Transaction on Magnet, Vol. 22, No.5, pp.1069-1071, September 1986.

[75] Nehl T.W., Fouad F.A., et al., "Dynamic Simulation of Radially Oriented Permanent Magnet-Type Electronically Operated Synchronous Machines with Parameters Obtained from Finite Element field Solutions," IEEE Transactions on Industry Application, Vol. 18, No.2, pp. 172-182, March/April 1982.

[76] Pilay P., and Krishnan R., "Modeling, Simulation and Analysis of Permanent Magnet Motor Drive, Part 1: The Permanent Magnet Synchronous Motor Drive," IEEE Transactions on Industry Application, Vol. 25, No.2, pp. 265-273, March/April 1989.

[77] Mihailovic Z., Prasad H.V., et al., "Computer Modelling and Analysis of VSI Fed Permanent Magnet Synchronous Motor Drive Systems with Adjustable Levels of Complexity," IEEE Applied Power Electronics Conference and Exposition, pp. 728-735, 1997.

[78] Ertugrul N., Eric Chong, "Modelling and Simulation of an Axial Field Brushless Permanent Magnet Motor Drive, " European Power Electrical Conference, Trondheim, Norway, 1997.

[79] "National Instrument LabVIEW User Manual," July 2000 Edition.

[80] Pillay P., "Modeling and Performance of Sinusoidal and Rectangular-Fed Permanent Magnet Motor Drives," Performance and Design of Permanent Magnet AC Motor Drives, IEEE-IAS Press, 1989.

[81] Peter Vas, "Electrical Machines and Drives: a Space-vector Theory Approach," Oxford University Press, 1992.

[82] Nakashima S., Inagaki Y., and Miki I., "Sensorless Initial Rotor Position Estimation of Surface Permanent-Magnet Synchronous Motor," IEEE Transactions on Industry Application, Vol. 36, No.6, pp. 1598-1603, November/December 2000.

[83] Kasa N., and Watanabe H., "A mechanical Sensorless Control System for Salient-Pole Brushless DC Motor With Autocalibration of Estimated Position Angles," IEEE Transactions on Industrial Electronics, Vol. 47, No.2, pp. 389-395, April 2000.

[84] Holtz J., "Is Snesorless Position Control of Standard Induction Motor a Feasible Technology?" Third International Power Electronics and Motion Control Conference IPEMC'2000, pp.21-32, Beijing, China, Aug. 2000.

[85] Hurst K.D., Habetler T.G., et al., "Zero-speed Tacho-less I.M. Torque Control: Sample a Matter of Stator Voltage Integration," IEEE APEC 1997, pp. 749-753, 1997.

[86] Chen Z., Tomita M., et al., "New Adaptive Sliding Observers for Position and Velocity Sensorless Controls fo Brushless DC Motors," IEEE Transactions on Industrial Electronics, Vol. 47, No.3, pp. 582-591, June 2000.

[87] Harnefors L., and Nee H. P., "A General Algorithm for Speed and Position Estimation of AC Motors," IEEE Transactions on Industrial Electronics, Vol. 47, No.1, pp. 77-83, February 2000.

[88] Emura T., and Wang L., "A High-Resolution Interpolator for Incremental Encoder Based on the Quadrature PLL Method," IEEE Transactions on Industrial Electronics, Vol. 47, No.1, pp. 84-90, February 2000.

[89] Moynihan J. F., Egan M.G., and Murphy J. M. D., "The Application of State Observers in Current Regulated PM Synchronous Drives," IEEE IECON 1994, pp. 20-25, 1994.

[90] Kim K. H., Baik I. C. and Youn M. J., "An Improved Digital Current Control of a PM Synchronous Motor with a Simple feedforward Disturbance Compensation Scheme" IEEE Power Electronics Specialists Conference PESC'1998, pp.101-107.

[91] Kang S. J., Sul S. K., et al., "Direct Torque Control of Brushless DC Motor with Nonideal Trapezoidal Back EMF," IEEE Transactions on Power Electronics, Vol. 10, No.6, pp. 796-802, November 1995.

[92] French C., and Acarnley P., "Direct Torque Control of Permanent Magnet Drives," IEEE Transactions on Industry Application, Vol. 32, No.5, pp. 1080-1088, September/October 1996.

[93] Zhong L., Rahman F., et al., "Analysis of Direct Torque Control in Permanent Magnet Synchronous Motor Drives," IEEE Transactions on Power Electronics, Vol. 12, No.3, pp. 528-535, May 1997.

[94] Chung S.K., Kim H. S., et al., "A New Instantaneous Torque Control of PM Synchronous Motor for High-Performance Direct-Drive Applications," IEEE Transactions on Power Electronics, Vol. 13, No.3, pp. 388-400, May 1998.

[95] Colby R.S., and Novotny D.W., "An Efficacy Optimizing Permanent Magnet Synchronous Drive," IEEE Transactions on Industry Application, Vol. 24, No. 3, pp. 462-469, May/June 1998.

[96] Vukosavic S. N., and Stankovic A.M., "Sensorless Induction Motor Drive with a Single DC-Link Current Sensor and Instantaneous Active and Reactive Power Feedback," IEEE Transactions on Industrial Electronics, Vol. 48, No.1, pp. 195-204, February 2001.

[97] Evans P.D., and Hill-Cottingham R. J., "DC Link Current in PWM Inverter," IEE proceedings, Vol. 133, Pt. B, No.4, pp. 217-224, July 1986.

[98] Boys J. T., "Novel Current Sensor for PWM AC drives," IEE proceedings, Vol. 135, Pt. B, No.1, pp. 27-32, January 1988.

[99] Chan C.C., Chau K.T., et al., "A Novel Dead-Time Vector Approach to Analysis of DC Link Current in PWM Inverter Drives," IEEE Applied Power Electronics Conference and Exposition, pp. 338-344, 1997.

[100] Jeong S. G., and Park M. H., "The Analysis and Compensation of Dead-Time Effects in PWM Inverters," IEEE Transactions on Industrial Electronics, Vol. 38, No.2, pp. 108-114, April 1991.

[101] Choi J. W., and Sul S. K., "Inverter Output Voltage Synthesis Using Novel Dead Time Compensation," IEEE Transactions on Industrial Electronics, Vol. 11, No.2, pp. 221-227, March 1996.

[102] "IRMDAC3 Reference Design Data Sheet," International Rectifier, October 1998.

[103] "High Performance DSP-Based Motor Controller, ADMC300," Analog Devices, 1998.

[104] "ADMC300 Processor Board," Analog Devices, 1998.

[105] "ADMC Connector Board," Analog Devices, 1998.

[106] "The Measurement and Automation Catalog 2001," National Instruments, 2001.

PUBLICATIONS

[1] Ying L. and Ertugrul N, "The Simulation of Permanent Magnet AC Motor drives with LabVIEW", Proceedings of AUPEC'99, pp. 484-489, Darwin, Australia, Sept. 1999.

[2] Ying L. and Ertugrul N., "The Intelligent Drive for Permanent Magnet AC Motors with the least number of sensors", Journal of Electrical and Electronics Engineering Australia, Vol.20, No.1, 2000.

[3] Ying L. and Ertugrul N., "A Novel Position Sensorless Control for Permanent Magnet AC Motors", Proceedings of IPEMC'2000, pp.169-174, Beijing, China, Aug. 2000.

[4] Ying L. and Ertugrul N., "A Novel Estimation of Phase Currents from DC Link for Permanent Magnet AC Motors", Proceedings of TENCON'2001, pp 606-612, Singapore, Aug. 2001.

[5] Ying L. and Ertugrul N., "A Novel Position Sensorless Technique for Permanent Magnet AC Motors", Proceedings of PESC'2002, pp 289-294, Cairns, Australia, June 2002.

[6] Ying L. and Ertugrul N., "A Novel, Robust DSP-Based Indirect Rotor Position Estimation for Permanent Magnet AC Motors without Rotor Saliency", Accepted by IEEE Transactions on Power Electronics.

[7] Ying L. and Ertugrul N., "An Observer-Based Three-Phase Current Reconstruction using DC Link Measurement in PMAC Motors", Submitted to IEEE Transactions on Power Electronics.

[8] Ying L. and Ertugrul N., "A PMAC Motor Drive with a Minimum Number of Sensors", to be submitted to IEEE Transactions on Industry Applications.